Self assembly for surface functionalization to improve biocompatibilities in Ti-based implants and enzyme immobilization in biofuel cells

Gu, Qiong

Self Assembly for Surface Functionalization to improve Biocompatibilities in Ti-based implants and Enzyme immobilization in Biofuel cells

Qiong Gu

A Thesis submitted for the degree of Doctor of Philosophy
in the Faculty of Engineering of the University of London

School of Engineering and Materials Science
Queen Mary, University of London

September 2010

ACKNOWLEDGEMENTS

I would like to take this opportunity to thank a number of people for their contributions to this work, without which this thesis would not have been possible. First, I am deeply indebted to my supervisor, Professor Z. X. Guo, who gave me such a great opportunity to work in this topical field of science, and also thankful for his expertise, encouragement, supervision and invaluable support through out the duration of my PhD research. As a scientist, his wide knowledge, enthusiasm and diligence set an inspirational model for me. I am also highly thankful to Dr. Dongmei Sun for her helpful instruction, training and also continuous encouragement and valuable discussion.

I would like to express my gratitude to the academic and technical staff in the Department of Materials, Queen Mary, University of London for providing all the research facilities and resources. Special thinks to Dr. Asa Barber, Dr. Geoffrey Hyett, Dr. Zimei Rong, Mr. John Caulfield, Dr. Monisha Phillips, Mrs. Sandra Wells and Miss Victoria Wells for their support. I also want to thank my colleagues in the group, particularly, Dr. Xuesong Lu, Dr. Coxia Shang, Dr. Steven Shevlin, Dr. Francois Aguey-Zinsou, Dr. Ting-Fu Hong, Dr. Jianfeng Jin, Dr. Zhaoyun Wu, Dr. Yang Lei, Dr. Weina Yang, Elnaz Ajami, Negar Amini, Yiwen Wang and Shahrouz Nayebossadri for all their help, support, interest and suggestions.

My great thanks are due to my parents for their continuous support, encouragement and endless love, which always make me feel strong and confident to face all the challenges during the period of my PhD study.

Especially, I would like to give my special thanks to my husband, Tong, whose patient love enabled me to complete this research.

ABSTRACT

Self-assembly is an effective biomimetic technique for surface functionalization and nanostructural synthesis. 3-Aminopropyltriethoxysilane (APTES) is a popular molecule that can assemble over substrates to modify surface properties. Titanium is a structural material with high weight-specific mechanical properties, corrosion-resistance and bioinertness. Here, a systematic investigation was carried out to optimize the self-assembly of an APTES-modified film on an oxidized titanium surface in order to improve its biocompatibility as an implant material and molecular selectivity, e.g. for CO_2 capture. A clean TiO_x layer was formed on titanium after the treatment in a *Piranha* solution of H_2SO_4 : H_2O_2 = 3:1. The IR spectra confirmed that the formation of the APTES-modified film (called APS film) on the surface by the presence of the Si-O-Ti and Si-O-Si covalent bonds. The ordering of the self-assembled film did not show strong temperature dependence from 30 to 70ºC, although a thicker film was noted at a higher temperature. Anhydrous toluene as the solvent is essential to the formation of a well-ordered and thin film, compared with hydrous toluene. The well-assembled film was formed on the oxidised titanium surface in the anhydrous toluene solution of ~0.2 v% APTES at 30°C for 16 hours. A higher APTES concentration leads to a disorder film with protonated $–NH_3^+$ groups, whereas a lower concentration causes end groups of the adsorbed APTES to loop with the -OH groups on the surface. The APS film with the free $–NH_2$ functional groups is more stable in aqueous solution with pH 10, although it is still hydrolyzed according to the intensity of the –Si-O-Si- bond in the IR spectra.

The well-ordered APS film with the $–NH_2$ groups cannot induce heterogeneous nucleation in a simulated body fluid (SBF), because the $–NH_2$ groups are neutral in the solution and the $–CH_2$- hydrophobic groups are exposed in the disordered structure of

the APS film. In the application of biofuel cells, the laccase from *Trametes versicolor* as an enzyme was immobilized on titanium and graphite with the APS film by the covalent bond, respectively. Compared with the native laccase, optimum pH of the immobilized laccase decreased to 3 because of the increase of turnover number (K_{cat}). Further comparison of Michaelis-Menten constant (K_m) of the immobilized laccase with the native one clearly shows that the increase of K_m value is mainly due to the change of configuration of the active site, further leading to the lower affinity of immobilized laccase towards the substrate. The laccase on graphite shows higher optimum temperature and twice lower the K_m value, compared with the laccase on titanium, which results from the surface morphology of graphite after oxidation. For electrochemical behaviour, graphite with the laccase as electrode does not show direct electron transfer (DET), due to the long electron tunnel between the T1 centre and electrode surface. However, the electrode with laccase shows good mediator electron transfer (MET) in the presence of mediator.

TABLE of CONTENTS

LIST OF TABLES

CHAPTER 2:

CHAPTER 3:

CHAPTER 4:

LIST OF FIGURES

CHAPTER 1:

CHAPTER 2:

CHAPTER 3:

CHAPTER 4:

CHAPTER 5:

ACRONYMS

ABTS	2,2'-azino-bis(3-ethylbenzthiazoline-6-sulphonic acid)
AFM	Atomic force microscopy
APTES	3-aminopropyltriethoxysilane
APS	3-aminopropylsilane
BOD	Bilirubin oxidase
BSA	Bovine serum albumin protein
CaP	Calcium phosphate
CE	Counter electrode
CV	Cyclic voltammogram
CVD	Chemical vapor deposition
Cyt *c*	Cytochrome *c*
DET	Direct electron transfer
ECM	Extracellular matrix
EDC	*N*-(3-dimethylaminopropyl)-*N*'-ethylcarbodiimide hydrochloride
EDX	Energy-dispersive X-ray spectrometer
ELISA	Enzyme-linked immunosorbent assay
EPD	Electrophoretic deposition
ESCA	Electron spectroscopy for chemical analysis
GLUTAL	Glutaraldehyde
GPES	General purpose electrochemical system
GPTS	3-Glysidoxypropyltrimethoxysilane
HA	Hydroxyapatite
HEPES	4-(2-hydroxyethyl)-1-piperazineethanesulfonic acid
HRP	Horseradish peroxidase
IZP	Isoelectric point

Lac	Laccase
LB films	Langmuir-Blodgett films
$\boldsymbol{K_{cat}}$	Catalytic rate constant / Turnover number
$\boldsymbol{K_m}$	Michaelis-Menten constant
MET	Mediator electron transfer
MFCs	Microbial fuel cells
11-MUA	11-Mercaptoundecanoic acid
MWCNTs	Multiwalled carbon nanotubes
NHS	*N*-hydroxysulfosuccinimide sodium salt
NHE	Normal hydrogen electrode
OTS	Octadecyltrichlorosilane
OPA	Octadecylphosponic acid
RA-FTIR	Reflectance-absorbance fourier transform infrared spectroscopy
RE	Reference electrode
RGD	Arg-Gly-Asp
SAMs	Self-assembled monolayers
SBF	Simulated body fluid
SEM	Scanning electron microscopy
SHE	Standard hydrogen electrode
SSCE	Sodium chloride saturated calomel electrode
α-TCP	α-Tricalcium phosphate
β-TCP	β-Tricalcium phosphate
TTCP	Tetracalcium phosphate
UHV	Ultrahigh vacuum
$\boldsymbol{V_0}$	Initial velocity
$\boldsymbol{V_{max}}$	Maximum velocity
WE	Working electrode
XPS	X-Ray photoelctron spectroscopy
XRD	X-ray diffraction

CHAPTER 1

INTRODUCTION

To date, 'nanotechnology' has become very popular and been widely applied in medicine, electronics, biomaterials, energy production, IT and communications, as it can create new materials and devices on an atomic and molecular scale. Why nanotechnology is better than other forms? Nanotechnology is dramatically changing materials' properties compared to that on macroscale, such as mechanical, electrical, thermal and catalytic properties, through the development of nano-systems. For example, gold, which is chemically inert at normal scales, can serve as a potent chemical catalyst at nanoscales. These systems incorporate novel nanostructures that integrate functional complexity directly into each individual nanoparticle, enabling the low-cost fabrication of high-value, high-performance applications.

Generally, nanotechnology has two strategies: top-down and bottom-up. The top-down approach is to create nanoscale devices by using larger, externally-controlled materials into the desired shape and order. Several excellent top-down type approaches including photolithography and electron-beam lithography have been used to produce nanostructures. However, the top-down method is very expensive and cannot control the size, shape and order of particles well. The bottom-up approach is to have smaller components build up into more complex assemblies, which relies on the chemical properties of single molecules to form expected nanostructure by self-assembly and/or molecular recognition, has been drawn attention recently. Among bottom-up approaches, self-assembly is a most popular method and become an important concept in nanotechnology [Ariga 2008]. Self-assembly is defined as the spontaneous formation of complex structures from pre-designed molecules by hydrogen bonds, aromatic π-stacking, van der Waal's interactions, etc [Ariga 2008; Schreiber 2000]. Self-assembly is ubiquitous in nature. Various natural structures are formed by self-assembly. For example, the self-assembly of the DNA double helix structures from two complementary oligonucleotides by base matching and of the cell membrane from two layers of lipid molecules by hydrophobic interactions.

Since it is original from the biological structure, the self-assembly has many advantages. Firstly, it carries out many of the most difficult steps in nanofabrication, involving atomic-level modification of structure. Secondly, the structure of self-assembly can be accurately and efficiently synthesized from relatively simple subunits. Moreover, this technology tends to produce structures that are relatively defect-free and self-healing [Van Alsten 1999].

The self-assembly method as a biomimetic technique has been developed to produce new materials by different driven forces. For instance, melamine and cyanuric acid in aqueous solution can be self-assembled to form a linear tap and/or cyclic rosette structures by hydrogen bonds (**Figure 1. 1**), which is the most symmetrical prototype for the arrays of hydrogen bonds between base pairs in nuclei acids [Whitesides 1991]. This structure is very stable and can be heated at 450°C without decomposition. Due to good thermal stability, melamine-cyanuric can be assembled to form three-dimensional nanotube crystal structures.

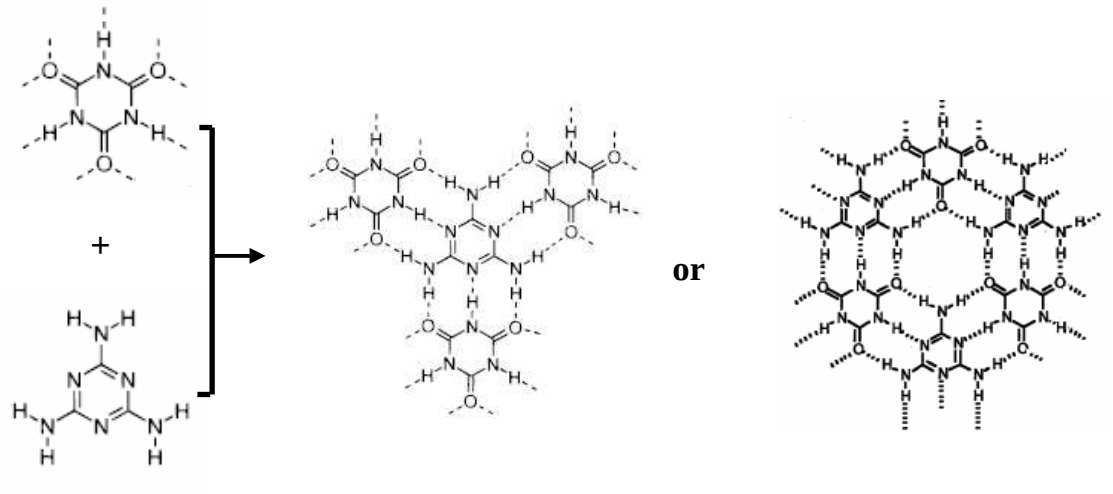

Figure 1. 1 Melamine-cyanuric acid hydrogen-bonded lattice. Two of the possible structures can be derived from the lattice: a linear tape and a cyclic rosette [Whitesides 1991].

Biomembrane is another good sample for self-assembled structure, which can provide most important structural units in the biological cell. In 1964 Bangham and Horne demonstrated that the bilayer structure forms spontaneously from aqueous lipid dispersions [Bangham 1964]. In bilayer structure lipids have normally three parts: hydrophilic head group, hydrophobic aliphatic chain (s), and the region linking with

other molecules [Antonietti 2003]. Usually, bilayer has a hydrophobic core and hydrophilic surface. Under special conditions, bilayer can reversely have hydrophilic core and hydrophobic surface. So far, various lipid designs can introduce hydrophilic/hydrophobic amphiphilic molecules to different structures through self-assembly processes, including vesicle, rod, micelle (reversed one), sheet and tube structures (**Figure 1. 2**), which has been successfully applied in drug delivery, biosensor, etc.

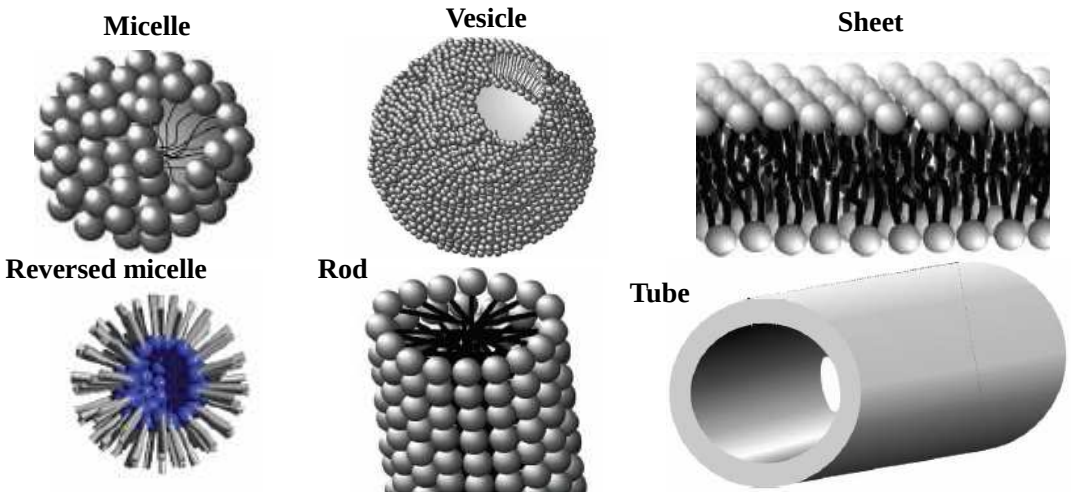

Figure 1. 2 Formations of higher order structures of amphiphilic molecules assemblies by bilayers [Ariga 2008].

Apart from organic molecules, metal ions can also be assembled into a designed structure. Recently, Metal Organic Frameworks (MOFs) are identified a class of porous polymeric material, consisting of metal ions linked together by organic bridging ligands (molecules) [James 2003]. For example, in MOF-5 (**Figure 1. 3**), $Zn_4O(CO_2)_6$ unit contains four Zn_4O tetrahedral and six carboxylated carbon atoms, which is called secondary build unit (SBU). According to inorganic metal-ligand interactions, materials can be produced an infinite one-, two-, or three-dimensional structures by self-assembly process, with high stability, tunable metrics, organic functionality and porosity. Due to the porosity in the structure, MOF materials are highly studied for gas purification, separation and storage [Mueller 2005].

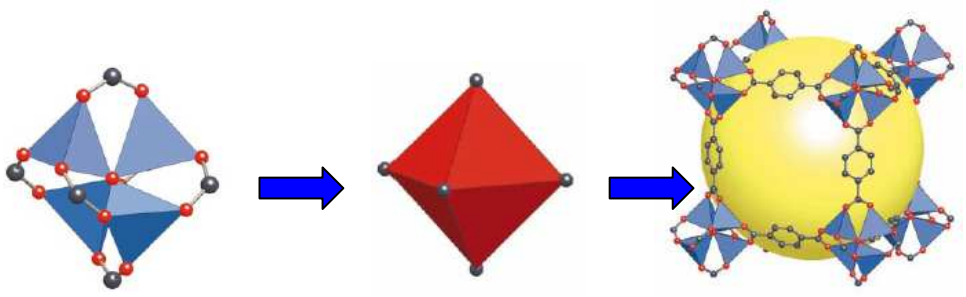

$Zn_4O(CO_2)_6$ **Octahedral SBU** **MOF-5**

Figure 1. 3 MOF-5 structure prepared from Zn and carboxyl acid. In $Zn_4O(CO_2)_6$ SBU (secondary build unit), O, red and C, black; metal-oxygen polyhedra are blue and polyhedron by carboxylate carbon atoms are red .

One of successful self-assembled structures is well-ordered molecules on a substrate, or self-assembled monolayers (SAMs) of ordered molecules. One of the early studies of SAMs on a substrate is the preparation of organic disulfide on a gold surface by Nuzzo and Allara [Nuzzo 1983]. Such molecules spontaneously assemble into ordered monolayers to form a nanometer-thick organic film on the surface. A strong interaction exists between a head group of a molecule and the substrate, involving the formation of a chemical bond. Because of the highly ordered nature and tight packing, the self-assembled monolayer has now effectively been used for chemical synthesis, nanotechnology, polymer science and surface engineering [Van Alsten 1999]. For example, SAMs have been used for the corrosion protection on metal surfaces and to control the wetting property of a surface by functional groups (hydrophilic or hydrophobic) [Schreiber 2000]. SAMs are also good candidates for boundary lubrication because of their strong chemical bonds with the substrate [Ulman 1990]. SAMs have been employed for many biological applications because of their capability of immobilizing proteins by functional end groups (e.g. –COOH and $–NH_2$).

Titanium and its alloys are very widely used as load-bearing implants in medicine because of its good mechanical properties such as relative low modulus, excellent corrosion resistant ability, good fatigue strength and low specific weight [Liu 2004]. However, titanium with the native surface oxide is known to be bioinert, so it is difficult to achieve good chemical bonding with bones and form new bones on its surface at the early stage after implantation [Liu 2004; Majewski 2006; Ratner 1996], compared with other bioactive implant materials, such as calcium phosphates (CaPs).

Although calcium phosphate can form strong chemical bonds with the surrounding bone, it cannot be applied along in the load-bearing implants due to its low fracture toughness and high elastic modulus [Legeros 2002]. Therefore, the remarkable biological activity of calcium phosphate with the excellent mechanical properties of titanium, makes suitable candidates as load-bearing implant materials.

Although various methods have been developed to coat calcium phosphate on titanium, they all possess two major problems: high processing temperatures and the poor coating integration with the metal surface. Low temperature biomimetic-based methods have been developed as alternative methods for coating calcium phosphate with the strongly chemical bond. Here, the use of self-assembled monolayers has been drawn attention. Moreover, the functional groups in SAMs can bind with bioactive molecules on the surface, such as Arg-Gly-Asp [Rezania 1999], extracellular matrix and growth factors [Oji 1999; Pan 1998], to elicit specific cellular responses [Faucheux 2004] and induce new tissue formation, finally to improve the biocompatibility of titanium.

SAMs are formed by the spontaneous two-dimensional organization of an active surfactant at an interface. Indeed, the formation of SAMs provides one easy route towards surface functionalization by organic molecules containing suitable functional groups like –SH, -CN, -OH, -COOH, -NH_2 with head groups on the surface [Love 2005]. So far, SAMs with thiol as head group on metallic surfaces (Au, Ag, and Pt) have been researched very well, including effect of molecular concentration, temperature and time on the preparation of SAMs as well as the structure of SAMs and its stability in aqueous solution [Imamura 1995; Love 2005; Poirier 1996; Schreiber 2000]. However, the thiol head group cannot form covalent bond with some solid surfaces, such as titanium (Ti), aluminum, silicon, glass and graphite. Since above mentioned surfaces can supply hydroxyl groups, which can form covalent bond (-M-O-Si-) with silanols, organic silane-based molecules can be chosen for SAMs on these surfaces. Although there is a very comprehensive investigation on the growth of silane-based SAM on silicon surfaces [Hsieh 2007; Ulman 1990] and other substrates, such as mica [Vallant 1998], glass [Chiang 1980] and aluminum [Lewington 2002], no much attention has been paid to the fundamental issues of the SAM formation on the

Ti substrates. There is only limited work on the growth of silane-based and phosphate-based SAM on Ti substrates, which has mostly been carried out on model silicon substrates coated with TiO_2. Obtaining a highly ordered and fully covering SAM on real Ti surfaces still remains a challenge.

Recently, the organic silane-based molecules with hydrophobic groups (-CH_3 and –$CH=CH_2$) on silica have been investigated widely, for example, octadecyltrichlorosilane (OTS) on silica. Compared with hydrophobic groups, hydrophilic functional groups (-OH, -COOH and –NH_2) are used widely in biochemistry and biotechnology. However, molecules with hydrophilic functional groups are very rare due to the formation of polymer after hydrolysis. For one-step preparation of SAMs by organic silane-based molecules, 3-aminopropyltriethoxysilane (APTES) is valid with the –NH_2 functional group, involving three-carbon chain. Although it has been reported to prepare on glass [Chiang 1980] and on silica [Golub 1996], APTES has not been systematically investigated on the metallic surface (e.g. Ti). Moreover, due to the wide applications of APTES, such as surface modification of bio-implant and protein immobilization, it is necessary to study its stability in aqueous solution and thermal stability.

Apart from the improvement of the biocompatibility of implants, self-assembled monolayers with the amine functional group could immobilize biomolecules by the functional groups. For example, enzyme as a kind of protein has been immobilized by thiol-based SAMs on gold surface [Gooding 1999; Mendes 2008]. Since enzymes are a particularly versatile class of catalysts, which are very effective and precise-catalysts that perform and regulate processes in living matter, they have been applied widely in many fields, such as in biosensors, nanotechnology and bioelectronic devices. In biofuel cells, SAMs with functional groups can be applied for the enzyme immobilization, which can convert chemical energy to electricity by redox reactions [Bullen 2006; Palmore 1994]. So far, among the varieties of enzymes, laccase has received much attention from researchers due to its ability to oxidize both phenolic and non-phenolic lignin related compounds as well as to reduce oxygen to water, which makes them very useful for its application to several biotechnological processes [Alexandre 2000; Reinhamm 1970; Yaropolov 1994].

Various immobilization methods of laccase have been applied on solid supports, including adsorption, covalent attachment, cross-linking and entrapment in polymers [Trevan 1980]. In general, adsorption and entrapment methods are easy to perform, but the interaction force between the enzyme and support surface is often weak causing leaching. The covalent attachment and cross-linking by the $-NH_2$ functional group could form chemical bond with enzymes, but suffer from a low reproducibility and a poor spatially controlled deposition, resulting in the lower activity of immobilized enzyme. Due to oxidation of substrate to product, laccase can be immobilized on functionalized titanium surface and its activity will be measured by UV-VIS spectrophotometer. According to the redox properties, laccase can also be immobilized on graphite as electrode by the APTES-modified film to investigate its electrochemical behaviour. There are two experimental approaches to study electron transfer reaction between laccase and electrode: Direct electron transfer (DET) and Mediated electron transfer (MET). The challenges for the laccase immobilized on electrode are: 1) to supply higher catalysis current from the redox reaction; 2) to be applied as long as they can.

1) DET — Direct evidence from observation of independent electrochemical activity;
2) MET — Indirect evidence from observing a catalytic response current in the presence of the substrate.

Since the thickness of APTES-modified film on titanium cannot be measured, here self assembled APTES with the $-NH_2$ groups is named 3-aminopropylsilane (APS) film. In order to clarify the above issues about the formation of the APS film and to improve further the biocompatibility on titanium and catalysis activity of the immobilized laccase, the investigation of the APS film on solid surfaces will focus on the following objectives:

1. To investigate the influences of selected factors on the formation of a well defined, uniform thin film on titanium; to identify the stability of the APS film in the dry condition and aqueous solutions at different pH values and its thermal stability;

2. To clarify the inducibility of calcium phosphate by the -NH_2 functional groups on titanium in simulated body fluid (SBF), so as to improve the biocompatibility of titanium surface;

3. To investigate the optimum conditions for immobilization of the laccase; to study the effects of pH and temperature on activity of laccases immobilized on the surface including titanium and graphite; to determine the Michaelis-Menten constant (K_m) of immobilized laccase for the study of enzyme kinetics.

4. To study the DET and MET electrochemical behaviour of immobilized laccase on electrodes.

To increase the likelihood of success in this research for preparation and application of the APS film on titanium, several avenues of investigation were explored. A synopsis of this thesis is described here. Following the brief Introduction, Chapter 2 gives a thorough literature survey on self-assembled systems mainly including the formation and applications of self-assembled films. For the formation of APS film, the structure, the preparation methods, the principle of reactions and its fabrication in a solvent on solid surfaces are reviewed in detail in this chapter. Meanwhile, applications of self-assembled films are also reviewed in this chapter, including calcium phosphate coating to improve biocompatibility on biomaterials and enzyme immobilization. Chapter 3 introduces the experimental process including the formation of the APS film, immobilization of laccase on substrates and sample characterization involved in this section.

The experimental results are separated into sub-sections in Chapter 4, each of which begins with a brief description of the specific objectives and method of the study, followed by the experimental investigation and analyses. Section 4.1 describes the effect of pre-treated titanium, APTES concentration, temperature and water content in toluene on the formation of the APS film. Moreover, stabilities of the APS film under different conditions and its thermal stability are studied in this section. Section 4.2 describes the investigation of inducibility of calcium phosphate by the -NH_2 functional groups on titanium in SBF with different ions concentration and different pH values. In

Section 4.3, a series of enzyme immobilization experiments are reported involving optimum conditions for laccase immobilized on titanium to clarify the effects of molar ratio of EDC/NHS, immersion time, pH and temperature on the activity of laccase immobilized, and calculate the Michaelis-Menten constant (K_m). To further identify catalytic activity of immobilized laccase, the electrochemical behaviour of laccase immobilized on graphite including DET and MET reactions, are mainly reported in Section 4.4.

Chapter 5 covers a general discussion of all the experimental findings, followed by concluding remarks of the investigation and future studies in Chapter 6 and Chapter 7, respectively. References cited in each chapter are listed together at the end of thesis. Lastly, the appendix cover some information related to this project.

CHAPTER 2

OVERVIEW OF SELF-ASSEMBLED FILMS

Self-assembly is dramatically drawn attention last twenty years. Research publications reveal a host of important self-assembled materials. **Figure 2. 1** displays the number of times that the term "self-assembly" appears in titles of articles catalogued by Science Citation Index and Social Science Citation Index over the past 30 years [Maasen 2006; Tollas 2000]. These data include not only those articles that have the term in the title, but also many additional publications with self-assembly concepts. Here, we will talk about self-assembled monolayers (SAMs), which have been applied in chemical synthesis, nanotechnology, polymer science and surface engineering. Although silane-based SAMs have been successfully formed on the oxidized silica, mica, glass and aluminium, limited work has reported on the titanium surfaces, especially with the hydrophilic functional groups (e.g. $–NH_2$). In order to study silane-based SAMs systematically, it is necessary to know the reaction conditions of formation of well-ordered and uniform structure in SAMs. Therefore, this review focuses on the preparation and applications of SAMs. A historical account of the overall self-assembled monolayers is briefly described as follows.

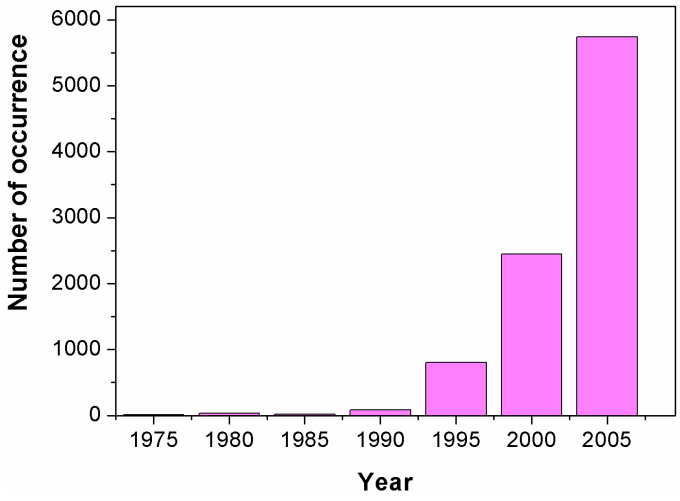

Figure 2. 1 "self-assembly" appears in titles of articles catalogued by Science Citation Index and social science citation index over the past 30 years [Maasen 2006; Tolles 2000].

2.1 Historical view of self-assembly films

The first case of self-assembly in nature was discovered by Benjamin Frankin in 1773 during a teaspoon of oil in a pond [Petty 1996]. Over a century later, Lord Rayleigh repeated Franklin's oil on water experiment in 1890 and calculated that the thickness of the film was 1.6 nm by knowing the volume of oil dropped and the area of coverage. Irving Langmuir was the first to perform systematic studies thin films and surface adsorption at General Electric. In 1917 Langmuir introduced the concept of a monolayer and the two-dimension physics that describe a surface, which was named 'Langmuir films'- floating monolayers [Petty 1996].

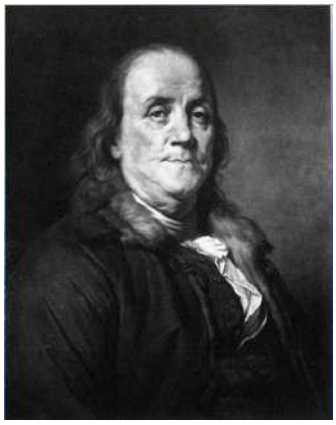

Figure 2. 2 Benjamin Frankin first discovered the phenomena of self-assembly when oil was in a pond.

Langmuir films are formed when amphiphilic molecules (hydrophilic heads and hydrophobic tails) interact with air at an air-water interface [Gainers 1996; Ulman 1991]. When molecular concentration is less than critical micellar concentration, the molecules arrange themselves as shown below in **Figure 2. 3**. The association behaviour of molecules in solution and their affinity for the air/water interfaces are determined by the physical and chemical properties of the head groups and tails [Petty 1996]. Since the tails are hydrophobic, their exposure to air is favoured over that to water. Since the heads are hydrophilic, the interaction of the heads with water is more favourable than air-water interaction. A classical example of an amphiphilic molecule is stearic acid ($C_{17}H_{35}CO_2H$) where the long hydrocarbon tail, ($C_{17}H_{35}$-), is hydrophobic, and the carboxylic acid head group (-COOH) is hydrophilic. The driving force behind the association is the reduction of the free energy of the system. Therefore, when molecules come in contact with water it accumulated at the air/water interface causing a decrease in the surface tension of water.

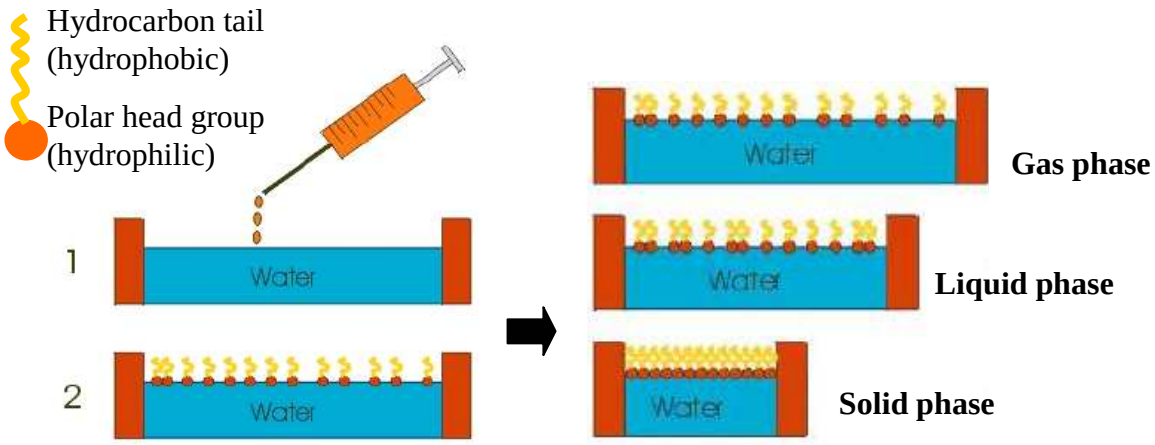

Figure 2. 3 Molecular arrangement of Langmuir film on air/water interface.

After 1926, Irving Langmuir and Katharine B. Blodgett discovered that a solid surface was inserted into an aqueous solution containing monolayers of organics then the film would deposit homogeneously over the surface. This process created Langmuir-Blodgett Films (LB films). A LB film is a set of monolayers, including a single layer or multilayer films deposited on a solid substrate. **Figure 2. 4** shows the commonest forms of LB films deposition. The substrate is hydrophilic and the first monolayer is transferred when the substrate is raised through the water. Therefore, the substrate may be placed in the sub-phase before the monolayer is spread. Subsequently, a monolayer is deposited on each traversal of the monolayers/air interface. As shown, multilayer of head-to-head and tail-to-tail in LB films are then formed later by hydrophilic or hydrophobic force.

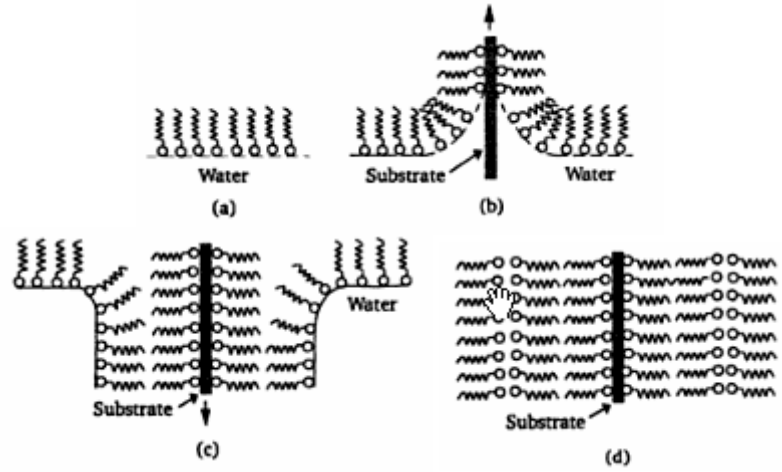

Figure 2. 4 Formation of assembled films on hydrophilic surface: (a) Langmuir film, (b) single layer of LB film on a solid substrate, (c) and (d) multilayer of LB films on the solid substrate [Petty 1996].

After Langmuir and Blodgett, Zisman and co-wokers prepared oleophobic molecules on platinum by Langmuir-Blodgett technique in 1946 [Zisman 1946]. Zisman reported that the molecules were close-packed and the outermost of the film was a plane surface with densely methyl groups. However, the reaction of heads with the surface was still poor due to physisorption. In 1983, Nuzzo and Allara prepared organic disulfides or alkanethiols on a gold surface by chemical bond of head group and surface [Nuzzo 1983], which is one of the successful self-assembled monolayers on the solid substrate.

Although SAMs are original from LB films, there is obvious difference between these two systems. The LB film is assembled vertically and usually composed of amphiphilic molecules with a hydrophilic head and a hydrophobic end. However, in SAMs, the molecules contain hydrophilic or hydrophobic end with a hydrophilic head. The key difference is that the LB films are on liquid surfaces and weakly bound to the solid surface by physisorption, while SAMs are on solid substrates and chemisorbed to form a strong bond [Petty 1996; Schreiber 2000]. Some of SAMs involve a three-dimensional polymer network (e.g., alkanesilanes). In other words, the molecules in the monolayers are connected to each other by strong chemical bonds, which explain its excellent material properties [Hoffmann 1997; Ulman 1991; Wang 2005]. Therefore, the SAMs created by the chemisorption are more stable than the physisorbed bonds of LB films.

2.2 Concept of self-assembled monolayers (SAMs): structures and components

Self-assembled monolayers are defined that organic molecules spontaneously assembly into ordered molecules to form nanometre-thick organic films on substrates. The strong specific interaction exists between a reactive group of molecules and the surface, containing chemical groups with a strong bond to the surface by chemisorption. The structure of self-assembled molecules can be divided into three parts, as shown in **Figure 2. 5**. The first part is the head group that provides the most exothermic process [Valiokas 2000], i.e., chemisorption on the substrate. The very strong molecular-surface interactions results in an apparent pinning of the head group

to specific site on the surface through a chemical bond. The second part is the backbone. After molecules are put in place on the surface, formation of an ordered and closely packed assembly can only start by interactions among the alkyl chains. Van der Waals interaction is the one of main forces in the case of simple alkyl chains. The third part is the end group, also called functional group, i.e., a methyl ($-CH_3$) group is the end group of a simple alkyl chain.

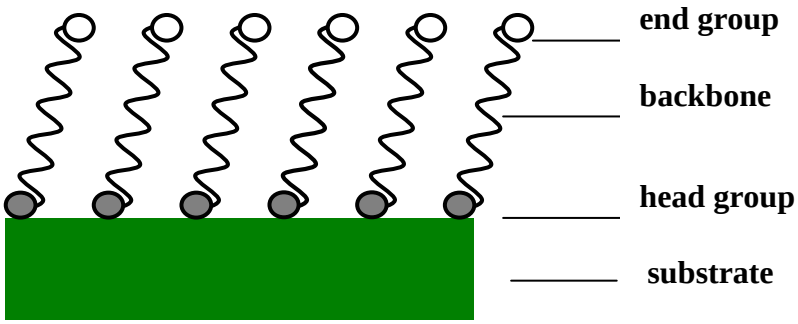

Figure 2. 5 Schematic structure of self-assembled monolayers.

2.2.1 Head groups

Typically, head groups are connected to a backbone with functional groups to vary the wetting and interfacial properties. According to difference in the head groups, there are different self-assembled molecules used so far, including alkanethiols (e.g. R-SH) and alkanesilanes (e.g. $R\text{-}SiCl_3$), which are the most thoroughly studied. Surface active alkanethiols compounds that form monolayers have increased in recent years. These compounds include alkylthiol, dialkyl disulfide, dialkyl sulphide, alkyl xanthate and dialkylthiocarbamate, structures of which are shown in **Figure 2. 6**. Alkanethiols compounds form very strong covalent bond with the surface by thiol to gold [Byloos 2001], silver, copper, platinum, iron [Love 2005; Schreiber 2000] and colloidal gold particles [Silin V 1997].

The alkanesilanes have hydrolyzed head groups on the silicon atom which permit covalent bond (Si-O) formation to a solid surface as well as cross-linking within the organosiloxane layer [Allara 1995; Zhao 1996]. According to hydrolyzed head groups, most used amphiphilic molecules among the alkanesilanes are alkylchlorosilanes and alkylalkoxysilanes. For example, octadecyltrichlorosilane (OTS) molecule has $-SiCl_3$

as the head group, while 3-aminopropyltriethoxysilane (APTES) molecule has $-Si(OCH_2CH_3)_3$ as the head group. No matter which alkanesilane is chosen for SAMs, the head group will be hydrolyzed by water to form silanol, which forms chemical bond with the surface.

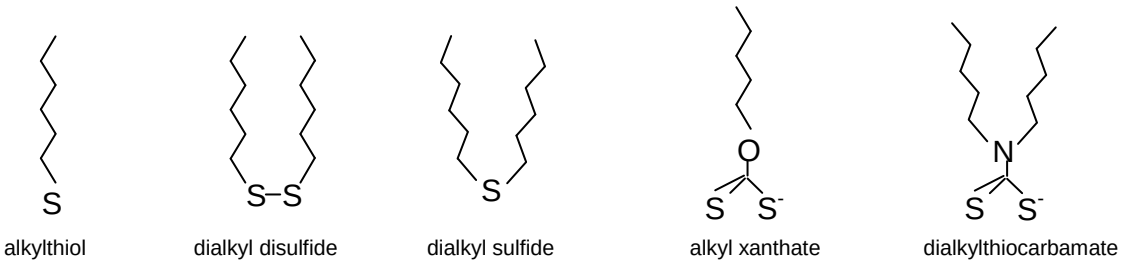

Figure 2. 6 Surface-active alkanethiol compounds that form SAMs on gold.

Selecting the type of head group in SAMs depends on the substrate. Alkanethiols and alkanedisulfides are the most commonly used for SAMs on noble metal substrates because of the strong affinity of sulphur for these metals, e.g. Au, Pt, Ag and Cu [Love 2005; Scherer 1997]. Due to the formation of silanol after hydrolysis of molecules, the alkanesilanes are generally used on non-metallic oxide surfaces, i.e. silica wafer, mica, glass and Al [Legrange 1993; Wang 2005; Xiao 1996]. Since titanium surface can supply hydroxyl groups, which can react with silanol to form covalent bond (-Ti-O-Si-), alkanesilanes will be chosen to form SAMs for titanium as substrate.

2.2.2 End groups

Functional groups are specific groups with molecules that are responsible for the characteristic chemical reactions. Alkanethiols have been reported to provide functional groups of the $-CH_3$ [Wirth 1997; Yamada 2000], $-CF_3$ [Love 2005], -OH [Tanahashi 1997], -Cl [Barrena 1999], -Br [Schweizer 2001], -COOH [Doudevski 2001; Patel 1997; Sato 2000], $-PO_4OH_2$ [Woodward 1996], $-CH=CH_2$ [Doudevski 2001], -CN [Hooper 2001], $-SO_3H$ [Poirier 1996], $-OCH_3$ [Brandriss 1993] $-NH_2$ [Hooper 2001], $-COOCH_3$ [Jung 1998] and $-CONH_2$ [Love 2005; White 2000] groups. However, it is quite difficult for alkanesilanes to find molecules with various terminal groups, because the alkanesilanes are sensitive to water, due to the hydrolysis of the head groups. The majority of alkanesilanes are molecules with hydrophobic groups,

i.e., -CH_3 [Balgar 2003; Peters 2002] or -$CH=CH_2$ [Liu 2002], while only a small part of them with hydrophilic groups, such as -NH_2 [Minier 2005; Zhu 2004], -SOOH [Majewski 2006], -SH [Toworfe 2006], -COOH [Toworfe 2006], -OH [Faucheux 2004], epoxide [Angst 1991]. Among these terminal groups mentioned above, some of terminal groups come from transforming of other terminal groups, i.e., hydroxyl (-OH) and carboxylic acid (-COOH) groups are normally generated from the -$CH=CH_2$ terminated SAMs [Wasserman 1989]. Among the silane-based SAMs, the -COOH, -OH, -SOOH and –SH terminated SAMs are negatively charged, while only the -NH_2 terminated SAMs is positively charged in acid media. The -NH_2 group as functional group which is similar to the -COOH group, is able to serve as a binding site for biomolecules such as enzymes, antibodies, and other proteins.

2.2.3 Backbone

The backbone is linking between head and functional groups in a molecule, and will stabilize the structure of self-assembled monolayers by interactions between molecules. According to the interactions, the backbone is classified into two groups: alkane chains and phenyl rings. The phenyl rings as backbone will introduce stronger interactions between molecules due to π-π bond, which might result in the difficulty to change the structure of SAMs on the surface. Moreover, in silane-based SAMs, functionalized molecules with the phenyl rings are not available so far. Thus, the alkane chains are only discussed further here.

In SAMs system, the monolayer packs tightly due to van der Waals or hydrogen bonding between backbones when the head group-surface interaction is nominally fixed, thereby reducing its own free energy [Love 2005]. In principle the molecular backbone does not need to be fully extended, and different backbones have different degrees of freedom to describe their conformational state [Schreiber 2000; Tao 1994]. For non-corrugated, i.e., smooth chains, one would expect the impact of the chain length to be small. This should result in at most a slight and continuous variation of the tilt structure with the chain length. On the other hand, for the more realistic picture of corrugated chains (due to their internal structure), certain relative positions of the chains with respect to each other would be preferred.

The alkane chains could determine the arrangement of complex molecules in polymer assemblies. The intimate correlation of the chains with structure has led to the use of infrared spectra as a diagnostic tool of the chain conformation and thus of the structure of the molecular assembly [Finklea 1986; Snyder 1982]. The C-H stretching region is usually the strongest feature in the infrared spectra. Snyder and Strauss found that symmetric mode at ~ 2856 cm^{-1} and antisymmetric mode at ~ 2928 cm^{-1} for the C-H stretching indicated that disordered polymethylene chain conformation [Snyder 1982]. Finklea and coworkers then reported that the peak positions for methylene ($-CH_2-$) symmetric and antisymmetric stretching modes of alkyl chains are typically to be in the range of 2846 – 2850 and 2915 – 2918 cm^{-1} for all-trans extended chains [Finklea 1986]. Therefore, the IR positions for the C-H stretching region can estimate the ordering of structure of SAMs.

In a broader sense, the chain-length dependence of the structure investigates the competition between the different interactions. For very long chains the interaction between alkane chains will be more important than the head group-substrate interaction, which results in the formation of the ordered structure of SAMs. For shorter chains (typically for $n< 8$) it is not easy to form well-defined monolayers because of the less interaction of alkane chains compared with longer alkane chains [Peterlinz 1996]. On the other hand, although the longer molecules will form more dense monolayers, chain length affects SAM thickness which will impact on the applications of SAMs, such as electrochemical field. For example, 3-mercaptopropionic acid (3-MPA) on gold with 2-carbon chain shows much better electric conduction than 11-mercaptoundecanoic acid (11-MUA) with 11-carbon chain on gold in the electrolyte with $Fe(CN)_6^{3-}$ [Mendes 2008].

2.3 Processing of self-assembled monolayers

2.3.1 Preparation methods of SAMs

The early literature on SAMs focused largely on the assemblies formed by the adsorption of organosulfur compounds from solution or the vapour phase onto planar metal substrates of gold and silver [Byloos 2001; Jung 1998; Love 2005; Vericat 2001].

Assembly from solution on laboratory is convenient and sufficient for most applications of SAMs, especially for those requiring contact with other liquid phases in subsequent experiments (e.g. supports for enzyme immobilization). Assembly from the gas phase is necessary when the SAMs are prepared under UHV conditions for analysis by certain spectroscopy [Schreiber 2000]. The following sections will discuss into details about these two methods.

The principle of gas phase deposition is very simple. The substrate is located in a generic ultrahigh vacuum (UHV) chamber, which allows for cleaning surface by, e.g. ion sputtering and annealing as done for metal single crystals. In this chamber, only one additional port is needed for attaching a valve through which the molecules can be dosed with a controllable flux from a little container (**Figure 2. 7a**). This method has been employed successfully [Eberhardt 1998; Poirier 1996; Poirier 1999]. Besides work in UHV it has also been shown that alkanethiols can be deposited by a nitrogen stream [Thomas 1991]. It should be noted for this method that the exact calibration of the vapour pressure is needed. The gas phase deposition in UHV has proven useful for studying the early-stage dynamics of assembly [Schreiber 2000]. However, this method cannot supply adequate vapour pressures for many precursors of SAMs and prepare low-coverage phase [Love 2005].

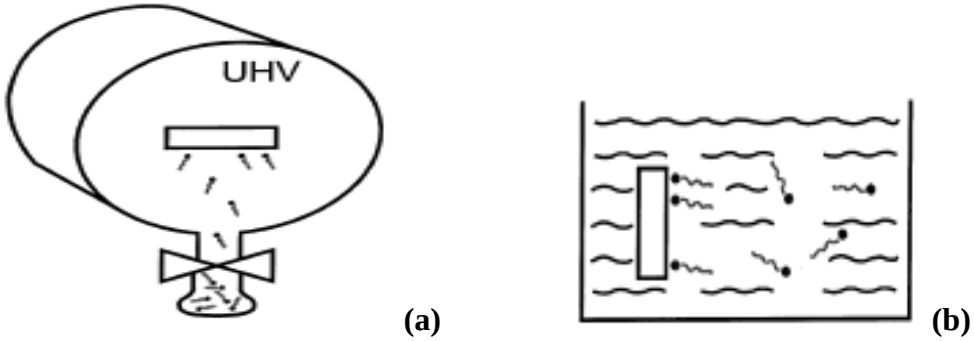

Figure 2. 7 SAMs formed from UHV chamber (a) and solvent (b) [Schreiber 2000].

In contrast to gas phase deposition, for the growth of SAMs in a solvent, a substrate is immersed into a solution of molecules for a certain period of time (**Figure 2. 7b**). After immersion, the substrate is rinsed with solvents (such as ethanol, acetone and distilled water) to wash away physisorbed molecules on the surface. Finally, it is dried in a steam of inert gas and the monolayer will assemble [Petty 1996; Schreiber 2000]. For

example, thiol-based SAMs produced by adsorption from solution are made by immersing a clean substrate into a dilute solution of alkanethiol in ethanol for 12 to 72 hours at room temperature and dried with nitrogen [Jung 1998; Love 2005; Vericat 2001]. This procedure is widely used and can be designed to optimize the reproducibility of the SAMs. Love and coworkers reported that dense coverage of molecules was obtained quickly from micromolar to millimolar solutions, but required a slow assembly process due to maximum the density of molecules and minimum the defects in the SAMs [Love 2005]. However, there are a number of experimental factors that can affect the structure of the SAMs and the rate of formation: solvent, temperature, concentration of molecules, immersion time, cleanliness of the substrate, and so on. All of factors mentioned above will be discussed further in Chapter 2.2.3.

The equilibrium structures should be equivalent to those from solution and gas phase deposition, but the growth exhibits some differences [Ulman 1991]. According to **Table 2. 1**, in solution deposition, the lying-down phase is more difficult to observe, although it was eventually found. This may be due to the facts that the standing-up phase can nucleate more easily and that the presence of the solvent molecules makes it more difficult to form the lying-down phase [Shreiber 2000]. Moreover, the method with a UHV chamber generally is more expensive than that with growth from solution, although it is in the clean environment. Therefore, the method of solution phase deposition is chosen in this project.

Table 2. 1 Simplified comparison of solution and gas phase deposition of SAMs, based on results from alkanethiols on Au [Schreiber 2004].

	Solution deposition	**Gas phase deposition in UHV**
Apparatus	Simple and inexpensive	Sophisticated and expensive
Environment	Contamination difficult to exclude	Clean
For lying-down phase	Formation might be hampered	Formation easier
For standing-up phase	Formation might be facilitated	Energy barrier can be higher for transition from lying-down

2.3.2 Principle of reactions of SAMs in solvent

Growth from solution is the traditional route for the preparation of SAMs. Two of the most widely studied SAMs systems have received the most attention. The first one is conveniently prepared by exposure of gold surfaces to a thiol or disulfide solution. It relies on the strength of sulphur-gold interactions, which is a covalent bond, but slightly polar [Jung 1998; Nuzzo 1983]. The second one is based on the reaction of alkanesilanes on silicon wafer [Schreiber 2000; Ulman 1990; Zhao 1996]. The following sections are devoted to the main principles for the two SAMs systems.

2.3.2.1 Alkanethiols on Au

From the first discovery of thiol-based SAMs on gold from the dilute solution produced by Nuzzo and Allara [Nuzzo 1983], we will see the functional organic molecules in regularly-oriented array on gold surface. So far, many other organosulfur compounds have been reported to form SAMs on gold, silver, copper, platinum and iron surfaces [Love 2005; Schreiber 2000]. However, SAMs of alkanethiols on Au are extensively studied and understood very well, such as the adsorption of alkanethiols and disulphides on gold, seen **Figure 2. 8**.

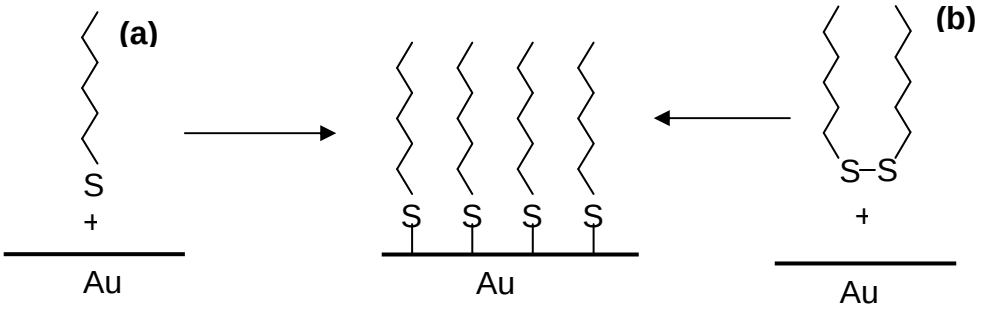

Figure 2. 8 Schematic illustration showing the self assembly of (a) *n*-alkanethiols and (b) disulphides on gold.

Its kinetics studies involve a two-step process [Bain 1989; Barrena 1999]. The first step, which proceeds via the physisorption of thiol-based molecules, takes a period of minutes. In the second step, which takes hours, significant rearrangement and reorganisation of the alkane chains occurs and the sulphur atoms bind to the gold surface by chemisorption (covalent bond) [Schreiber 2000]. The formation of SAMs of

alkanethiols on gold and the structure of the resulting monolayer are controlled by a complex interplay between competing head group-substrate and chain–chain interactions.

2.3.2.2 Alkanesilanes on silicon

Alkanesilanes are very well-known as adhesion promoters of polymers to silica [Bourkherroub 1999; Linford 1993; Wang 2003], glass[Christenson 2001; Mrksich 1998], quartz [Brandriss 1993; Mathauer 1993], mica [Woodward 1996; Xiao 1996] and various metal oxides(e.g. Al_2O_3 [Lewington 2002; Oberg 2001] and ZnSe [Buriak 2002]). They were successfully used not only for the attachment of synthetic polymers but also for immobilization of various peptides (e.g. enzymes and proteins) with at least partial retention of their biological activity. The reaction of alkanesilane has been reported by several groups [Balgar 2003; Wang 2003; Wang 2005]. Alkanesilanes with different head groups (e.g. Cl and OR) react with the hydroxylated surface (M-OH) to yield M-O-Si chemical bond. For example, the scheme of silanization reaction of alkyltrichlorosilane on silicon includes three steps as seen in **Figure 2. 9**. At the first step, alkanesilanes are hydrolyzed by water to form silanols (-Si-OH) and HCl (**Figure 2.9a**). Secondly, silanols link hydroxyl groups on the substrate surface by hydrogen bond and dehydrate to form the chemical bond of M-O-Si (**Figure 2.9b**). Finally, a condensation reaction is assumed to occur in which hydroxyl groups from silanols react with each other to form Si-O-Si cross-link within the monolayers (**Figure 2.9c**).

This initial hydrolysis step can occur either in solution or at the substrate surface depending on the amount of water present in the system. If water is present in the solvent, condensation reaction will happen first and then dehydration will do, which might affect the ordering of the structure of SAMs on the surface. Due to the formation of cross-link between molecules, the silane-based SAMs are more stable compared with thiol-based SAMs. The stability and optically transparent substrates make silane-based SAMs attractive for a number of technological applications. However, the quality of the monolayers is highly dependent on surface oxidation and hydration and the atmospheric conditions under which silanization is carried out [Plueddemann 1982]. Consequently, reproducibility of high quality silane-based monolayers between

laboratories has been poor, although continual improvement in understanding is changing this situation.

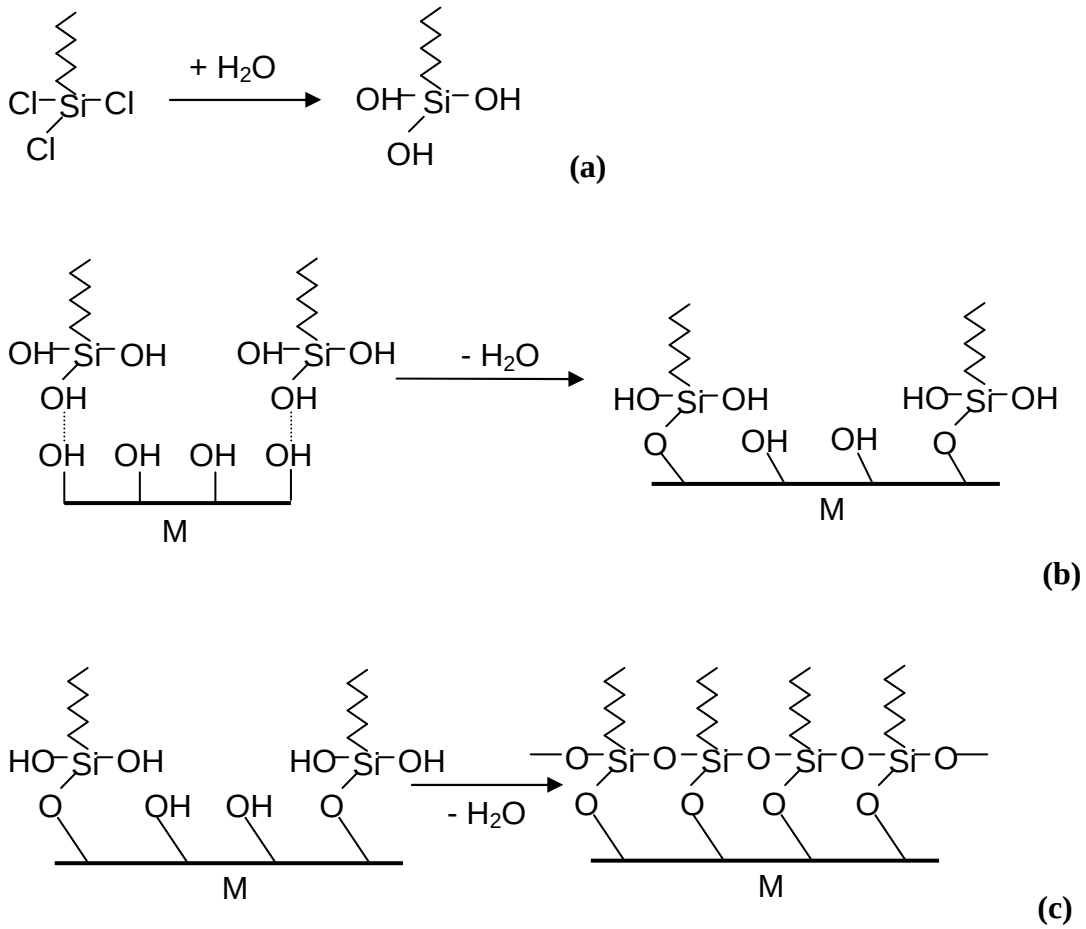

Figure 2. 9 Schematic diagram illustrating reactions leading to the deposition of SAMs on M substrate: (a) hydrolysis reaction of alkyltrichlorosilane with water; (b) dehydration reaction of silanols on the surface; (c) condensation reaction with monolayers.

2.3.2.3 3-Aminopropyltriethoxysilane (APTES)

Due to the water sensitivity of silane-based molecules, there is a limit to the variety of terminal functional groups in alkylsilanes. So far, molecules with the -CH=CH_2, -CH_3 and -NH_2 functional groups are supplied directly from alkylsilanes, while molecules with the -COOH and -OH groups need to be diverted from the –CH=CH_2 group [Toworfe 2006]. Currently aminated silanes (with the -NH_2 group) are employed in a wide variety of both research and industrial applications. For example, aminated silane as a coupling agent is commonly used for the surface modification to increase adhesion [Plueddemann 1982]. It is also utilized to promote adhesion of polymer films on glass

or to produce temperature and photoresponsive films on silica [Howarter 2006]. Moreover, aminated film is used to attract protein to promote cell adhesion in biotechnology applications [Toworfe 2006; White 2000]. Since the amine group can react with carboxyl group, the aminated film is able to capture CO_2 to reduce the influence of global warming of the planet [Rao 2002]. Molecules with longer carbon chain which present a higher degree of coverage are not suitable for substrates intended for electrochemical applications because they passivate the transduction interface, making it difficult to transfer electrons and reducing electrode sensitivity. For example, in relation to enzyme immobilization on gold electrode, it has been referred that monolayers that possess the $-NH_2$ terminal groups with short chain length provide the best results [Mendes 2008] among various molecules with different end groups and carbon chains.

Here, APTES was selected as the molecule in the self-assembly system, because it provides Si-OH as head group which form the covalent bond (-Si-O-Ti-) on the titanium surface and the $-NH_2$ functional group for reaction with peptides, proteins and enzymes by the peptide bond (-NH-CO-). Moreover, SAMs with the $-NH_2$ groups might induce calcium phosphate in a simulated body fluid to improve the bioactivity of implant [Toworfe 2006; Zhu 2004]. The structure of this molecule is shown in **Figure 2. 10**, including three ethoxy groups ($-OC_2H_5$) as head groups, primary amine group as functional group and a 3-carbon chain. Triethoxy groups in APTES are rapidly hydrolyzed to produce ethanol and trisilanols. Since the Si-C bond is not hydrolyzed further, the aminopropyl group is not be cleaved from APTES molecule. This molecule usually exists liquid phase as the melting point is -70°C (**Table 2. 2**). Due to the sensitivity of carbon dioxide and water, a bottle of APTES is normally stored in a glove box under argon.

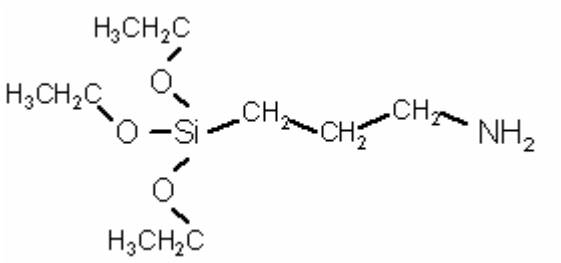

Figure 2. 10 Structure of 3-aminopropyltriethoxysilane.

Table 2. 2 Physico-chemical properties of APTES.

Property	**Value**	**Comment**
Melting point	-70°C	
Boiling point	223°C	
Relative density	0.95 at 25°C	
Vapour pressure	0.02 hPa at 20°C	
Water solubility	7.6 x 10^5 mg/l at 25°C	Estimated. This value may not be applicable because the material is hydrolytically unstable.

Although APTES is one of the most popular coupling agents, the controversy is brought over its molecular structure. The problem is the variety of process conditions used in sample preparation, especially on metallic surfaces. Moreover, the head group (-Si-OH) after hydrolysis and the functional group (-NH_2) are both hydrophilic, so it is possible for the amine group to form hydrogen bonds with hydroxyl groups from silanols and/or substrate surface, which leads to the disordered structure of the –NH_2 functionalized film. Many studies attempted to elucidate the molecular structure of the polysiloxane interphase with the amine groups [Arya 2007; Howarter 2006; White 2000], because silane-based molecules with the –NH_2 group reaction with solid surfaces lacks reproducibility in film quality, which arises from an acute sensitivity to reaction conditions. People reported that the structure of the APTES-modified film was highly dependent on deposition conditions and underlying substrate [Hooper 2001; Howarter 2006; Plueddemann 1982]. Factors, such as surface preparation, reaction temperature, silane concentration, incubation time, solvent and its water content, will all affect the final structure of the adsorbed aminated layer on the solid surface. Therefore, it is important to optimize the reaction conditions of the preparation of the APTES-modified film on the titanium surface from liquid phase.

2.3.3 Formation of SAMs on substrates

The early literature on SAMs focused largely on the assemblies formed by the adsorption or organosulfur compounds from solution onto planar metal substrates of

gold and silver [Bain 1989; Gun 1984; Nuzzo 1983]. Although the thiol-based and silane-based SAMs are slightly different on the head groups, the kinetics is quite similar for the formation of these two kinds of SAMs on solid substrate. According to the study of alkanethiols on Au [Love 2005; Schreiber 2000], dense coverage of molecules adsorbed on the surface is obtained quickly from solution, but a slow reorganization process requires hours to minimize the defects in the SAMs. To obtain densely packed and well-ordered self-assembled monolayers, substrate, molecular concentration, temperature, solvent, silanization time and residual water content in solvent during reaction of molecules on the substrate, should be considered. The following sections are devoted to further information of the effect of above factors on the fabrication of SAMs on the solid substrate.

2.3.3.1 Pre-treatment of substrates

2.3.3.1.1 Substrates for SAMs

Types of substrates range from planar surfaces (e.g., glass or silicon, metal foils, single crystals) to highly curved nanostructures (colloids, nanocrystals, nanorods) [Love 2005]. To select the type of substrate is dependent on the application for which the SAM is used. For example, gold is a standard substrate for alkanethiols due to the covalent bond of gold and thiol. For alkanethiols, the most common planar substrates are gold, silver, copper, palladium, platinum, nickel and their alloys [Schreiber 2000]. Due to the formation of silanols in molecules after the hydrolysis, it is necessary for substrates to supply hydroxyl groups on the surface. Therefore, mica, glass, silicon and alumina are widely used as the substrates for alkanesilanes.

In this project, titanium is used as substrate to study the formation of self-assembled monolayers. As known, a native oxide film grows spontaneously on the titanium surface when it exposes to air. The characteristics of the oxide film grown at room temperature on pure titanium are schematically shown in **Figure 2. 11** and summarized as follows:

1) The amorphous or nanocrystalline oxide film is typically 3-7 nm thick and mainly composed of the stable oxide TiO_2.

2) Hydroxide and chemisorbed water bond with Ti cations lead to weakly bound physisorbed water on the surface. In addition, some organic species like hydrocarbons and metal-organic species, such as alkoxides or carboxylates of titanium also exist on the outmost surface layer. The organic concentrations depend on not only the surface conditions, such as cleanliness, but also the exposure time to air during storage [Brunette 2001].

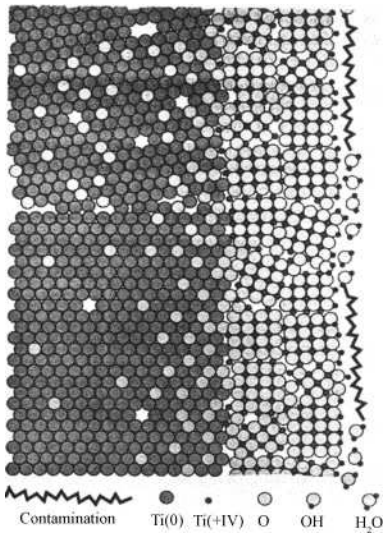

Figure 2. 11 Schematic view of the oxide film on pure titanium [Liu 2004].

A nonstoichiometric, amorphous, insoluble titanium oxide layer (~3-7 nm thick) forms spontaneously on the Ti upon contact with air. The oxide layer has a crucial role in the adsorption of cations and anions on the Ti surface. On the titanium surface, the TiO_2 molecule becomes a dipole with positive Ti^+ and negative O^- sites. In an aqueous electrolyte, OH^- bonds to the Ti^+ cation of TiO_2 and forms Ti-OH groups [Diebold 2003; Liu 2004]. Since hydroxides or hydro-complexes of multivalent (e.g. Ti^{IV}) cations are generally exhibiting both acid and base properties, depending on the pH of the electrolyte, acidic or basic Ti-OH groups could form on the surface as outlined below. According to **Equation 2. 1** & **2.2**, the titanium surface charge depends on the pH value of the solution. The isoelectric point (IEP) of titanium oxide is 5-6 [Diebold 2003; Liu 2004]. Therefore, at lower pH (< 5), the formation of $[Ti - OH_2]^+$ from a basic Ti-OH group causes a positive surface charge, whereas at higher pH (>6) acidic Ti-OH gives off proton and becomes $[Ti - O]^-$ causing a negative surface charge. Between pH 5-6, both acidic and basic hydroxyl coexist on the Ti surface.

$$Ti\text{-}OH + H_2O \longleftrightarrow [Ti-O]^- + H_3O^+ \quad \text{(basic reaction)}$$

Equation 2. 1

$$Ti\text{-}OH + H_2O \longleftrightarrow [Ti-OH_2]^+ + OH^- \quad \text{(acidic reaction)}$$

Equation 2. 2

Besides the requirement of chemical properties, the crystalline state of the substrate needs to be considered, which will influence the morphology of the substrate. It is easier to form disordered SAMs on a rough surface. So far, single crystals are very frequently used in surface science (e.g. silicon and gold) because they constitute well-defined substrates after pre-treatment. Therefore, no matter the substrate is planar or curved, the surface has to be as flat as possible. Since displacement with molecules first requires desorption of the contaminants and impurities, maintenance of the contaminants will affect the kinectics of SAMs formation. Therefore, the cleanliness of the substrate has a strong impact on the growth behaviour of SAMs [Jung 1998].

2.3.3.1.2 Treatment methods of substrates for SAMs

As mentioned above, the hydroxyl groups are required for the self-assembly of alkanesilanes on the surface. In other words, the hydration state of the oxide surface was found to greatly influence the packing of the monolayers [Hoffmann 1997]. Allara and coworkers showed that adequate substrate hydration was critical for the deposition of densely-packed, highly organized alkylsilane monolayers of similar structure on solid substrates [Allara 1995]. Therefore, many of surface studies focused on the formation of hydroxyl groups on the surface, especially for titanium.

Table 2. 3 gives an overview of different surface treatments used for titanium recently and the main effects obtained with each type of methods. The effects of the listed methods can be divided into three categories: a) cleaning and removal of native surface layers, b) modification of surface structure and topography, c) modification of composition and structure of the oxide layer or controlled formation of a new surface layer. It is necessary to descale and remove dirt firstly for the titanium surface.

Compared with other methods, hydrogen peroxide-treatment not only gives a clean surface, but also gives OH groups by hydroxylation. Pan *et al.* suggested that the oxide had a two-layer structure with a thin (< 5 nm) and dense inner oxide and an outer porous layer. Hydrogen peroxide treated surfaces often show extremely low carbon signals in surface analyses, typically 5% or less [Pan 1998]. However, this treatment needs longer treatment time, which will lead to roughening the surface on the sub-micron scale and a significant growth in oxide thickness [Legrande 1993; Lewington 2002].

Table 2. 3 Overview of commonly used surface treatment methods for titanium, and the main effects they have on different surface properties [Brunette].

Methods	Main effect / Purpose of treatments	References
Grinding, polishing	Descaling, removal of native layer, Smooth surface finish	
Solvent cleaning	Removal of contamination	
Etching in HF/HNO_3 or HCl/H_2SO_4	Descaling, removal of native layer, Surface roughening, cleaning, Removal of stresses	[Ungersbock 1994; Wong 1995]
Alkaline etching	Hydroxylation, Improve apatite formation, Surface roughening	[Kim 1997; Wen 1998]
Passivation in HNO_3 or by heat treatments	Oxidation, minimize ion release	[Kilpadi 1998; Oji 1999]
H_2O_2 treatment	Oxidation, hydroxylation, Roughening/etching, Cleaning/sterilization, Removal of native layer	[Pan 1998; Suzuki 2000; Tengvall 1989]
Electropolishing	Removal of stresses, Smooth surfaces	[Larsson 1994; Petitjean 1990; Walivaara 1994]

The total amount of oxygen on the titanium surface is very important, which indicates the quantity of OH groups. The oxygen functionalities depend on the oxidation conditions and the overall amount of oxygen increase with increasing power of the oxidation agents. **Figure 2. 12** shows the amount of oxygen on the surface of

multiwalled carbon nanotubes (MWCNTs) as detected by XPS measurements for different treatments [Datsyuk 2008]. They reported that the increase of surface oxygen per type of oxidation treatment follows the trend: hydrochloric acid < ammounium hydroxide/hydrogen peroxide < piranha < refluxed nitric acid. Many researchers reported the piranha solution has been used in pre-treatment of substrates [Ulman 1990; Depalma 1989; Mathauer 1993; Nyquist 2000], which involves H_2SO_4 and H_2O_2. For example, silicon, a very popular substrate for SAMs, has the clean and smooth surface with oxide layer after oxidation in the piranha solution [Allara 1995; Angst 1991; Bourkherroub 1999; Depalma 1989; Mathauer 1993; Nyquist 2000; Ulman 1990]. This oxide layer on silicon is hydrophilic and will form plenty of OH groups in the aqueous solution. Since nitric acid cannot hydrolyte the titanium surface according to **Table 2. 3**, hence the piranha method is chosen as oxidant for pre-treatment of titanium.

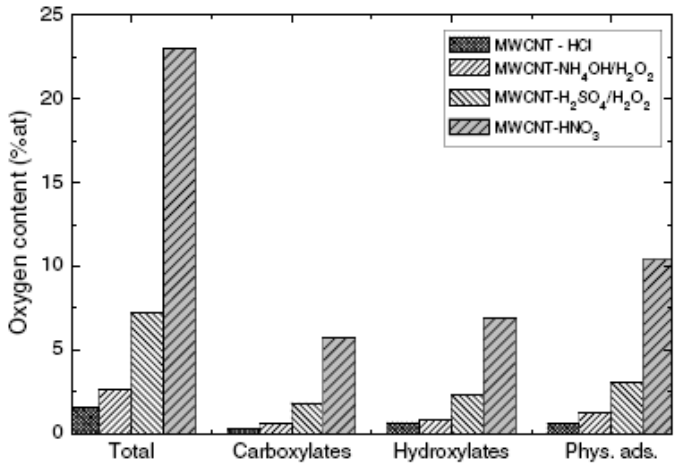

Figure 2. 12 Oxygen content (at%) on the MWCNT walls after treatment with different oxidation agents [Datsyuk 2008].

The *Piranha* solution is a mixture of concentrated sulphuric acid and hydrogen peroxide, which is frequently employed for cleaning procedure. As the mixture is a strong oxidizer, it can remove most organic matter, and also oxidize/hydroxylate most metal surfaces, making them extremely hydrophilic. Usually, the piranha solution is prepared by adding the peroxide to the acid. Although the solution is a strong oxidizer with strong acid, there is almost no effect on surface roughness of single crystal substrates. However, it is quite difficult to control surface roughness on polycrystalline surface (e.g. commercial pure titanium) due to different oxidized states. Therefore, the oxidizing ability of the piranha solution, including the oxidizing time and temperature,

and the mixture ratio, will affect quantity of hydroxyl groups, surface roughness, and further the quality of SAMs.

So far, different mixture ratios of H_2SO_4:H_2O_2 are used to form a *Piranha* solution. Silberzan used a solution of 1:1 at 80°C for 30 minutes to oxidize silicon surface [Silberzan 1991]; Love reported a solution of 3:1 for gold at 50°C for 1 hour [Love 2005]; a solution of 1:1 at room temperature for 1 hour was used by Majewski for titanium [Majewski 2006]; other protocols may use a 7:3 or even 4:1 mixture. For polycrystalline titanium as substrate, it is an issue to optimize the oxidizing condition of *Piranha* solution in order to obtain the clean and flat surface with hydroxyl groups.

2.3.3.2 Effect of silanization time

Length of immersion time (also called silanization time in alkanesilane-based system) normally affects the final structure of SAMs. Generally, SAMs formation occurs in two steps, an initial fast step of adsorption and a second slower step of monolayers organization [Schreiber 2000]. The former step happen within minutes according to various molecules, but the latter step may take minutes to hours, even to days to eliminate defects in the final SAMs structure. For example, Britt and Hlady investigated that the mica surface was almost completely covered with octadecyltrichlorosilane (OTS) after 300 seconds expect many small 'pinholes' [Britt 1996]. **Figure 2. 13** shows the silanization process of OTS on the hydrated mica within 300 seconds at 25°C. The bright features in these images are condensed OTS islands or clusters and the darker features in the background is the mica surface.

Macanovic and coworkers studied that the silanization time of 3-glycidoxypropyltrimethoxysilane (GPTS) on silicon chips by varying the times (30, 60, 90, 120, 360 and 480 minutes) by fluorescein-labelled bovine serum albumin protein (BSA) [Macanovic 1993]. The results show that optimal silanization time is 4 hours for GPTS on silicon chips, as shown in **Figure 2.14**. Although molecules can be covered on substrates within a few hours, there are still defects in the self-assembled films. Barrena *et al.* investigated the long-term effects on the island growth of hexadecanethiol by atomic force microscopy (AFM) [Barrena 1999]. At the beginning

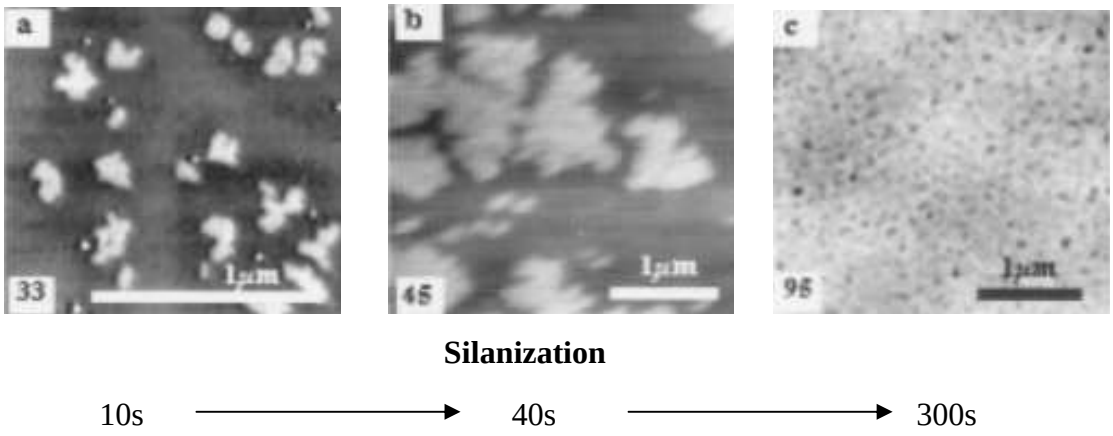

Figure 2. 13 AFM images of the effect of silanization time from 10 to 300 seconds on growth of OTS on the hydrated mica at 25°C, and water contact angles shown at the bottom left corner of each image [Britt 1996].

within a couple of hours, the small islands are formed on the substrate due to the diffusion of molecules in the solvent. From several hours to days the islands exhibit a combination process, leading to the formation of fewer and larger islands and further resulting in a densification of the layer and the removal of defects.

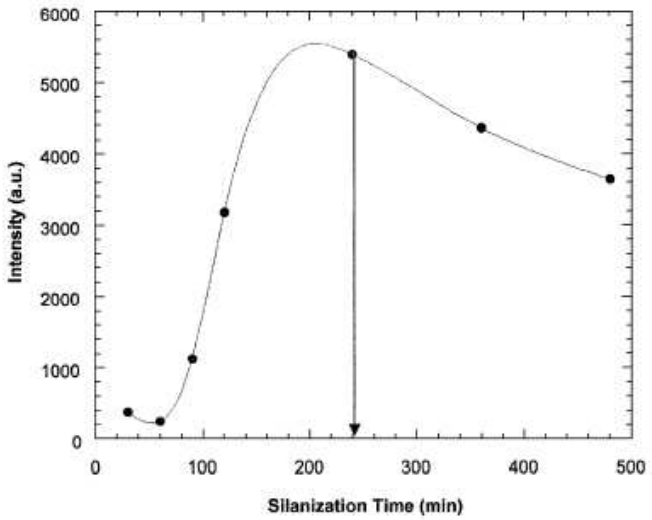

Figure 2. 14 Fluorescence intensity of BSA as function of the silanization time of GPTS on silicon [Macanovic 1993].

So far, these different time scales are reported for the formation of SAMs. DeBono *et al.* demonstrated that hexane, dodecane, and hexadecane thiol adsorptions on gold surface were best fit by a two-step process (around 10 hours) using surface plasma resonance spectroscopy and surface plasmon microscopy [DeBono 1996]. However, Peterlinz and Georgiadis reported that there were at lest three distinct kinetics steps

(around 18 hours) in the film formation in ethanol [Peterlinz 1996]: the first step is the most rapid; the second step is depend on alkanethiol chain length, concentration, and practical film thickness; the third is slowest. Himmelhaus [Himmelhaus 2000] and Schreiber [Schreiber 2000] studied that the kinetics of film formation in the solution within 16 hours, and found that three different steps with significantly different time scales were identified. The first step in the formation process is the fastest step, related to the chemisorption of the head group (e.g., the formation of the Au-S bond). The second step (3-4 times slower than the first) comprises the straightening of the hydrocarbon chains. The third step (again 35-70 times slower than the second step) is related to the reorientation of the terminal groups.

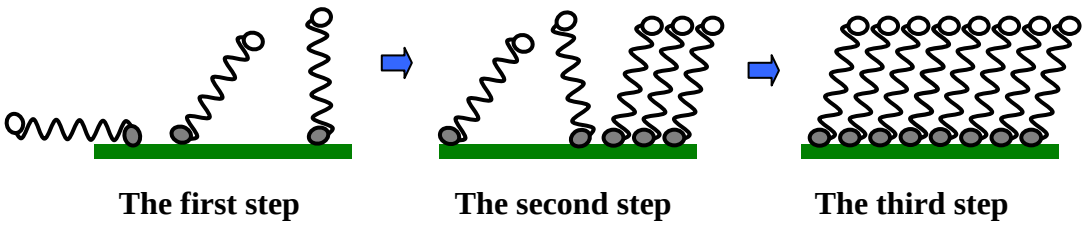

Figure 2. 15 Schematic illustration showing the formation of a SAM.

According to the investigation of adsorption of docosanethiol ($CH_3(CH_2)_{21}SH$) onto polycrystalline gold by Himmelhaus, 1000 minutes (about 16 hours) was needed for the total three steps of SAMs formation [Himmelhaus 2000]. Moreover, the common protocol for preparing SAMs on gold, silver, palladium and other materials is immersion of clean substrate into a solution of thiols for 12-18 hours [Love 2005]. These results imply that the coverage of the surface increases with extended immersion time and suggest two consequences: (1) the number of pinhole defects in the SAMs decreases and (2) the conformational defects in the alkane chains decrease. Therefore, according to the above conclusions, in this project the titanium surface will be silanized for 16 hours in the solvent with APTES.

2.3.3.3 Effect of molecular concentration in solution

Molecular concentration in solution during preparation of SAMs can influence the thickness and structure of the film. Many researches proved that low concentrations

require longer immersion times and often create highly crystalline domains [Finklea 1986; Rozlosinik 2003; Schreiber 2000; Wasserman 1989]. For SAMs formed from alkanethiols on gold, the typical surface density of molecules is ~ 4.5 × 10^{14} molecules/cm^2 [Schreiber 2000]. Thus, the minimum concentration for forming a dense SAM is ~ 1 μM, or ~ 6 × 10^{14} molecules/cm^2, but substrates need immerse for a week in solutions. For the immersion time of 16 hours, thiol-based SAMs should be prepared in the solution with concentrations from 1 – 10 mM [Love 2005].

Rozlosnik *et al.* reported under a wide range of concentrations from 25 μM to 2.5 mM and normal laboratory air humidity (RH 45-85%) OTS dissolved in heptane caused the formation of a full-coverage self-assembled monolayer on hydrophilic silicon oxide [Rozlosinik 2003]. Doudevski *et al.* investigated self-assembled monolayers of octadecylphosphonic acid (OPA, $CH_3(CH_2)_{17}PO(OH)_2$) on mica by different concentrations from 0.01, 0.08, 0.17 to 0.45 mM [Doudevski 2001]. They found a solution concentration of 0.45 mM leads to the formation of larger island number density and full coverage on the surface, shown in **Figure 2. 16**.

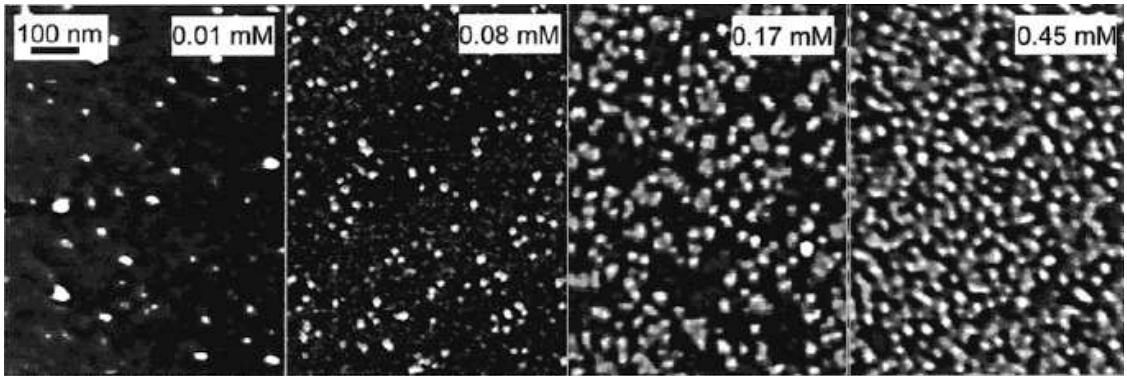

Figure 2. 16 AFM images (2μm× 2μm) of the surfaces topology of an OPA monolayer prepared with different concentrations [Doudevski 2001].

Karpovich and Blanchard reported that the growth rate of octadecanethiol (CH_3-$(CH_2)_{17}$-SH) increased with molecular concentrations [Karpovich 1994]. Peterlinze and Georgiadis changed the concentration of $CH_3(CH_2)_{15}SH$ in ethanol from 1.0 μM to1.0 mM for film growth on a single gold film [Peterlinz 1996]. Kinetics results (**Figure 2. 17A**) clearly demonstrate a decrease in the overall film growth rate as concentration decreases. Film thickness was monitored for the 1.0 mM, 10 μM, and 1.0 μM solutions

up to 20 h (**Figure 2. 17B**). A sudden increase in film growth rate happened at 8-9 Å for the 10 µM film (**Figure 2. 17B**, triangle labelled line). This increased rate matches the second step growth rate for the 1.0 mM solution, which also starts at 10-11 Å. This kinetic step does not occur for the lowest concentration studied (1.0 µM). Clearly, for these solutions, the self-assembly rate for the second kinetic step depends on molecular concentration. However, $CH_3(CH_2)_{15}SH$ molecules at lowest concentration assembled thinner layer on the surface (**Figure 2.17B**).

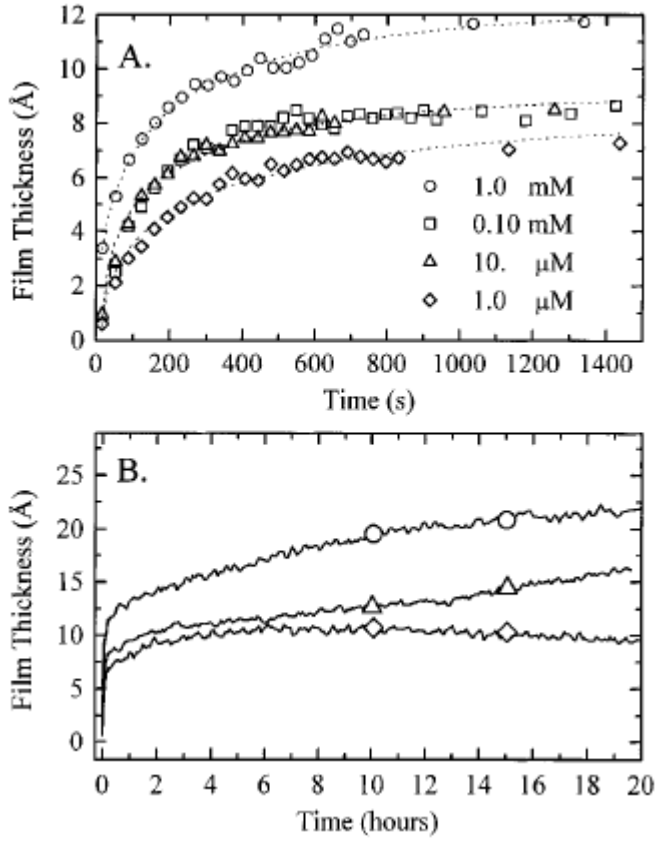

Figure 2. 17 Concentration dependence of formation kinetics for hexadecanethiolate (C_{16}) film from ethanol solutions. Shown are the thicknesses calculated from *in situ* SPR spectra measured during film formation from four different solutions, 1.0 mM, 0.10 mM, 10 *µ*M, and 1.0 *µ*M $CH_3(CH_2)_{15}SH$ in ethanol [Peterlinz 1996].

According to the above conclusions, the well-ordered thin film with full-coverage should be prepared at lower molecular concentration (~ 10 mM) in solution, especially with hydrophobic functional groups (e.g., -CH_3). However, this conclusion does not suit for hydrophilic functional groups (e.g., -SH, -COOH and –OH). Akkerman *et al.* reported that high-concentration dithiol solutions result in a preferential standing-up phase [Akkerman 2008]. They found that SAMs with long alkanedithiols prepared

with 30 mM concentration is almost with full standing-up phase, but SAMs with 0.3 mM concentration leads to a highly looped monolayer. The length of C14 was calculated to be 22.6 Å, including a 2.3 Å Au-S bond. When a tilt angle of 30° is assumed, a layer thickness of 1.93 nm is expected, which is the same as that from the experiment (**Figure 2. 18**). Moreover, from 0.03 mM and 0.3 mM concentration the peak intensity of unbound ^{H}S-C is found to be very low compared to the bound S-Au, which implies that almost all molecules are attached with both thiol end groups to the gold surface to form looping phase.

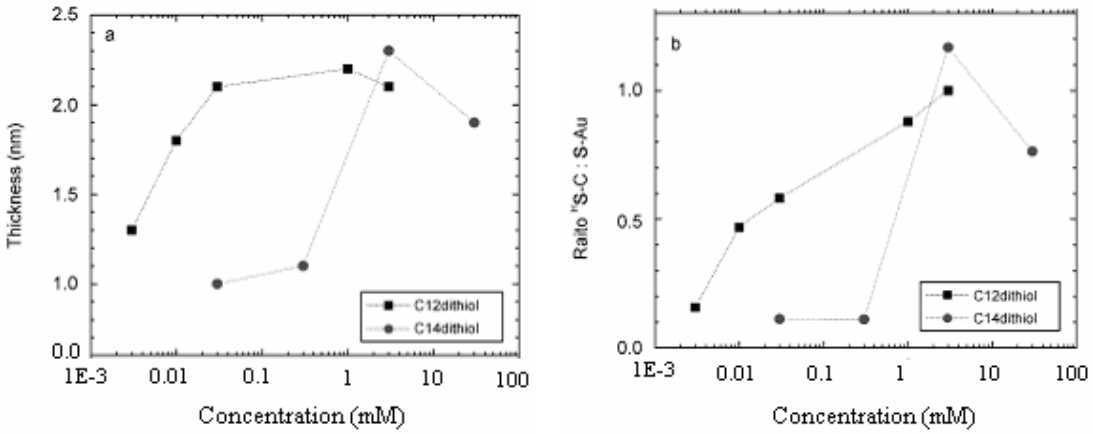

Figure 2. 18 Results for concentration-dependent SAM formation of HS-$C_{14}H_{28}$-SH and HS-$C_{12}H_{24}$-SH: (a) the layer thickness by Ellipsometer and (b) the ^{H}S-C:S-Au ratio in each layer by XPS [Akkerman 2008].

So far, APTES-modified self-assembled film was reported to be prepared in ethanol or toluene with molecular concentration from 1 to 3 vol% (422 mM ~ 1.266 M) [Golub 1996; Majewski 2006; Zhu 2004]. Compared with OTS or thiol-based molecules, optimum molecular concentrations are obviously different in preparation of SAMs from solution deposition, because of the functional groups. However, there is no report about the effect of molecular concentration on the well-ordered APTES-modified film on titanium in the literature. Therefore, further investigation need to be carried out in the aspect.

2.3.3.4 Effect of temperature during silanization

Only a few studies exist concerning the influence of temperature on the formation of the self-assembled monolayers. On the early study, in order to reduce the density of

defects of SAMs, it is reported that thermal annealing of SAMs at >100°C resulted in the healing of the defects [Schreiber 2000], especially alkylchlorosilanes and alkanethiol monolayers. However, unexpected phenomenon is happened during thermal annealing process. For example, it is found for OTS to aggregate and form islands of multilayer at 150°C after for 5 hours [Britt 1996]. It is also found for octadecanethiol to desorb from Au after incubating at 120°C for several hours [Yamada 2000]. So a precise control of the temperature is needed to avoid desorption of the molecules during the annealing. Moreover, surface contamination could take place during the annealing process.

Therefore, different research groups apply different temperatures during the formation of SAMs. Yamada *et al.* studied the self-assembled process of alkanethiols on an Au surface in 1 mM ethanol solutions at temperature from -20, 5, 25, 60 to 78°C, which was examined by scanning tunnelling microscopy [Yamada 2000]. They discovered that the higher temperature of the solution leaded to the larger size of the well-ordered domain structure. Nyquist and co-workers also suggested that the effect of temperature was particularly relevant during the first few minutes of the formation of SAMs when most of the adsorption and reorganization of the SAMs were taking place [Nyquist 2000]. Tian *et al.* discovered the temperature range of 20-80°C had a negligible effect on the formation of octadecyltriethoxysilane monolayer in low humidity. However, in high humidity, the multilayers are formed on the surface at higher temperature [Tian 2004].

Forming SAMs at temperatures above 25°C can improve the kinetics of formation and reduce the number of defects in them [Love 2005]. Brzoska *et al.* demonstrated *n*-alkyltrichlorosilane monolayers on the oxidized silicon wafer as a function of the temperature of the silanization reaction [Brzoska 1992]. They reported that 28 ± 5 °C was well-defined temperature for the formation of OTS on silicon. Britt and Hlady employed two silanization temperatures (25 and 9°C) on mica surface during silanization [Britt 1996]. A uniform distribution of OTS clusters on the surfaces is seen in all three images (**Figure 2. 19a-c**), while no large islands were present. However, at 9°C, after 40 seconds of silanization (**Figure 2. 19e**) larger aggregates of condensed OTS are clearly seen and even larger after 300 seconds (**Figure 2. 19f**).

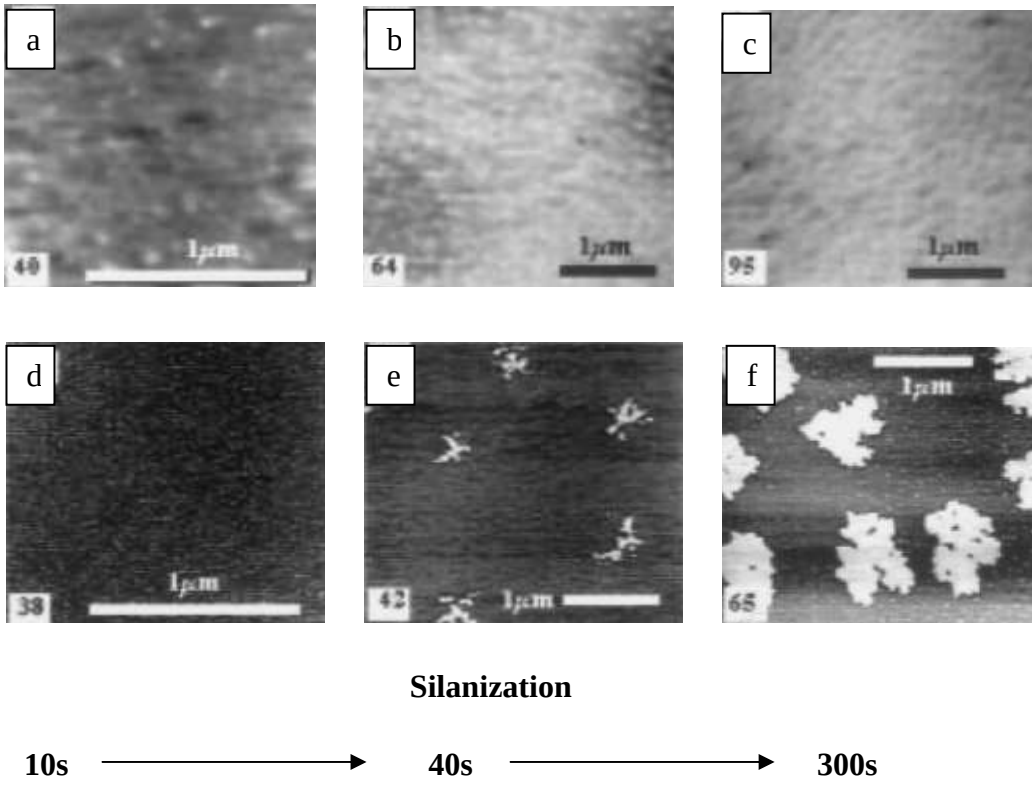

Figure 2. 19 AFM images of the effects of silanization temperature versus silanization time on the formation of OTS monolayers for 10, 40, 300 seconds on partially dehydrated mica at different temperatures: samples from a, b and c are prepared at 25°C; d, e and f are at 9°C, and water contact angles shown at the bottom left corner of each image [Britt 1996].

The above findings do not clearly show the effect of temperature on the formation of SAMs, especially on the film structure. The effect of temperature may be dependent on individual molecules or environment. Certain achievement has been obtained so far, but further investigation is still required for APTES molecules in order to prepare the well-ordered film on titanium and satisfy practical requirements.

2.3.3.5 Effect of solvent during silanization

The studies of the effect of solvent on the SAMs of alkanethiols on gold indicate that the choice of solvent clearly is an important parameter for determining the resulting quality of a SAM prepared from solution. However, the influence of solvent on the kinetics of formation and the mechanism of assembly are complex and poorly understood [Love 2005]. Studies on this topic have led to some qualitative understanding of how solvent can affect the assembly process. The presence of a solvent adds additional parameters to the dynamic equilibrium during the adsorption of

thiols: solvent-substrate and solvent-adsorbates interactions complicate the thermodynamics and kinetics of assembly. Solvent-substrate interactions can hinder the rate of adsorption of thiols from solution because the solvent molecules must be displaced from the surface prior to adsorption of thiols [Love 2005; Schreiber 2000].

Ethanol as solvent is most widely used for preparation of SAMs. It is not noticeable difference for thiol-based SAMs with hydrophobic functional groups formed in ethanol compared with that from other solvents (tetrahydrofuran, dimetylformamide, acetonitrile, cyclooctane and toluene) [Schreiber 2000]. Peterlinz and Georgiadis compared the kinetics of formation in ethanol, a relatively weak alkanethiol solvent, with that in heptane, a relatively strong alkanethiol solvent [Peterlinz 1996]. Studies suggest that the rate of formation of SAMs of alkanethiolates is faster in certain nonpolar solvents (hexanes) than ethanol. As shown in **Figure 2. 20**, the kinetics of growing a self-assembled film in 1.0 mM hexadecanethiol in heptane and ethanol

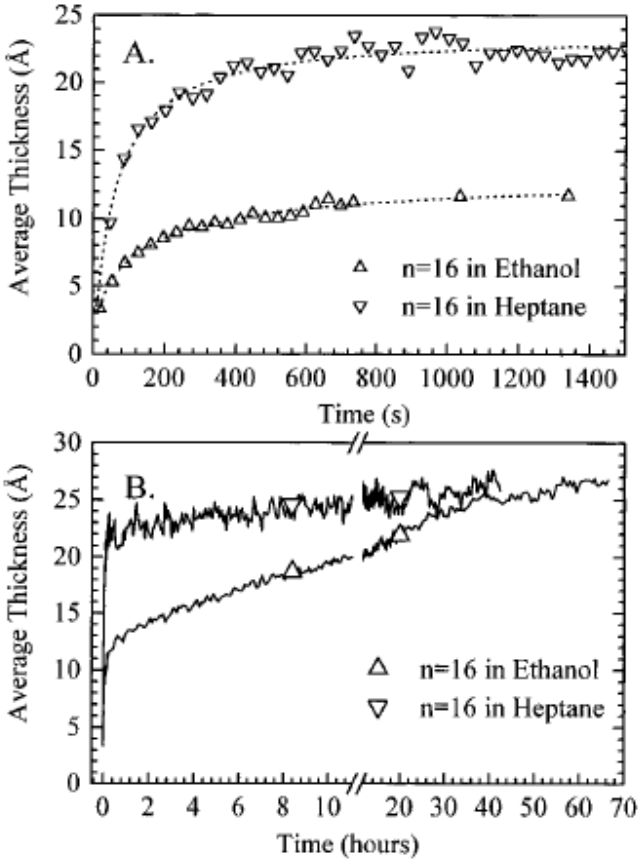

Figure 2. 20 Solvent dependence of formation kinetics for hexadecanethiolate (C_{16}) film in 1.0 mM hexadecanethiol solutions. Shown are the thicknesses calculated from *in situ* SPR spectra measured during film formation from two different solutions, 1.0 mM $CH_3(CH_2)_{15}SH$ in ethanol and in heptane [Peterlinz 1996].

are dramatically different. The rate for the film grown in heptane at the initial step is notably larger. At the end of this first step, the film thickness in heptane is 22 Å versus 12-13 Å for ethanol. Although there appears to be a 4 Å increase in film thickness over the next 43 h for the film grown in heptane, the thickness is largely increased with the film grown in ethanol. Therefore, there is relatively rapid kinetic step in heptane, compared with the formation in ethanol. However, Karpovich did not observe significant differences between hexane and cyclohexane as solvents for the formation of 1-octadecanethiol (CH_3-$(CH_2)_{17}$-SH) on gold [Karpovich 1994].

The use of long hydrocarbons, such as dodecane and hexadecane, as solvents reduces the rates of formation such that they are comparable to those for forming SAMs from ethanol solutions [Love 2005]. Hydrocarbon solvents may improve the kinetics of formation in some cases, but the strong solvent-adsorbate interactions in these solutions impede the organization of SAMs formed from alkanethiols. Dannenberger *et al.* studied the impact of the solvent chain length on the growth of dodecanethiol (CH_3-$(CH_2)_{11}$-SH) [Dannenberger 1998]. They found that the initial rate of chemisorption was significantly slower for longer-chain solvents. The slower adsorption for solvents with longer chains is considering that the interaction of the solvent molecules with the surface (from which they have to be displaced by the thiols) is larger for longer chains and that also the mobility of the molecules in solution is reduced for longer chains.

Therefore, the chemical nature of a solvent will influence many parameters, such as polarity, mobility, solubility for SAM molecules, etc. Most of the research work in the literature reports that ethanol, toluene or a mixture of ethanol and water solvents are usually used for growth of SAMs with the -NH_2 group. Kang and coworkers found, in a polar solvent (ethanol or acetone), although a polar SAM can be stabilized by solvent interactions, the -NH_2 functional groups will connect to the solvent molecule by hydrogen bond, instead of free amine groups [Kang 1998]. Moreover, ethanol as the solvent will occupy the position of hydroxyl group on the surface by hydrogen bond, so that coverage of SAMs on the surface will decrease. Toluene as a dipolar solvent can overcome the above issues for growth of SAM with the -NH_2 group on a hydroxylated surface. Some researchers investigated the solvent effects for the preparation of modified NH_2-funcitonalized surface in different solvents (toluene,

ethanol and acetone) [Hsieh 2007]. After certain immersion time, they found NH_2/Toluene combination provided the best and most repeatable signal (shown in **Figure 2. 21**), which implies that toluene is a better solvent than ethanol and acetone for growth of SAMs with the -NH_2 group. According to the physical-chemical property of APTES, its solubility in toluene is much great than that in ethanol, which results in the better diffusion of APTES in solvent. Therefore, toluene is chosen as solvent for APTES during self-assembly on titanium in this project.

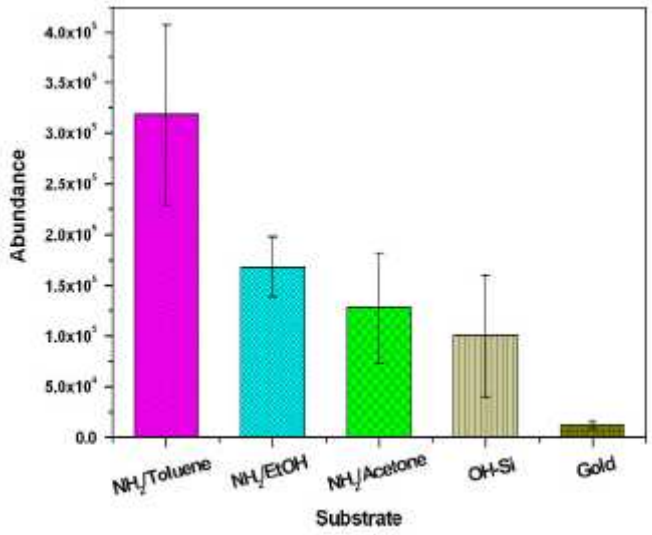

Figure 2. 21 Bradykinin fragment abundance for several NH_2-terminated SAM modified Si substrates, an OH-rich Si substrates, and standard gold substrate [Hsieh 2007].

2.3.3.6 Effect of residual water content in solvent

Compared with thiol-based SAMs, water is necessary for silane-based SAMs to hydrolyze head groups, which will form covalent bonds (Si-O-M) with the surface and three dimensional condensations (Si-O-Si) through polymerization, according to the reaction principle of SAMs on the surface in Chapter 2.2. Angst *et al.* showed that OTS molecules attached to a dry SiO_2 surface to form disordered film [Angst 1991]. Tripp *et al.* reported that high water content of the solvent leaded to polymerization of alkanesilanes in bulk solution [Tripp 1992]. Therefore, the water content in solvent is an important parameter that plays a major role in quality of the final silane-based SAMs. However, the dependence of the monolayer growth kinetics on water content is still far from being understood.

Water, which is either in solvent or present in the surface of substrate, hydrolyzes the alkanesilanes to form silanols [Silberzan 1991]. These silanols then form stable bonds to the substrate upon reacting with the hydroxylated surface and release water. Mcgovern *et al.* suggested a moisture quantity of 0.15 mg/100 mL of solvent as the optimum condition for the formation of closely packed monolayers for OTS [McGovern 1994]. It was reported that increasing age of the solution favours island-type growth more strongly. Vallant and Burnner also reported that an island type growth of OTS on the surface was strongly favoured with increasing water content in solvent [Vallant 1998]. However, Silberzan *et al*. recommended that small amount of water in solvent would lead to the formation of large aggregates, which would block vacant adsorption sites on the surface. Consequently, the formation of well-defined SAMs will be prevented [Silberzan 1991], as shown in **Figure 2.22a**.

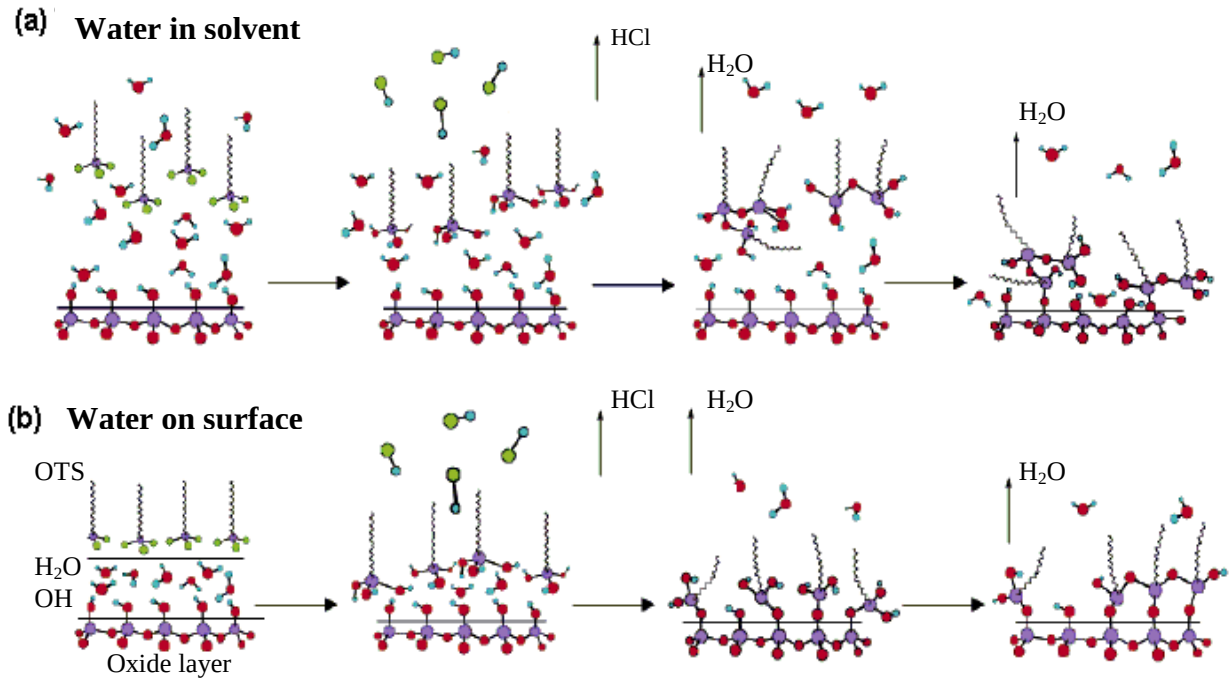

Figure 2. 22 Schematic of OTS growth mechanisms on an oxide layer in (a) wet and (b) anhydrous conditions [Silberzan 1991].

In an anhydrous environment, a thin water on the substrate surface could act as a water reservoir for hydrolysis of the molecules and as a lubricating layer for the adsorbed molecules to move laterally on the surface and gather into a densely packed monolayer [Schreiber 2000]. Angst and Simmons found that a water film on the silica substrate

was necessary for the formation of a complete monolayer [Angst 1991]. Tripp and Hair used infrared spectroscopy to provide direct evidence for the full hydrolysis of methylchlorosilanes to methylsilanols, at the solid-gas interface, by surface water on a hydrated silica [Tripp 1995], as shown in **Figure 2.22b**. Britt and coworkers reported that a thinner water layer might result in the formation of an incomplete monolayer, which will affect its further applications. While, a thick water layer may eliminate the non-covalent interactions between the polar head group of monolayer molecules and the surface as well as prevent covalent bond formation between monolayer molecules and any surface hydroxyl groups [Britt 1996]. Therefore, water content during silanization needs to be carefully controlled.

From the above assessment, where water comes from during silanization, is still a dispute for the formation of well-ordered silane-based SAMs. In order to clarify this point for the formation of the APTES-modified film, different solvents will be used to investigate this purpose according to the limitation of current laboratory: hydrous toluene (90%), which is assumed that residual water presents in solvent, and anhydrous toluene (+99.9%), which is assumed that water presents on the substrate surface.

2.3.3.7 Stability of SAMs

The stability of SAMs is an important parameter to be considered especially for its applications. For example, in biology-related applications, hydrolysis stability of SAMs in aqueous solution will determine the stability of protein on the surface. On other word, immobilized protein with SAMs will be dropping off from the surface when covalent bonds in SAMs (e.g. Si-O-M and Si-O-Si) are broken. Therefore, assessment of SAMs stability with time, under temperature and in solution is required and in this regard, several investigations were carried out in the past for SAMs with hydrophobic functional groups.

Wang *et al*. have investigated the systematic stability of various alkylsilane SAMs on a silicon surface *in vitro* in a saline solution (0.9% NaCl in deionised water) at 37 ^{o}C for up to 10 days [Wang 2005]. They showed that SAMs with hydrophobic end groups and longer chains (e.g. OTS) show better stability compared to SAMs with hydrophilic

end groups and shorter chains. The reason could be that the hydrophobic SAMs prevent water penetration and longer chain of molecules form closely packed films due to increased van der Waals attractions between the backbone alkyl chains. The stability of alkyltrichlorosilane SAM was also investigated by Wassserman *et al*. [Wasserman 1989]. They showed that CH_3-terminated siloxanes were stable for 18 months storage in air. They also confirmed the stability of tetradecyltrichlorosilane in contact with the acid (0.1N HCl) at room temperature, however, in the basic solution (0.1N NaOH) 50 % of the film was etched within 80 min.

McElwee *et al*. have speculated that monolayer packing and mobility may affect its thermal stability [McElwee 2005]. They showed by the thermogravimetric analysis curves that the degradation of alkylsilane SAMs happens through pyrolysis of the hydrocarbon chains via cleavage of the C-C and Si-C bonds and the inorganic portion of the molecule remains attached to the surface. The maximum weight loss was obtained at ~ 400 - 450 ^{o}C for trifunctional and ~ 250 ^{o}C for mono-functional alkylsilanes. Furthermore, according to Cohen *et al*., OTS-based SAMs on silicon surfaces are stable up to 125 ^{o}C [Cohen 1998].

2.4 Enzyme immobilization

Since the amine functional groups in APTES-modified SAMs can immobilized protein by covalent bond, this self-assembly technique is often applied for biosensors, bioelectronics. Here, we will talk about special protein – enzyme for biofuel cell. Enzymes as biocatalysts exhibit a number of features that make their use advantageous as compared to conventional chemical catalysts. Foremost among them are a high level of catalytic efficiency, often far superior to chemical catalysts, and high degree of specificity that allows them to discriminate not only between reactions but also between substrates (substrate specificity) and between optical isomers (stereospecificity) [Trvan 1980]. In addition, enzymes generally operate at mild conditions of temperature, pressure and pH with reaction rates compared with those achieved by chemical catalysts at more extreme conditions [Elsenthal 1993; Trevan 1980]. Enzyme as biocatalysts, can also offer cost advantages over metallic catalysts.

Moreover, enzymes practically do not present disposal problems since being mostly proteins and peptides, and they are biodegradable and easily removed from contaminated streams. Therefore, enzymes as biocatalysts have been widely applied for industries.

Reports on immobilization of proteins and enzymes first appeared 30 years ago [Zaborsky 1974]. Since then, immobilized proteins/enzymes have been widely used for the processing of a variety of products spanning industries from food to environmental control [Messing 1975]. In addition to their use in processing, immobilized enzymes have also been found useful in many fields, including bioanalysis, synthetic chemistry, industrial use, waste utilization, nanobiotechnology and etc. [Duran 2002]. For example, immobilized enzymes are used routinely in the medical field, such as in the diagnosis and treatment of various diseases. Immobilized antibodies, receptors, or enzymes are used in biosensors and Enzyme-linked immunosorbent assay (ELISA) for the detection of various bioactive substances in the diagnosis of disease states [Zaborsky 1974]. Encapsulated enzymes are also used in bioreactors for the removal of waste metabolites and correction of inborn metabolic deficiency. Moreover, the use of artificial cells as well as the development of controlled release drug delivery systems to release encapsulated enzymes or proteins may also be considered a form of immobilized enzyme use [Hanefeld 2009].

For the implementation in a commercial process, all beneficial and detrimental effects of whether an enzyme is chosen, and whether a free or immobilized enzyme is used, have to be weighed taking into account all relevant aspects, health and environmental included, in addition to obvious economical viability. Laccase, a copper-containing oxidase enzyme, is found in many plants, fungi and microorganisms and often used as the cathode in enzymatic biofuel cells and waste water treatment [Yaropolov 1994]. In order to re-use enzyme in a commercial process, it is essential to understand fully fundamental mechanisms of catalysis of enzyme, advantages and disadvantages of each immobilization method, and molecular structure and electrocatalytic properties of enzyme.

2.4.1 Introduction of enzyme immobilization

Enzymes are protein molecules that catalyze chemical reactions of living cells. In enzymatic reactions, the molecules at the beginning of the process are called substrates, and the enzyme converts them into different molecules, called the products. Like all catalysts, enzymes work by lowering the activation energy (E_a or ΔG) for reaction, thus dramatically increasing the rate of the reactions (**Figure 2.23**) [Elsenthal 1993]. The substrates need a lot of energy to reach a transition state which then decays into products, while the enzyme can stabilize the transition state by reducing the energy needed to form products. Most enzyme reaction rates are millions of times faster than those of comparable un-catalyzed reactions. As with all catalysts, enzymes are not consumed by the reactions they catalyze, nor do they alter the equilibrium of these reactions.

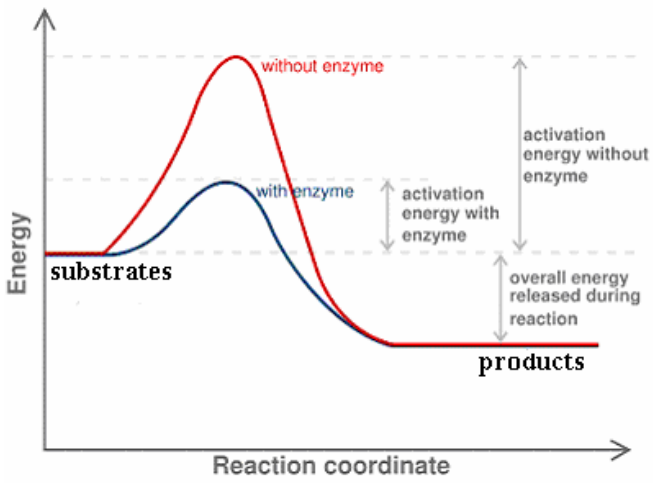

Figure 2. 23 Energies of the stages of a chemical reaction with or without enzyme [W3].

Enzymes are generally globular proteins and contains up to 2,500 amino acid residues. In the structure of enzymes, a specific region is know as the active site, which contains the catalytic residues, binds the substrate and then carries out the reaction. In 1894 Emil Fischer suggested 'the lock and key' model for enzymatic reactions [Elsenthal 1993]. However, this model fails to explain the stabilization of the transition state that enzymes achieve. In 1958, Daniel Koshland modified this model, shown in **Figure 2. 24**. When the substrate interacts with the enzyme, it does not simply bind to a rigid active site. So the active site changes the shape until the substrate is completely bound [W3].

Enzyme/substrate complex is catalyzed to enzyme/products complex, and finally the product is separately from the enzyme. The activities of enzymes are determined by their three-dimensional structure of the activity site, and can be affected by other molecules (e.g. inhibitors), temperature, chemical environment (e.g. pH) and the concentration of substrate.

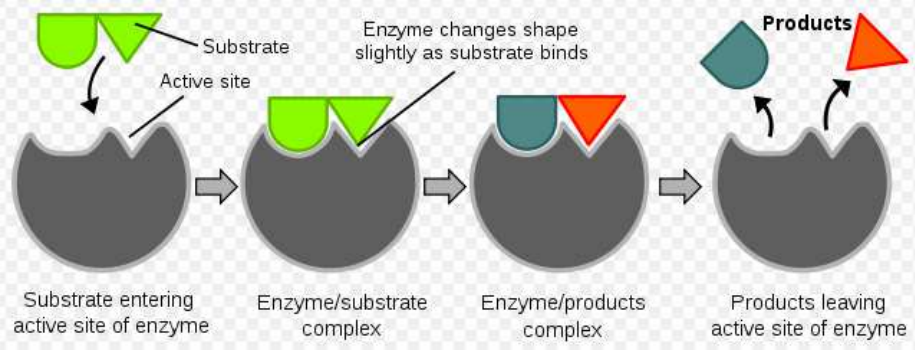

Figure 2. 24 Process of enzymatic reaction with substrates in the 'lock and key' model [W3].

Enzymes are able to catalyze the most complex chemical processes under the most experimental and environmental conditions, because of their excellent functional properties (activity, selectivity, and specificity). Obviously, in addition to their excellent catalytic properties, enzymes also have some characteristics that are not very suitable for industrial applications: they are soluble catalysts, usually very sensitive and unstable, and may be strongly inhibited by substrates and products. Some enzymes only work well on natural substrates and under physiological conditions. In order to overcome above limitations and allow longer duration of activity of enzymes, one of the most successful technologies is enzyme immobilization.

Enzyme immobilization may be defined as the 'imprisonment' of an enzyme molecule in a distinct phase by physical or chemical bonds and still act on its substrate [Treven 1980]. General operational advantages of enzyme immobilization are reusability, possibility of continuous operational modes, rapid termination of reactions, controlled product formation, greater variety of engineering designs for continuous processes, and possible greater efficiency in consecutive multistep reactions (**Table 2. 4**). Therefore, it has to be emphasised that enzyme immobilization can help in the utilization of the enzyme [Hanefeld 2009]. However, immobilization often causes the reduction of enzyme activity and diffusion limitation during catalysis. Therefore, the

immobilization is required to optimize enzyme dispersion to improve accessibility for the substrates, as well as to avoid the aggregation of the hydrophilic protein particles. In addition, immobilization ensures that these biocatalysts can be readily recycled. The anchoring of an enzyme onto a solid insoluble support should be straightforward and cost efficient.

Table 2. 4 Technological properties of immobilized enzyme systems.

Advantages	Disadvantages
Catalyst reuse	Loss or reduction in activity
Easier reactor operation	Diffusion limitation
Easier product separation	Additional cost

2.4.2 Methods of enzyme immobilization

Immobilization of an enzyme involves two species: enzyme and carrier. The enzymes have been introduced on the above section. An essential requirement for any carrier is to match either of these surface properties of the enzyme. The carriers can be small-particle-size materials, though it will make separation difficult, or with highly porous materials with pores of sufficiently large dimensions that do not limit diffusion of the substrates. In the latter case the pores of the carrier have to be of sufficient size to guarantee unhindered diffusion of the substrates while ensuring that enzyme remains locked inside. Alternatively the carrier can immobilize enzymes by surface functional groups. For example, primary amine groups (-NH_2) react with carboxyl groups (-COOH) to form peptide bonds (-NH-CO-). Reactive functional groups can be introduced in the matrix of polymeric supports by choosing appropriate organic monomers. Moreover, the carrier needs to be chemically and mechanically stable. Therefore, many methods are available for enzyme immobilization. The most frequently used immobilisation techniques fall into four categories: adsorption, entrapment, cross-linking and covalent binding.

Several techniques may be applied to immobilize enzymes on solid supports. They are mainly based on physical and chemical mechanisms. Physical immobilization methods

involve entrapment and adsorption through van der Waals, hydrogen bonds, etc. Chemical immobilization methods mainly include covalent binding and cross-linking using multifunctional reagents, such as carbodiimide and glutaraldehyde. Both physical and chemical methods of enzyme immobilization have advantages and disadvantages (**Table 2. 5**). In general, the entrapment and adsorption immobilization methods typically change the structure of enzyme much less and consequently offer retention of the enzyme properties resembling those in solution [Bailey 1986], but they results in the cleavage of immobilized enzymes from the carrier because of weak bonds. Although chemical immobilization methods tend to reduce the activity of the enzyme due to the change of the enzyme native structure, they can be used for longer time because of strong chemical bonds [Trvan 1980]. Usually, a long-time applicable immobilized enzyme with a lower initial activity is preferable to that with a high level of initial activity but with a short-time activity retention [Duran 2002]. In the following, the immobilization processes will be briefly discussed especially cross-link and covalent binding immobilization methods.

Table 2. 5 Methods for enzyme immobilization [Hanefeld 2009; Treven 1980].

Method	Advantages	Disadvantages
Adsorption	Gently treatment of enzyme; no modification of enzyme; matrix can be regenerated	Very weak bonds; susceptible to changes in pH, temperature, ionic strength
Entrapment	Gentle; no direct chemical modification; specificity and analyte interaction retained	High diffusion barrier; only good for small analyses; continuous loss of enzyme
Cross-linking	Used in conjunction with entrapment to reduce loss of enzyme	Covalent links formed between protein molecules rather than matrix and protein; may involve harsh/toxic chemicals
Covalent binding	Low diffusion resistance; strong binding force between enzyme and matrix; resistant to adverse conditions of pH, ionic strength	Matrix not regenerable

2.4.2.1 Adsorption

Immobilization of enzymes by adsorption is probably the mildest method available, being mediated by ionic, hydrophobic or hydrogen bonds [Hanefeld 2009]. Adsorption of enzymes onto insoluble supports is a very simple method of applications and capable of high enzyme loading. Simple mixing of the enzyme with a suitable adsorbent, under appropriated conditions of pH and ionic strength, followed after a sufficient incubation period, by washing off loosely bound and unbound enzyme, will produce the immobilized enzyme in a directly usable form. The driving force causing this physical binding is usually due to the combination of hydrophobic effects, van der Waals force, π-π bond, etc. [Piacquadio 1997]. For example, enzymes with a large lipophilic surface area will interact well with a hydrophobic carrier. Sugar residues of glycosylated enzymes can ensure adsorption by hydrogen bonds; large hydrophilic surface areas of the enzyme will interact with a hydrophilic carrier [Zaborsky 1974]. The suitable carriers for adsorption of enzymes are ion-exchange matrices, porous carbon, hydrous metal oxides, glasses and polymeric aromatic resins [Hanefeld 2009].

2.4.2.2 Entrapment

Apart from adsorption, the entrapment is one of most important physical immobilization methods and provides relatively small perturbation of the enzyme native structure and function. Generally, the entrapment of an enzyme molecule can be achieved in one of three ways [Treven 1980], as shown in Error! Reference source not found.**25**:

1) Inclusion within the matrix of a highly cross-linked polymer;
2) Separation from the bulk phase by a semipermeable ‘microcapsule’ (encapsulation);
3) Dissolution in a distinct non-aqueous phase.

In entrapment, the enzymes are not directly attached to the carrier, but simply trapped inside the polymer matrix by physical caging. Therefore, there is none of the steric problems associated with electrostatically binding an enzyme on to a polymer, which

results in the minimum of loss of enzyme activity. In general, entrapment methods are performed by dissolving the enzyme in a solution, followed by polymerization initiated

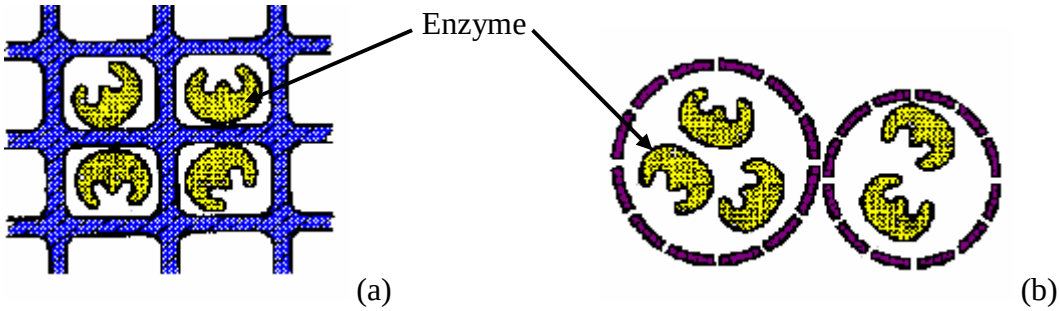

Figure 2. 25 Modes of enzyme immobilized by entrapment: (a) entrapment with crosslinked polymers; (b) encapsulation.

by a change in temperature or by a chemical reaction. The polymer is formed either in particulate form or a block which can be disrupted to form discrete particles. The most commonly methods of entrapment use polyacrylamide, collagen, cellulose acetate, calcium alginate or carrageenan as the carriers [Elsenthal 1993; Hanefeld 2009]. Entrapment of enzymes within gels or fibres is a convenient method for use in process involving low molecular weight substrate and products. However, the difficulty which large molecules have in approaching the catalytic sites of entrapped enzymes precludes the use of entrapped enzymes with high molecular weight substrates.

2.4.2.3 Cross-linking

Immobilization of enzymes by chemical cross-linking is based on the formation of covalent bonds between enzyme molecules by functional groups (e.g. -NH_2 and -SH), by means of bi- or multifunctional reagent, leading to three-dimensional cross-linked aggregates. Instead of fixing the enzyme directly to a carrier, a linker is necessary between enzyme and carrier. In general, ***N***,***N***'- bisdiazobenzidine-2,2' – disulphonic acid or 2,4- dinitro-3,5-difuorobenzene and glutaraldehyde (GLUTAL) regents have been used to cross-link enzymes. 2,4-Dinitro-3,5-difluorobenzene requires highly alkaline solutions to react and the presence of organic solvent to dissolve it; N,N'-bisdizaobenzidine-2,2'-disulphonic acid is a potentially explosive carcinogen [Trevan 1980]. Therefore, the most commonly used multifunctional reagent is GLUTAL because it reacts with enzymes readily under relative mild conditions.

GLUTAL ($CH_2(CH_2CHO)_2$) is an amine-reactive homo-bifunctional cross-linker containing an aldehyde residue at both ends of a 5-carbon chain. The amino group as nucleophile can attack an aldehyde to form the imine, which the reaction is shown in Error! Reference source not found.. When a carrier can supply the $–NH_2$ functional groups, GLUTAL can both cross-link enzyme molecules and the carrier. This method produces multilayers of enzymes on the electrode surface [Imamura 1995]. Creager and Olsen reported that glucose electrodes where the enzyme was bound to the thiol using glutaraldehyde have at least 64 layers of glucose oxidase [Creager 1995]. This net effect is to increase the distance of the enzyme molecules to supports, so that the ability of transferring electrons will be affected between supports and enzymes. Moreover GLUTAL often preferentially attacks the active site of the enzyme, thus rendering it inactive [Trevan 1980].

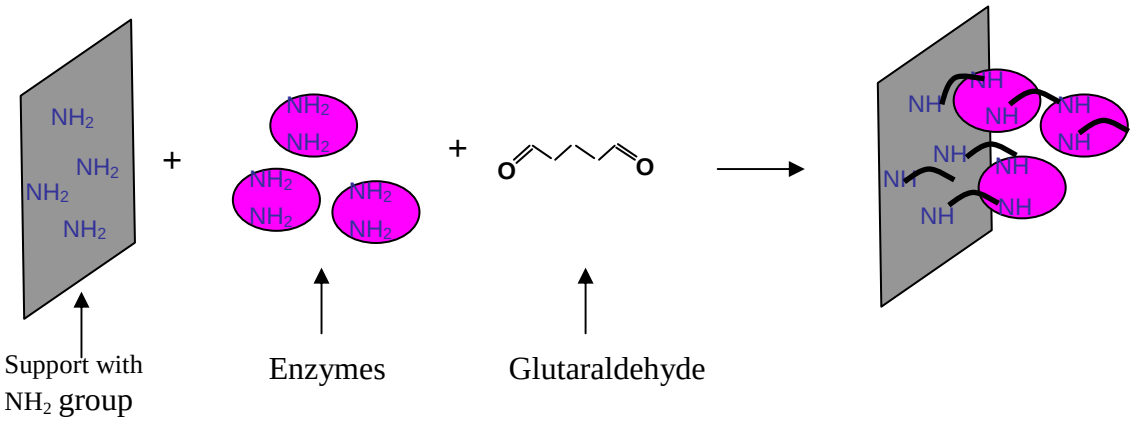

Figure 2. 26 Schematic diagram of enzyme immobilization by cross-linking with glutaraldehyde.

2.4.2.4 Covalent binding

Covalently binding enzymes has flourished since the 1950s and is now an important method of enzyme immobilization, because covalent bonds usually provide the strongest linkages between enzyme and carrier, compared with non-covalent adsorption-based enzyme immobilization. Thus leakage of enzyme from the carrier used is often minimized with covalently binding. Normally, enzyme immobilization by covalent binding is preferred when working in aqueous solution and when denaturing factors exist. This is due to the fact that the formation of multiple covalent bonds

between the enzyme and the carrier reduces conformational flexibility and thermal vibrations thus preventing protein unfolding and denaturation [Hanefeld 2009].

In general, covalent binding of an enzyme to a carrier is based on chemical reaction between the active amino acid residues located on the enzyme surface and functional groups from the carrier surface. The functional groups from the carrier that may take part in this binding include amine ($-NH_2$), carboxyl (-COOH), hydroxyl (-OH), imidazole (**Figure 2. 27a**), phenolic (**Figure 2. 27b**), thiol (-SH) and indole (**Figure 2. 27c**) groups. **Table 2. 6** shows various covalent bonds in enzyme immobilization and most useful covalent bond is the amide bond (-CO-NH-).

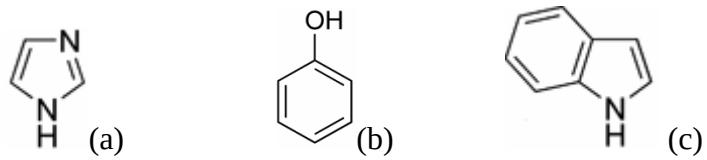

Figure 2. 27 Structures of imidazole (a), phenolic (b) and indole (c).

Table 2. 6 Various covalent bonds between enzymes and carriers [Messing 1975; Trevan 1980].

Diazotization	-N=N-
Amide bond formation	-CO-NH-
Arylation	$-CH_2$-NH-
Schiff's base formation	-CH=N-
Amidation reaction	-C=N-NH-
Thiol-disulfide interchange	-S-S-

To achieve efficient linkage, the functional groups of the carrier or the enzyme must be activated before immobilization. A popular and highly versatile method for covalently attaching proteins to the carrier is by using carbodiimide coupling which couples carboxylic acids to amines [Hanefeld 2009]. A carbodiimide is a functional group consisting of the formula RN=C=NR, which hydrolyzes to form urea (H_2N-CO-NH_2). In carbodiimide family, 1-ethyl-3-(3-dimethylaminopropyl) carbodiimide (EDC, shown in **Figure 2. 28a**) is the most useful activator and converts the carboxyl groups

into a reactive unstable intermediate and then yield the amide bonds with primary amine groups. The formation of an amide using a carbodiimide is straightforward. The carboxyl group reacts with the EDC to produce the intermediate **A**: the O-acylisourea, which is with an activated leaving group and then reacts with amines to form the amide. If the intermediate reacts with an additional carboxyl group to form an acid anhydride, which can react further to form the amide. Apart from the carboxyl groups, the EDC can also activate phosphate groups.

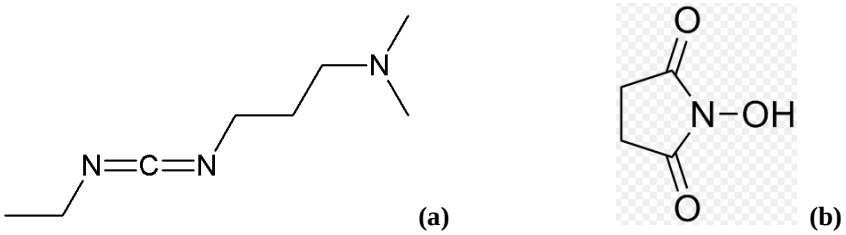

Figure 2. 28 Molecular structures of EDC and NHS.

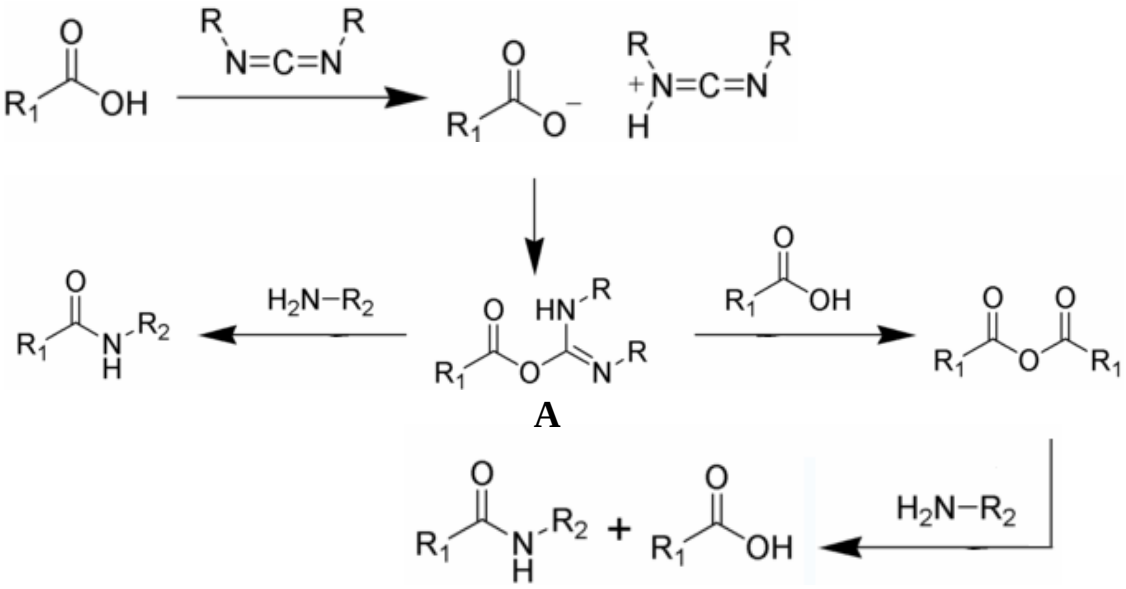

Figure 2. 29 Formation of amide bond by the reaction of carboxyl group with amine group under activation of EDC [modified from W2].

However, the intermediate is not stable because two o-acylisourea molecules can react to form the stable N-acylurea. In order to decrease the side reaction, EDC is often used in combination with *N*-hydroxysuccinimide (NHS, shown in **Figure 2. 28b**) to increase coupling efficiency and create a stable amine-reactive product. In Figure 2.29, the

intermediate **A** is formed by the activation of carboxyl group with EDC and further reacts with NHS to form a stable intermediate **B**. The latter will react with primary amine groups to obtain the amide bonds. Gooding *et al.* reported that XPS was used to determine the percentage of 3-mercaptopropionic acid (MPA) molecules which are activated with EDC alone and EDC with NHS. The XPS spectra reveal that with EDC alone only 40% of carboxyl groups on the surface are activated while 70% of those are activated by EDC/NHS [Gooding 2001].

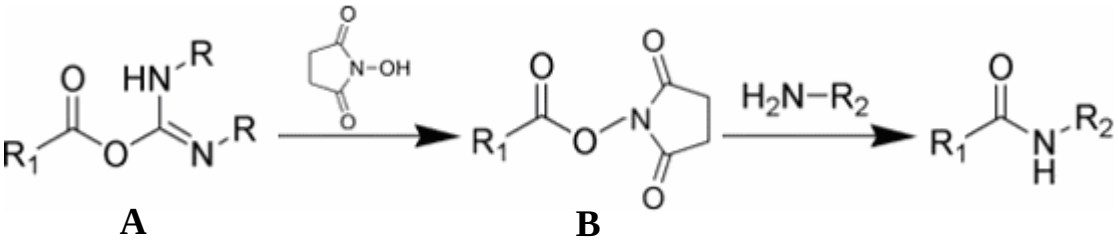

Figure 2. 30 Formation of amide bond by the reaction of carboxyl group with amine group under activation of EDC and NHS, which is modified from [Gooding 1999].

In this project, covalent binding by amide bond will be applied for the enzyme immobilization as the APTES-modified SAMs can supply the primary amine groups. The carboxyl groups from enzyme surface will be activated by EDC/NHS and then react with the $-NH_2$ groups from the carrier surface, which might avoid attaching of active site of enzyme. However, covalent binding might alter the conformational structure of the enzyme (especially active site), resulting in loss of activity. Therefore, in order to obtain the maximum of enzyme activity, the optimum conditions for immobilization need to be investigated by covalent binding with the NH_2-SAMs, such as EDC/NHS molar ratio, pH, temperature and immobilization time.

2.4.3 Immobilization of laccase

2.4.3.1 Introduction of laccase

Laccase is one of the very few enzymes that have been studied since the end of 19th century [Yaropolov 1994]. It was first demonstrated in the exudates of *Rhus vernicifiera*, the Japanese lacquer tree (Yoshida, 1883). A few years later it was also

demonstrated in fungi (Bertrand, 1896). Laccases are typically found in many plants [Mayer 1979], fungi [Thurston 1994] and microorganisms [Alexandre 2000]. Plant laccases participate in the radical-based mechanisms of lignin polymer formation [Boudet 2000; Sterjiades 1992], but fungi laccases probably have more roles including morphogenesis, fungal plant-pathogen/host interaction, and lignin degradation [Baldrian 2006]. A very wide range of substrates has been shown to be oxidized by fungal laccases [Baldrian 2006], such as 2,2'-azinobis(3-ethylbenzothiazoline-6-sulfonic acid) (ABTS), 2,6-dimethoxyphenol (DMP), 2-methoxyphenol (guaiacol) and 4-hydroxy-3,5-dimethoxybenzoic acid (syringaldazine). There are also some reports about laccase activity in bacteria [Boudet 2000]. Probably the best characterized bacterial laccase is that isolated from *Sinorhizobium meliloti*, which has been described as a 45-kDz periphasmic protein with isoelectric point at pH 6.2 and the ability to oxidize syringaldazine [Baldrian 2006].

In the last decades laccases have received much attention from researchers. Although known for a long time, laccases are attracted considerable attention only after the beginning of studies of enzymatic degradation of wood by white-rot wood-rotting fungi [Yaropolov 1994]. Due to their ability to oxidise both phenolic and non-phenolic lignin-related compounds, laccases have been used for some applications in several biotechnological processes. Such applications include the detoxification of industrial effluents, mostly from the paper and pulp [Camarero 2004], textile and petrochemical industries [Hou 2004], use as a tool for medical diagnostics, pesticides and certain explosives in soil [Susana 2006]. Laccases are also used as the cathode in novel enzyme-based catalyzed fuel cells [Palmore 1999], as cleaning agents for certain water purification systems and as catalysts for the manufacture of anti-cancer drugs and even as ingredients in cosmetics [Golz-Berner 2004; Lang 1999]. In addition, their capacity to remove xenobiotic substances and produce polymeric products makes them a useful tool for bioremediation purposes [Susana 2006]. The following sections are devoted to the structure and electrocatalytic properties of the laccase and its active sites.

2.4.3.1.1 Molecular structure of laccase

Laccase is an oxidoreductase enzyme that can catalyze the oxidation of various aromatic compounds with the concomitant reduction of oxygen to water [Duran 2002].

Apart from plants and bacteria, the most studied laccases appear to be from fungi, such as *Cerrena unicolor* [Nogala 2006; Zawisza 2006], *Rhus vernicifera* [Reinhamm 1970], *Rhizoctonia practicola* [Leonowicz 1988; Palmore 1999], *Trametes* or *Polyporus versicolor* [Freire 2001; Liu 2007; Piacquadio 1997; Piontek 2002] and *Coriolus hirsitus* [Shleev 2005a; Xu 1997]. The molecular masses of laccases vary in a wide range and major discrepancies may well be related to the carbohydrate moiety of the molecule. The amino acid chain contains about 500 amino acids.

The laccase from *Trametes versicolor* was determined by X-ray and the crystal structure of the fully active enzyme is shown in **Figure 2. 31** [Piontek 2002]. The structure of *T. versicolor* laccase is a monomer, and has dimensions of about 65 ×55×45 Å. Each of the three domains is of similar β-barrel type architecture. Domain 1 (D1) comprises two four-stranded β-sheets and four 3_{10}-helices. Domain 2 (D2) has one six-stranded and one five-stranded β-sheet. Domain 3 (D3) consists of a β-barrel formed by two five-stranded β-sheets, together within a α-helix and a β-turn, form the cavity in which the type-1 copper is located [Piontek 2002]. A 3_{10}-helix between D2 and D3 forms part of a loop region.

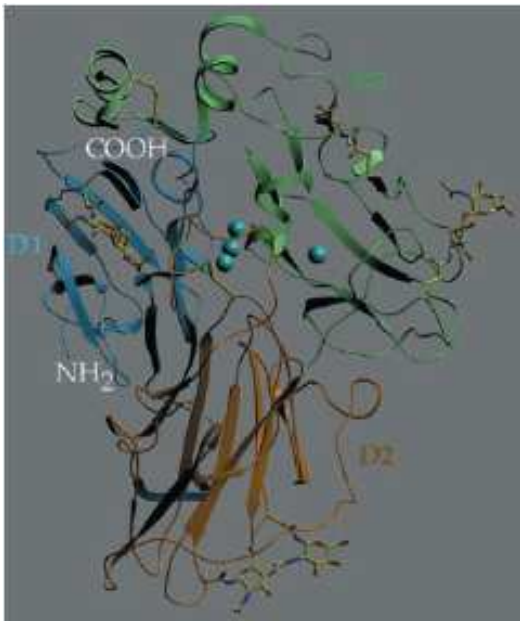

Figure 2. 31 Crytal structure of *Trametes versicolor* laccase (ribbon diagram). The arrangement of the domain structure is depicted in different colour coding (D1-D3). Copper ions are drawn as blue spheres; Carbohydrates and disulfide bonds are included as stick models [Christenson 2004; Piontek 2002].

In general, laccase is a copper protein and contains 4 copper ions classified into 3 types: type-1(T1), type-2(T2) and type-3(T3) [Christenson 2004; Duran 2002; Solomon 1996], which play an important role in the enzyme catalytic mechanisms. It was shown that laccase has a minimum of one mononuclear copper site containing one T1 copper, and a trinuclear copper cluster containing one T2 and two T3 coppers. The different copper centres can be identified on the basis of their spectroscopic properties. The T1 copper lies embedded in D3 about 6.5 Å below the surface of the enzyme, which is characterized by a strong adsorption around 600 nm [Piontek 2002]. The T1 copper involved in substrate binding, occupies a room of the enzyme surface, delimited by a β-turn, belonging to D1, and two β-turns of D3 [Christenson 2004; Thurston 1994]. The trinuclear cluster (T2/T3) connects the T1 copper by a His-Cry-His tripeptide which is highly conserved among blue multicopper oxidases, as shown in **Figure 2. 32**. The T2 centre is 3-coordinate with two histidines (His) ligands and water as ligands and the T3 coppers are each 4-coordinate, having three His ligands and bridging hydroxide, where the reduction of molecular oxygen takes place.

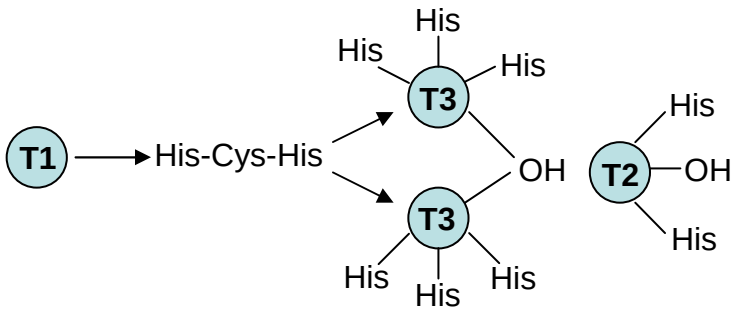

Figure 2. 32 Pictorial mode of laccase (T1 and T2/T3 copper centres) [Baldrian 2006; Duran 2002].

2.4.3.1.2 Electrocatalytic redox properties of laccase

The electrocatalytic redox properties of laccase involve the copper centres: the T1, T2, and T3. Neither the electron transfer nor the oxygen reduction to water mechanisms is fully understood. Since the T1 centre is involved in substrate binding, some researchers have proved for some laccases that T1 is the primary centre at which electrons are accepted from reducing substrates [Solomon 1996; Xu 1999]. When substrates are oxidized by the T1 copper, the extracted electrons are transferred,

probably through a strong conserved His-Cys-His tripeptide to the trinuclear T2/T3, where molecular oxygen is reduced to water. The summary reaction of the electroreduction of oxygen to water is shown in **Equation 2.3**.

$$O_2 + 4e^- + 4H^+ \xrightarrow{\text{laccase}} 2H_2O \qquad \textbf{(Equation 2. 3)}$$

Figure 2. 33 shows the proposed mechanisms for the reduction and reoxidation of the copper sites in the laccase. The major question remaining in the reductive part of the cycle is the mechanism by which the trinuclear cluster is reduced. In this figure (centre) starting from the "native intermediate," the substrate reduces the T1 site (**C**), which in turn transfers the electron to the trinuclear cluster. Two possible mechanisms for the reduction of the trinuclear cluster are shown [Solomon 1996]: (**A**) The T1 copper transfers its electron to the T2 copper (**A1**)and then is re-reduced (**A2**); the T1 and T2 coppers transfer its electron to the T3 copper (**A3**) and gets re-reduced (**A4**), ultimately resulting in the fully reduced form of the enzyme (**D**). This possible mechanism would be consistent with the fact that in resting fully oxidized laccase the T3 centre acts as a strictly two electron acceptor. (**B**) The trinuclear cluster is sequentially reduced by three one-electron transfer steps from the T1 site. The T1 transfers one electron to the T3 copper (**B1**) and then gets re-reduced (**B2**); the T1 transfers one electron to the T2 (**B3**) and then is reduced (**B4**), which transfers one electron to T3 copper again, leading to the full reduction of the laccase.

The fully reduced site reacts with O_2 to generate a peroxide-level intermediate, best described as a bridged hydroperoxide species [Duran 2002; Solomon 1996]. This is activated for further oxidization to generate the native intermediate which is more appropriately described as a hydroxide product bridging the T2 and one of the T3 coppers in the trinuclear copper cluster. Solomon *et al.* pointed to the fact that the rate limiting step could be found in the reaction sequence in the molecular mechanism of the 4 e^- reduction of oxygen to water by laccase [Solomon 1996]. The enzyme binds one dioxygen and one water molecule prior to the formation of bound peroxide-level intermediate. Reduction of oxygen by laccase appears to occur in two $2e^-$ steps. The first is rate-determining and the second is fast [Liu 2007; Xu 1999]. In this T3 bridging mode for the first $2e^-$ reduced (oxidization of T3 coppers), the peroxide-level

intermediate would facilitate the second $2e^-$ reduction (oxidization of T1 and T2 coppers) in that the peroxide is directly coordinated to reduce T2, and the reduced T1 is coupled to the T3 by the covalent Cys-His linkages.

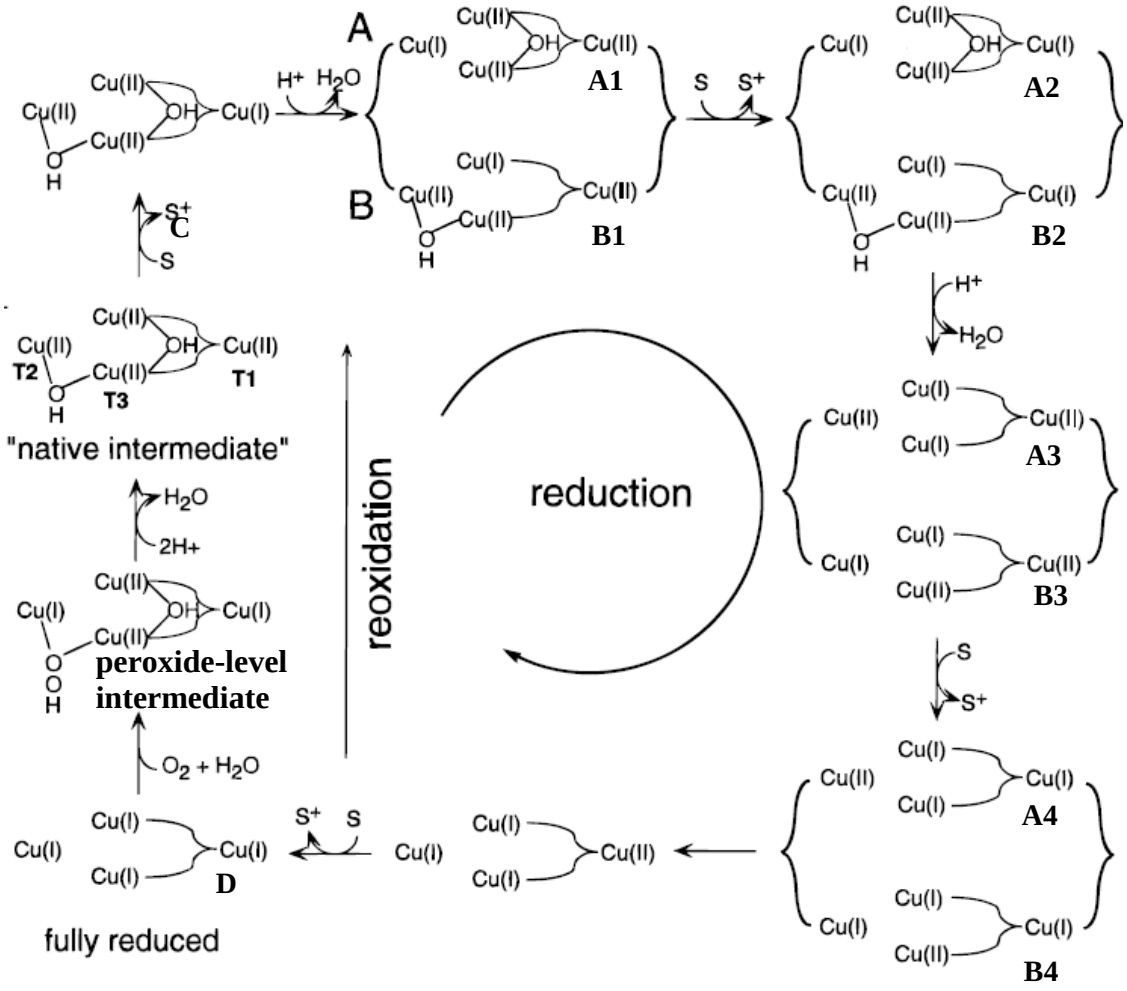

Figure 2. 33 Catalytic cycle of laccase shows the proposed mechanisms for the reduction and reoxidation of the copper sites (S stands for substrate) [Duran 2002; Solomon 1996].

The redox potential of the T1 copper-site has been determined using potentiometric titrations with redox mediators for a great number of different laccases and varies between 420 and 790 mV (vs. Standard Hydrogen Electrode (SHE)) [Call 1997; Reinhamm 1970; Xu 1999]. The catalytic efficiency depends on the redox potential of the T1 site [Duran 2002], which suggests that higher potential of the T1 site will result in higher catalytic efficiency. Therefore, from an electrochemical point of view, all laccases can be divided into three groups depending on the potential of the T1 site: low,

middle and high potential laccases. **Table 2. 7** shows potentials of sites of laccases from different sources. The low potential group includes laccases from trees, e.g., *Rhus vernicifera* [Reinhamm 1970]; the middle group includes laccases from basidiomycetes, *Rhizoctonia solany* [Xu 1999], and *Coprinus cinereus* [Yaropolov 1994]; The high potential laccases include *Trametes* (*Polyporus. Coriolus*) *hirsute*, *T. versicolor*, *T. villosa* [Christenson 2004; Reinhamm 1970]. Thus, laccase from *T.versicolor* is chosen as enzyme in this project to obtain the higher catalytic efficiency.

Table 2. 7 Potentials of sites of laccases from different sources.

Active sites	Low potential laccase(vs.SHE) (mV)	Middle potential laccase(vs.SHE) (mV)	High potential laccase(vs.SHE) (mV)
T1	420 ~ 450	470 ～710	780
T2	390	-	-
T3	450	-	785

2.4.3.2 Immobilization of laccase

The methods used in the immobilization procedures greatly influence the bioactivity of the resulting biocatalyst. This implies that the immobilization strategy may differ for different enzymes. They include several parameters such as overall catalytic activity, effective kinetics of the catalysis, and cost. Also toxicity of immobilization reagents should be considered in connection with the immobilization process, waste disposal and final application of the immobilized enzyme catalyst [Arica 2000; Messing 1975; Zaborsky 1974]. Therefore, a proper immobilization method is important to affect the activity of the immobilized enzyme.

Laccases from different sources have different immobilization methods. For example, the laccase from *Polyporus versicolor* is immobilized by entrapment and adsorption on several carriers (i.e., gelatine, polyurethane and a metal-chelate affinity matrix) and used for different purposes [Arica 2000]. Laccases from *Coriolus versicolor* entrapped in calcium alginate gel beads or covalently immobilized on activated carbon are used in the treatment of effluents from the pulp and paper industry [Freire 2001]. The two methods (cross-linking and covalent bond) are used to immobilize the enzyme on the

activated carbon [Duran 2002]. Laccase immobilized on diimide-activated carbon shows a considerably higher activity and is used in large batches for both batch and reactor experiments [Davis 1992]. For the laccase from *Pyricularia oryza*, the enzyme can be linked by covalent bond to sugar carriers (e.g. CH-sepharose 4B), by adsorption, followed by treatment with GLUTAL, on both silica gel and florisil, by entrapment and by radiation polymerization on colloidal silica [Duran 2002].

Apart from the fungal laccases mentioned above, laccase from *T.versicolor* is extensively studied for several years because it has the high-potential T1 site. **Table 2. 8** reports this kind of laccase immobilized on different supports by different methods. The type of its supports and methods of immobilization used are specified in the catalytic process. Many researchers reported that glass beads activated with APTES and GLUTAL immobilized *T. versicolor* laccase in literature [Christenson 2004; Duran 2002; Liu 2007]. The reports show a very good immobilizing capability of retained activity (90%). Leonowicz also reported that a specific activity of immobilized enzyme higher than that of the free enzyme was also observed [Leonowicz 1988]. Laccase from *T.versicolor* is often immobilized for possible use as a biosensor. Biosensors are prepared on different pre-treated carbon fibres and utilizing different methods. For example, covalent binding of laccases onto the surface of glassy carbon electrode using polyethylene bis-glycidyl ether as a redox polymer linker [Leech 1998]. Freire *et al.* reported that the laccase from *T.versicolor* was immobilized by physical adsorption, carbodiimide coupling, GLUTAL activation, and combined use of carbodiimide and GLUTAL. They found that the carbodiimide/GLUTAL procedure gave the best results and the percentage of GLUTAL was the most important influencing parameter; 10% GLUTAL shows the most sensitivity for fungal laccase immobilization [Freire 2001].

Though it is advantageous, the immobilization will lead to a number of adverse effects degrading the activity of the enzymes. Compared with the native enzyme, the immobilized enzyme shows reduced activity and a higher Michaelis-Menten constant (K_m) [Jiang 2005; Quan 2004; Zawisza 2006]. These alterations result from structural changes introduced to the enzyme by the applied immobilization procedure and from the creation of a microenvironment in which the enzyme works, different from the

bulk solution. The latter is strongly dependent on the reaction taking place, the nature of the support and on the design of the reactor. Therefore, the stable immobilization of enzymes on substrate with complete retention of their bioactivity is a crucial problem for practical commercial applications.

Table 2. 8 Laccase from *Trametes versicolor* immobilized on different supports [Duran 2002].

Support	Immobilization	Reference
Self-assembled monolayers	Covalent bonding	[Leonowicz 1988]
Sepharose CL-6B	Adsorption	[Milstein 1989]
Porous glass (activated)	Covalent-APTES-GLUTAL	[Rogalski 1991]
Redox hidrogel eletrode	Adsorption	[Leech 1998]
Hydrophilic PVDF, microfiltration membrane	Covalent bonding	[Jolivalt 2000]
Carbon-fibers microelectrodes	Adsorption, cross-linking, covalent bonding	[Freire 2001]
Polyacrilamide gel 80%	Entrapped	[Osiadacz 1999]

2.5 Applications of Self-Assembled Monolayers

The applications of self-assembled monolayers in materials are very diverse, ranging from the preparation of surfaces for protein and devices for nanoelectronics to strategies for biomimetic material synthesis. Protective coatings are ‘passive’ applications of SAMs. One example is their use for corrosion protection of copper [Scherer 1997]. SAMs can also be employed for mechanical protection of surfaces. Depalma *et al.* modified iron and steel surfaces with SAMs to make them more ‘resistant’ to aqueous environment [Depalma 1989]. SAMs coatings on engineering metals has also been discussed by Van Alsten [Van Alsten 1999]. Variation of the reactive groups (hydrophilic or hydrophobic) leads to control of the wetting properties of surfaces. In particular, mixed SAMs are attractive, since these allow for a continuous change of the contact angle as a function of relative concentration [Mandler 1996; Tao 1994]. SAMs represent an attractive alternative to these lubricants because of their strong adsorption to the surface; i.e., they are expected not to migrate on the

surface and not to transfer from one solid surface (e.g., the magnetic disk) to the other (e.g., the magnetic head) [Xiao 1996]. Due to the reaction between the $–NH_2$ and CO_2, the $-NH_2$ as a functional group in SAMs is able to capture CO_2 to reduce the influence of global warming of the planet.

The biomimetic environment of SAM surface renders noble metal surfaces suitable substrates for biomolecular immobilization, e.g. for biofuel cells and bioelectronics applications (**Figure 2. 34**). For example, the affinity of thiols for gold surface makes alkanethiols ideal for the preparation of modified electrodes. The well ordered monolayers formed by alkanethiols on gold can be used to immobilise enzyme close to an electrode surface with a high degree of control over the molecular architecture of the recognition interface [Creager 1995; Imamura 1995; Gooding 1999]. As a consequence of this ability, SAMs have been used for the fabrication of a variety of biosensors including immunosensors [Jones 1998], for DNA hydridisation biosensors and enzyme biosensors.

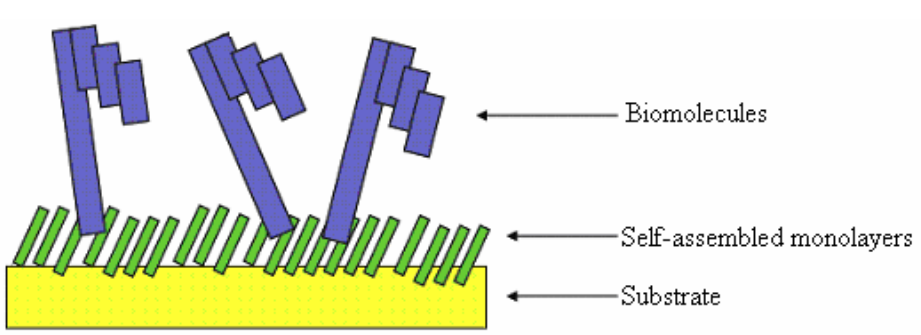

Figure 2. 34 Example for SAM-based biointerfaces, involving both components for specific adsorption of proteins and components for avoiding unspecific adsorption.

Deposition of SAMs is very versatile, and several studies have shown possible directions of bio-compatible applications [Nyquist 2000; Wirth 1997]. They have been used to modulate the nucleation and growth of minerals [Zhu 2002], promote the attaching and spreading of neurons [Kleinfeld 1988], fix antigen / antibody [Chowdhury 1998], attach peptides to promote cell adhesion [Kam 2002], immobilize heparin and hyaluronate to enhance biocompatibility [Chen 2004]. Generally, SAMs form the link between organic and inorganic matter to modify material interface.

2.5.1 SAMs on bone implant materials

The world wide orthopaedic implant and equipment market is $22 billion in 2007 [Stryker 2008]. In fixing bone fracture and treating bone diseases, traditional synthetic materials such as metals, ceramics and polymers are used to repair load-bearing bones. Among these biomaterials, titanium and its alloy exhibit favourable biocompatibility and mechanical properties for applications as surgical implants, as well as non-load bearing situations, such as facial bone reconstruction [Liu 2004]. However, Ti and its alloys do not bond to bone within the first 6 months after implantation [Oji 1999]. Therefore, various methods have been employed to introduce hydroxyapatite (HA, $Ca_{10}(PO_4)_6(OH)_2$) or calcium phosphate (CaP) coatings onto Ti and its alloys implant surfaces to improve biocompatibility and accelerate their integration with natural bone matrix. The existing techniques for making CaP layers (e.g. thermal spraying, sputter coating, dip coating, sol-gel and electrophoretic deposition), still have an issue of lack of biological and chemical bonding between Ti implant surface and the natural bone [Ratner 1993]. In order to target the above problem, it is essential to know basic compositions of natural bone. With an understanding of the process of bone biomineralization, the properties of CaP and surface modification methods for CaP deposition will be introduced below.

2.5.1.1 Bone biomineralization in vivo

Bones of the skeletal system differ greatly in size and shape from person to person, but both compact and cancellous bones have a very similar basic composition, which is composed of collagen (organic phase) and inorganic salts (inorganic phase) [Currey 2002; Olszta 2007]. Collagen gives bone its strength and resilience, whereas inorganic salts make it hard and resistant to crushing. These two phases have multiple components which consist of minerals, collagen, water, non-collagenous protein, lipids and cells [Williams 2004]. An overall composition of the bone is given in **Table 2. 9**. The inorganic phase of bone, also called bone mineral, is mainly composed of HA crystals that account for 69% of the weight of the bone [Van Blitterswijk 1986]. The organic phase is composed mainly of a protein, type I collagen. In bone, collagen acts

as a structural framework in which plate-like tiny crystals of HA are embedded to strengthen the bone [Currey 2002].

Table 2. 9 Composition of Bone [Park 1984].

Inorganic phase	wt%	Organic phase	wt%
Hydroxyapatite	~ 69	**Collagen**	~ 20
Carbonate	~ 4	**Water**	~ 9
Citrate	~ 0.9	**Non-collagenous proteins**	~ 3
Sodium	~ 0.7	**Other trace:lipids, cytokins**	--
Magnesium	~ 0.5	**Primary bone cells: Osteoblasts, osteoclasts, osteocytes**	--
Other traces: Cl^-, F^-, K^+, Zn^{2+}, Cu^{2+}, Fe^{2+}, Sr^{2+}, Pb^{2+}	--		

Bone is a hierarchically structured composite material. An excellent review was provided by Weiner and Wagner, who broke down the structure of bone into seven levels of hierarchy [Weiner 1998]: nanoscale platelets of HA are oriented and aligned within self-assembled collagen fibrils; the collagen fibrils are layered in parallel arrangement within lamellae; the lamellae are arranged concentrically around trabecular network of microporous bone, as spongy or cancellous bone. Therefore, the mineralization of the bone occurs predominantly extracellularly within a matrix supersaturated with respect of calcium and phosphate, and then mineral of calcium phosphate is deposited on collagen.

From the above process, there are two necessary requirements for bone mineralization: one is matrix with collagen and another one is inorganic phase of calcium and phosphate. The collagen fibrils in the bone are secreted by osteoblasts. They assemble into a highly organized, close-packed lamellar structure [Glorieux 2000]. The collagen alone took many years to resolve, and various permutations models are accepted as providing a reasonable description of the fibrillar organization. A schematic structure of collagen molecules is shown in **Figure 2. 35**. The repetitive nature of the amino acid sequences of collagen allows the protein to assemble into triple helical structures, referred to as tropocollagen molecules, where many $-NH_2$, -COOH, -OH groups are

exposed out the surface. Interactions between tropocollagen units leads to self-organization into fibrillar structures in the microfibril [Veis 1970]. Type-I collagen, the primary constituent of bone tissues, assembles its tropocollagen units in a quarter-staggered array, which leads to hole and overlap zones. The quarter-stagger arrangement leaves a regular array of 40 nm gaps within each periodic unit, and these are reportedly and the locations where crystal nuclei of mineral phase are first observed in systems [Christoffersen 1991]. When hydroxyapatite crystals embed within the collagen and then encases the self-assembled fibrillar collagen, the high degree of mineral phase is forming by intrafibrillar mineralization. According to the mineralization process in bone, self-assembled monolayers with functional groups as a biomimetic coating method for implant surface modification, are given much attention recently. SAMs are not only for the design of biomimetic materials with bioactive molecules such as growth factor, but also can build a three dimensional biomimetic scaffold to direct new bone formation on the surface by deposition of CaP.

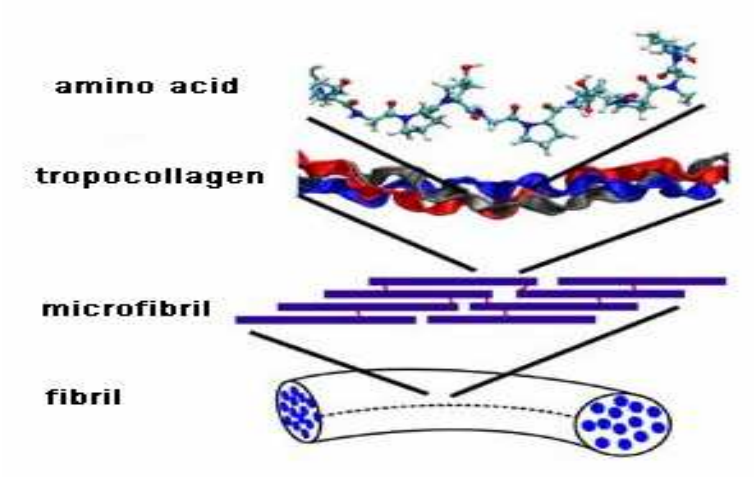

Figure 2. 35 Schematic structure of collagen molecules (tropocollagen), microfibril and fibril [Veis 1970].

Calcium and phosphate crystals as calcium apatite, not unlike the organic matrix organization, remain a central part of the mineralization process. These crystals are composed of a specific amount of calcium, phosphate and carbonate in a ratio that is critical to the process of mineralization [Rey 1995; Sauer 1988]. During the early phases of this process, a Ca-P solid phase is produced which is amorphous rather than crystalline. With maturation, crystalline development occurs. Most of the initial crystals deposited in the newly developed collagen microfibrils are located in hole

zones between connecting microfibrils. Further calcification occurs both by primary heterogeneous nucleation and by secondary and tertiary nucleation from crystals already formed and propagated in the collagen pores [Glimcher 1968]. In addition, collagen fibrils expand in the regions of the hole zones, permitting additional deposition of crystals. Eventually, all the available space within the fibril becomes a continuous hard substance.

The amorphous calcium phosphates do not have a rigidly defined chemical composition. The molar Ca/PO_4 ratios are found to vary from 1.44 to 1.55 [Rey 1995]. Hydroxyapatite crystal forms a simple hexagonal lattice, the atomic contents of which is given by the formula $Ca_{10}(PO_4)_6(OH)_2$. Olszta *et al.* found that the Ca/P molar ratio ranged from 1.37 to 1.71. The ratio was age-dependent, with the lowest values being obtained for the bones of children and the elderly [Olszta 2007].

2.5.1.2 Calcium phosphate deposition on Ti-based implant

Titanium as bioinert material provides a limited response to surrounding tissue and a thin fibrous capsule will be formed around the material [Liu 2004]. In other words, titanium after implantation does not bond directly to bone resulting in loosening of the implant and undesirable movements at the implant-tissue interface results in failure cracks of the implant. So far, much work has been devoted to the improvement of biocompatibility of titanium surface. One of them is to coat a bioactive material on the surface, such as calcium phosphate [Brunette 2001]. Calcium phosphate coatings have been widely used as bioactive materials that have been shown experimentally to promote early bone apposition on the surface of metallic implants [Dlecrin 1994; Maxian 1993]. Therefore, the application of bioactive coatings to titanium and its alloys will enhance the bonding of Ti-based implants to the existing bone via formation of an apatite layer on their surfaces [Murai 1996], resulting in significantly better implant lifetimes than can be achieved with materials in use today. The current methods used for calcium phosphates coatings on metallic implant substrates include plasma spraying, sputter coating [Ding 1999, 2003; Wolke 1994], chemical vapour deposition, alkaline etching, sol-gel coating [Chai 1998; Manso 2002], electrophoretic deposition [De Sena 2002; Han 2001; Manso 2000] and biomimetic coating

[Habibovic 2002; Oliveira 1999; Yang 2005]. The advantages and disadvantages for each coating method are discussed below in **Table 2. 10**. However, these processes mentioned above have limitations associated with their applications, including high temperatures and multistep, which prohibit for incorporation of biological molecules. Furthermore, many of these techniques cannot be applied to complex shapes and/or porous implants. Biomimetic coating can overcome these drawbacks and be mimicked in vitro to prepare calcium phosphate layers on implants surfaces by immersing the implant substrates at low temperatures in aqueous solutions.

A self-assembled monolayer technique as biomimetic coating, allows for the systematic modification of surface chemical properties, and has advantages over conventional methods of calcium phosphate deposition. Traditional coating methods often clog or fill the implant porosity after coating on porous substrates, but self-assembled method does not. Moreover, this method is very easily adaptable to most implant materials and does not need specialty equipment---lower coating costs. SAMs with highly ordered structure can incorporate a wide range of groups both in the alkyl chain and at the reactive group due to low-temperature process. Molecules are self-assembled on the surface, so the structure of SAMs is more like that of collagen in nature bone and biomineralization will be easily happened on the surface with SAMs.

Different researchers obtain different results about the inducibility of calcium phosphate by functional groups in SAMs. For example, Majewski and Allidi found that the –SOOH functionalized SAMs have better inducibility of CaP compared with the –NH_2 and -SH [Majewski 2006]. Zhu *et al.* reported that SAMs with OH groups show the best inducibility of CaP [Zhu 2002]. Moreover, they observed that the -NH_2 functional groups cannot induce CaP in simulated body fluid (SBF), pH 7.2 ~ 7.4, while it can do in SBF, pH 7.6 [Zhu 2004]. However, Toworfe *et al.* reported that the –NH_2 functional groups have inducibility of CaP in SBF, pH 7.4 [Toworfe 2006]. Therefore, it is still a debate whether the SAMs with the –NH_2 functional group can induce calcium phosphate in SBF solution.

Table 2. 10 Different techniques to deposit HA coatings [Hench 1997; Li 1996; Li 2002; Liu 2001; Liu 2002; Mavis 2000; Ong 1994; Yang 2005; Zhitomirsky 2000].

Technique	Thickness	Advantages	Disadvantages
Thermal spraying	30-200 µm	High deposition rates; low cost	Line of sight technique; high temperatures induce decompositions; rapid cooling produces amorphous coatings
Sputter coating	0.5 – 3 µm	Uniform coating thickness on flat substrates; dense coating	Line of sight technique; produces amorphous coatings
Dip coating	0.05-0.5 mm	Inexpensive; coatings applied quickly; can coat complex substrates	Requires high sintering temperature, thermal expansion mismatch
Sol-gel	< 1 µm	Can coat complex shapes; low processing temperature; relatively cheap as coatings are very thin	Some processes require controlled atmosphere processing; expensive raw materials
Electrophoretic deposition	0.1-2.0 mm	Uniform coating thickness; rapid deposition rates; can coat complex substrates	Difficult to produce crack-free coatings; requires high sintering temperatures
Biomimetic coating	< 30 µm	Low processing temperatures; can form bonelike apatite; can coat complex shapes; can incorporate bone growth stimulating factors	Time consuming; Requires replenishment and a constant of pH of simulated body fluid

2.5.2 SAMs for immobilization of biomolecules

2.5.2.1 Introduction of biomolecules immobilized by SAMs

The immobilization of biomolecules, in particular for proteins and enzymes, onto solid supports is fundamental in the development of advanced biosensors, bioreactors, affinity chromatographic separation materials and many diagnostic techniques. So far,

different methods have been investigated to increase the adhesion of individual molecules to a surface, including modifications of the substrate surface, e.g. surface charges, surface functionalization, surface porosity and particle size [Clarke 2006; Kasemo 1986]. Among the methods mentioned above, the functionalization of the surface with self-assembled monolayers is a popular method for the physical and chemical immobilizations of biomolecules, especially for enzymes. **Table 2. 11** shows biomolecules immobilized on substrates by different SAMs.

Table 2. 11 Biomolecules immobilized by different SAMs on substrates.

Biomolecules	Molecules of SAMs	References
Nucleotides	3,3'-dithiopropionic acid	[Okahata 1998]
Glucose oxidase	3-mercaptopropionic acid	[Gooding 2001]
Bovine serum albumin	16-mercaptohexadecanoic acid; 16-mercaptohexadecanol; 2-aminoethanethiol	[Silin 1997]
Immunoglobulin G		
Catalase	11-mercaptoundecanoic acid (11-MUA)	[Patel 1997]
Poly(L-lysine)hydrobromide	11-MUA	[Brian 1996]
Horseradish peroxidase	Cystamine & Thioctic acid	[Mendes 2008]
Laccase	11-MUA	[Quan 2004]

Lisdat and co-workers used the layer-by-layer self-assembly technique to immobilize cytochrome *c* (cyt *c*) and bilirubin oxidase (BOD) on gold electrodes with the self-assembled MUA layer and polyelectrolyte network [Lisdat 2009]. Due to the electroactive cyt *c*, a direct protein-protein electron transfer is achieved, although proteins and enzymes are assembled in complexes on electrodes, as shown in **Figure 2. 36**. This design does not need a redox mediator and the electrode facilitates the electron transfer from the electrode via multiple protein layers to molecular oxygen resulting in a catalytic reduction current.

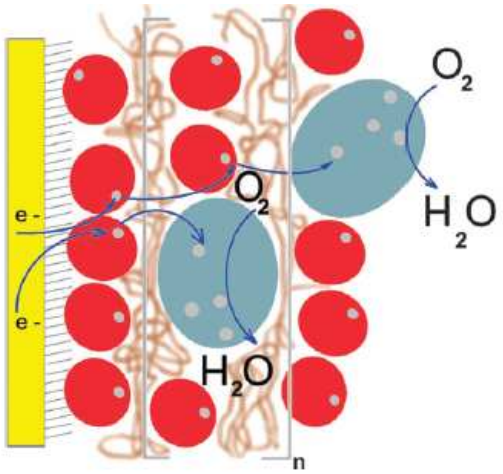

Figure 2. 36 Schematic illustration of the cyt *c*/BOD assembly on gold electrode with MUA and electron transfer: red circles = cyt *c*, blue shapes = BOD enzyme, brown lines = polyelectrolyte network, arrows indicate electron transfer pathways between cyt *c* and BOD within the polyelectrolyte network and the four-electron oxygen reduction process [Lisdat 2009].

The SAMs can be tailored to present a hydrophobic or charged surface, hence enabling hydrophobic or electrostatic interactions with molecules by physical methods. For chemical immobilization of proteins onto the SAMs, the general procedure involves the formation of either a disulfide or an amide by the covalent bond. For example, the immobilization of enzymes on the surface of electrodes modified with SAMs provides a number of advantages as a method for the fabrication of enzyme electrodes. Using SAMs has the potential to provide enzyme electrodes with a high degree of reproducibility, molecular level control over the spatial distribution of the immobilized enzymes and the immobilization of the enzyme close to the electrode thus allowing direct electron transfer to be achieved. These advantages have resulted in a recent surge in research into self-assembled monolayers for biosensor and electrochemical applications in general, and enzyme electrodes in particular [Blanford 2007; White 2000; Quan 2004].

2.5.2.2 Introduction of enzyme-based biofuel cells

The enzyme electrode mentioned above can be used for biosensors, bioanalysis, nanobiotechnology, etc [Hanefeld 2009]. Today, one of major applications of the enzyme electrode is biofuel cells, which are able to directly transform chemical to electrical energy via electrochemical reactions involving biocatalysts, either

biomolecules (enzymes) or whole living organisms (bacterial) [Palmore 1994]. Biofuel cells are highly renewable, and capable of using naturally available biomass as fuel, which are excellent alternative compared with conventional fuel cells and batteries are plagued by non-renewability, non-implantability, size/weight, operating conditions (high temperature, acidity and toxicity) and waste issues [Bullen 2006].

The first discovery of the connection between biology and electricity has been known from the experiments of Galvani in the 1780s, when it was discovered that the current from a static electricity generator could cause a severed frog's leg to twitch, revolutionising the understanding of the nervous system [Trevan 1980]. The expansion of interest in fuel cells triggered by the USA space program, in the late 1950s and early 1960s, lead to the development of microbial biofuel cells as a possible technology for a waste disposal system for space flights that would also generate power [Katz 1999]. Also in the late 1960s, the biofuel cell using cell-free enzyme systems began to be used, with the early goal of a power supply for a permanently implantable artificial heart [Bullen 2006]. Presently there are two practically applied systems by biofuel cells: a test rig operating on starch plant wastewater, which has been operating for at least 5 years has been demonstrated as a bioremediation method [Gil 2003] and as a biological oxygen demand sensor. The most obvious target for biofuel cell research is still for applications where the fuel used could provide higher voltage with a long-term or even permanent power supply for such devices.

According to the source of the biocatalysts, biofuel cells can be divided into two categories: Microbial and Enzymatic fuel cells. Microbial fuel cells (MFCs) are devices that use living organism (e.g. bacteria) as the catalysts to oxidized organic and inorganic matter and generate current [Logan 2006]. Electrons produced by the bacteria from these substrates are transferred to the anode and flow to the cathode, which are usually capable of oxidizing the substrate completely to carbon dioxide and water. For example, bacteria in the anode compartment transfers electrons obtained from an electron donor (glucose) to the cathodic electrode, as shown in **Figure 2. 37**. During electron production protons are also produced in excess. These protons migrate through the cation exchange membrane into the cathode chamber, which will react with the final electron acceptor-oxygen to produce water.

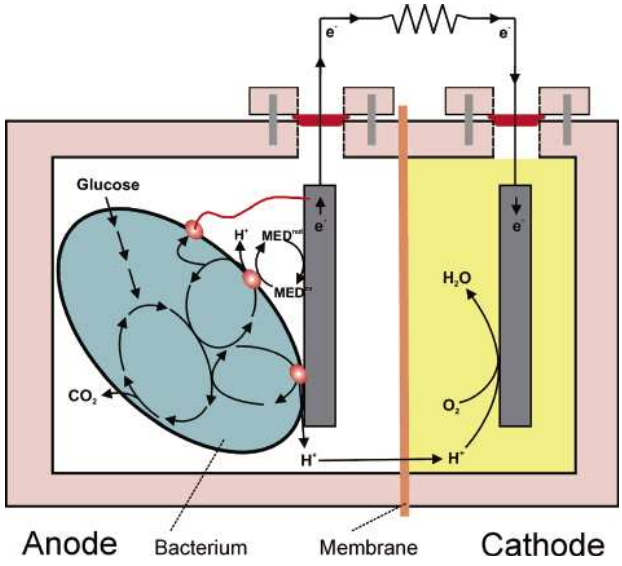

Figure 2. 37 Operating principles of a MFC [Logan 2006].

The MFCs are successfully applied in wastewater treatment, but it depends on the concentration and biodegradability of the organic matter in the influent, the wastewater temperature, and the absence of toxic chemicals [Bullen 2006; Palmore 1994]. Moreover, carbon dioxide will be produced in the microbially catalysed system leading global warming. Therefore, the enzymatically catalysed system is developed using biological molecules as catalysts for achieving their redox reaction, either purified enzymes or enzyme derivatives to catalyse a specific reaction [Bullen 2006]. For example, **Figure 2. 38** shows the configuration of the biofuel cell element with two enzyme electrodes: the anode is functionalized by a surface reconstituted glucose oxidase, and the cathode is presented by the reconstituted cytochrome *c*/cytochrome oxidase couple. At the GO_x functionalized electrode, glucose is oxidized to gluconic acid by bio-electrocatalysis, resulting in electrons moving from the anode to cathode electrodes, whereas at the Cyt.*C* | CO_x layered electrode, the reduction of O_2 to water takes place by receiving the electrons. Since the current occur between the electrodes by the movement of the electrons, it is successfully transforming from the chemical to electrical energy.

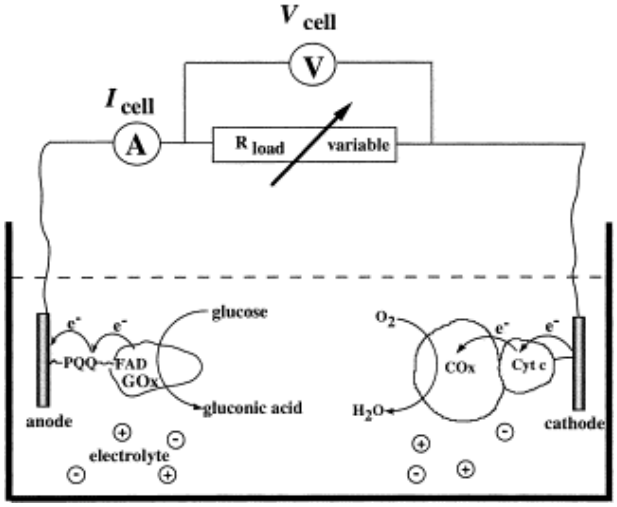

Figure 2. 38 Schematic configuration of a biofuel cell employing glucose and O_2 as a fuel and an oxidizer, respectively, and PQQ-FAD | GO_x and Cyt. *C* | CO_x-functionalized electrodes as biocatalytic anode and cathode, respectively [Bullen 2006].

In order to study the enzymatic fuel cells, the electrochemistry method is normally chosen to evaluate the catalytic activity of the enzyme. Generally, electrons can transfer between the reaction site and the electrode via a direct electron transfer between the reaction site and the electrode or via a mediator molecule that repeatedly cycles [Bullen 2006], which can be divided into direct electron transfer (DET) and mediated electron transfer (MET). The DET is covering only systems where the electron tunnels directly from the active site fixed in the enzyme to the electrode. The very first reports on DET with a redox active protein were published in 1977 when Eddowes and Hill showed that cytochrome *c* on the bipyridyl modified gold with reversible electrochemistry [Eddowes 1977]. Due to realizing electron transferring between enzymes and an electrode is an indirect, the MET is using a small redox molecule serving as an electron transfer mediator and encompassing all forms of regenerative mediation whether diffusive or non-diffusive [Barton 2004]. However, most of the redox enzymes, lack direct electrical communication with electrode supports, and various electron mediators were used to contact the biocatalyst electrically with the electrode [Katz 1999]. So far, the methodology based on the application of purified redox enzymes for the reduction of specific fuel and oxidization of substrates at the electrode supports and the generation of the electrical current output is more successful for the development of biofuel cells. Recent examples of biofuel cells devices employing purified enzymes are summarised in **Table 2. 12**.

Table 2. 12 Summary of enzymatic bioelectrochemical devices [Bullen 2006].

System (oxidation/reduction)	Bio-catalysts	Electrodes	Current density ($\mu A\ cm^{-2}$)
MET CH_3OH to CO_2, reducing NAD^+, NADH reducing BV^{2+}, BV^+/oxygen	ADH, AldDH, FDH and diaphorase	Graogute okate abidem platinised platinum gauze cathode.	2.6
H_2/MET O_2	-/laccase	Platinum gauze anode, either glassy carbon or platinum foil cathode.	0.12
MET glucose or hydrolysed corn syrup/MET H_2O_2	GO_x/HRP	GO_x/ferrocene-modified graphite anode, the same matrix on cathode.	0.00594
MET glucose/ MET O_2	GO_x/laccase	Carbon fibre electrodes. Anode has GO_x with redox polymer. Cathode has laccase with redox polymer.	0.36
MET glucose/O_2	GO_x/laccase		0.45

However, enzyme-based electrodes in biofuel cell exist a number of practical problems in the use of enzymes: the instability of their structures once they are isolated from their natural environments to results in less catalysis activity, and their sensitivity both to process conditions other than the optimal ones and to trace levels of substances that can act as inhibitors. The latter two result in enzymes' short operational lifetimes. In the system of the enzymatic fuel cells, the major barrier to any successful application is component lifetime, particularly in view of the limited enzyme lifetime and problems of electrode fouling/poisoning.

2.5.2.3 Laccase-based biofuel cells

Laccase (EC 1.10.3.2) is a multi-copper oxidase that catalyzes the reduction of O_2 to water through receiving four electrons, so it is immobilized on an electrode as the cathode [Baldrian 2006]. Recently, the electroreduction of oxygen and electron transport were studied in the system of the oxygen-laccase-electrode with various sources of laccases. The achievement of a DET between electrodes and enzymes is a breakthrough, providing a simply and efficient way with signal transduction. DET avoids the use of redox mediators, reducing potential interferences and side reactions,

as well as being more compatible with *in vivo* conditions. The first publication on DET for a redox laccase was from the *T.versicolor* with high potential [Tarasevich 1979]. The authors showed that the laccase modified carbon electrode exhibited DET in the presence of the molecular oxygen. They also found that the redox potential shifting from 30 to 380 mV, was dependent on the electrode material, its method of preparation and immobilization methods. The DET for the native laccase from *T.hirsuta* at the highly ordered pyrolytic graphite was studied by cyclic voltammograms [Christenson 2004], as shown in **Figure 2. 39**. It obviously shows the catalytic current when the laccase on the electrode reacts with the oxygen.

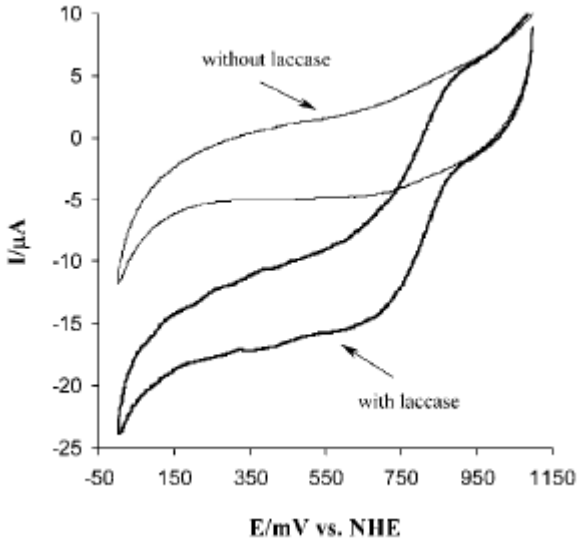

Figure 2. 39 Cyclic voltammograms of laccase absorbed on highly ordered pyrolytic graphite, 0.1 M phosphate buffer pH 6.5 with air-saturated oxygen. Scan rate 10 mV/s [Christenson 2004].

Lee and co-workers immobilized laccase from *Polyporous versicolor* on the pyrolytic graphite electrode by the physisorption, and found that the reduction proceeded quantitatively to water at potential as positive as ca. 0.5 V vs. sodium chloride saturated calomel electrode (SSCE) [Lee 1984]. The catalytic activity of the enzyme is greatest between pH 3 and 4. Shleev and co-workers entrapped the Lac from different sources, such as *Trmetes ochracea*, *Cerrena maxima*, *Coriolopsis fulvocinerea* and *Cerrena unicolor* under a dialysis membrane at spectrographic graphite electrodes, respectively [Shleev 2005b]. They found the DET from the laccase on the electrode by cyclic voltammetry at potentials of oxygen electroreduction from 800 to 740 mV vs. NHS, as shown in **Figure 2.40**.

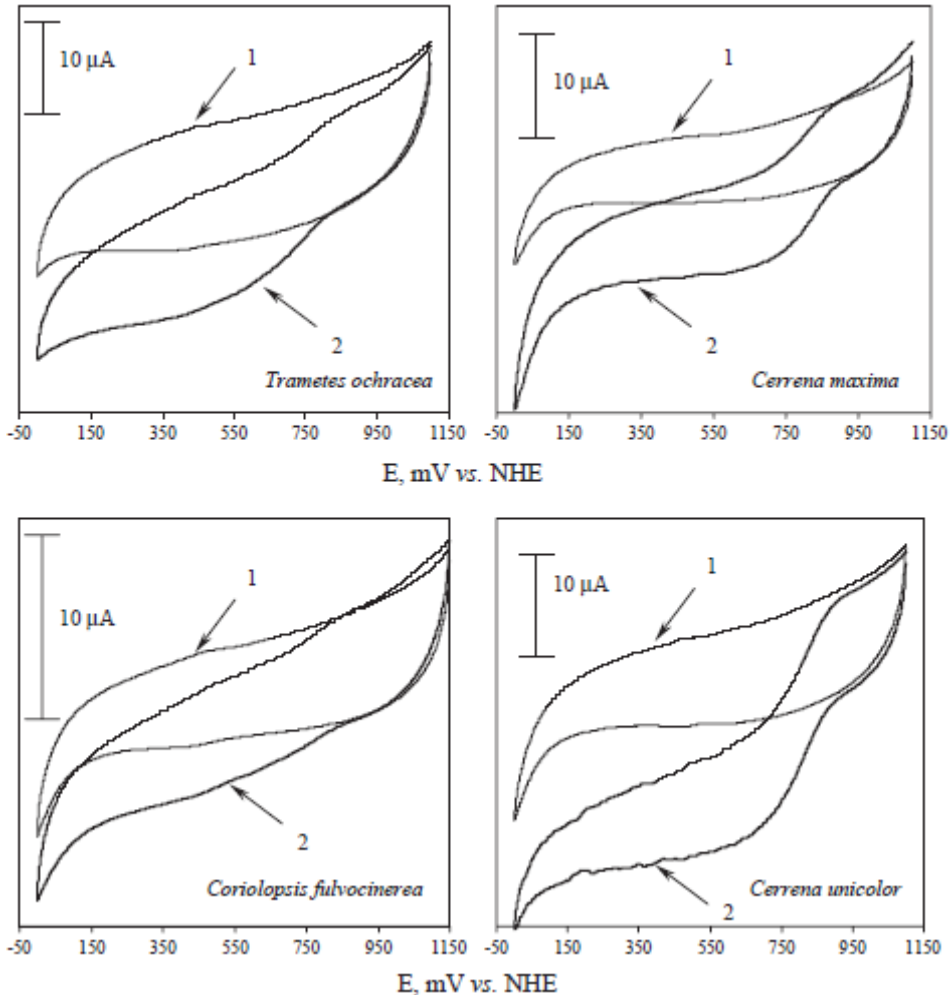

Figure 2. 40 Electroreduction of molecular oxygen on: (1) naked spectrographic graphite; (2) electrodes modified with adsorbed laccases. Citrate-phophate buffer, 50 mM, saturated oxygen pH 3.0; ionic strength-100 mM $NaClO_4$; scan rate-10 mV/s [Shleev 2005b].

Direct electron transfer can avoid the use of redox mediators, reducing potential interferences and side reactions. However, it is not possible to obtain a stable response without the presence of excess laccase due to the weak bond at the electrode [Duran 2002]. Moreover, the catalytic current produced by the immobilized laccase is generally less 20 $\mu A/cm^{-2}$ in the O_2-saturated solution. Therefore, MET using redox molecule as mediator is developed to transfer electrons from the mediator to the enzyme. **Figure 2. 41** shows the principle of a mediator transferring electrons to the laccase reducing O_2 to water.

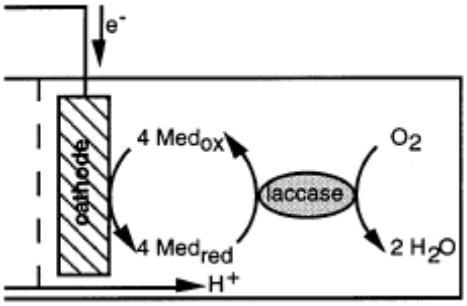

Figure 2. 41 Electro-enzymatic reduction of dioxygen to water using laccase and the mediator in the cathode of a biofuel cell [Palmore 1999].

There are six different commercially available mediators for the laccase, including the organic compounds 2,2'-azino-bis(3-ethylbenzthiazoline-6-sulphonic acid) (ABTS), syringaldazine, acetosyringone, promazine, hydroquinone and the inorganic compound ferrocyanide [Fernandez-Sanchez 2002]. They measured the catalytic activity of the physisorbed laccase on glassy carbon electrode and found that ABTS was chosen as the most suitable substrate for the laccase due to the better affinity between the enzyme and the mediator. Liu and co-workers entrapped the laccase on graphite electrode surface by nanotubes-ionic liquid gel and found that the laccase would reach the maximum activity at 70°C in the presence of ABTS [Liu 2007]. However, the stability of the electrode with the laccase is about 1-2 weeks. Zawisza *et al.* reported that the laccase immobilized in thin hydrophilic silicate gel on gold electrode, exhibited maximum activity in pH range 4.2 – 5.2 at temperature ranging from 40 to 50°C [Zawisza 2006]. Therefore, the mediated electron transfer can improve the catalysis of the enzyme, but the mediator still affect the lifetime of the immobilized enzyme.

2.5.2.4 Graphite as electrode for biofuel cells

So far, electrodes in biofuel cells are made of various materials, such as gold [Lisdat 2009; Shleev 2005a; Zawisza 2006], platinum[Quan 2004], graphite [Bourbonnais 1998; Christenson 2004; Fernandez-Sanchez 2002; Liu 2007; Shleev 2005b], TiO_2 nanotubes [Liu 2005]. Among above electrodes, graphite is a most popular material as electrode to be applied in bioelectronics devices, such as glassy carbon, pyrolytic graphite and activated carbon.

It is unique in that graphite has properties of both a metal and a non-metal. It is flexible but not elastic, has a high thermal and electrical conductivity, and is highly refractory and chemically inert. Moreover, graphite has a low adsorption of X-rays and neutrons making it a particularly useful material in nuclear applications [W7]. The unusual combination of properties is due to the crystal structure, as shown in **Figure 2. 42**. The carbon atoms are arranged hexagonally in a planar condensed ring system. The layers are stacked parallel to each other. The atoms within the rings are bonded covalently, whilst the layers are loosely bonded together by van der Waals forces.

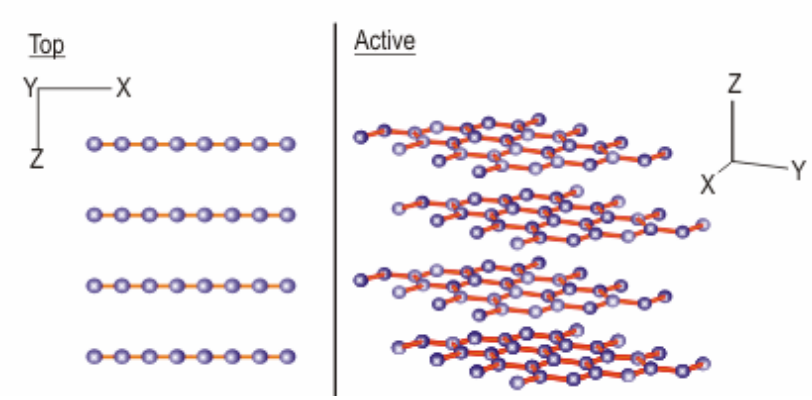

Figure 2. 42 Crystal structure of graphite [W7].

According to the above figure, graphite is composed of sheets of carbon atoms and each of these is bonded to only three atoms. This leads to the fourth valence electron of the carbon atom delocalized, which means it is free to move between the different sheets, therefore carrying the electrical charge through the network of carbon atoms which makes up the structure of graphite. Compared with other metal electrodes (e.g. gold and platinum), graphite is relatively cheap and a good conductor. Therefore, in this project, graphite is chosen as an electrode for the electrochemistry measurement of the immobilized laccase.

CHAPTER 3

EXPERIMENTAL METHODS

3.1 Materials and methods

3.1.1 Preparation of self-assembled films on titanium

3.1.1.1 Materials

Self-assembled films with the functional -NH_2 groups have been built as a bionic interface to investigate the thermodynamic and dynamic properties of some important biomolecules (especially proteins). Titanium and its alloys are most widely applied for biomedical materials because of its biocompatibility and high corrosion resistance. Therefore, titanium was selected as a support material for the fabrication of a well-defined biofunctional membrane with good coverage by the self-assembly method.

Table 3. 1 shows all of solvents and chemicals used during preparation of self-assembled films with the -NH_2 groups (also called APS film) on titanium. Since it is easily hydrolyzed by water and reacted with carbon dioxide, 3-aminopropyltriethoxysilane (APTES), together with as-received toluene, was stored in a glove box under argon. Hydrogen peroxide as received was stored in a refrigerator at 4°C. It is important to ensure a clean environment when preparing self-assembled film. Before use, all vials were soaked in a dilute hydroxychloride acid solution in a fume cupboard overnight, then washed again with the detergent and rinsed with deionized water (18.2 MΩ cm, Barnstead Easypure II) in order to remove potential organic and inorganic contaminants. Finally, these vials were dried in a vacuum oven for several hours and wrapped with foil for further use.

Table 3. 1 Solvents and chemicals used for preparing APS film.

Chemicals	Purity	Formula	Supplier
Commercially pure titanium	99.9%	Ti	
3-aminopropyltriethoxysilane (APTES)	99%	$(H_5C_2O)_3Si$-$(CH_2)_3NH_2$	Aldrich
Toluene	99.8% anhydrous	$C_6H_5CH_3$	Aldrich
	90% hydrous		
Hydrogen peroxide	30 wt.% A.C.S. reagent	H_2O_2	Sigma-Aldrich
Sulfuric acid	98%, Analytical reagent grade	H_2SO_4	VWR
Ethanol	96%, GPR	C_2H_5OH	VWR
Deionized water	18.2 Ω cm	H_2O	water purification from Fisher
Standard phosphate buffer pH 4, pH 7, pH 10	—	—	Acros Organics

3.1.1.2 Experimental procedure

Ti samples were firstly cut into approximately 10 ×10 ×1 mm^3 squares from a commercially pure titanium sheet (grade 4, 99.9%). The small piece of titanium sample was consecutively ground on silicon carbide papers of 600#, 1200# and 2400# (Struers), respectively, and subsequently polished using polycrystalline diamond pastes of 3, 1 and 0.5 µm (Buehler), respectively, in order to remove the native titanium oxide layer and create a flat surface. Each polished sample was placed in a clean vial and sonicated with ethanol and then deionized water, respectively. Each cleaning stage was repeated 3 times with a fresh solvent for 5 minutes. Finally, the samples were dried under argon-gas stream (BOC) and stored in a desiccator (Fisher) at room temperature.

Since ethoxy groups ($R\text{-}OC_2H_5$) in the APTES molecule is very easily hydrolyzed in water to produce hydroxyl groups (R-OH), the silanization process of titanium was carried out in a glove box under argon. The overall experiment of procedure is schematically shown in **Figure 3. 1**. Briefly, in order to form a uniform layer with -OH functional groups on the pretreated clean Ti surface, titanium samples were oxidized in a piranha solution (a mixture of sulfuric acid and hydrogen peroxide) as described in the following:

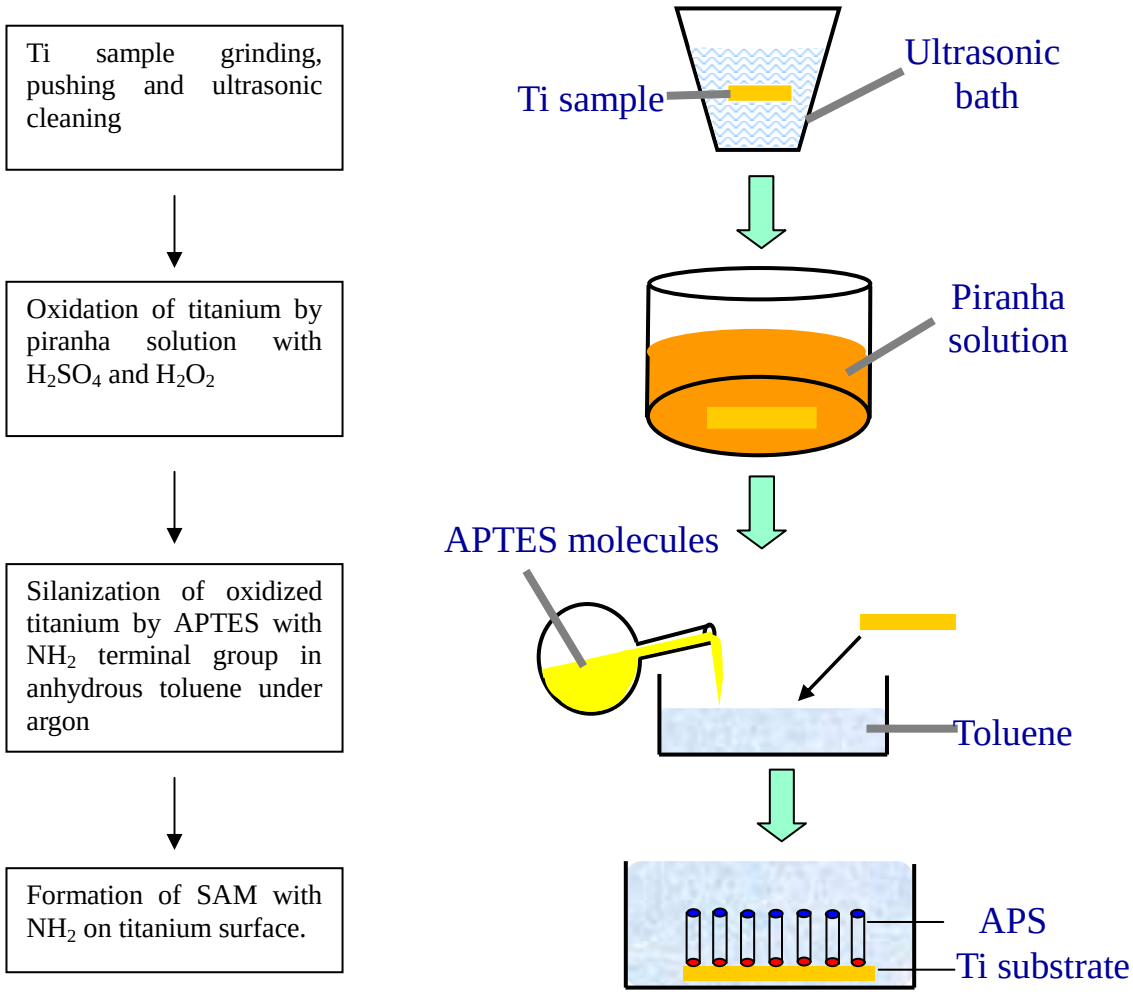

Figure 3. 1 Procedures of producing APS film on titanium.

Here a typical *Piranha* solution (20 ml) of H_2SO_4:H_2O_2 = 3:1 was used for the introduction of oxidation process. Firstly, H_2SO_4 of 15 ml was poured out into a small beaker in a fume cupboard. Then, H_2O_2 of 5 ml was added into the above container. After that, polished titanium samples were placed thoroughly into the *Piranha* solution for different time to form -OH groups on the titanium surface. Once cooling down, the *Piranha* solution was transferred into a closed glass container for waste storage. Titanium samples after oxidation were cleaned in an Ultrasonic bath (Fisher) with distilled water for three times, each lasting 3 minutes, in order to remove residuals of H_2SO_4 and H_2O_2. Finally, oxidized titanium samples were dried under dry argon stream, stored in a desiccator for the next step of silanization.

From the literature review, it is clear that different *Piranha* solutions have been used in the past under conditions. Therefore, it is important to clarify the effect of *Piranha* solution on the oxidation of titanium and the growth of SAMs. In order to obtain a clean and smooth TiO_x layer on titanium, the effects of different temperatures and immersion durations in the *Piranha* solution of H_2SO_4:H_2O_2 = 1:1 were studied (**Table 3. 2**). In order to investigate the effect of the *Piranha* solution on the formation of hydroxyl groups on titanium, polished titanium samples were cleaned and immersed in the solution with different ratios of H_2SO_4 to H_2O_2, from 1:3, 1:1, 2:1, 3:1 to 4:1, as shown in **Table 3. 3**.

Table 3. 2 Different temperatures and immersion durations used in 1:1 *Piranha* solution.

Temperature / Duration / Sample Code	Room Temperature	50°C	100°C
5 minutes	**S_{RT_5}**	—	—
15 minutes	**S_{RT_15}**	—	—
30 minutes	**S_{RT_30}**	**S_{50C_30}**	**S_{100C_30}**

Table 3. 3 Different oxidation solutions used at room temperature for 15 minutes during pre-treatment of titanium.

Sample Code	Piranha solution (20 ml)		Ratio of H_2SO_4: H_2O_2
	Volume of H_2SO_4 (ml)	Volume of H_2O_2 (ml)	
S_{H2SO4}	20	-	-
S_{H2O2}	-	20	-
$S_{1:3}$	5.0	15.0	1:3
$S_{1:1}$	10.0	10.0	1:1
$S_{2:1}$	13.3	6.7	2:1
$S_{3:1}$	15.0	5.0	3:1
$S_{4:1}$	16.0	4.0	4:1

From the literature, a period of 16 hours is the optimum silanization time for the formation of self-assembled monolayers on a substrate. Following the oxidation of titanium in the *Piranha* solution, the titanium surface was silanized for 16 hours in a toluene solution of APTES, and placed in a glove box under argon (**Figure 3. 2A**). To

study the effect of APTES concentration, the titanium samples were placed in 5 ml anhydrous toluene with an APTES concentration of 0.02, 0.05, 0.1, 0.2, 0.5, 1 and 3 volume%, respectively at 70°C (**Table 3. 4**).

Table 3. 4 Different concentrations of APTES used in the toluene at different temperatures.

Sample Code	Volume of APTES in 5 ml solvent (µl)	Temperature (°C)	Solvent (toluene)
$S_{0.02\%}$	1	70	Anhydrous
$S_{0.05\%}$	2.5		
$S_{0.1\%}$	5		
$S_{0.2\%}$ (S_{70})	10		
S_{60}		60	
S_{50}		50	
S_{40}		40	
S_{30}		30	
$S_{anhydrous}$			
$S_{hydrous}$			Hydrous
$S_{0.5\%}$	25	70	Anhydrous
$S_{1\%}$	50		
$S_{3\%}$	150		

For example, APTES of 0.2 v% was prepared from 10 µl APTES mixed with 5 ml anhydrous toluene. Therefore, in the glove box under argon, anhydrous toluene of 5 ml was transferred into a vial by a syringe (10 ml, VWR), and then APTES of 10 µl was dropped into the anhydrous toluene by a pipette (Standard Eppendorf, Fisher). Before the sample was put into the vial, the vial was shaken by hands to ensure that the APTES molecules can diffuse uniformly in the solvent. In order to avoid cross contamination, one vial was just soaked in one titanium plate and sealed by parafilm (Fisher). To evaluate the temperature effect, samples in 0.2 v% APTES were held in an incubator (Fisher) (**Figure 3. 2B**) at 30, 40, 50, 60 and 70°C, respectively (**Table 3. 4**). Titanium samples were also immersed in an anhydrous and a hydrous toluene solutions, respectively with 0.2 v% APTES at 30°C for 16 hours to investigate the effect of residual water content in the solvent (**Table 3. 4**). After silanization, the samples were repeatedly washed in the ultrasonic bath by toluene and ethanol for 3 times, each time for 3 minutes, in order to remove physically adsorbed APTES molecules on the surface. Finally, the samples were washed by deionized water in order to remove residual ethanol. After cleaning, the samples were dried under argon and analyzed with a few

hours. Stabilities of the APS film on the titanium surface were also investigated under vacuum and in aqueous solutions of pH range of 4 – 10 up to 72 hours at room temperature. The thermal stability of thin layers was performed at the temperature range 110 – 170°C under vacuum.

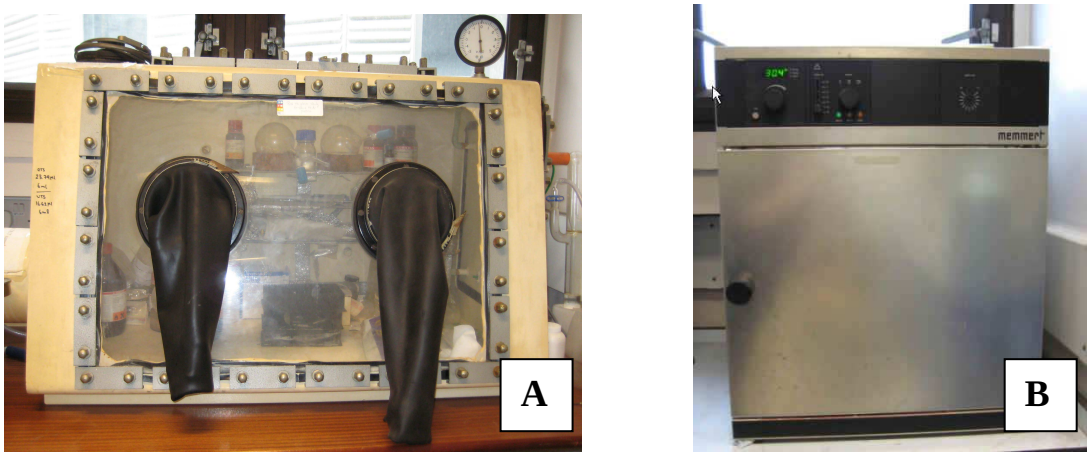

Figure 3. 2 (A) an anaerobic glove box and (B) Memmert incubator.

3.1.2 Calcium phosphate deposition by APS film on titanium

3.1.2.1 Preparation of simulated body fluid

Simulated body fluid (SBF) is the solution with ion concentrations approximately equal to those of human blood plasma, which has been widely used for in vitro assessment of the bioactivity of artificial materials and for the formation of bone-like apatite on various substrates [Kokubo 2003]. As known, the SBF is normally used to measure inducibility of calcium phosphate (CaP) by materials in vitro. Since it takes more than 2 weeks to induce CaP in the SBF, 1.5 SBF has also been applied for experiments, which is 1.5 times higher ion concentrations than those in the SBF. **Table 3.5** shows ion concentrations in human blood plasma and two different SBF. Simulated body fluid is a highly saturated solution, so a careful preparation route is necessary to avoid apatite precipitation during preparation. Since glass containers or edge of scratches will induce apatite nucleation, a plastic container with smooth surface is used for SBF preparation. **Table 3.6** below lists the recipe used in this study for

Table 3. 5 Ion concentrations of simulated body fluids and human blood plasma.

	Ion concentration (mM)							
	Na^+	K^+	Mg^{2+}	Ca^{2+}	Cl^-	HCO_3^-	HPO_4^{2-}	SO_4^{2-}
Blood plasma	142.0	5.0	1.5	2.5	103.0	27.0	1.0	0.5
SBF	142.0	5.0	1.5	2.5	103.0	10.0	1.0	0.5
1.5 SBF	213.0	7.5	2.3	3.8	154.5	15.0	1.5	0.8

Table 3. 6 Recipe of preparing 1L SBF and 1.5 SBF solutions.

Order	Reagent	Purity and supplier	Amount	
			SBF	1.5 SBF
1	Deionized water	-	750 ml	750 ml
2	NaCl	99+%, ACS, Aldrich	5.403 g	8.104 g
3	$NaHCO_3$	99.5%, ACS, Aldrich	0.504 g	0.756 g
4	Na_2CO_3	99.5+%, ACS, Aldrich	0.426 g	0.639 g
5	KCl	99+%, ACS, Aldrich	0.225 g	0.337 g
6	$K_2HPO_4 \cdot 3H_2O$	99+%, ACS, Aldrich	0.230 g	0.345 g
7	$MgCl_2 \cdot 6H_2O$	98+%, ACS, Aldrich	0.311 g	0.466 g
8*	0.2 M NaOH	97+%, ACS, Aldrich + distilled water	0.293 g	0.439 g
9*	HEPES	99.5+%, ACS, Aldrich	17.892 g	26.838 g
10	$CaCl_2$	96+%, ACS, Aldrich	0.293 g	0.439 g
11	$NaSO_4$	99+%, ACS, Aldrich	0.072 g	0.108 g
12	1.0 M NaOH	97+%, ACS, Aldrich + distilled water	15 ~ 20 ml	15 ~ 20 ml

***: HEPES previously are dissolved in 100 ml and 150 ml of 0.2 M NaOH for SBF and 1.5 SBF, respectively.**

preparations of the SBF and 1.5 SBF. In order to prepare 1000 ml solution, the deionized water of 750 ml was firstly poured into a 1000 ml plastic container with a stirring bar. The water was heated to 36.5°C under stirring on the hot plate. Chemicals in **Table 3. 6** were then added into the deionized water one by one in the order given, after each reagent was completely dissolved. The solution was adjusted to expected pH value by 1 M NaOH at 36.5°C before transferred to a 1000 ml plastic volumetric flask. When temperature of the solution was fallen to 20°C, the deionized water was added up to the marked line. Finally, the prepared simulated body fluid was preserved in the refrigerator at 4°C.

3.1.2.2 Bioactivity treatment

Titanium with the APS film was produced by a self-assembly technique as described in Chapter 3.1.1. The samples were then immersed into the prepared SBF solution to test their bioactivity by inducibility of calcium phosphate. Each Ti sample was placed into a vessel with SBF of 15 ml. To study the effect of ions concentrations in simulated body fluid, the titanium samples were placed in the SBF and 1.5 SBF solutions, respectively at 37°C for 5-10 days. To evaluate the pH effect in the solution, the titanium samples were placed in 15 ml SBF with pH value of 7.0, 7.45 and 7.98, respectively at 37°C for 5 days. After being kept in the incubator, the samples were taken out from the solution and washed with the deionized water in the ultra bath for 3 times, each time for 3 minutes to remove calcium phosphate deposited by the solution. All the samples were then dried in a vacuum oven at 50°C for overnight and stored at the desiccator for further analysis.

3.1.3 Immobilization of laccase on Ti by the APS film

In order to improve stability and re-usability, enzymes are normally immobilized on supports, such as glass, Pt, Au, etc. Solid-phase organic synthesis makes it possible to build a functional monolayer, which could act as an effective interlayer for enzyme immobilization, by a multistep route under simple and economic conditions in a clean and efficient way. The most employed functional groups of self-assembled monolayers for enzyme immobilization are amine and carboxylic groups, which could react with amino acids residues of enzymes to covalently bond them on SAMs.

The most common immobilization strategies available to laccase (Lac) comprise physical adsorption, crosslinking and covalent binding. Although it is a fast and easy way to building up bio-recognition interfaces, physical adsorption approach is known to give sensing surfaces with the shortest stability [Treven 1980]. Crosslinking only forms covalent linkage between enzymes rather than between matrix and enzymes [Treven 1980], which may lead to the less stability of enzymes on substrates. Covalent binding, e.g., the formation of an amide bond between amino acids of enzymes and the functionalized matrix by the help of activation reagent of carbodiimide, is reported to

be a competitive method to immobilize laccase on titanium. The bound enzyme is expected to have long stability with good performance.

3.1.3.1 Materials

In this thesis, laccase from *Trametes versicolor* was covalently immobilized on the -NH_2 functionalized titanium substrate using *N*-ethyl-*N'*- (3-dimethylaminopropyl) carbodiimide (EDC) and *N*-hydroxysuccinimide (NHS) as activation reagents. A titanium sample was silanized in 5 ml anhydrous toluene containing 0.2% APTES at 30°C for 16 hours as mentioned above. The samples were then successively washed by toluene, ethanol and distilled water for 3 times, respectively. Finally the –NH_2 functionalized titanium sample was ready for immobilization of the laccase after being dried under argon. Since after silanization the titanium surface has plenty of -NH_2 groups, a carbodiimide activation approach (EDC/NHS) was used to activate -COOH groups from the amino acid residues of the laccase, and form amide bond with -NH_2 groups from APS (3-aminopropyltrisilanol which is a hydrolyzed APTES molecule) bound to titanium. **Table 3. 7** below shows all of chemicals used for immobilization of laccase by EDC/NHS on titanium.

3.1.3.2 Experimental procedure

A solution with a buffered pH will supply a stable environment for enzymatic activity than a non-buffered solution (deionized water), so a buffer solution will be used both for immobilization and activity measurements of enzymes. In order to maximize the immobilization of laccase, 4-(2-hydroxyethyl)-1-piperazineethanesulfonic acid (HEPES) is selected for the buffer solution with EDC/NHS to active the -NH_2 groups on titanium instead of a phosphate buffer solution, because EDC can also activate phosphate groups. The preparations of different solutions including HEPES buffer, EDC, NHS and laccase, are very important before immobilization of the laccase and introduced as follows.

Table 3. 7 Chemicals for laccase immobilization on Ti with the APS film.

Name	Formula	Molecular mass (g/M)	Purity	Supplier	Storage temperature
4-(2-hydroxyethyl)-1-piperazineethanesulfonic acid (HEPES)	$C_8H_{18}N_2O_4S$	238.3012	> 99%	Fisher	Ambient
Sodium hydrate	NaOH	40	99+%	Sigma-Aldrich	Ambient
Laccase from *Trametes versicolor*	—	—	22.4 U/mg	Sigma	-18°C
N-(3-Dimethylaminopropyl)-*N*'-ethylcarbodiimide hydrochloride (EDC)	$C_8H_{17}N_3 \cdot HCl$	191.70	> 99.9%	Sigma-Aldrich	-20°C
N-hydroxysulfosuccinimide sodium salt (NHS)	$C_4H_4NNaO_6S$	217.13	≥ 98.5%	Aldrich	Ambient

1) Preparation of 20 mM HEPES buffer: The require mass (m) in the solution can be calculated by the following equation:

$$m = C \times V \times M \qquad \textbf{(Equation 3. 1)}$$

where C is the concentration, V is the total volume of the solution and M denotes the molar mass of the chemical. Therefore, the amounts for 20 mM, 100 ml HEPES and 0.1 M, 100 ml NaOH are shown below, respectively:

$$m_{HEPES} = (20 \times 10^{-3}) \times (100 \times 10^{-3}) \times 238.3012 = 0.4766 \text{ g}$$

$$m_{NaOH} = 0.1 \times (100 \times 10^{-3}) \times 40 = 0.4 \text{ g}$$

NaOH powder of 0.4 g was weighed on a high precision balance (Fisher, shown in **Figure 3. 3A**), and then dissolved in a baker with 100 ml deionized water by a stir bar on a magnetic stirrer hotplate (Fisher) for 2 minutes. As the same procedure, HEPES

power of 0.4766 g was dissolved in 100 ml deionized water and then pH value of the solution was adjusted by 0.1 M NaOH using a pH meter (S20, Fisher, shown in **Figure 3. 3B**). To evaluate the pH effect during the immobilization of laccase, the HEPES buffer was prepared with the pH value range of 3 – 8. After preparation, the HEPES buffer was sealed and then stored in a refrigerator at 4 °C.

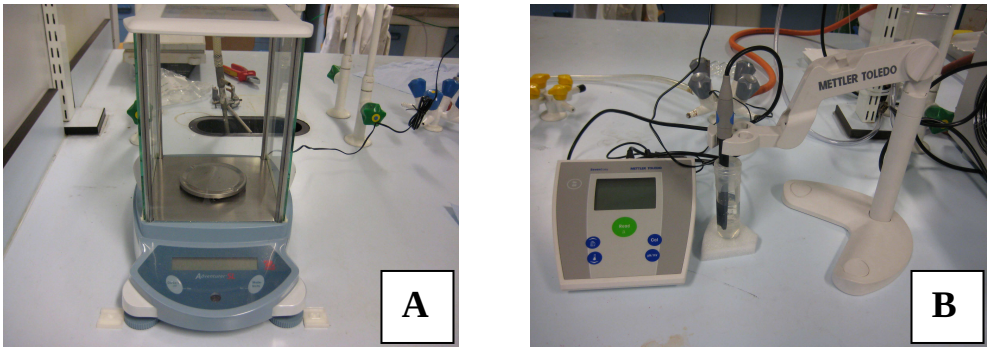

Figure 3. 3 (A) Adventurer SL 64 balance and (B) Fisher S20 pH meter.

2) Preparations of EDC and NHS solutions in 20 mM HEPES buffer, respectively: Here 5 mM of EDC and NHS solutions are introduced for preparations. According to Equation 3.1, the masses of EDC and NHS in 1 ml are shown below, respectively:

$$m_{EDC} = (5 \times 10^{-3}) \times (1 \times 10^{-3}) \times 191.70 = 0.9585 \text{ mg} \approx 1.0 \text{ mg}$$

$$m_{NHS} = (5 \times 10^{-3}) \times (1 \times 10^{-3}) \times 217.13 = 1.08565 \text{ mg} \approx 1.1 \text{ mg}$$

EDC of 1.0 mg was weighed in a microcentrifuge tube (1.5 ml, Fisher) with the balance, and then transferred into a tube with 1 ml of 20 mM HEPES buffer by the pipette. In order to dissolve EDC well in the HEPES buffer, the solution was mixed by a Vortexer (PV1, Fisher, shown in **Figure 3. 4A**) at a high speed for 1 minute. After that, the tube was centrifugated for 30 seconds by a microcentrifuge mini (1.5/2.0 ml rotor, Fisher, shown in **Figure 3. 4B**), in order for the EDC solution attached on the tube lid and side walls to flow back to the bulk solution. Eventually, the tube was sealed with parafilm (Fisher), labeled and stored in the refrigerator at − 21°C. The preparation procedure for the NHS solution in HEPES buffer was the same as that of the EDC solution. Briefly, NHS of 1.1 mg was dissolved in 1 ml of 20 mM HEPES by the

vortexer. After centrifugated and labeled, the prepared NHS solution was preserved in the refrigerator at − 21°C, too. In order to investigate the effect of the molar ratio of EDC/NHS on the activity of immobilized laccase on the titanium with APS film, different concentrations of EDC and NHS from 5 – 20 mM were prepared, as shown in **Table 3. 8**.

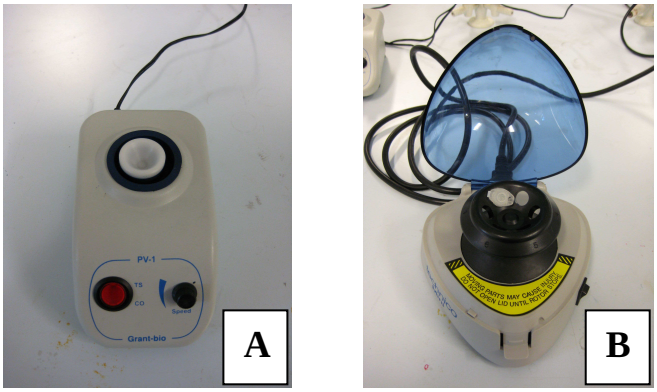

Figure 3. 4 (A) Fisher PV1 vortex mixer and (B) 1.5/2.0 ml microcentrifuge.

Table 3. 8 Different molar ratios of EDC and NHS for immobilization.

Molar Ratio of EDC/NHS	EDC (1ml)		NHS (1ml)	
	Concentration (mM)	Amount (mg)	Concentration (mM)	Amount (mg)
1:3	5.0	1.0	15.0	3.3
1:2			10.0	2.2
1:1			5.0	1.1
2:1	10.0	2.0		
3:1	15.0	3.0		
4:1	20.0	4.0		

3) Preparation of 10 mg/ml Lac solution: laccase of 10 mg was weighed in a tube with the balance, dissolved in 1 ml of 20 mM HEPES by the vortexer and finally stored in the refrigerator at – 21°C.

In order to avoid inactivation of the above prepared solutions, EDC, NHS and Lac solutions were put in an ice-box when transferred from the refrigerator for experiments. For the immobilization of Lac, HEPES buffer of 400 µl, EDC solution of 200 µl and NHS solution of 200 µl were added into a conical tube (Fisher) and mixed together by the pipette. Then 200 µl of 10 mg/ml Lac solution was added into the mixture

mentioned above and mixed well. Finally, the titanium sample with APS film was immersed into the above mixture at 4°C. To evaluate the time effect on the immobilization, the titanium samples were placed in 1 ml mixed solution with laccase for 2, 6, 12, 18, 20 and 24 hours, respectively. After immobilization, the samples were rinsed with 20 mM HEPES buffer for 3 times, to remove physisorbed Lac on the surface. Finally, the titanium samples were stored in a dry condition and 20 mM HEPES buffer at the range of 3-8, respectively at 4°C for subsequent Lac activity measurement to investigate the effect of storage conditions on Lac activity.

3.2 Characterization techniques

3.2.1 Reflectance-Absorbance Fourier Transform Infrared spectroscopy (RA-FTIR)

Infrared (IR) spectroscopy is a chemical analytical technique, which detects the vibration characteristics of chemical functional groups in a sample. When an infrared light (wavelength from 0.75 to 300 μm) interacts with matter, the permanent dipole is changed, leading to the vibrations of bonds (stretching, bending, rocking, etc). As a result, a chemical functional group tends to adsorb infrared radiation in a specific wavenumber range regardless of the structure of the rest of the molecule. Hence, the correlation of the band wavenumber position with the chemical structure is used to identify a functional group in a sample [Smith 1996].

Since substrates in the whole experiments are titanium or graphite and the IR could not be transmitted through the samples, Reflectance – Absorbance Fourier Transform Infrared spectroscopy (RA-FTIR) was used here. Reflection occurs when light impinges on the surface of a material and is partially reflected, as shown in **Figure 3. 5**. Light that passes into the material may be absorbed or reflected out again. Finally, such scattered IR energy is collected by a spherical mirror that is focused onto the detector. The detected IR light is partially absorbed by the sample and provides the vibrational information of the sample.

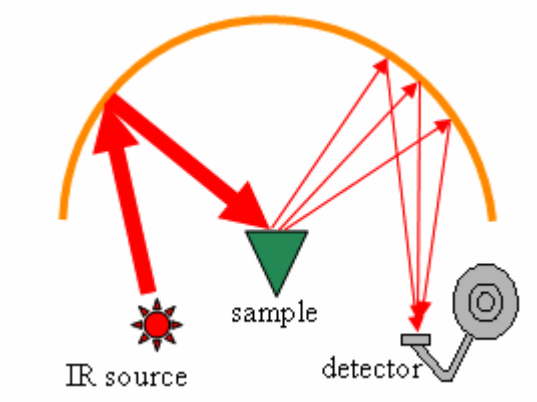

Figure 3. 5 Schematic procedure of RA-FTIR working.

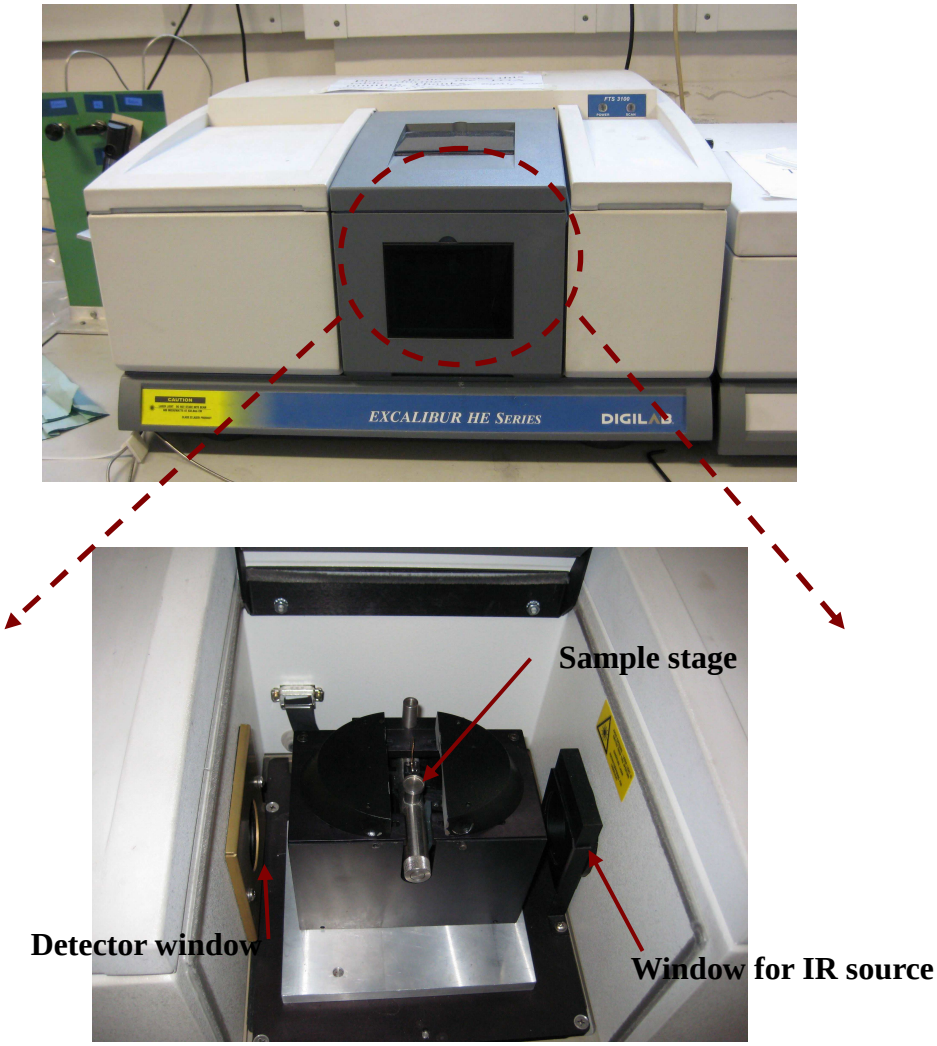

Figure 3. 6 Digilab Varian 3100 FTIR (above) and sample chamber (bottom).

According to the principles of RA-FTIR, the outmost layer on the sample will be detected, such as -NH_2 functionalized monolayers and calcium phosphate layers on

titanium. All of spectral analysis was performed throughout the spectral range (400 – 4000 cm^{-1}) by RA-FTIR (Varian 3100 FTIR, Excalibur HE series, Netherlands). The number of scans was 128, the scan speed was 5 kHz and the resolution was 4 cm^{-1}. During the measurement, the accessory chamber was closed under purged air condition (**Figure 3. 6**). The spectra were collected between 4000 and 400 cm^{-1}, and processed mathematically including normalizing and baseline correction to make the spectra comparable and to minimize noise. The backgrounds were collected from TiO_x for titanium-based samples and oxidized graphite for graphite-based samples. All of samples were measured at room temperature after drying under an argon stream.

3.2.2 Contact angle goniometry

Contact angle, $\boldsymbol{\theta}$, is the angle at which a liquid/vapor interface meets the solid surface, and determined by the interactions across the three interfaces. Therefore, once the chemical components on the solid surface are changed, the interactions between liquid and solid are changed, leading to the change of the contact angle. As shown below (**Figure 3. 7**), it is the angle between the solid and the tangent to the drop profile at the intersection point.

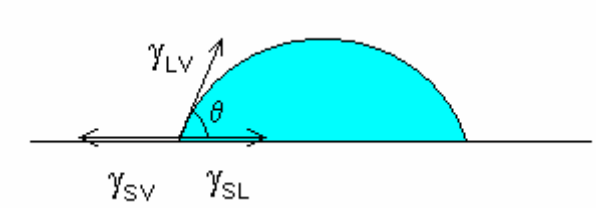

Figure 3. 7 Interfacial free energies of liquid dropped on solid. The surface energies forces, γ, γ_{LV}, γ_{SV}, γ_{SL} refer to the interfacial energies of the liquid/vapour interface, the solid/vapour interface and the solid/liquid interface. [Ulman 1991].

Equation 3.2 presents the relationship between the three phases given by the Young equation. Therefore, contact angle measurement gives information about surface tension /free surface energy indirectly with the shape of a drop placed on the sample surface. If there is no interaction between the solid and the liquid, the contact angle will be 180°. If the angle is less than 90°, the liquid is said to wet the solid. A zero contact angle represents complete wetting. Lower value of $\boldsymbol{\theta}$ indicates that the surface

has great tension or free surface energy, while high values indicate poor surface tension and free surface energy [Hartland 2004].

$$\gamma_{LV} \text{Cos}\theta = \gamma_{SV} - \gamma_{SL} \qquad \textbf{(Equation 3. 2)}$$

Contact angle measurements were carried out in the Interdisciplinary Research Center (IRC) in Biomedical Materials at Queen Mary, University of London. The contact angle goniometry (CAM 100 system) equipped with a 1 milliliter syringe (Hamilton Company, UK), is manufactured by KSV Instruments Ltd. As shown in **Figure 3. 8**, the machine also includes a FireWire video camera, an adjustable sample stage and a LED light source. The static sessile drop method was employed in the whole experiments. Deionized water of 10 µl was dropped on the sample surface at room temperature, and calculated with KSV C200 software (Static Sessile Drop analysis). The results represent the average of three measurements for each sample and images of the droplet were taken by the video camera interfaced with a computer.

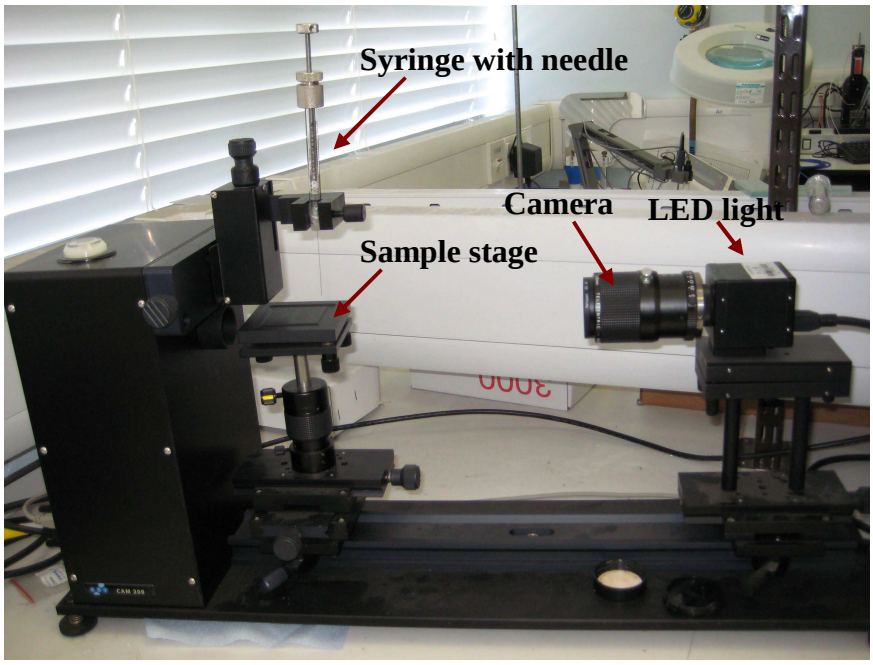

Figure 3. 8 CAM 100 contact angle goniometry.

3.2.3 Atomic Force Microscopy (AFM)

An atomic force microscopy (AFM) determines the topography and roughness of surfaces including defects or mixtures of different structures and generates high-resolution 3D images at the nanometer scale without sample pre-treatment. **Figure 3. 9** below shows the main principle sketch of AFM. The probe tip, which is mounted to the end of the cantilever, scans across the sample surface, by direct physical contact with the sample. A light beam from a small laser is bounced off from the cantilever and reflected on to a four-section photodetector. As the probe tip scans, the photodetector will supply information of varying topographic features that cause the deflection of the tip and the cantilever.

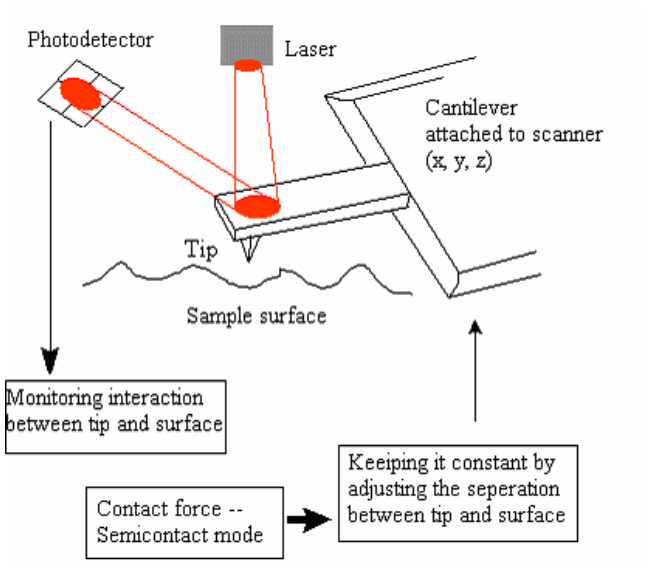

Figure 3. 9 Main principle sketch of AFM [modified from W4].

Since scanning a sample surface not only involves attractive but also repulsive forces, as demonstrated in **Figure 3. 10**, oscillations can take place in C*ontact*, *Semicontact* and *Non-contact* modes. Compared with the contact mode, the force of the cantilever onto the surface is less in semicontact mode, which will not damage the sample surface and cause the cross-contaminant between the tip and sample. In non-contact mode, although the tip cannot touch the surface, lower resolution will be obtained compared with the semicontact mode. Therefore, the semicontact mode is more sensitive and will investigate truly characteristics of the surface than other two modes.

Multimode NTEGRA AFM (NT-MDT, Moscow, Russia) equipped with a head including cantilever stage, laser and photodetector, sample stage and anti-vibrator, are shown in **Figure 3. 11**. Images were acquired in the semicontact mode using an integral cantilever with attached silicon tips (PPP-FMR, Nanosensors, UK). The force constant of the tip was between 42 N/m and the resonance frequency was 330 kHz. Quantitative measurements of the local root-mean-square (RMS) surface roughness were determined from the 30 × 30 μm^2 sample area, which was evaluated based on a standard formula integrated in the imaging software with NoVa.

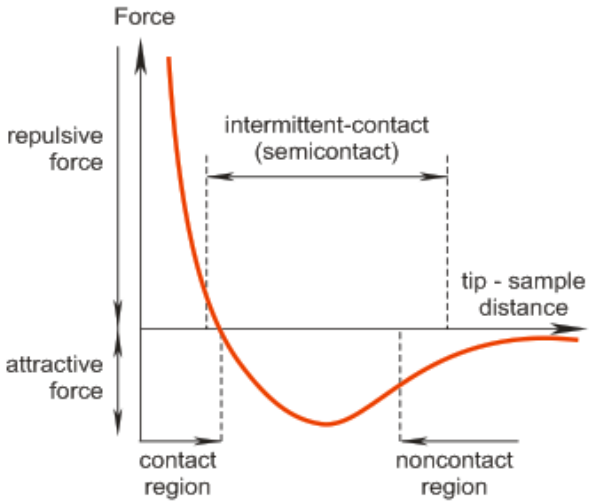

Figure 3. 10 Different oscillations of tip by force and distance between tip and sample [W5].

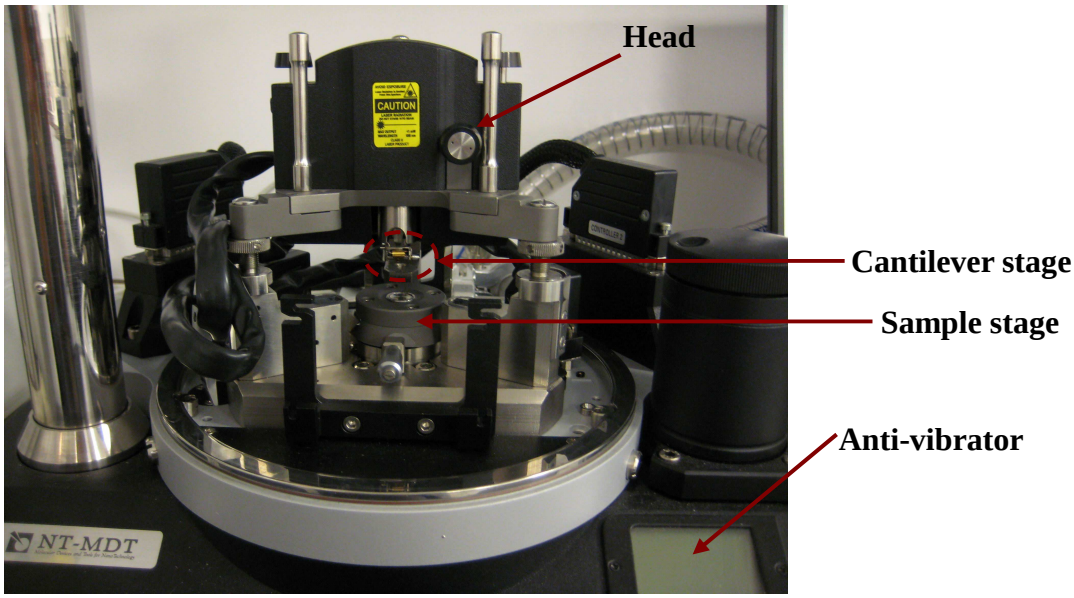

Figure 3. 11 Multimode NT-MDT AFM with anti-vibrator.

3.2.4 X-ray photoelectron spectroscopy (XPS)

X-ray photoelectron spectroscopy (XPS), also known as Electron Spectroscopy for Chemical Analysis (ESCA), is a surface chemical analysis technique that can be used to analyze the surface chemistry of a material. It is a quantitative spectroscopic technique that measures the elemental composition (top 1 – 10 nm usually), chemical state and electronic state of the elements that exist within a material.

As shown in **Figure 3. 12**, in XPS system, when a beam of X-rays irradiates a material, the photon is adsorbed by an atom in a molecule or solid, leading to ionization and the emission of a core (inner shell) electron from the top layer of the material. The kinetic energy distribution of the emitted photoelectrons can be measured by electron energy analyser and a photoelectron spectrum can thus be recorded.

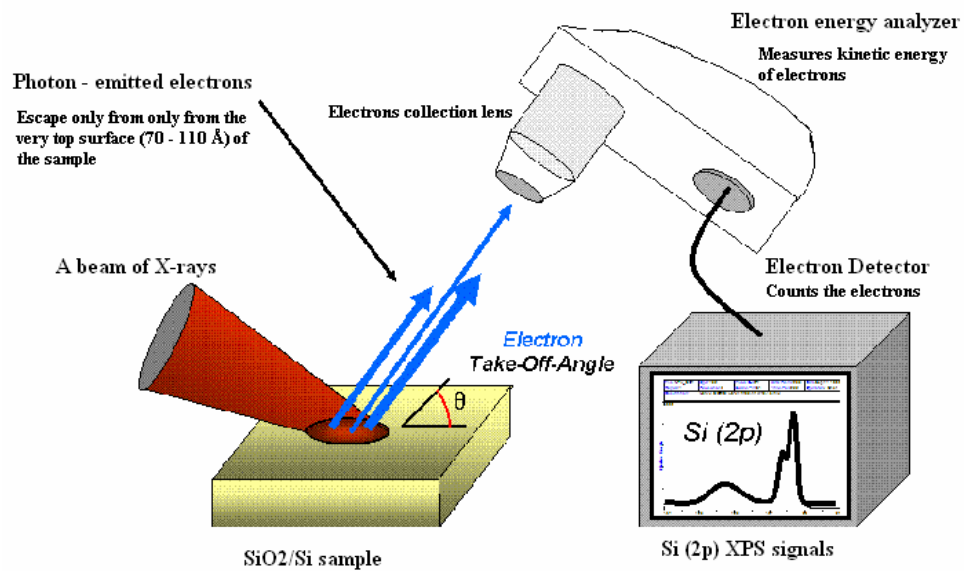

Figure 3. 12 Main principle sketch of XPS [modified from W1].

Since the energy of a particular X-ray wavelength equals a known quantity, the electron binding energy (BE) of each of the emitted electrons can be determined by the following equation, according to Ernest Rugherford (1914):

$$E_{binding} = E_{photon} - E_{kinetic} - \Phi \qquad \textbf{(Equation 3. 3)}$$

Where $\boldsymbol{E}_{\text{binding}}$ is the energy of the electron emitted from one electron configuration within the atom, $\boldsymbol{E}_{\text{photon}}$ is the energy of the x-ray photons being used, $\boldsymbol{E}_{\text{kinetic}}$ is the kinetic energy of the emitted electron as measured by the instrument and $\boldsymbol{\Phi}$ is the work function of the spectrometer.

In this project, XPS was used to determine the OH group on titanium surface oxidized in the different piranha solutions. In the whole experiments, the XPS was performed using an Escalab 220i-XL instrument with monochromatized Al Kα radiation at 1486.6 eV under ultra high vacuum. Survey scans were recorded in the range of 0 – 110 eV (binding energy), and then small-range and high-resolution scans were used to record of the principal peaks of Ti (2p), C (1s) and O (1s). The peaks were modelled using the CasaXPS software to determine their area.

3.2.5 Scanning Electron Microscopy (SEM)

Scanning electron microscopy (SEM) was used to characterise the particle morphology, phase distribution and particle size of material surface. The SEM apparatus used for obtaining high-resolution images is a field emission scanning electron microscopy (FE-SEM, JEOL JSM 6300F), which consists of a cold cathode field emission gun that requires a vacuum better than 10^{-8} Torr. For sample preparation, after inducibility of calcium phosphate in SBF and dried under vacuum, the sample was placed on a smooth metal stub with carbon sticker and ready for the SEM analysis. The phase composition on the surface was analysed on a JEOL JEM 6300 thermionic SEM equipped with an Energy Dispersive X-ray spectroscopy (EDX) detector of INCA Energy 300 Microanalysis System by Oxford Instruments Analytical.

3.2.6 X-ray Diffraction (XRD)

Thin Film X-ray Diffraction (XRD) is an analytical technique to reveal the information of phases present (peak position), phase concentrations (peak heights), amorphous content (background hump) and crystallite size/strain (peak width) in the materials. Since each crystalline substance has characteristic arrangement of atoms which

diffracts X-rays in a unique pattern. X-ray reflection takes place from lattice planes according to Bragg's Law:

$$n\lambda = 2d\sin\theta \ (n=1,2,3\ldots) \qquad \textbf{(Equation 3. 4)}$$

where λ is the wavelength, d is the lattice plane distance, θ is an angle between the incident ray and the relevant crystal planes and n is integer number.

The XRD measurements were performed on a Siemens D-5000 diffractometer. The X-ray source was Cu Kα radiation generated from a conventional water-cooled X-ray tube. The Diffracplus Basic 4.0 software was used to analyze the obtained data. The XRD was performed at 2θ angles from 20° to 60° at a scanning speed of 1.5°/min. For specimen preparation, after immersed in simulated body fluid and dried in a vacuum oven, the samples then were placed in the middle of a plastic specimen holder and flattened by a clean glass plate. XRD used in this project are mainly for detecting the compound of calcium phosphate on the titanium surface.

3.2.7 Laccase activity assay by UV-VIS spectrophotometer

3.2.7.1 Enzyme activity assay --- Initial rate experiments

Enzyme assays are laboratory procedures that measure the rate of product formation or substrate utilization during the enzyme-catalyzed reaction. For many enzymes there are several alternative assay procedures available and the choice between them may be made on the grounds of convenience, cost, the availability of appropriate equipment and reagents and the level of sensitivity required [Elsenthal 1993]. So far, the most commonly used type of experiment in enzyme kinetics is Initial rate experiments.

Initial rate experiments are to measure the rate of reaction at very short time before any significant changes in concentration occur. When an enzyme is mixed with a large excess of the substrate, the enzyme-substrate intermediate builds up in a fast initial transient. Then the reaction achieves a steady-state kinetics in which the intermediates

remain constant over time and the reaction rate changes relatively slowly. Rates are measured for a short period by monitoring the accumulation of product with time. A typical progress curve for an enzyme-catalysed reaction with time is shown below (**Figure 3. 13**). The rate of product formation with time is decreasing, which results from product inhibition, substrate depletion, the enzyme-substrate intermediate instability and so on. However, at the beginning for a very short period of time, these effects should not be significant. Since the measurements are carried out for a very short period with the large excess of substrate, the initial substrate can be approximately considered as free substrate. Therefore, this linear initial rate is often related to the enzyme activity.

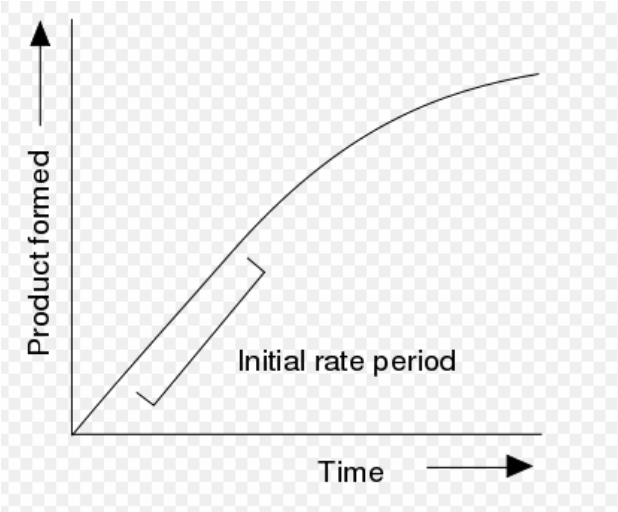

Figure 3. 13 A typical progress curve of an enzyme-catalyzed reaction [Elsenthal 1993].

Normally, the initial rate over enzyme concentration is used to express the activity of an enzyme quantitatively. In this project, it is assumed that the quantities of immobilized Lac on titanium under different conditions are the same. Therefore, the initial rate can evaluate the catalysis activity of the enzyme. The linear initial rate is defined as the change in the concentration of the product (C) formed by the enzyme catalyzed reaction per unit time (minutes).

$$\text{Reaction rate} = dC / dt \qquad \textbf{(Equation 3. 5)}$$

The change of the concentration of the product is related to that of the substrate because of single-substrate enzyme. Therefore, the change of the concentration of the

substrate can be monitored by the absorption of light to the properties of the substrate through the light is travelling. According to **Beer-Lambert law** [Elsenthal 1993], the absorption of light over the concentration of the substrate is expressed in Equation 3.6:

$$\boldsymbol{A} = \boldsymbol{\varepsilon} \times \boldsymbol{l} \times \boldsymbol{c} \qquad \textbf{(Equation 3. 6)}$$

where A is the absorbance of light, ε is the molar adsorptivity of substrate, l is the pathlength and C is denoted as the concentration of the substrate. Substituting Equation 3.6 into Equation 3.5, the linear initial rate of the enzyme catalyzed reaction could also be expressed as below:

$$\text{Reaction rate} = (d\boldsymbol{A} / \boldsymbol{\varepsilon l})/d\boldsymbol{t} \qquad \textbf{(Equation 3. 7)}$$

In this project, 2,2'–azino-bis(3-ethylbenzthiazoline-6-sulphnic acid) (ABTS) is employed as the substrate for the Lac. In Equation 3.7, dA/dt is the slope of the initial curve, ε of ABTS is 3.6 $\times 10^4$ $M^{-1}cm^{-1}$ at 420 nm and l is 1 cm (width of cuvette). According to the above equation, within the same time, the reaction rate is changing with that of absorbance of light.

3.2.7.2 Michaelis-Menten constant (K_m)

The Michaelis-Menten kinetic mode is the basis for most single-substrate enzyme kinetics. The Michaelis-Mental equation relates the initial reaction rate to the substrate concentration. Two crucial assumptions underlie this equation: the total enzyme concentration and the concentration of the intermediate complex do not change over time. The enzymatic reaction is assumed to be irreversible and the product does not bind to the enzyme. Therefore, single-substrate mechanism for an enzyme reaction is expressed as follows:

$$E + S \underset{\kappa_{-1}}{\overset{\kappa_1}{\rightleftharpoons}} ES \xrightarrow{\kappa_{cat}} E + P \qquad \textbf{(Equation 3. 8)}$$

where κ_1, $\kappa_{-1}$and κ_{cat} are the rate constants for the individual steps.

The first key assumption for the Michaelis-Menten equation is that the concentration of the substrate-bound enzyme ([*ES*]) changes much slowly than those of the product ([*P*]) and the substrate ([*S*]). This allows the rate of change [*ES*] to be set to zero:

$$\boldsymbol{d[ES] / dt = \kappa_1[E][S] - [ES](\kappa_{-1} + \kappa_{cat}) \approx 0} \qquad \textbf{(Equation 3. 9)}$$

The second key assumption is that the total enzyme concentration ($[E]_0$) does not change over time, thus the total concentration of enzyme $[E]_0$ is the sum of the free enzymes in the solution [*E*] and those which bound to the substrate [*ES*]:

$$\boldsymbol{[E]_0 = [E] + [ES] \approx \text{constant}} \qquad \textbf{(Equation 3. 10)}$$

Substituting Equation 3.10 into Equation 3.9, an expression for [*ES*] is shown below:

$$\boldsymbol{0 = \kappa_1 [S] ([E]_0 - [ES]) - [ES](\kappa_{-1} + \kappa_{cat})}$$

$$\boldsymbol{[S][E]_0 = [S][ES] + [ES] \underbrace{\{(\kappa_{-1} + \kappa_{cat}) / \kappa_1\}}_{K_m}}$$

$$\boldsymbol{[ES] = [S] [E]_0 / (K_m + [S])} \qquad \textbf{(Equation 3. 11)}$$

According to Equation 3.8, the rate of product formation (*V*) is written as:

$$\boldsymbol{V = d[P] / dt = \kappa_{cat} [ES]} \qquad \textbf{(Equation 3. 12)}$$

Substituting Equation 3.11 into Equation 3.12, an expression for the rate of product formation is shown below:

$$\boldsymbol{V = d[P] / dt = \kappa_{cat} [ES] = \underbrace{\kappa_{cat} [E]_0}_{V_{max}} \{[S] / (K_m + [S])\}}$$

$$V = V_{max}\,[S] / (K_m + [S]) \qquad \textbf{(Equation 3. 13)}$$

$$K_m = (\kappa_{-1} + \kappa_{cat}) / \kappa_1 \qquad \textbf{(Equation 3. 14)}$$

where K_m and V_{max} are defined as the Michaelis constant and maximum rate, respectively.

The Michaelis constant K_m is an inverse measure of the affinity or strength of binding between the enzyme and its substrate, since the value of K_m is decreasing with κ_1 increasing. It means that the lower K_m, the greater the affinity between enzyme and substrate. According to Equation 3.14, K_m is the constant for certain enzyme under certain substrate, which cannot be changed by the concentrations of enzyme and substrate, pH value of the solution, etc. Equation 3.13 above describes how the initial reaction rate depends on the concentration of a substrate under a certain concentration of enzyme, normally named as the Michaelis-Menten equation. The Michaelis-Menten equation predicts a hyperbolic relationship between initial reaction rate (V) and substrate concentration ([S]), as shown in **Figure 3. 14A**. Therefore, according to Equation 3.13, K_m is experimentally defined as the concentration at which the rate of the enzyme reaction is half V_{max}.

$$1 / V = (K_m / V_{max}) \cdot (1 / [S]) + 1 / V_{max} \qquad \textbf{(Equation 3. 15)}$$

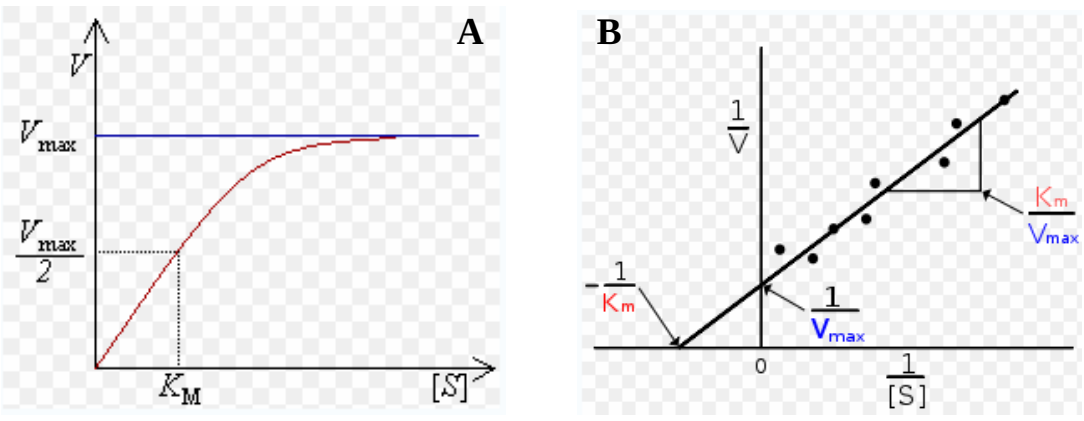

Figure 3. 14 Schematic picture showing the relation between the concentration of substrate the initial velocity (A) and the Lineweaver – Burk plot (B) [W6].

Equation 3.14 can also be rewritten in Equation 3.15 which uses the inverse of V and [S], which makes it easier to determine the constants from measured data using Lineweaver – Burk plot [Elsenthal 1993]. Plotting the reciprocals of the same data points (**Figure 3. 14A**) yields a Lineweaver-Burk plot (**Figure 3. 14B**). This provides a more precise way to determine V_{max} and K_m. V_{max} is determined by the point the line crosses the 1/V axis and K_m is determined by the point the line cross the 1/[S] axis.

3.2.7.3 Measurement of enzyme activity

Laccase is a multi-copper oxidoreductase and able to catalyze the oxidation of various phenols, substituted polyphenols, aromaticamines and benzenethiols. Among these organic compounds, 2,2'-Azino-bis(3-ethylbenzothiazoline-6-sulfonic acid) (ABTS) is most commonly used as a substrate. This compound is easily oxidized by the Lac, turning it into a green and soluble end-product, which can be measured by UV-VIS spectrophotometer with absorbance of light at 420 nm. Chemicals for activity assay of immobilized Las on the surface are listed in **Table 3. 9**.

Table 3. 9 Chemicals for activity assay of immobilized laccase on Ti.

Name	Formula	Molecular mass (g/M)	Purity	Supplier	Storage temperature
2,2'-azino-bis(3-ethylbenzthiazoline-6-sulphonic acid) (ABTS)	$C_{18}H_{24}N_6O_6S_4$	548.68	≥ 99%	Fluka	4°C
Sodium citrate dehydrate	$Na_3C_6H_5O_7 \cdot 2H_2O$	294.10	> 99%	Fisher	Ambient
Citric acid	$C_6H_8O_7 \cdot H_2O$	210.14	99.8%	Fisher	Ambient

1) Preparation of 0.1 M citrate buffer: Fist of all, sodium citrate dehydrate solution of 0.1 M and citric acid solution of 0.1 M were prepared, respectively. Briefly, according to Equation 3.1, masses for 100 ml of 0.1 M sodium citrate dehydrate and citric acid solutions are as follows, respectively:

$m_{\text{sodium citrate dehydrate}} = (100 \times 10^{-3}) \times (100 \times 10^{-3}) \times 294.10 = 2.941$ g

$m_{\text{citric acid}} = (100 \times 10^{-3}) \times (100 \times 10^{-3}) \times 210.14 = 2.1014$ g

The powders of 2.941 g for sodium citrate dehydrate and 2.1014 g for citric acid were dissolved in 100 ml deionized water, respectively. Then 0.1 M sodium citrate dehydrate solution as base was poured into the 0.1 M citric acid solution and the pH value of the mixture was adjusted by the pH meter at room temperature. In order to evaluate the optimum pH for the activity of laccase, the citrate buffer of 0.1 M was prepared at 2.6, 3, 4, 4.5, 5 and 6, respectively. After preparation, the citrate buffer of 0.1 M was then stored in the refrigerator at 4°C.

2) Preparation of 5 mM ABTS in 0.1 M citrate buffer: The mass for 1 ml of 5 mM ABTS is shown below:

$m_{\text{ABTS}} = (5 \times 10^{-3}) \times (1 \times 10^{-3}) \times 548.68 = 2.74 \text{ mg} \approx 2.7 \text{ mg}$

The preparation procedure of 1 ml of 5 mM ABTS in 0.1 M citrate buffer is the same as that of 5 mM EDC solution in 20 mM HEPES buffer. Briefly, ABTS solid powder of 2.7 mg was dissolved in a microcentrifuge tube with 1 ml of 0.1 M citrate buffer. After mixing, ABTS solution of 5 mM was labeled and then preserved in the refrigerator at -21°C.

3) Measurement of the laccase activity: At the first, the citrate solution 0.1 M of 1ml with 0.2 mM ABTS was prepared from 40 µl of 5 mM ABTS diluted into 960 µl of 0.1 M citrate buffer to measure laccase activity. To measure the K_m, titanium samples were immersed in 1 ml citrate solution with different ABTS concentrations from 0.005 to 0.45 mM, as shown in **Table 3. 10**. Then the solutions with ABTS were transferred into a reference and sample cuvettes in UV-Vis spectroscopy, respectively. A titanium sample without laccase was placed into the reference cuvette as control, while another titanium sample with laccase was immersed into the sample cuvette. **Figure 3. 15** shows UV-visible absorbance curve of the immobilized laccase on titanium with SAM-NH_2

in ABTS solution for 2 minutes. In this figure, the linear part of the curve is within the first 30 seconds in the initial period. According to Equation 3.7, the initial reaction rate of immobilized laccase on titanium is as follows:

Reaction rate = $(0.13223-0.00289)/(0.5 \times (3.6\times10^{4}) \times 1) = 7.26$ μmol/min

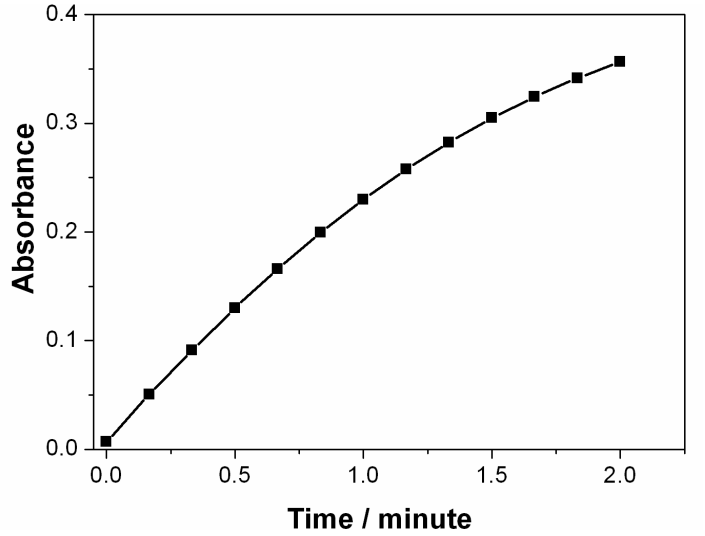

Figure 3. 15 A progress curve of immobilized laccase-catalyzed ABTS reaction.

Table 3. 10 Different ABTS concentrations used for measurement of K_m.

Volume of 5 mM ABTS (μl)	Volume of 0.1 M citrate buffer (μl)	Final concentration of ABTS (mM)
1	999	0.005
2	998	0.01
8	992	0.04
20	980	0.1
30	970	0.15
40	960	0.2
50	950	0.25
60	940	0.3
70	930	0.35
80	920	0.4
90	910	0.45

3.2.7.4 Introduction of UV-VIS spectrophotometry

UV-VIS spectrophotometry measures the absorbance of a given molecule in a solution at a special wavelength corresponding to the special molecule. Activity assay of the immobilized laccase on titanium or graphite will be obtained from Equation 3.7. **Figure 3. 16** demonstrates the main working principle of a typical spectrometer. The UV-Visible spectrophotometer uses two light sources (coloured yellow), a deuterium (D_2) lamp for ultraviolet light and a tungsten (W) lamp for visible light. After bouncing off a mirror (mirror 1), the light beam passes through a slit and hits a diffraction grating. The grating can be rotated allowing for a specific wavelength to be selected. At any specific orientation of the grating, only a monochromatic (single wavelength) wave successfully passes through a slit. A filter is used to remove unwanted higher orders of diffraction. The light beam hits a second mirror before it gets split by a half mirror (half of the light is reflected, the other half passes through). One of the beams is allowed to pass through the reference cuvette, the other passes through the sample cuvette. The intensities of the light beams are then measured at the end.

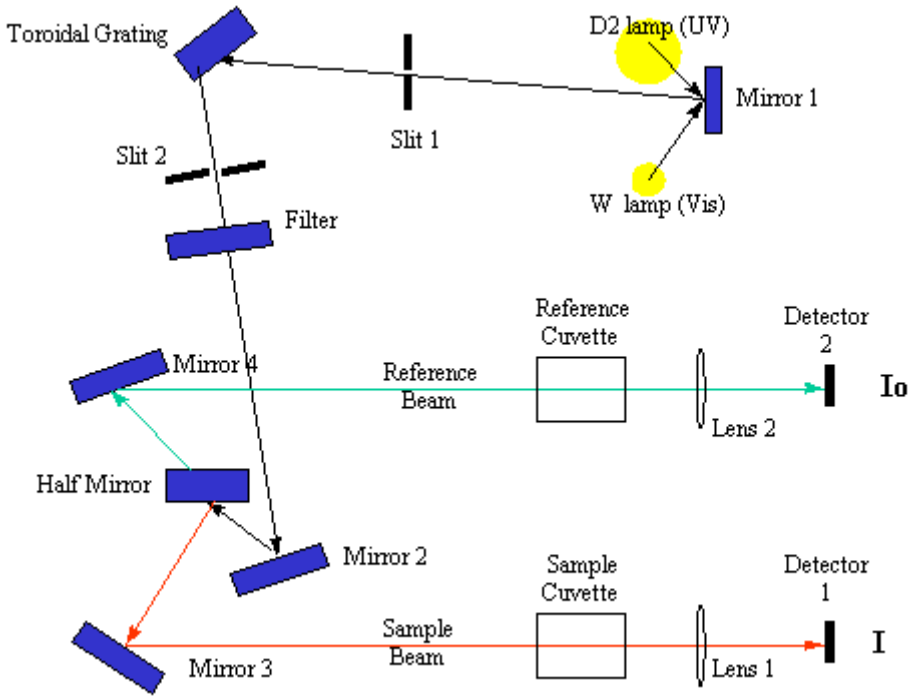

Figure 3. 16 Schematic of a UV-VIS spectrometer and its working principle.

According to **Beer-Lambert Law**, there exists a logarithmic dependence between the transmission (T) of light through a substance and the product of the adsorption coefficient of the substrate (α), and the distance that the light travels through the solution (l). The adsorption coefficient can be written as product of a molar adsorptivity (ε) and the concentration of absorbing products in the solution (C).

$$T = \boldsymbol{I/I_0} = 10^{-\alpha l} = 10^{-\varepsilon l c} \qquad \textbf{(Equation 3. 16)}$$

Where $\boldsymbol{I}$ is the intensity of light at a specified wavelength that has passed through a sample and $\boldsymbol{I_0}$ is the intensity of the light before it enters the sample on incident light intensity.

According to Equation 3.7, Equation 3.16 can be expressed as:

$$\mathbf{A = - \log (I/I_0)} \qquad \textbf{(Equation 3. 17)}$$

In the whole experiments, a Lambda 25 UV-VIS spectrophotometer (PerkinElmer LAS, UK) was used with UV Winlab V 2.85 software to measure laccase activity, as shown in **Figure 3. 17**. The reference and sample cuvettes were sealed with clean film in order to minimize the oxidization of ABTS by air. During the measurement, to remedy the limitation of diffusion of immobilized laccase, the sample cuvette was shaken by the vortexer every 10 seconds.

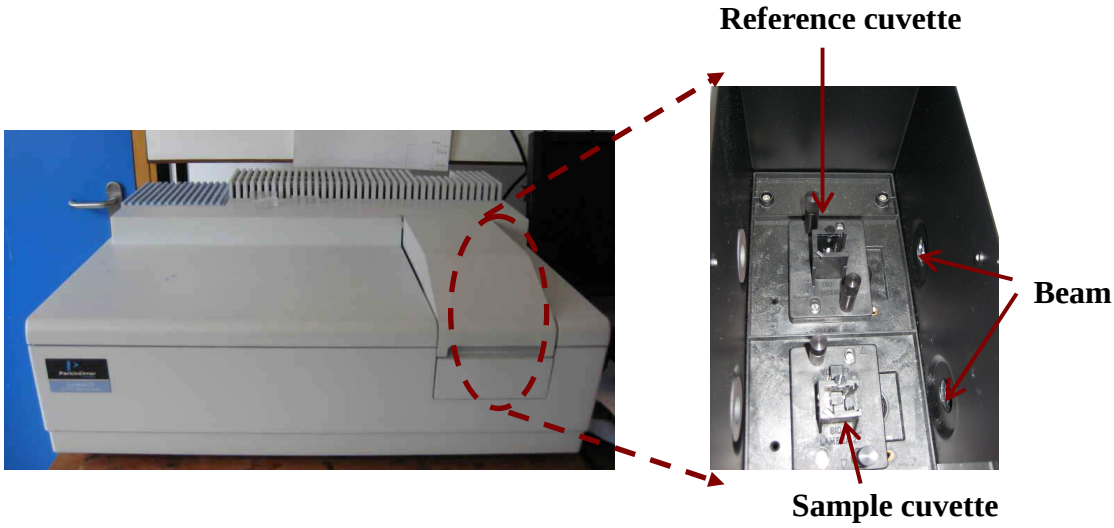

Figure 3. 17 Lambda 25 UV-VIS spectrophotometer (right) and sample chamber (left).

3.2.8 Electrochemical technique -- Cyclic voltammetry for the electrocatalytic activity of laccase

3.2.8.1 Introduction of Cyclic Voltammetry

Cyclic voltammetry (CV) is a most widely technique for studying electrochemical reactions. The power of cyclic voltammetry results from its ability to rapidly provide considerable information on the thermodynamics of redox processes and the kinetics of electron-transfer reactions. CV is often the first experiment performed in an electron-analytical study and offers a rapid location of redox potentials of the electro-active species, and convenient evaluation of the effect of media upon the redox process.

Cyclic voltammetry consists of scanning linearly the potential of a stationary working electrode, using a triangular potential waveform (potential vs. time), as shown in **Figure 3.18**. The complex waveform is composed of two isosceles triangles. The voltage is first held at the initial potential where no electrolysis occurs and hence no faradaic reduced compound is oxidised at the electrode surface. At a particular set value, the scan direction is reversed and the material that was oxidised in the outward excursion is then reduced. During the potential sweep, the potentiostat measures the current resulting from the applied potential. The resulting plot of current vs. potential is termed a cyclic voltammograms (**Figure 3. 19**).

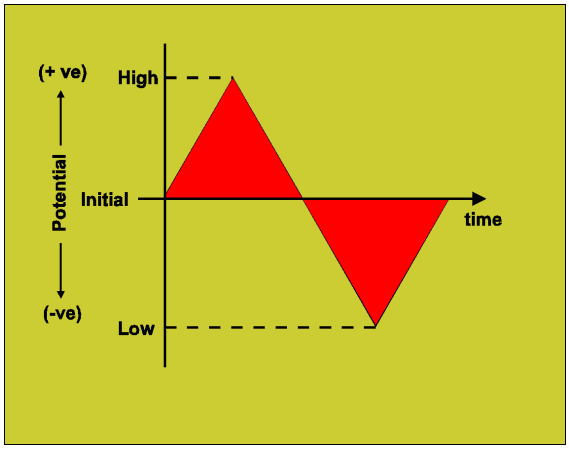

Figure 3.18 Cyclic voltammetry waveform [W3].

In typical cyclic voltammetry, a solution component is electrolyzed (oxidized or reduced) by placing the solution in contact with an electrode surface, and then making the surface sufficiently positive or negative in voltage to force electron transfer. The electrode voltage is changed to a higher or lower voltage at a linear rate. The voltage is then changed back to the original value at the same linear rate. When the surface of the electrode becomes sufficiently negative or positive, a solution species may gain electrons from the surface or transfer electrons to the surface. This results in a measurable current in the electrode circuitry. When the voltage cycle is reversed, the case that the electrons transfer between electrodes and chemical species will also be reversed, leading to an inverse current peak.

$[Fe(CN)_6]^{3-}/[Fe(CN)_6]^{4-}$ redox system is used frequently as a standard system in electrochemistry to study ideal reversible charge transfer behaviour because of the redox couple of Fe^{2+} and Fe^{3+}, as shown in **Equation 3.18**. When the potential is applied on a working electrode from lower to higher voltage, Fe^{2+} is oxidized to Fe^{3+} as the surface of the working electrode will lose electrons; otherwise, Fe^{3+} is reduced to Fe^{2+} when the voltage is returned to the starting value. Cyclic votammogram of the redox reaction of $[Fe(CN)_6]^{3-}/Fe(CN)_6]^4$ is obtained from Autolab (**Figure 3. 19**).

$$[Fe(CN)_6]^{3-} + e^- \underset{\text{oxidation}}{\overset{\text{reduction}}{\rightleftharpoons}} [Fe(CN)_6]^{4-} \qquad \textbf{(Equation 3. 18)}$$

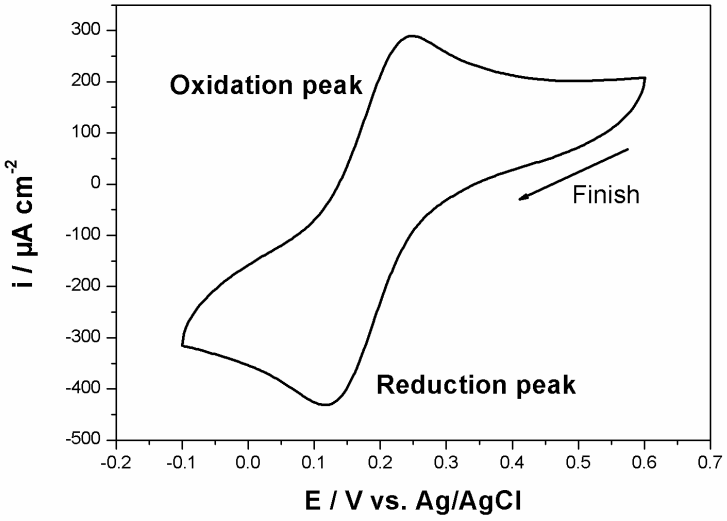

Figure 3. 19 Cyclic voltammogram (second scan) at the bare graphite electrode in 0.1 M citrate buffer, pH 4.5 with 4 mM $Fe(CN)_6^{3-}$. Scan rate: 50 mV/s.

The important parameters obtained from a cyclic voltammograms are the anodic peak current (i_a) (referred to oxidation peak), cathodic peak current (i_{cat}) (referred to reduction peak), anodic peak potential (E_a) and cathodic peak potential (E_c). All of these values can be readily obtained from the voltammograms. The formal reduction potential (E_0) for a reversible system is centered between E_a and E_c. For example, from **Figure 3. 19**, i_a = 290 μA, i_{cat} = 440 μA, E_{pa} = 250 mV, E_{pc} = 125 mV, E_0 = 185 mV (vs. Ag/AgCl). In this project, the catalysis activity of laccase can be monitored with oxygen since the oxidation of the substrate is paired with the reduction of oxygen to water. Therefore, the value of i_{cat} and the ratio of i_{cat} to i_a are more important than other parameters for evaluating the catalysis activity of laccase.

3.2.8.2 Electrocatalytic measurements

The electrochemical cell is needed during electrocatalytic measurements, which includes three electrodes: a reference electrode (RE), counter electrode (CE) and working electrode (WE). The RE acts as a reference in measuring and controlling the WE potential by a potentiometer and at no point does it pass any current, and the CE passes all the current needed to balance the current observed at the WE by a amperometer, as shown in **Figure 3. 20**. For the WE, it makes contact with the analyte, applies the desired potential and facilitates the transfer of electrons to and from the analyte.

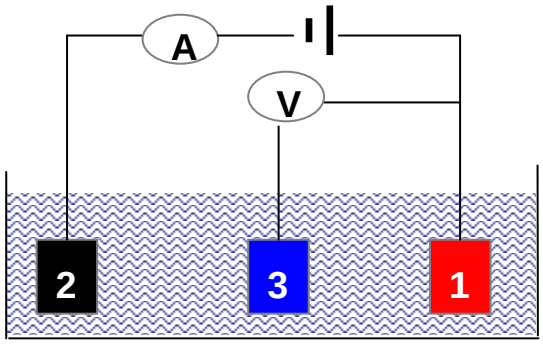

Figure 3. 20 A electrochemical cell with Three electrodes: (1) WE, (2) CE and (3) RE. A: amperometer and V: potentiometer.

In this project, a bright platinum wire (99.9%, Fisher, D0.3mm) was used as the CE, and Ag/AgCl (saturated KCl, MF-2079, BASi) as the RE was used throughout the experiments and stored in 3 M NaCl after experiments, as shown in **Figure 3. 21**. Titanium and graphite are both WE. For preparation of the samples during cyclic voltammetry experiments, in order to avoid reaction of copper wire in the electrolyte, copper wire was wrapped completely by a mixture of Araldite resin and hardener (Bostik Findley Ltd, Staffordshire, UK). An electrochemical cell with cables connected to Autolab is shown below in **Figure 3. 22**.

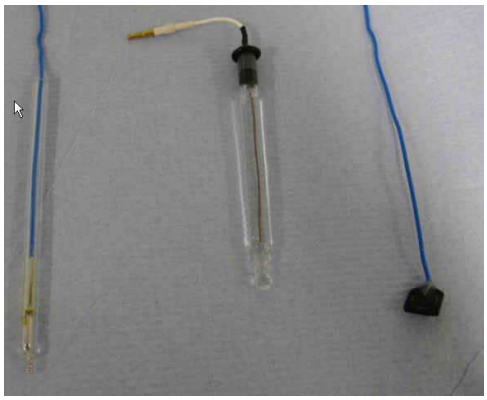

Figure 3. 21 Pt electrode (CE), Ag/AgCl electrode (RE) and graphite electrode (WE), from left to right.

Figure 3. 22 An electrochemical cell with cables connected with the potentiostat: blue connector for RE, red one for WE and black one for CE.

For titanium WE, bare TiO_x and TiO_2 electrodes were placed in 10 ml citrate buffer of 0.1 M with 4 mM $Fe(CN)_6^{3-}$, respectively at room temperature to measure the conductivity. Potassium heacyanoferrate (III)($K_3Fe(CN)_6$, 329.24 g/mol, 99.0+%,

Fisher) 4 mM of 10 ml was prepared by dissolving 13.17 mg of potassium heacyanoferrate in 10 ml citrate buffer of 0.1 M, pH 4.50.

For graphite WE, in order to investigate that laccase reduces oxygen to water, each working electrode was performed with and without oxygen, respectively. For anaerobic experiments, solutions were bubbled through with argon for 1 hour before being used and pure argon was maintained throughout the experiments. For aerobic experiments, pure oxygen (supplied from BOC) was bubbled the solution for at least 10 minutes prior to application, and oxygen gas was also maintained throughout the experiments. For experiments of direct electron transfer (DET), the WE was immersed in 10 ml of 0.1 M citrate buffer, pH 4.50 at room temperature for study of voltammetric responses of immobilized laccase. For experiments of mediated electron transfer (MET), cyclic voltammogram was performed in 10 ml citrate buffer solution of 0.1M with 0.2 mM ABTS at a scan rate of 5, 10, 20 and 50 mV/s, respectively at room temperature. In ABTS – medicated system, to evaluate temperature effect on the catalytic activity of immobilized laccase, graphite electrodes in 10 ml ABTS solution, pH 4.50 were held in a water bath at the rang of 7 to 62°C, respectively. In order to investigate the pH effect of the citrate buffer, the electrodes were immersed in 10 ml ABTS solution with a pH range from 2.5 to 6, respectively.

3.2.8.3 Introduction of Autolab

The Autolab electrochemical instrument is a potentiostat, which can be further configured to needs by adding one ore more of the available modules. The instrument is controlled by powerful windows based software that allows you to perform a wide variety of electrochemical techniques as well as sophisticated data analysis. In this project, electrochemical experiments were performed with an Autolab PGSTAT302 potentiostat (Eco Chemie, Netherlands) and controlled by General Purpose Electrochemical System (GPES) software, version 4.9 (**Figure 3. 23**).

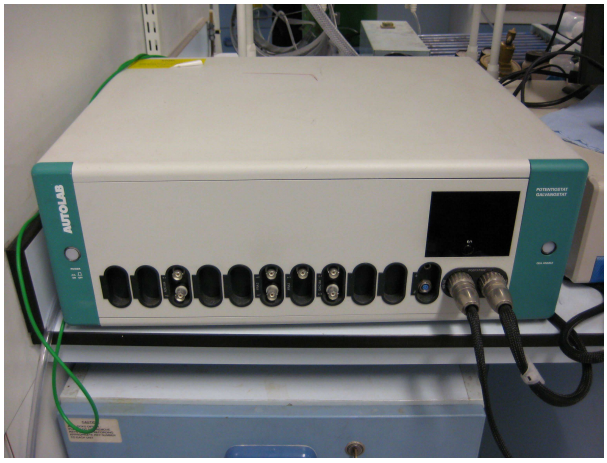

Figure 3. 23 Autolab PGSTAT302 potentiostat.

CHAPTER 4

EXPERIMENTAL RESULTS

4.1 Formation of the APS film on Ti

There are several factors that might influence the growth behaviour of self-assembled film on titanium, such as pre-treatment of substrate, molecular concentration and reaction temperature during silanization, water residual in solvent, etc. The aim of this work is to establish the optimum reaction conditions to form well-ordered thin film of APTES on the titanium surface. The following sections were focused on how the above factors affect the final structure of APTES on surface.

4.1.1 Pre-treatment of titanium

In order to clarify the above factors, the effect of titanium pre-treatment was first investigated since the quality of the APS (after the hydrolysis of APTES) film is dependent on both the effective surface area (cleanliness and roughness of titanium surface) and density of the –OH groups for silanization [Ulman 1991]. In order to obtain a clean and smooth TiO_x layer with a high dense of hydroxyl group, the *Piranha* solution (98% H_2SO_4 + 30 wt% H_2O_2) is commonly used, but there is little mechanistic report on the resulting surface characteristics. Since titanium used here is a polycrystal and has various oxidized status (Ti^{I}, Ti^{II}, Ti^{III} and Ti^{IV}), it is quite difficult to prepare the flat surface. Therefore, a comprehensive research on the effect of piranha treatment on the surface properties of titanium was investigated, including temperature, time, and the volume ratio of H_2SO_4 and H_2O_2 during the oxidation.

4.1.1.1 Temperature effect of oxidation on titanium

Temperature applied during oxidation is known to affect considerably wetting property

of a surface. This is indeed the case for titanium surface. **Figure 4. 1** shows the wettability of pure and hydrolyzed titanium surfaces prepared in a *Piranha* solution (H_2SO_4: H_2O_2 = 1:1) for 30 minutes at different temperatures, as described in Chapter 3.1.1.2. Static water contact angles by contact angle goniometer for titanium samples are presented in **Table 4. 1**. The pure titanium surface is noted to be about 78.2° of a contact angle (**Figure 4. 1a**). Oxidation in the 1:1 *Piranha* solution at room temperature resulted in a significant reduction of the water contact angle to 24° (**Figure 4. 1b**). Increasing temperature to 50°C does not seem to introduce obvious additional reduction of contact angle (**Figure 4. 1c**). Further increasing temperature to 100°C leads to a reduction of the contact angle to 16°, which is almost completely spread out on the surface (**Figure 4. 1d**).

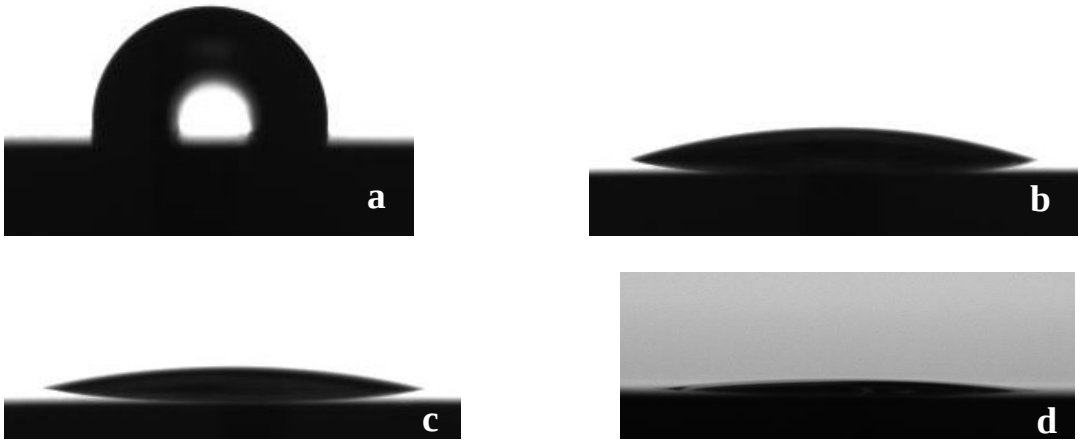

Figure 4. 1 Images of water contact angles for surfaces of pure titanium (a) and TiO_x prepared in the *Piranha* solution of H_2SO_4 : H_2O_2 = 1:1 for 30 minutes at different temperatures: (b)S_{RT_30}, (c) S_{50C_30} and (d) S_{100C_30}.

Table 4. 1 Summary of the samples surfaces in terms of wettability (contact angle) and roughness (n=3).

	Pure titanium	**Oxidized titanium**		
		S_{RT_30}	**S_{50C_30}**	**S_{100C_30}**
Contact angle (°)	78.2±1.3	24±2.7	22±3.1	16±4.9
Roughness (nm)	4.18±1.1	12.94±2.1	29.08±2.4	37.71±3.6

The sudden decrease of water contact angle of the titanium surface in **Figure 4.1a-b** is mainly due to removal of organic contaminant and formation of titanium oxide. The

Piranha solution is very strong oxidant. The first and faster process is dehydration by the concentrated sulphuric acid to carbonise of common organic materials. The second step is oxidation of Ti to TiO_x by hydrogen peroxide. The final step is conversion of TiO_x to TiOH in the aqueous solution. When water is dropped off the surface, compared with pure titanium surface, OH group from the surface forms the bond with water molecules on the boundary, which results in the decrease of surface tension of water surface. In order to equilibrize intermolecular forces of boundary and interior molecules, more and more water molecules attach the surface to equilibrize, which leads to the decrease of water contact angle after oxidation.

Atomic force microscopy (AFM) is used to study the surface topography. To this aim, micrographs of different surfaces were carried out by AFM with each scan $5 \times 5\ \mu m^2$. Surface roughness of the sample surfaces (root mean square (RMS) measured by AFM using Nova software) are presented in **Table 4. 1**. It can be seen in **Figure 4. 2** that the appearance of surfaces strongly depends on the oxidation temperature. Polished pure titanium surface with fine scratch (**Figure 4. 2a**) is smoother than other three surfaces. After oxidation at room temperature, needle-like structures are observed on the surfaces and there are more and more produced as the temperature increases. The RMS values dramatically increase from 4.18 to 12.94 nm, which implies that oxidation in the *Piranha* solution resulted in a roughened surface. When the temperature increases to higher temperatures, the images show aggregated particles on the surfaces (**Figure 4. 2c-d**) and the roughness increases significantly to 29.08 and 37.71 nm for S_{50C_30} and S_{100C_30}, respectively.

Generally, the wetting response is a result of two factors: the exposed chemical components at the surface and the surface roughness. When the pure titanium is oxidized in the *Piranha* solution, two reactions happened: first one is that organic contaminants are oxidized. At the same time, the surface is oxidized to TiO_x and form Ti-OH in the aqueous solution according to the surface properties of titanium [Brunette 2001]. Hydroxyl group (-OH) is a polar group which will strongly interact with the dipole of water molecules making the surface more wettable. Therefore, this is the reason that the water contact angle is changed significantly after oxidation from pure titanium. During the oxidation at the higher temperatures, the water contact angles are

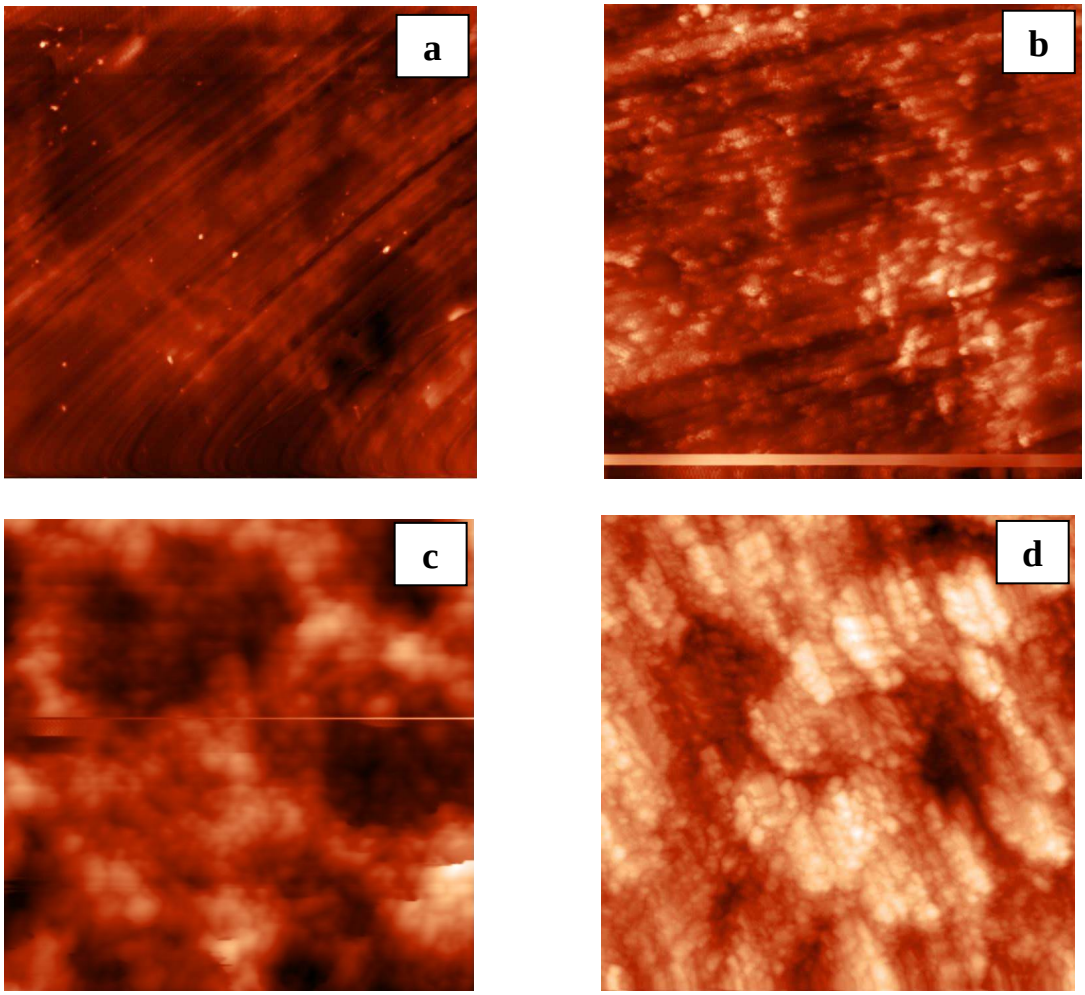

Figure 4. 2 AFM images of titanium surfaces: (a) pure titanium, (b) S_{RT_30}, (c) S_{50C_30} and (d) S_{100C_30}. Scan size: 5 µm × 5 µm.

slightly changed. One of the main reasons is the increase of the surface roughness. If a sample has similar chemical components on the surface, for a rough surface, the contact angle is defined by Wenzel equation:

$$\mathbf{Cos}\boldsymbol{\theta}_{\mathbf{apparent}} = \boldsymbol{r}\,\mathbf{Cos}\boldsymbol{\theta}_{\mathbf{true}} \qquad \textbf{(Equation 4. 1)}$$

where $\boldsymbol{\theta}_{\mathbf{apparent}}$ is the apparent contact angle which corresponds to the stable equilibrium state, $\boldsymbol{r}$ is donated to the ratio of true area of the solid surface to the apparent area and $\boldsymbol{\theta}_{\mathbf{true}}$ is the Young contact angle as defined an ideal surface.

According to the Wenzel equation, the roughness of a surface further decreases the

contact angle if the contact angle is < 90°, while the roughness further increases the contact angle if the contact angle is > 90°, as shown in **Figure 4. 3**. In this case, the greater the surface roughness, the lower the water contact angle. When the temperature is increasing, oxidants accelerate the reaction speed. Polycrystal titanium is oxidized to different oxidation states (TiO, Ti_2O_3, and TiO_2) on the surface, which results in the change of surface roughness. Another reason that results in decrease of the water contact angles, is assumed that the quantity of the -OH groups is increasing with temperature during the oxidation.

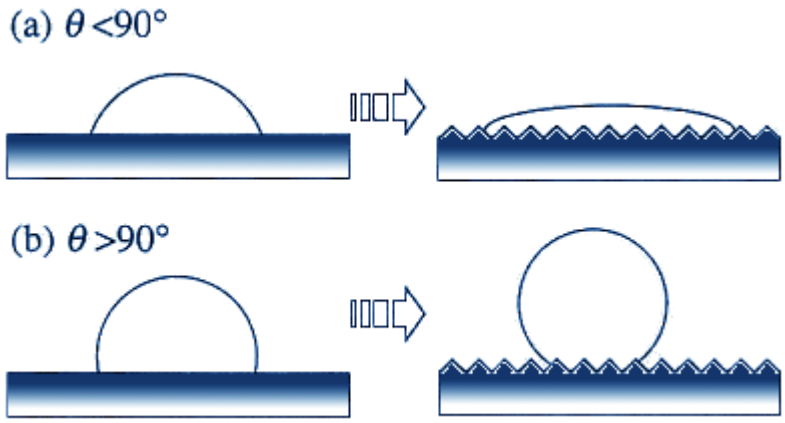

Figure 4. 3 Schematic illustration of the relationship between surface roughness and contact angle.

4.1.1.2 Time effect of oxidation on titanium

On the above experiments, although S_{100C_30} and S_{50C_30} show more hydrophilic surfaces due to water contact angles, their RMS values show surfaces are very rough compared with the length of APTES molecule (about 1.2 nm). Therefore, the water contact angle and AFM analyses reveal that S_{RT_30} results in a relative clean and smooth titanium surface. In this continued study, oxidation of samples was carried out in the *Piranha* solution of 1:1 at room temperature for 5, 15 and 30 minutes, respectively, as described in Chapter 3.1.1.2. The surface roughness and water contact angles for the samples are presented in **Table 4. 2**. **Figure 4. 4** shows the evolution of water contact angles of TiO_x surfaces oxidized up to 30 minutes. The water contact angle of S_{RT_5} is 39° (**Figure 4. 4a**) with big variation after 5-minute oxidation. Further increasing up to 15 minutes resulted in the decrease of the contact angle to 26°. Since

the surface roughness is changed slightly from 6.12 to 7.57 nm (**Figure 4. 5a-b**) when the time increases to 15 minutes, it suggests that the titanium surface is not oxidized completely after 5 minutes at room temperature. In other words, OH groups on the surface might be increased greatly from 5 to 15 minutes. With increasing time up to 30 minutes, there is no noticeable change for the water contact angles (**Figure 4. 4b-c**), while the surface roughness is increased to 11.26 nm (**Figure 4. 5c**). It is assumed that the surface roughness instead of OH groups results in the reduction of water contact angle during the oxidation from 15 to 30 minutes, which indicates that *Piranha* solution does react with titanium and will etch the surface if the samples are left in for a long period of time. Therefore, in order to obtain a relative thin and smooth TiO_x layer, the titanium surface is oxidized completely for 15 minutes at room temperature.

Table 4. 2 Summary of the samples surfaces in terms of wettability (contact angle) and roughness (n=3).

	Oxidized titanium		
	S_{RT_5}	**S_{RT_15}**	**S_{RT_30}**
Contact angle (°)	39±7.1	27±1.4	24±2.9
Roughness (nm)	6.12±1.3	7.57±1.8	11.26±2.0

Figure 4. 4 Images for water contact angles of TiO_x surfaces prepared in *Piranha* solution (1:1) at room temperature for different immersed time: (a) S_{RT_5}, (b) S_{RT_15} and (c) S_{RT_30} (n=6).

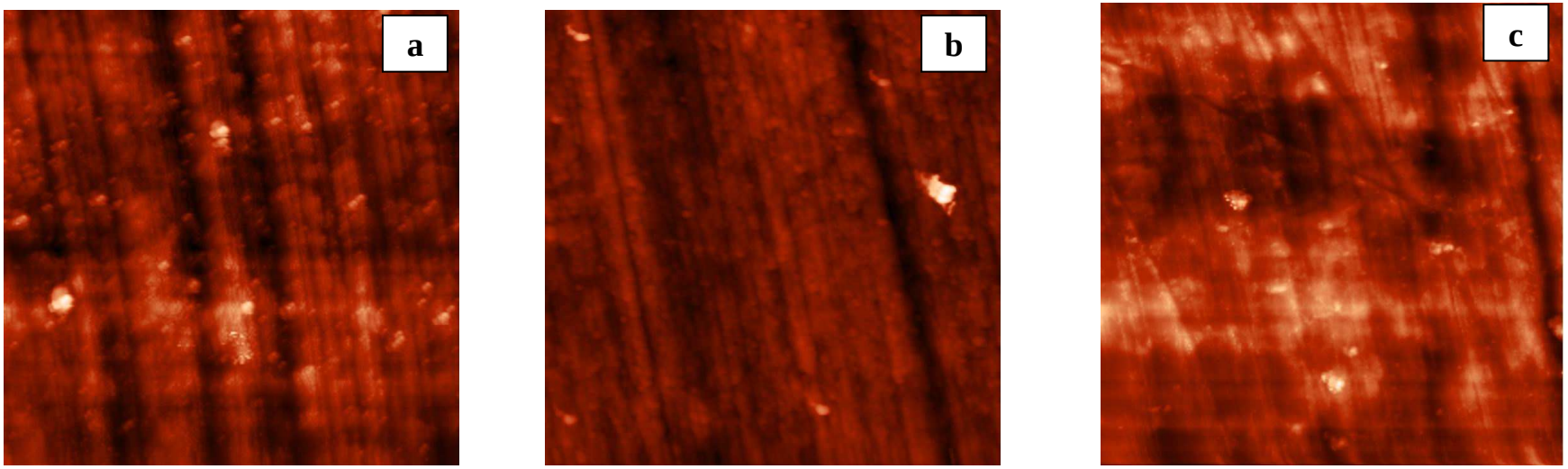

Figure 4. 5 AFM images of oxidized titanium surfaces prepared in the *Piranha* solution (1:1) at room temperature: (a) S_{RT_5}, (b) S_{RT_15} and (c) S_{RT_30} under laboratory atmosphere, scan size 5 µm × 5 µm.

4.1.1.3 Effect of different oxidation solutions on titanium

In order to get very thin, cleaned and smooth TiO_x layer on titanium surface, water contact angle of the titanium surface was measured from different oxidation solutions at room temperature for 15 minutes (each solution is about 20 ml), as described in Chapter 3.1.1.2. In **Figure 4. 6**, the contact angle is reduced from 78.2° to 50° and 46.5°, respectively, after the titanium was immersed in the concentrated H_2SO_4 or the as-received H_2O_2 solution. For a mixture of H_2SO_4 and H_2O_2, increase of H_2SO_4 concentration further reduces the water contact angle from 46.5° to 15.2°. When the ratio of H_2SO_4 and H_2O_2 in the piranha solution is ≥ 3:1, the contact angle of the titanium surface seems to be stable around 15°.

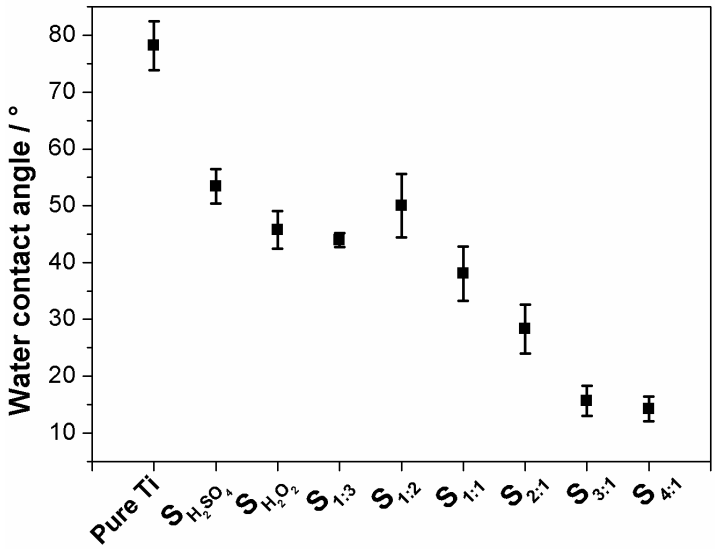

Figure 4. 6 Water contact angles for pure titanium and TiO_x prepared in different oxidized solution for 15 minutes at room temperature (n=6).

Figure 4. 7 shows the key XPS core-level regions (Ti(2p), C(1s) and O(1s)) for oxidized titanium surfaces prepared in four different oxidation solutions (H_2SO_4 to H_2O_2 of 1:3, 1:1, 2:1 and 3:1). For all samples, curve fitting indicated that the O1s peaks were located at 530.4 and 531.8 eV, corresponding to O from the TiO_x and TiOH species, respectively. A slight increase of the amount of oxygen from the TiOH species is observed from all the O1s components: 30.38%, 33.14%, 34.45% and 39.14% for $S_{1:3}$, $S_{1:1}$, $S_{2:1}$ and $S_{3:1}$, respectively. In the Ti 2p regions there were two peaks at 459 and 464.7 eV, respectively, corresponding to the TiO_x species on the surface. On $S_{1:1}$ and

$S_{1:3}$ a small Ti2p peak at 453.8 eV is corresponding to pure titanium, which is non-oxidized. A C1s peak was observed at 284.8 eV corresponding to the contaminants on titanium surfaces under vacuum, which indicates that the C1s peak area decreases with the increase of H_2SO_4 concentration in the piranha solution. The Ti2p peak at 453.8 eV combined with the C 1s peak indicates that titanium surfaces were not oxidized completely within 15 minutes for $S_{1:1}$ and $S_{1:3}$.

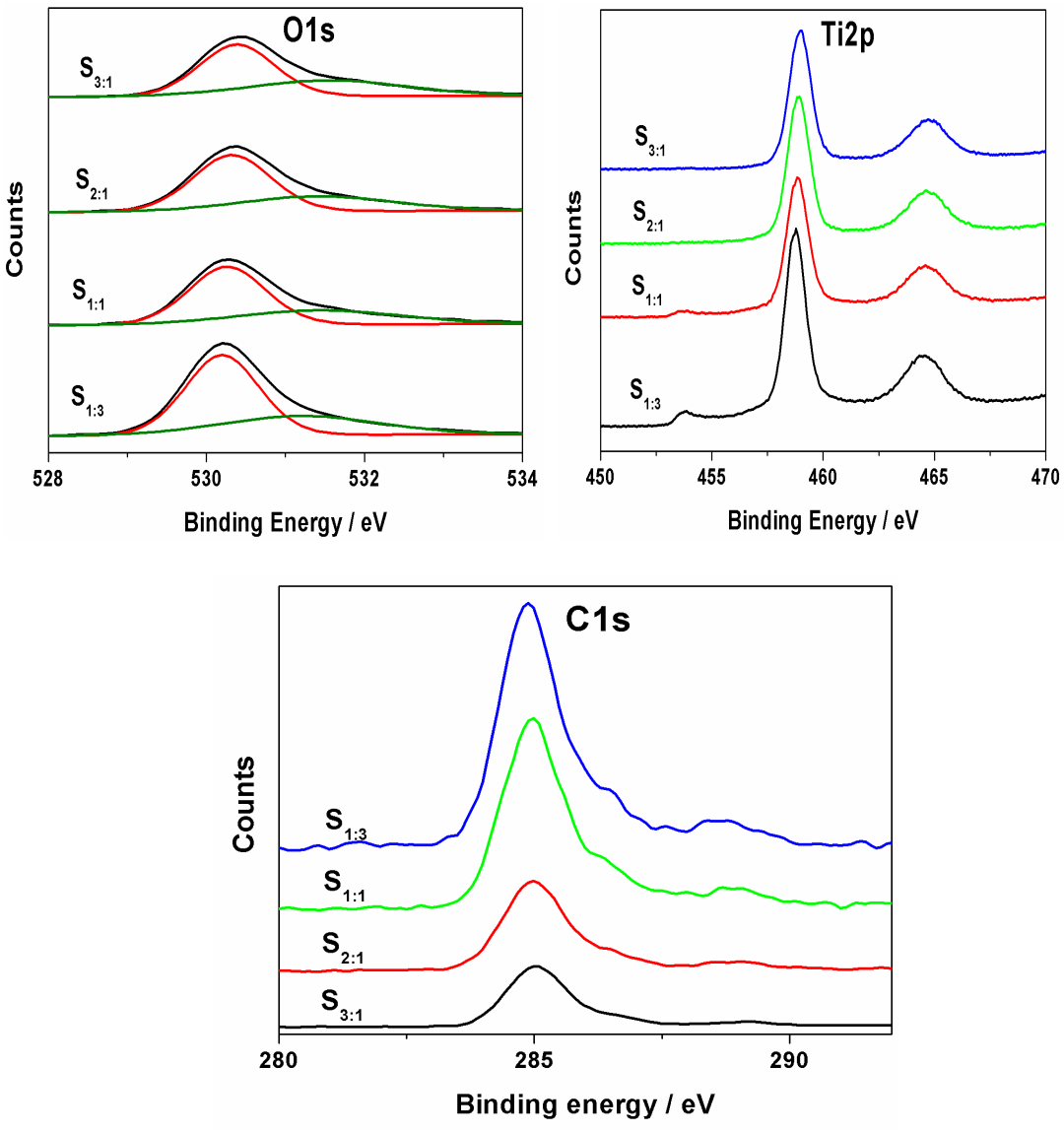

Figure 4. 7 XPS core-level regions for key elements (O, Ti and C) in oxidized titanium prepared in the different piranha solutions.

During oxidation of titanium, acid treatment is often used to remove the native oxide and contamination to obtain clean and uniform TiO_x surface and generally leads to a thin surface oxide layer (< 10 nm). Hydrogen peroxide treatment yields a two-layer

titania gels, which consists of a thin (< 5 nm) and dense inner oxide and an outer porous layer [Wang 2002]. When H_2SO_4 and H_2O_2 are mixed together, the speed of the oxidation is accelerated compared with either H_2SO_4 or H_2O_2 solutions. According to contact angles and the XPS results, the oxidation of the solution is improved with increasing H_2SO_4 concentration in the *Piranha* solution. However, the quantity of the -OH functional groups on the surface is not increased dramatically with the oxidation ability of the *Piranha* solutions. It is assumed that the majority of the – OH functional group comes from the original titanium surface, instead of oxidation of the *Piranha* solution. From the above results, during a short chemical treatment time, the *Piranha* solution of 3:1 will oxidize titanium to obtain more cleaned, smooth and hydrophilic TiOH layer compared with other *Piranha* solutions.

4.1.1.4 Summary

In this section, a systematic investigation of pre-treatment of titanium was reported in order to obtain a relative clean and smooth TiOH layer. Water contact angles and AFM analyses reveal that the *Piranha* solution can only etch the titanium surface at higher temperatures for longer periods of time instead of oxidizing titanium. Further comparison of the different oxidation solutions clearly shows that there is no large difference on the quantity of the – OH functional groups on the titanium surface, which is confirmed by the XPS results. Compared with other solutions, the *Piranha* solution of 3:1 at room temperature for 15 minutes is the optimum condition for the pre-treatment of titanium in order to obtain the well-ordered self-assembled monolayers.

4.1.2 Synthesis of the APS film on Ti

The above section clearly shows that the *Piranha* solution of 3:1 (H_2SO_4 : H_2O_2) for 15 minutes is sufficient to oxidize the titanium surface and to supply a clean and smooth TiOH layer. In order to obtain a well-ordered APS film on titanium, molecular concentrations and temperature during silanization, water content in a solvent and stability of the film were investigated in the following sections. For all the experiments,

the chemical components on the surface were characterized by water contact angle and FTIR, and surface topography was investigated by Atomic force microscopy (AFM).

According to the physical - chemical properties of APTES (3-aminopropyltriethoxy silane) in Chapter 2, this molecule is hydrolyzed very quickly once it meets H_2O, which results in the formation of polysiloxane. In order to prevent the loss of the reactive amine functional groups and the formation of the polysiloxane, the anhydrous toluene was used as the solvent at the beginning. After pre-treatment of titanium, the sample was immersed in 5 ml anhydrous toluene with 1 volume% APTES for 16 hours at 70°C for silanization, as described in Chapter 3.1.1.2. The structural characteristics of a APS film after washed were obtained by FT-IR analysis in the regions 800 – 2000 and 2800 – 2950 cm^{-1} (**Figure 4. 8**).

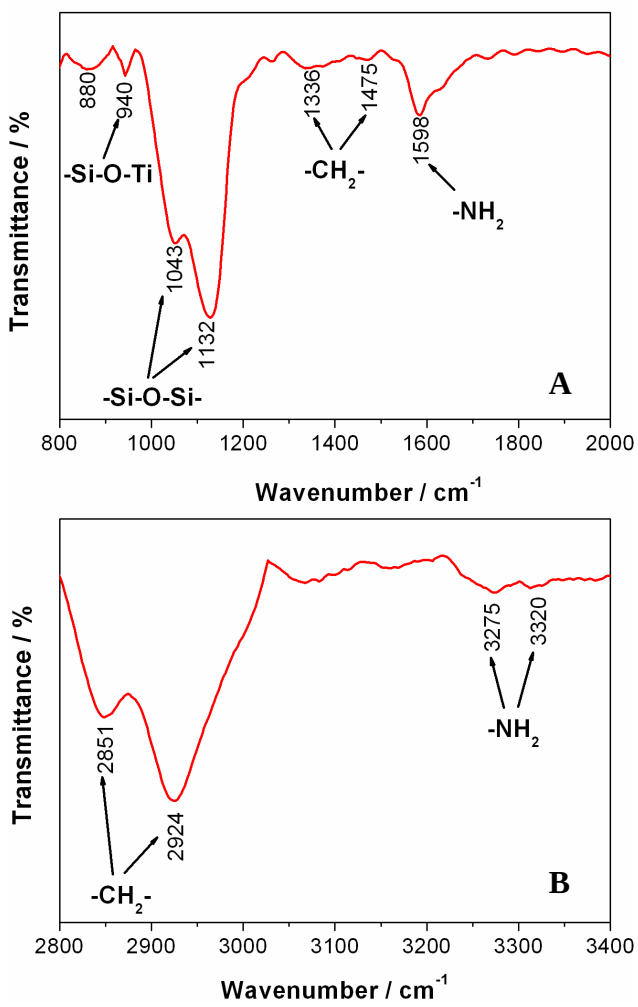

Figure 4. 8 IR spectra of titanium with the APS film produced in 5 ml toluene with 1 v% APTES: (A) the Si-O-Si and the NH regions (800 – 2000 cm^{-1}); (B) the CH region (2800 – 3400 cm^{-1}).

The possible interactions of APTES molecules with the TiOH surface involve the formations of covalent Ti-O-Si and Si-O-Si bonds. According to [Socrates, 1980], a tabulation of the key bands and their assignments are provided in **Table 4. 3**, which shows noticeable differences between the IR spectra of pure APTES and the APS film on titanium. First, **Table 4. 3** shows the vibrations corresponding to the ethoxy groups (ν (C-O) and δ (CH_3)) are missing from the IR spectrum of the APS film between the region of 800 – 2000 cm^{-1}, indicating that APTES was fully hydrolyzed when absorbed onto the TiO_x surface (**Figure 4. 8A**). A weak band at 880 cm^{-1} is assigned to the Si-O stretching from Si-OH, which implies that APS molecules are not completely cross-linked to form Si-O-Si. A very weak band at 940 cm^{-1} is assumed to be the stretching vibration of Si-O-Ti, which indicates that APS molecules are covalently bonded on the titanium surface. In **Table 4. 3**, the two peaks at 1082 and 1103 cm^{-1} were disappeared and the new peaks at 1043 and 1132 cm^{-1} were formed instead. This change is assigned to the formation of Si-O-Si bonds, which can confirm further that ethoxy groups have been totally hydrolyzed. Normally, the primary amine vibration is confirmed by N-H deformation instead of stretching, so the wavenumber for the -NH_2 free groups on titanium is 1592-1605 cm^{-1}.

Table 4. 3 FTIR peak frequencies and infrared spectroscopic group assignments for bulk APTES [www.sigmaaldrich.com] and the APS film on titanium.

Bulk APTES		**APS film on titanium**	
Frequency (cm^{-1})	Assignments	Frequency (cm^{-1})	Assignments
956	ν_s (Si-O-C)	935	ν (Si-O-Ti)
1082	ν_a (Si-O-C)	1043	ν_s (Si-O-Si)
1103	ν_a (Si-O-C)	1132	ν_a (Si-O-Si)
1167	ν (C-O)		
1311	δ (CH_2)	1336	δ (CH_2)
1390	δ (CH_3)		
1477	δ (CH_2)	1475	δ (CH_2)
1596	δ (NH_2)	1598	δ (NH_2)
2885	ν_s (CH_2)	2851	ν_s (CH_2)
2927	ν_a (CH_2)	2924	ν_a (CH_2)
2974	ν_a (CH_3)		
3292	ν_s (NH_2)	3275	ν_s (NH_2)
3366	ν_a (NH_2)	3320	ν_a (NH_2)

Figure 4. 8B shows the spectrum in the range from 2800 to 3400 cm^{-1} correspond to the experimental C-H stretching mode spectra of the APS film on the hydrated titanium surface. In **Table 4. 3**, there are two strong peaks for the CH_2 stretching vibration: 2851 (ν_s (C-H)) and 2924 cm^{-1}(ν_a (C-H)), which are shifted to the left 34 cm^{-1} for ν_s (C-H) and 3 cm^{-1} for ν_a (C-H), respectively. Compared with frequencies from the bulk APTES, there is no CH_3 asymmetric mode observed on **Figure 4. 8B**. It proves that APTES molecules are totally hydrolyzed on the surface. The two very weak peaks observed at 3275 and 3320 cm^{-1} shows the N-H stretching modes. Since the peak positions for symmetric and antisymmetric of alkyl chains are reported typically to be in the range ~ 2850 and ~ 2919 cm^{-1} for all-*trans* extended chains and at ~ 2856 and ~ 2930 cm^{-1} for liquid-like disordered chains [Snyder 1982]. Therefore, it is concluded that the chains are predominantly in the liquid-like disordered conformation on the titanium surface. According to the FTIR results above, APTES molecules are all hydrolyzed and the APS film is formed on the titanium surface by Si-O-Ti and Si-O-Si bonds after 16-hour silanization. However, the film on the surface is not well-ordered, which will affect the applications of the amine functional group.

4.1.2.1 Effect of APTES concentrations on self-assembly

To investigate the effect of molecular concentrations, different concentrations of APTES in anhydrous toluene from 0.02 to 3 v% were used to study the growth behaviour of the APS film on the titanium surface and the preparation conditions of each sample was described in **Table 3.4**. The water contact angles of surfaces with the APS film prepared under different APTES concentrations are shown in **Figure 4. 9**. The water contact angle of $S_{3\%}$ shows increases to 78° from the oxidized titanium of 15°, which suggests that the APS film has already been formed on the titanium surface. When the molecular concentration further reduces to 0.1 – 0.2 v%, the surface with the APS film produces a more hydrophilic surface with the contact angle of 67°. The interesting thing is, when the concentration reduces further to 0.02 v%, the water contact angle of the surface rises dramatically to 90°. The water contact angle results also show a large measurement error on $S_{0.05\%}$ and $S_{0.02\%}$, which indicates hydrophobic groups (e.g. -CH_2-) are probably formed on the titanium surface apart from the –NH_2 functional group and structures of the APS film is schematically shown in **Figure 4. 10**.

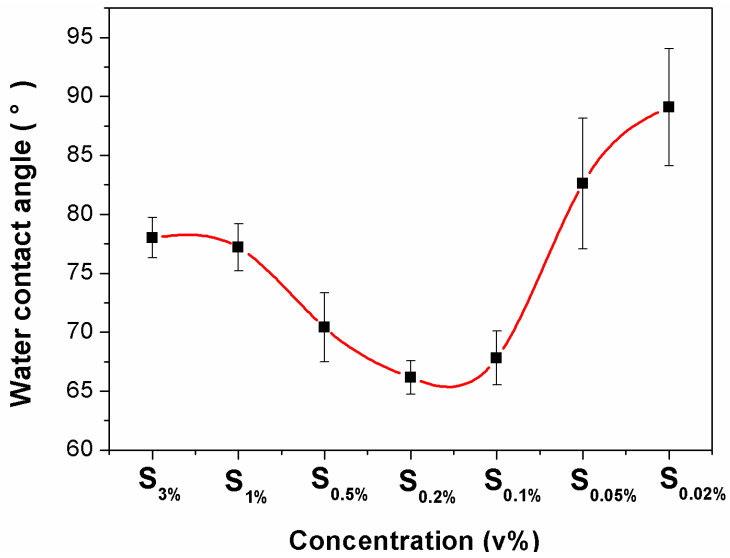

Figure 4. 9 Water contact angles for titanium surfaces with the APS films prepared in 5 ml anhydrous toluene with different APTES concentrations at 70°C for 16 hours (n=6).

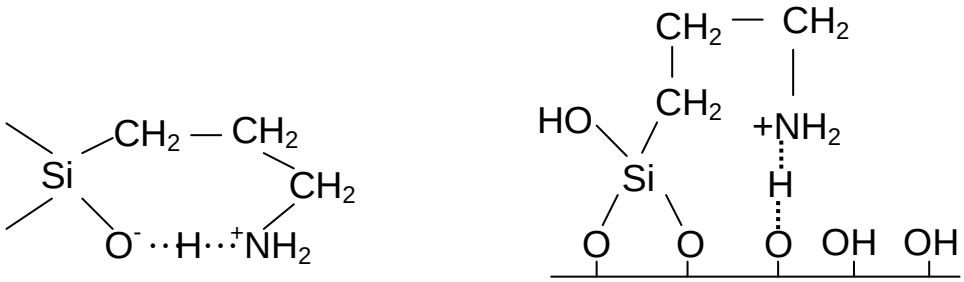

Figure 4. 10 Two possible schematic structures for APS molecules on Ti.

Figure 4. 11 shows the IR spectra from titanium surfaces with the APS film prepared at different concentrations. The intensity of the two doublet peaks for the Si-O-Si stretching increases with APTES concentrations (**Figure 4. 11A**). However, Si-O-Si and N-H bonds cannot be detected on the IR spectra of $S_{0.02\%}$ and $S_{0.05\%}$. When the APTES concentration increases up to 0.5 v%, the IR band observed at 1595 cm^{-1} on the spectra is assigned to the deformation mode of the free $–NH_2$ functional group on the surface (**Figure 4. 11A**). When the APTES concentration is greater or equal to 1 v%, apart from the free $–NH_2$ deformation band, another band at 1655 cm^{-1} is also found on the IR spectra of $S_{1\%}$ and $S_{3\%}$, which is assigned to the $–NH_3^+$ asymmetric deformation according to the reference [Socrates 1980]. This result reveals that a network structure of $OH\cdots{}^{+}NH_2–$ in the APS film is formed.

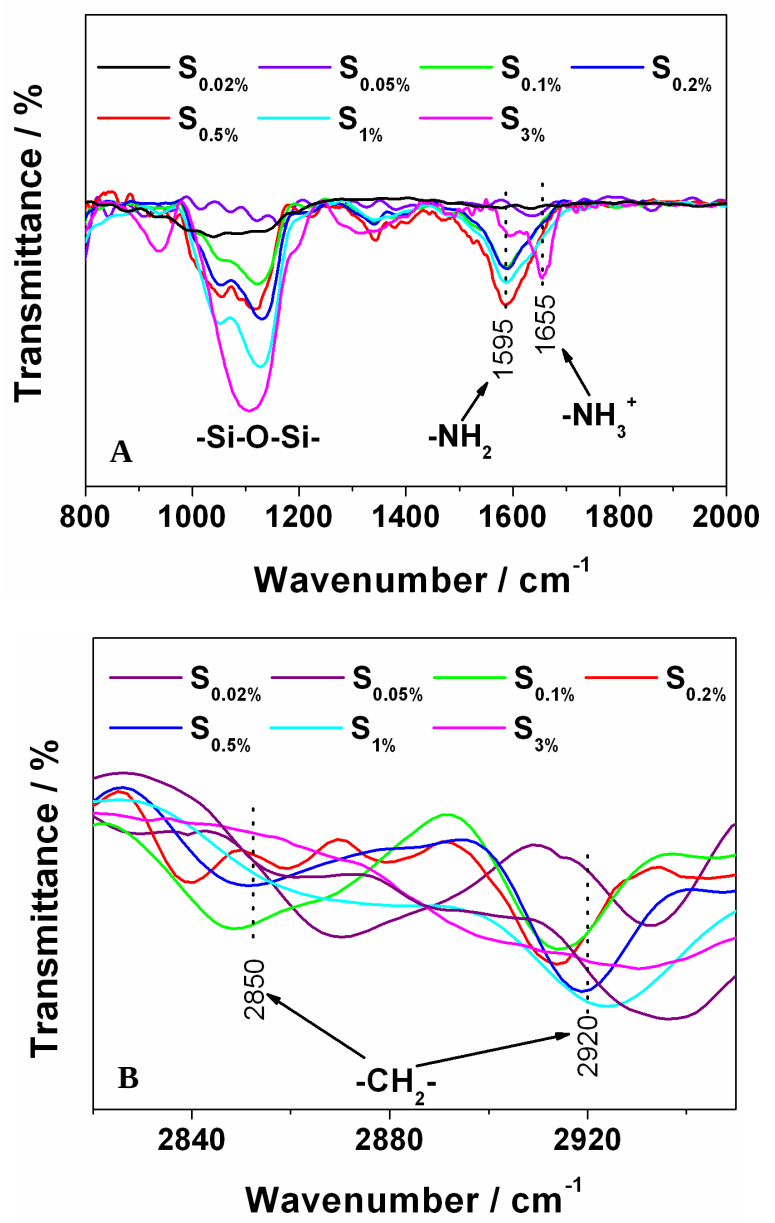

Figure 4. 11 IR spectra of the APS film prepared at different APTES concentrations: (A) the Si-O-Si and the NH regions (800 – 2000 cm^{-1}); (B) the CH region (2800 – 2950 cm^{-1}).

Figure 4. 11B shows the IR spectra of different samples in the 2800-2950 cm^{-1} region of the C-H vibrations, which can suggest the ordered structure of the self-assembled film on the surface [Socrates 1980]. The C-H stretching vibrations on the IR spectra of $S_{0.05\%}$ and $S_{0.02\%}$ are at 2869 and 2936 cm^{-1}, which suggests that the structure of the APS film on the surface is disordered. In the same way, the structures of the APS film with the concentrations of 1 v% and 3 v% are disordered as the C-H stretching vibrations on the IR spectra are at 2858 and 2923 cm^{-1}. However, $S_{0.1\%}$, $S_{0.2\%}$ and $S_{0.5\%}$ show well-ordered structure of the APS film as the positions of C-H stretching modes

of alkyl chain are in the range of ~ 2950 cm^{-1} and ~ 2920 cm^{-1} [Snyder 1982], because the APS film is closed packed, resulting in the formation of more chemical bonds (e.g. Si-O-Si), which leads to the redshifting (lower wavenumber).

Several spectra are markedly different essentially due to varying structures of the APS film on titanium. According to [Socrates 1980], the N-H deformation mode for the free amine groups is observed between 1590 – 1605 cm^{-1}. If it is out of this range, the $–NH_2$ group may participate in the formation of a weak hydrogen bonding ($-NH_3^+$). The ordering of the APS film should be reflected on the IR spectra of the C-H stretching region. When the concentration of APTES in anhydrous toluene is lower than 0.1 v% or greater than 0.5 v%, the two predominant bands of the C-H stretching are blueshifted by 5 – 18 cm^{-1} (higher wavenumber), indicating an increasingly disordered state for the aminopropyl segments, in comparison with those on the IR spectra of $S_{0.1\%}$, $S_{0.2\%}$ and $S_{0.5\%}$. Therefore, from the IR spectral characteristics of the APS film and the water contact angles, the range of the optimum APTES concentration on titanium should be between 0.1 – 0.5 v% in 5 ml anhydrous toluene.

4.1.2.2 Stability of the APS film on Ti

The APS film prepared by self-assembly is commonly employed as an adhesion promoter or molecular glue between substrates and molecules. For example, the APS film is used to promote the protein adhesion for biological implants. However, the APTES molecule includes 3-carbon chain length, which indicates that the structure of APS film on the surface will not be stable because of weak van der Waals interactions between chains, leading to the poor applications. Therefore, to further clarify the stability of the APS film, titanium samples were placed in a desiccator and in different solutions at room temperature up to 72 hours for measurement of hydrolytic stability of the APS film, such as phosphate buffer (pH 4 and pH 10) and distilled water (pH 6.5). According to the above section, titanium samples were prepared in 5 ml anhydrous toluene with 0.2 v% APTES at 70°C for 16 hours.

Figure 4. 12 shows the water contact angles of the APS film on the titanium surface immersed in the phosphate buffer, pH 4 within 72 hours. The contact angle of the

surface slightly decreased to 66.5° from 68° within 10 hours. Immersion for 30 hours resulted in an obvious reduction of the contact angle to 47.1°. Further immersion up to 72 hours, the surface produces a more hydrophilic surface with the contact angle of 32.6°. The water contact angles are dramatically decreasing with large measurement errors from 10 to 72 hours, which indicates that hydrophilic groups (e.g. –HO-P(O)-) are probably produced on the titanium surface apart from primary amine groups.

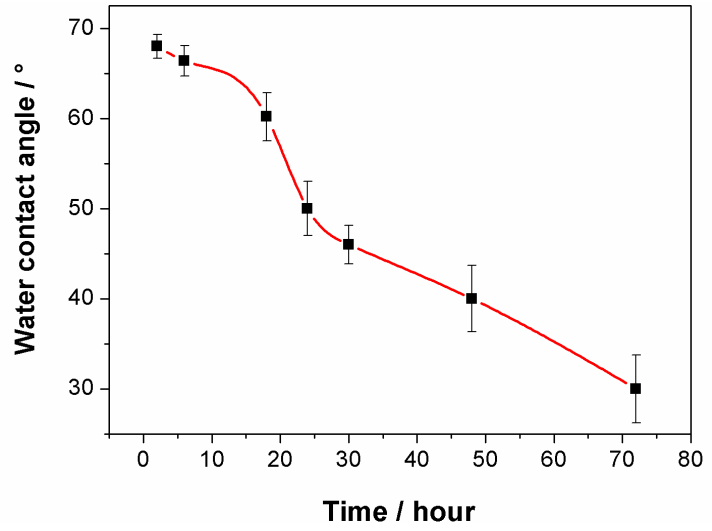

Figure 4. 12 Water contact angles for the APS film in a phosphate buffer, pH 4 vs. time (n=6).

Figure 4. 13 reveals the structure of the APS film on the surface immersed in the phosphate buffer, pH 4 up to 72 hours at room temperature. During the first two hours in the buffer, the N-H deformation bands red-shifts from 1595 to 1578 cm^{-1}, which is assigned the symmetric vibration of the $–NH_3^+$ according to the reference [Socrates 1980]. This is due to the high concentration of hydrogen ions in the phosphate buffer, pH4. When samples were immersed from 18 to 72 hours, the IR spectra show two peaks at 1557 and 1644 cm^{-1}, respectively in **Figure 4. 13A**. Normally, the amine functional groups can easily react with –COOH groups or phosphate groups (HO-P(O)-) under the acidic condition to form amide bond, which are located at 1520 and 1655 cm^{-1} according to the reference [Socrates 1980]. Therefore, the peaks at 1557 and 1644 cm^{-1} on the IR spectra are assumed to be the vibration of physical adsorped $–NH_2\cdots$HO-P(O)-, which leads to the formation of hydrophilic surface. The band at 1396 cm^{-1} is assigned to the deformation of CH_3 according to the **Table 4. 3**, which suggests that the new molecules attach on the APS film. The intensities of Si-O-Si,

-CH_2- and -NH_2 bands on the IR spectra decrease with immersion time in the buffer, which indicates that the APS film is rapidly hydrolyzed in the acidic aqueous solution. However, the intensity of Si-O-Ti band does not decrease when immersion up to 48 hours. Especially immersion up to 72 hour results in the disappearance of the Si-O-Ti bond on the IR spectrum, which implies that the APS film is almost hydrolyzed away from the surface.

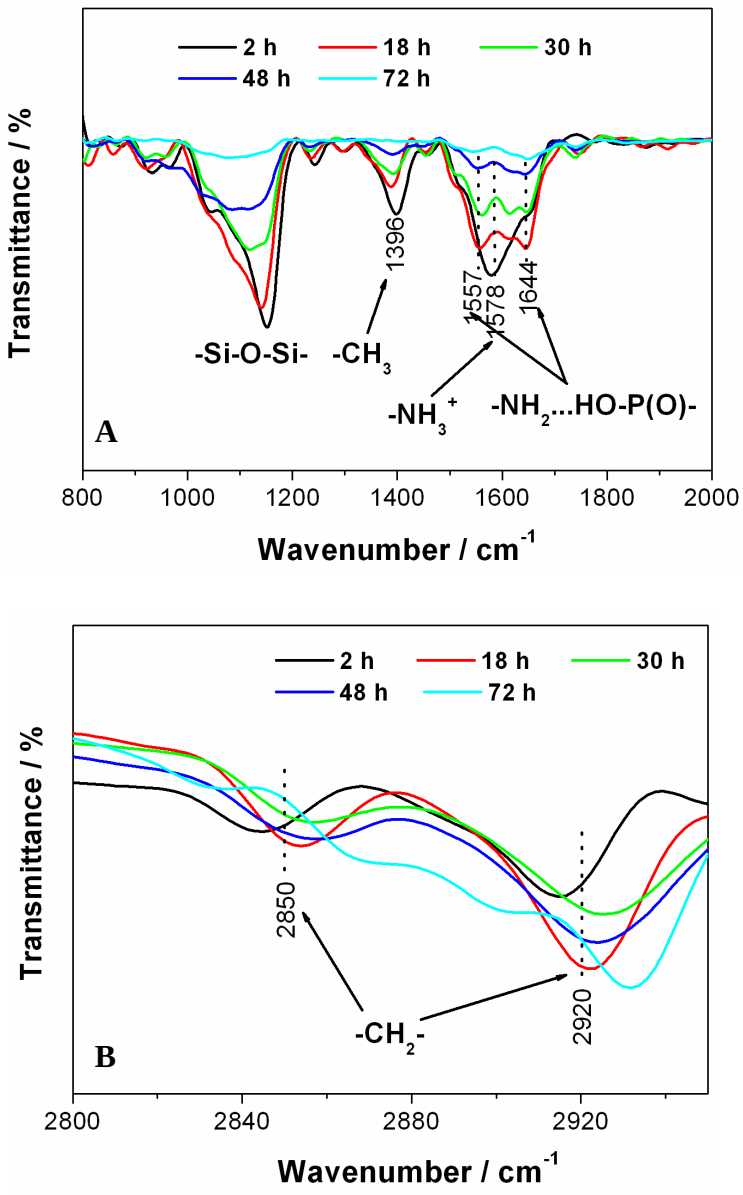

Figure 4. 13 IR spectra of the APS film in the phosphate buffer, pH 4: (A) the Si-O-Si and the NH regions (800 – 2000 cm^{-1}); (B) the CH region (2800 – 2950 cm^{-1}).

Figure 4. 13B shows that the structure of the APS film is still well-ordered within 2-hour immersion in the phosphate buffer, pH 4 because the C-H stretching modes

appear at 2844 and 2914 cm^{-1}. However, immersion up to 72 hours results in that the structure of the APS film becomes disordered. Therefore, from the water contact angles and IR spectra, the APS film can be rapidly hydrolyzed in the acidic aqueous solution and primary amine functional groups can be easily protonated or form the new chemical bonds with other molecules.

The stability of the APS film on titanium was studied in the distilled water (pH 6) for 72 hours at room temperature and the results are shown in **Figure 4. 14** and **Figure 4. 15**. The water contact angle is dramatically decreased to 47° from 68° with immersion time up to 35 hours (**Figure 4. 14**), which indicates that a hydrophilic chemical components are formed on the surface (e.g. –OH). However, immersion up to 72 hours results in the increase of the water contact angles to 63°, which implies hydrophobic groups (e.g. -CH_2-) are probably formed on the titanium surface besides the primary amine groups.

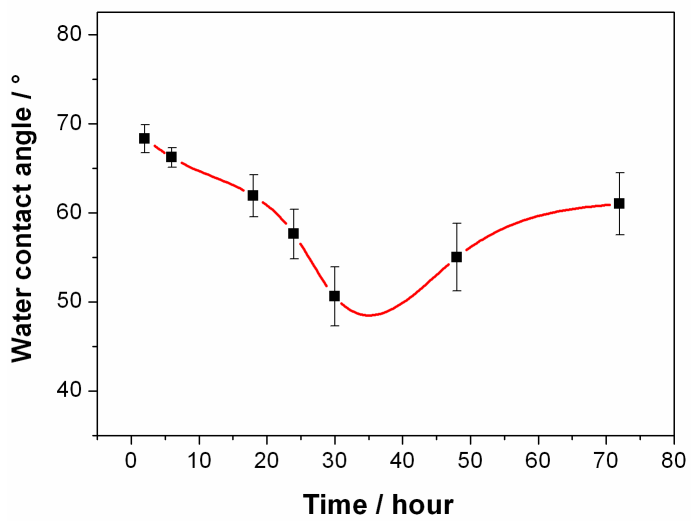

Figure 4. 14 Water contact angles of the APS film on titanium in the distilled water, pH 6.5 vs. time (n=6).

Figure 4. 15 shows transformation of the structure of the APS film in the distilled water, pH 6.5 for 72 hours. Within 48 hours for the immersion time, the intensity of Si-O-Si stretching modes on the IR spectra is slightly decreased, which implies that the APS film is partly hydrolyzed to form the silanol. The formation of silanol is the reason that the contact angle decreases with immersion time up to 35 hours. During the whole

immersion time, the intensity of the Si-O-Ti stretching mode observed at 930 cm^{-1} in the IR spectra is not changed (**Figure 4. 15A**), which implies that APS molecules is not dropped off from the titanium surface by the hydrolysis. Also this result firms that the Si-O-Ti bond is more stable than the Si-O-Si stretching mode in the distilled water, pH 6. Apart from the primary amine deformation at 1604 cm^{-1}, other two peaks at 1559 and 1663 cm^{-1} are observed on the IR spectra, which results from the $–NH_2$ groups to form the $–H_2N…HO-$ bond by the hydrogen bond. The hydrolysis of Si-O-Si bond results in the less interaction between the carbon chains in the APS film. It is assumed that the free amine functional groups are bended to link the hydroxyl groups from the

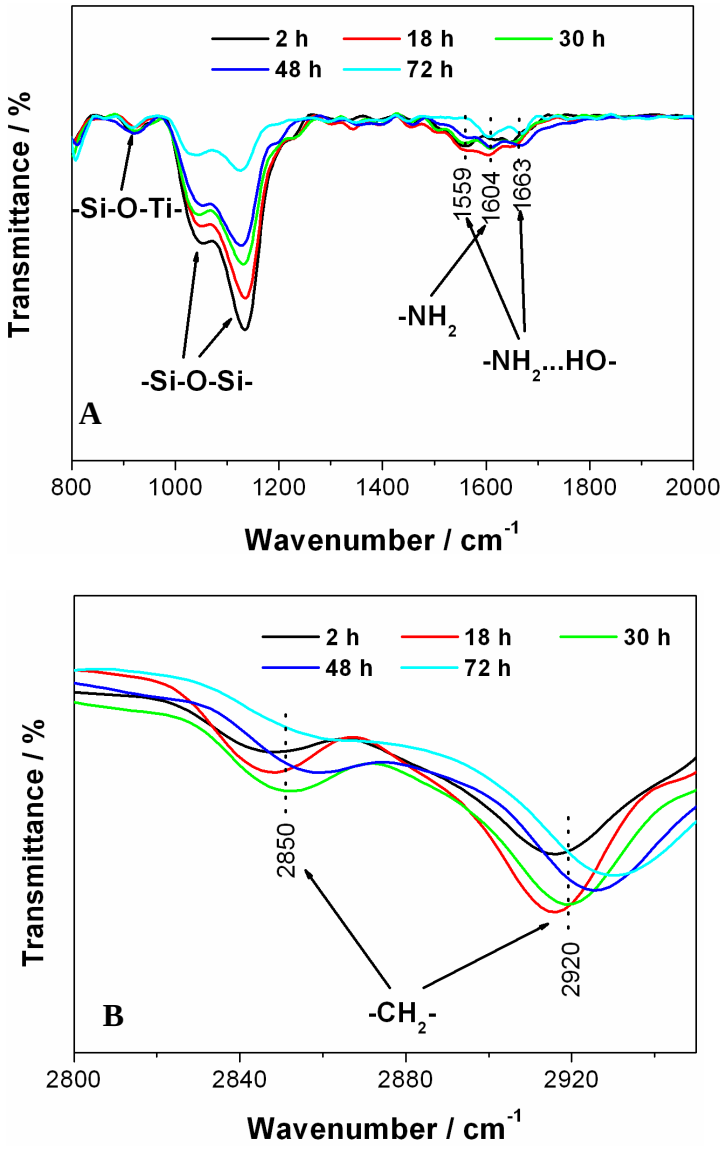

Figure 4. 15 IR spectra of the APS film on the titanium surface in the distilled water, pH 6.5: (A) the Si-O-Si and the NH regions (800 – 2000 cm^{-1}); (B) the CH region (2800 – 2950 cm^{-1}).

silanol, as shown in **Figure 4. 10**, which could result in the exposure of the -CH_2- groups on the surface, leading to the increase of the contact angle during the immersion of 35 to 72 hours. The IR spectra in **Figure 4. 15B** show the positions of the C-H stretching models of the alkyl chain are in the ordered range of ~ 2850 and ~ 2920 cm^{-1} when the titanium sample was immersed in the distilled water for 30 hours. Immersion up to 72 hours results in the disordered structure of the APS film because of the peaks of the C-H stretching modes at 2855 and 2929 cm^{-1} on the IR spectra, which can support the assumption of the disordered structure of the APS film on the surface.

The above two sections show that the APS film on the surface is more stable in the distilled water compared with in the acidic aqueous phosphate buffer, although the $–NH_2$ groups are protonated by the hydrogen bond. In this continued study, the titanium sample with the APS film was immersed in the phosphate buffer, pH 10 for 72 hours to study the stability. **Figure 4. 16** shows the water contact angles of the sample immersed in an alkali solution. The water contact angle of the sample decreases slowly to 58.1° from 68.3° with increasing immersion time. According to the results of the IR spectra of the APS film (**Figure 4. 17A**), the intensity of –Si-O-Si- stretching modes reduces with increasing immersion time, which indicates that the –Si-O-Si- bond is also easily hydrolyzed in the alkali condition. Up to 48 hours of the immersion time, the free $–NH_2$ functional groups maintain on the APS film due to peak at 1598 cm^{-1}.

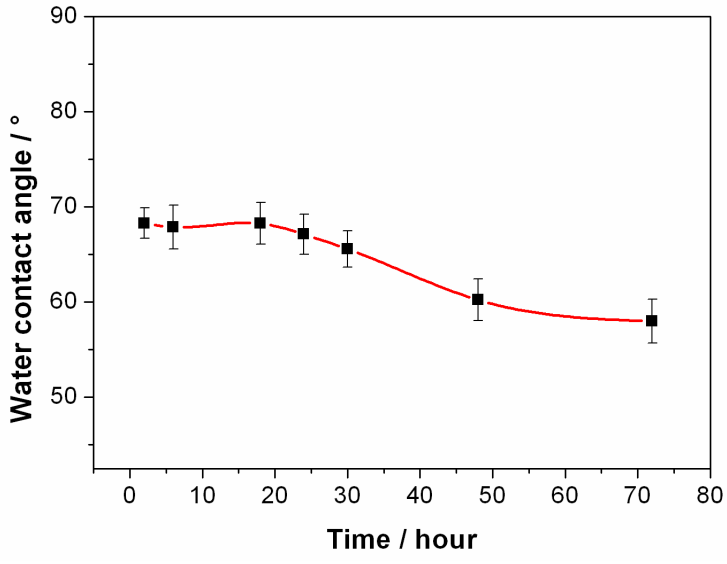

Figure 4. 16 Water contact angles of the APS film in the phosphate buffer, pH 10 vs. time (n=6).

Further immersion up to 72 hours leads to the formation of a small shoulder at 1671 cm^{-1} on the IR spectrum, which is assigned for $–NH_3^+$ deformation mode and renders the APS film disordered, as the positions of ν_s (CH_2) and ν_a (CH_2) at 2860 and 2931 cm^{-1}, respectively, as shown in **Figure 4. 17B**.

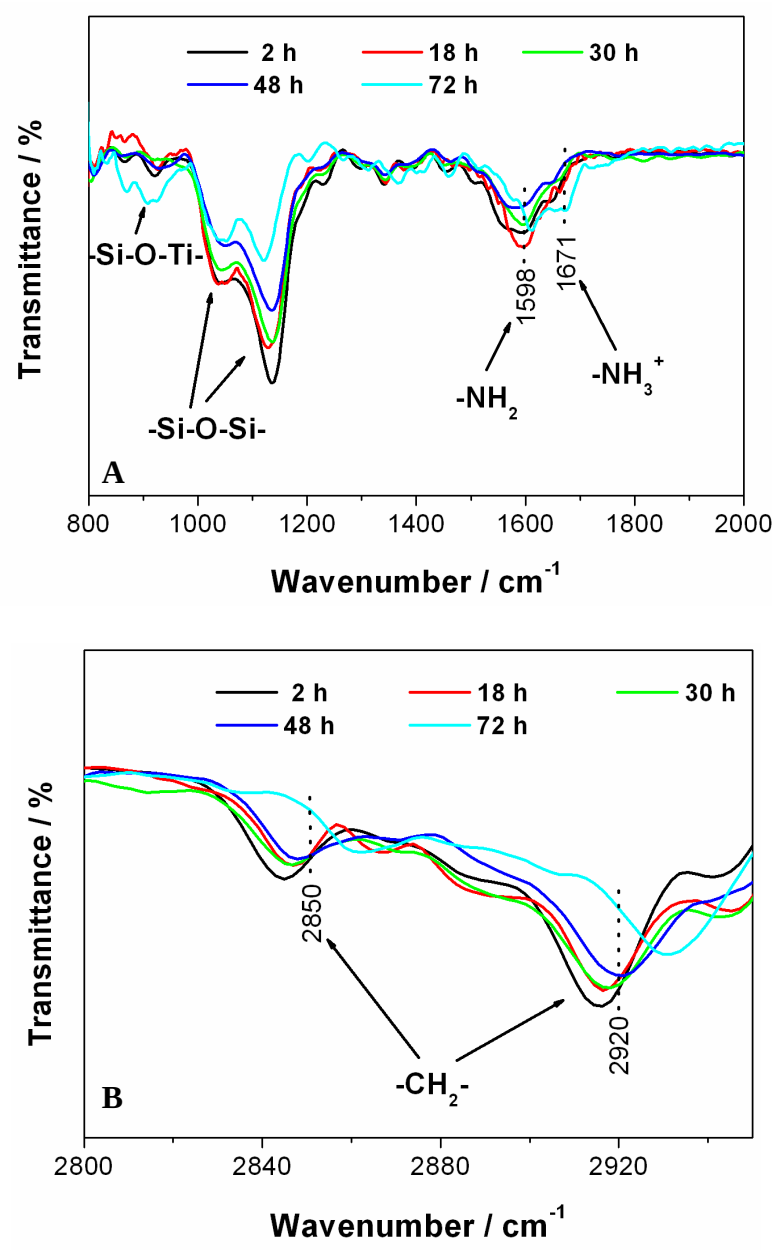

Figure 4. 17 IR spectra of the APS film in the phosphate buffer, pH 10: (A) the Si-O-Si and the NH regions (800 – 2000 cm^{-1}); (B) the CH region (2800 – 2950 cm^{-1}).

In the aqueous solution, the free amine functional groups easily form the $-NH_3^+$, leading to the disordered structure in the APS film. In order to avoid the formation of the protonated amine groups on the surface, titanium samples with the APS film were

stored in a desiccator for 72 hours and the results are shown in **Figure 4. 18-4.19**. In **Figure 4. 18**, it is noted that the contact angle increases significantly to 102.5° from 68.1° with increasing storage time, which confirms that the APS film produces a hydrophobic surface. Due to the sample stored under vacuum, it is assumed that the structure of the APS film is changed with 72 hours in the desiccator.

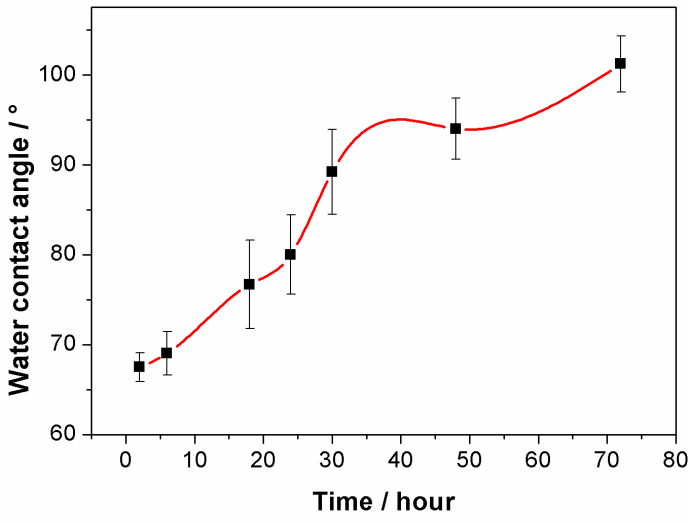

Figure 4. 18 Water contact angles for the APS film in a desiccator vs. time (n=6).

Figure 4. 19 shows the IR spectra of titanium samples with the APS film stored in the desiccator for 72 hours. The free amine functional groups observed at 1605 cm^{-1} on the IR spectra always exist on the APS film, as shown in **Figure 4. 19A**. A small shoulder peak at 1671 cm^{-1} is found on the IR spectrum with the immersion time up to 72 hours, which is assigned to the $–NH_3^+$. Moreover, the intensity of the Si-O-Si stretching vibration is reduced after immersion for 72 hours. It is probably because the water in the ambient might protonate the $–NH_2$ groups or hydrolyze the Si-O-Si bonds, respectively. **Figure 4. 19B** reveals that the structure of the APS film is disordered after 2 to 72 hours in the desiccator, which might result from that the three-carbon chain of the APTES molecule shows less interactions in the APS film, leading to the unstable structure and further resulting in the increase of the contact angle.

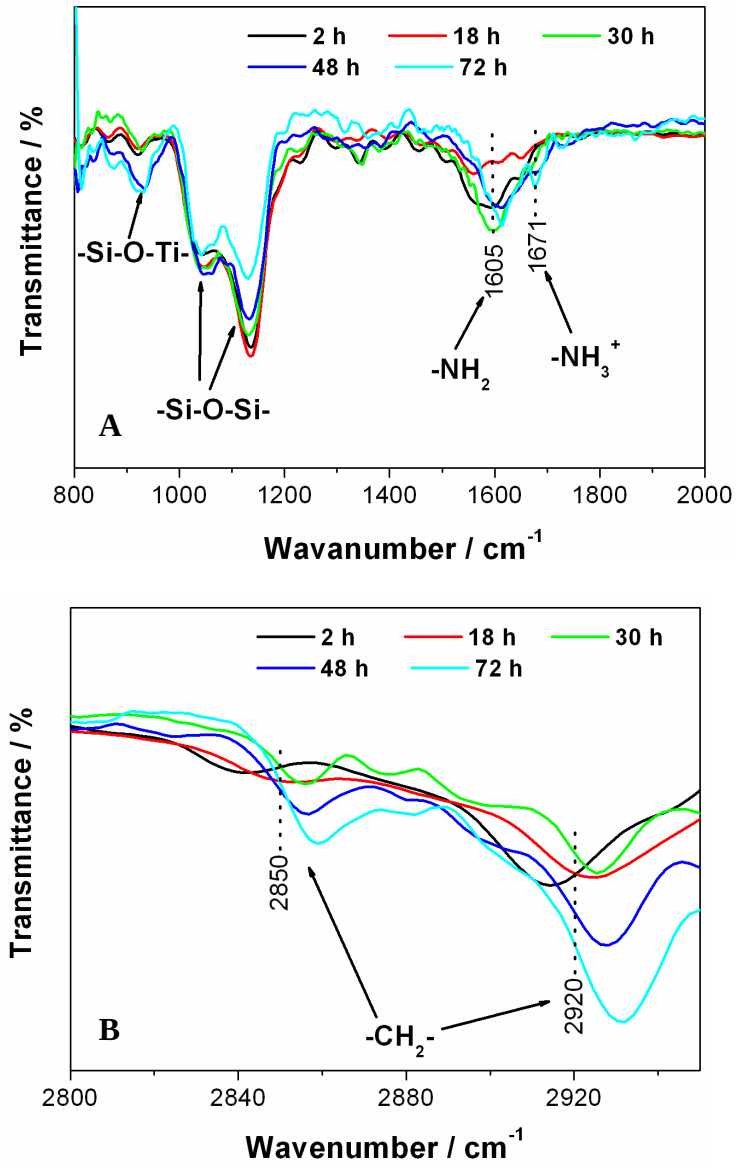

Figure 4. 19 IR spectra of the APS film on the titanium surface in the desiccator: (A) the Si-O-Si and the NH regions (800 – 2000 cm^{-1}); (B) the CH region (2800 – 2950 cm^{-1}).

4.1.2.3 Growth behaviour of APTES on self-assembly

In order to understand the kinetics of silanization of APTES molecules on titanium, the growth process of the APS film prepared in anhydrous toluene with 0.2 v% APTES was studied from 5 to 960 minutes at 70°C by the contact angle goniometer and AFM. **Figure 4. 20** shows the water contact angles of different titanium surfaces, including pure titanium, oxidized titanium and titanium with the APS film prepared for different durations in the solvent. The contact angle of the oxidized titanium decreases to 22°

from the pure titanium of 79°, which confirms that a clean titanium surface with TiOH is formed after treated by the piranha solution (3:1). When the titanium surface was treated in the solvent with APTES up to 120 minutes, the water contact angle of the surface rises dramatically to 63°, which indicates that the surface with the APS film produces a more hydrophobic surface compared with the oxidized titanium. When the immersion time lasts up to 960 minutes, the contact angle of the titanium surface trends to be stable around 65°.

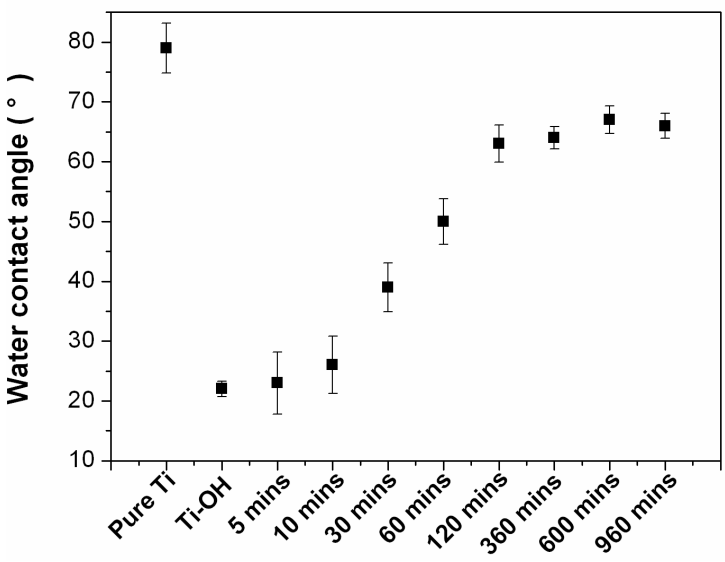

Figure 4. 20 Water contact angles of the pure titanium, oxidized titanium and titanium surfaces with the APS film for different immersion time (n=6).

Different durations in the anhydrous toluene with 0.2 v% APTES were used to investigate the growth behaviour of the APS film on the titanium surface and the topography of each sample measured by AFM is shown in **Figure 4. 21**. After the silanization for 5 minutes, small white specks like islands around ~ 50 nm in diameter are observed on the surface. Immersion up to 120 minutes results in that the islands grow in size and number on the titanium surface with time. The globular islands then agglomerate together when the silanization time lasts up to 960 minutes and the surfaces show a patchy dense topography. **Table 4. 4** reveals the roughness of different surfaces prepared with different conditions. The pure titanium and oxidized titanium samples both show relative smooth surfaces with the roughness of 4.22 and 7.67 nm, respectively, compared with that with the APS film. When titanium samples were

silanized in the solvent, the surface is getting rougher and rougher after 60 minutes. However, immersion up to 120 minutes results in a relative smoother surface with the roughness of 12.53 nm, which indicates that APS molecules are totally covered on the surface. The roughness of the surface then increases dramatically to 33.41 nm until the silanization of 960 minutes, which is probably attributed to the agglomeration of APTES molecules on the surface.

Table 4. 4 Surface roughness for different titanium samples by AFM (10 μm ×10 μm) (n=3).

Samples		**Surface roughness (nm)**
Pure titanium		4.22±0.9
Oxidized titanium (TiOH)		7.67±1.2
Titanium samples with the APS film prepared for different time	5 minutes	9.30±1.4
	10 minutes	11.65±2.1
	30 minutes	17.61±2.9
	60 minutes	19.66±4.0
	120 minutes	12.53±2.2
	360 minutes	16.82±2.6
	600 minutes	21.77±3.1
	960 minutes	33.41±3.3

Several things can be noted from the results of the water contact angles and surface topography by AFM. First of all, the water contact angle of the surface increases after the silanization compared to the TiOH surface, which indicates a general trend towards decreasing the wettability by the APTES self-assembly. Secondly, APS molecules seem to totally cover on the surface at 70°C in 0.2 v% APTES solvent for 120 minutes. The Silanization up to 960 minutes at 70°C results in the formation of multilayer on the surface, which might cause that the APS film is not stable. Finally, from AFM images the growth behaviour of the APS film on the surface is the formation of islands first, and then each island as a centre extends and links each other to form the layer.

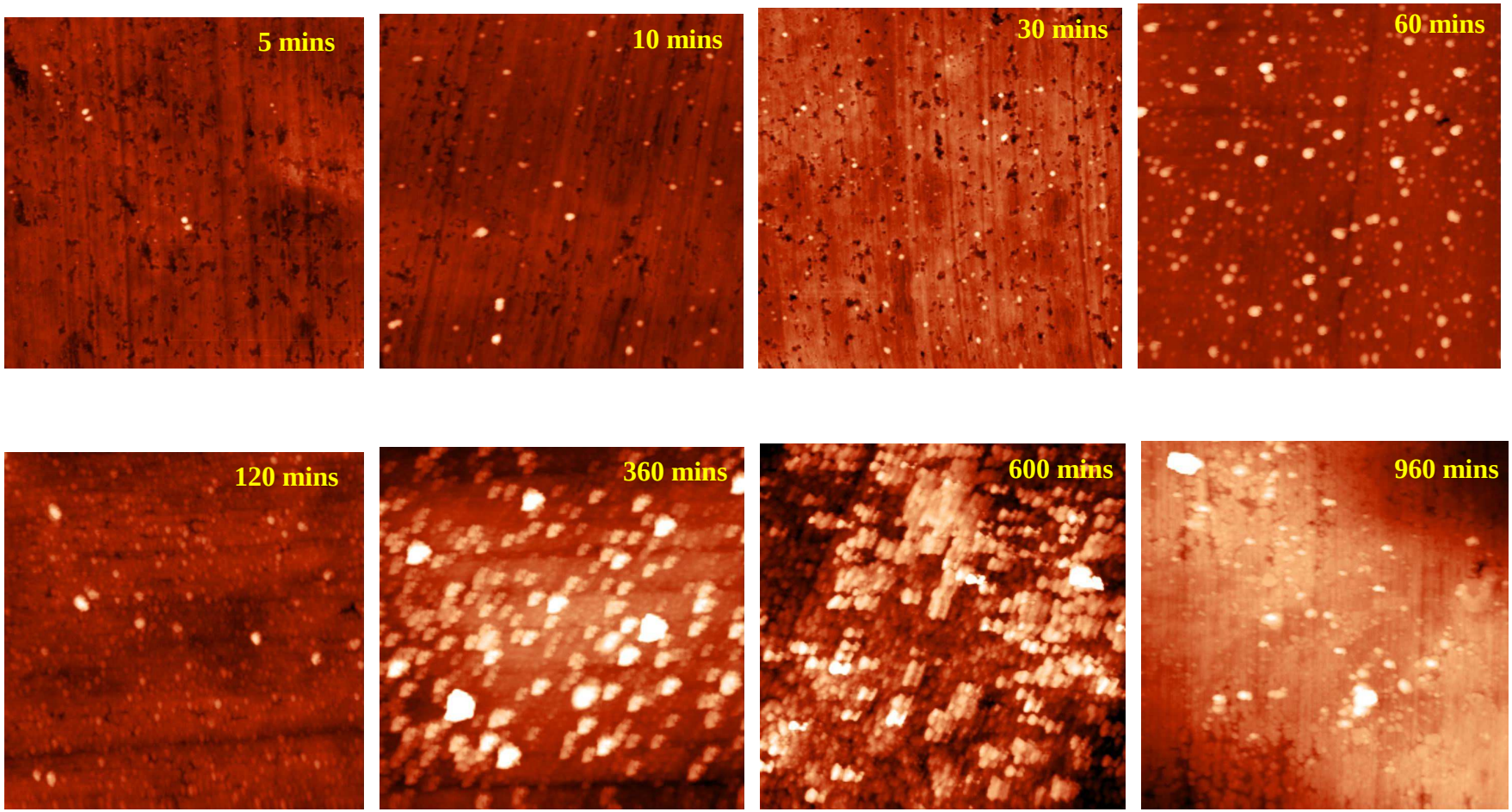

Figure 4. 21 AFM images of the APS film on titanium surfaces prepared in the anhydrous toluene with 0.2 v% APTES at 70°C for different immersion times, scan size 10 µm × 10 µm.

To further clarify the growth behaviour of the APS film on the surface, the APS film silanized for 5 minutes at 70°C was investigated by AFM and the topography of the surface is shown in **Figure 4. 22**. From the line measurement by AFM the height of islands is about 3.5 and 5 nm, respectively. According to the length of one APTES molecule (1.1 nm), the islands as shown are composed of 3 ~ 5 molecules on the vertical direction. It means that APS molecules cross-link to form the oligomer first in the solvent and then attach on the surface by the Si-O-Ti covalently bond. Apart from the humidity in the ambient during the silanization, the higher temperature leads to the molecular cross-linking, which probably accelerates the reaction rates including hydrolyzation and condensation of APTES molecules in the solvent. Therefore, lower temperature should be better for the silanization to obtain a well-ordered structure of the APS film on the surface.

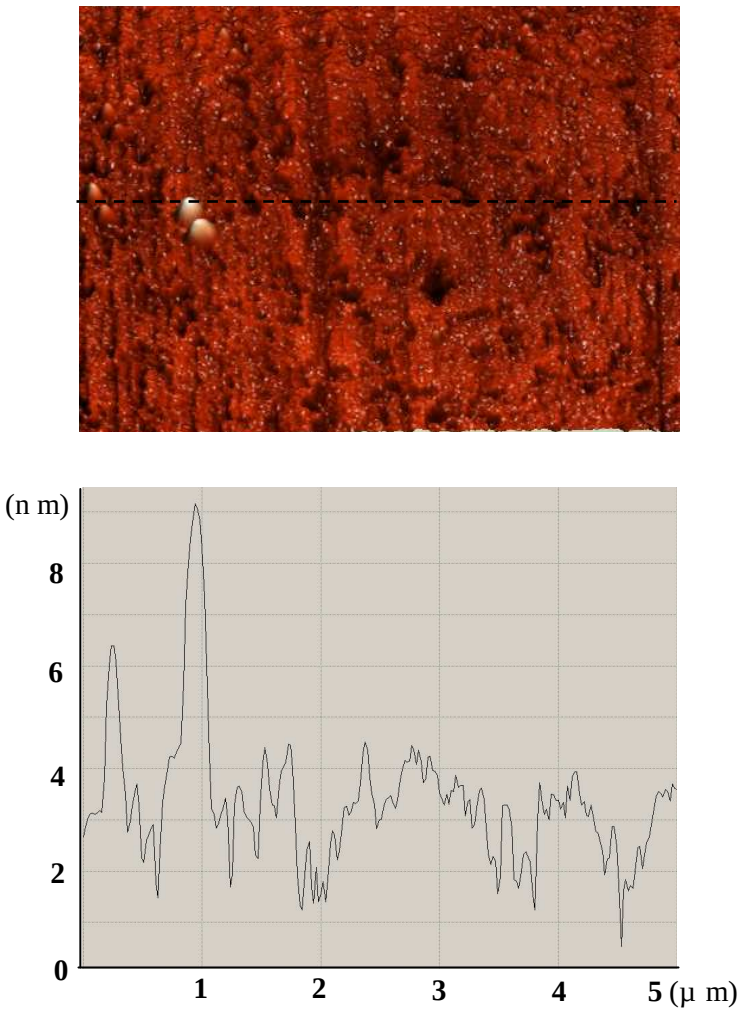

Figure 4. 22 AFM image of the APS film prepared in the anhydrous toluene with 0.2 v% APTES for 5 minutes at 70°C (top) and line measurement by AFM (bottom). Scan size: 5 µm × 5 µm.

4.1.2.4 Effect of silanization temperature on self-assembly

The results from the above experiments show the APS film contains multiple layers instead of monolayer. Even at the beginning of the silanization, the polysiloxane can be happened at higher temperature. In order to prepare a relatively thin and ordered molecular layer on the surface, the effect of temperature was investigated in the following experiments. The oxidized titanium samples were prepared in anhydrous toluene with 0.2 v% APTES for 16 hours at 30, 40, 50, 60 and 70°C, respectively.

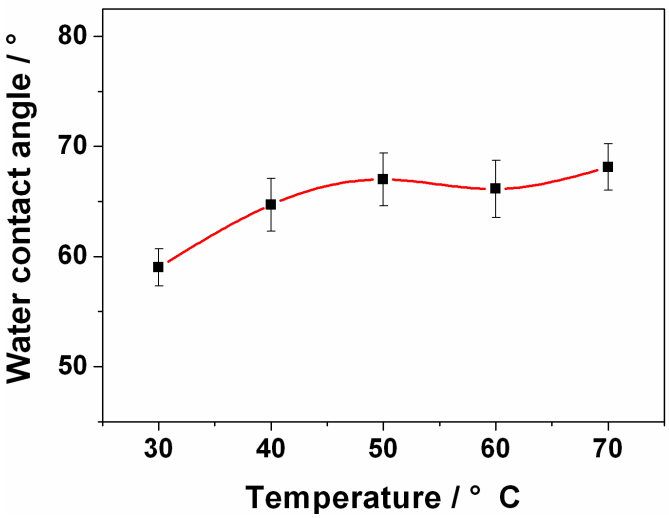

Figure 4. 23 Water contact angles for the APS film prepared for 16 hours at different temperatures (n=6).

The water contact angles of titanium surfaces with the APS film prepared at different temperatures are shown in **Figure 4. 23**. When the temperatures decreases from 70 to 30°C, the value of contact angles drops slightly from 68° to 60°. **Figure 4. 24** shows the temperature dependence of the IR spectra of the APS film on titanium. The peaks at 1592-1603 cm^{-1} on the IR spectra of S_{30} – S_{70} are assigned to the free amine group deformation vibration (**Figure 4. 24A**). Between 30 – 70°C, the IR spectra in **Figure 4. 24B** shows no remarkable shift of the C-H stretching variations in frequency: ~2850 and ~2919 cm^{-1}, respectively. This indicates that the environment of the propyl segments of the APS on titanium is thermally stable during the silanization. However, the intensity of the Si-O-Si and the N-H vibration modes on the IR spectra increase with the temperature, which implies a thick layer with $–NH_2$ functional groups is formed on the titanium surface.

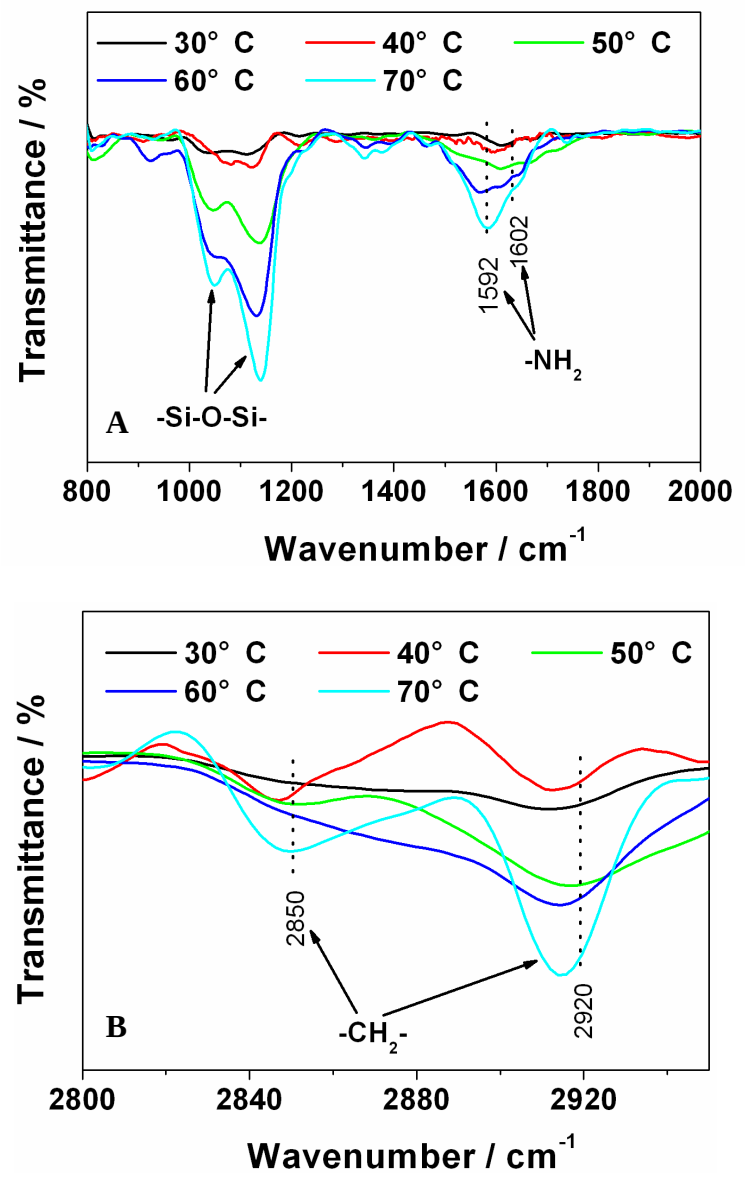

Figure 4. 24 IR spectra of the APS film on titanium surfaces prepared at different temperatures: (A) the Si-O-Si and the NH regions (800 – 2000 cm^{-1}); (B) the CH region (2800 – 2950 cm^{-1}).

At a higher temperature, the increase of the collision between molecules in toluene leads to an increase of the reaction rate during the silanization, which further accelerate the kinetics of the APS growth on titanium. Moreover, as the temperature increases, water is able to desorb from the substrate and enter the toluene phase, resulting in the formation of polysiloxane. Because of the increased reaction rate, the initial film is formed and increased in thickness more quickly. From the intensity of Si-O-Si bond, the films created at 70°C were over at least three times as thick as that at 30°C, which implies a more aggressive initial deposition. Therefore, the lower temperature will result in the formation of a thinner film on titanium.

4.1.2.5 Effect of the residual water content in solvent on self-assembly

As known, the hydrolysis of silane results in the attachment of the APTES to the substrate by the formation of Si-OH bonds at the surface. However, it is still debatable whether the initial hydrolysis step could occur either in solution or at the substrate surface. In order to further clarify this issue, according to the residual water content in solvent, two different organic solvents were used in the following experiments: anhydrous toluene (99.9+%, Sigma) and hydrous toluene (90%, Sigma). Titanium samples were immersed in the 5 ml above mentioned solvents with 0.2 v% APTES, respectively for 16 hours at 30°C and analyzed with the contact angle goniometer and FTIR immediately after silanization.

Figure 4. 25 Images of the water contact angles for titanium samples with the APS film prepared with 0.2 v% APTES in: (a) anhydrous toluene and (b) hydrous toluene.

Figure 4. 25 shows the water contact angles of APS films prepared in two solvents. $S_{anhydrous}$ has more hydrophilic surface compared with $S_{hydrous}$ with a contact angle of 61° and 86°, respectively. **Figure 4. 26** shows the IR spectra of APS films on the Ti surfaces. The intensity of the Si-O-Si stretching vibration on the IR spectrum of the $S_{hydrous}$ is evidently greater than that from the $S_{anhydrous}$, which implies the formation of thick layers on the $S_{hydrous}$ (**Figure 4. 26A**). Moreover, due to extra water in the hydrous solvent, the $-NH_3^+$ vibrations at 1567 and 1647 cm^{-1} were observed on the IR spectrum of the $S_{hydrous}$, instead of the $–NH_2$ vibration at 1598 cm^{-1} on that of the $S_{anhydrous.}$ **Figure 4. 26B** shows that the APS film on the $S_{hydrous}$ is disordered because of the C-H vibrations at 2876 and 2933 cm^{-1} on the spectrum. Therefore, under the hydrous condition, the APS film will form a thick layer with disordered structure.

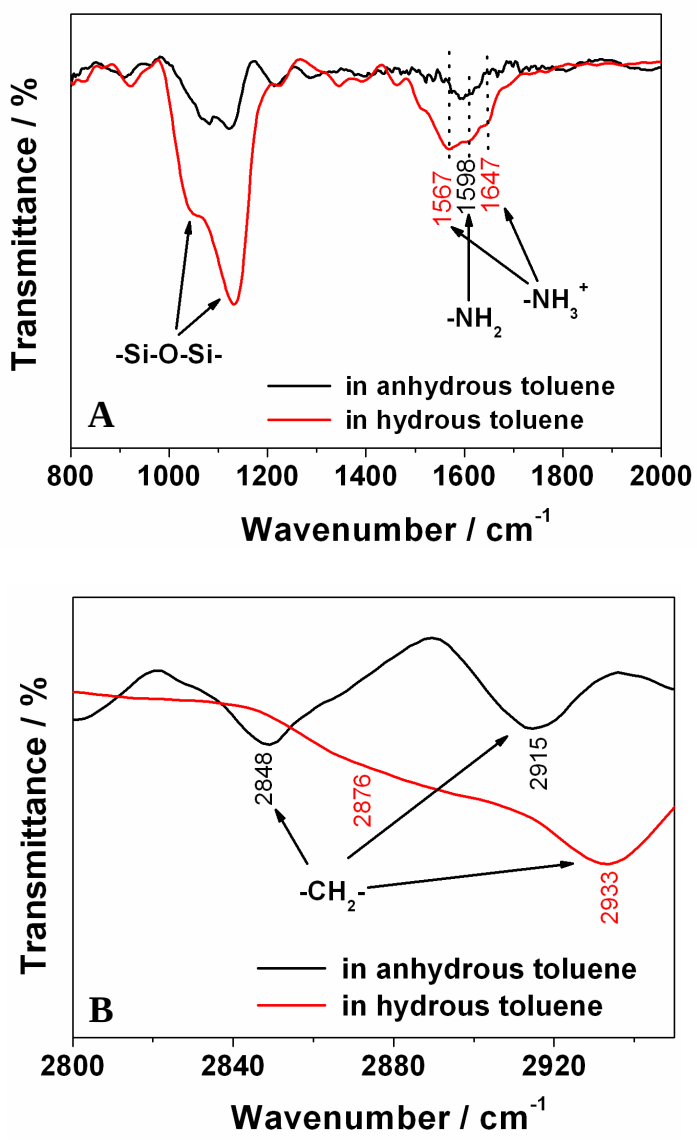

Figure 4. 26 IR spectra of the APS film prepared in anhydrous and hydrous toluene, respectively: (A) the Si-O-Si and the NH regions (800 – 2000 cm^{-1}); (B) the CH region (2800 – 2950 cm^{-1}).

According to literature, the residual water content in the solvent must be carefully controlled during the silanization. If water comes from the solvent, APTES will easily form polysiloxane in the solvent and then form the covalent bond with TiOH on the surface, which leads to the formation of disordered thick layers. Due to the rapid hydrolysis of APTES in the solvent, it is possible for the $-NH_2$ functional groups to partly form $–NH_3^+$ groups with the –OH groups from the silanols, which affects the quality of the APS film and its applications. If water comes from the surface, the APTES will first be hydrolyzed slowly to form the covalent bond of Si-O-Ti and then crosslink between molecules to form the Si-O-Si bond. Therefore, the application of anhydrous solvent will result in a relative thin film with the well-ordered structure.

4.1.2.6 Thermal stability of the APS film on Ti

The APS film by self-assembly is widely used for the development of advanced materials with a desirable interface. Since substrates with the APS film are applied at high temperature (up to 200°C), it is necessary to investigate the thermal stability of the APS film, especially for the stabilities of the amine functional group (N-H), the crosslinker (Si-O-Si) and covalent bond (Si-O-Ti).

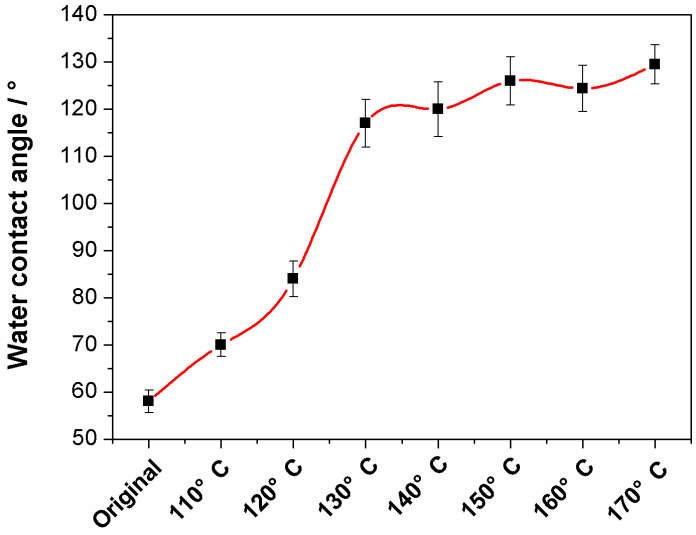

Figure 4. 27 Water contact angles of Ti the APS film in a vacuum oven vs. temperatures (n=6).

Titanium samples were prepared in anhydrous toluene with 0.2 v% APTES at 30°C for 16 hours and then heated from 110 to 170°C in a vacuum oven, each time for 30 minutes. The water contact angles of titanium surface with the APS film treated at different temperatures are shown in **Figure 4. 27**. When the temperature increases to 130°C, the value of contact angles increases dramatically from 58° to 117°, which is assumed that hydrophobic groups (e.g. -CH_2-) are probably exposed on the outermost of the titanium surface. **Figure 4. 28** shows the IR spectra of the APS film on the regions of 800 – 2500 cm^{-1} and 2800 – 2950 cm^{-1}. When the temperature increases up to 130°C, the peak at 1604 cm^{-1} assigned the –NH_2 vibration is disappeared on the IR spectra (**Figure 4. 28A**), which indicates that the C-N bond is broken. This also confirms that the -CH_2- functional groups result in the hydrophobic surface after the APS film was treated at 130°C. From the IR spectra the intensity of the Si-O-Si vibrations seems not to change on the whole experiments, which is assumed that the Si-O-Ti bond is not broken

at higher temperatures. The IR spectra in **Figure 4. 28B** implies that the structure of the APS film is disordered after the treatment at 110°C because of the C-H vibrations.

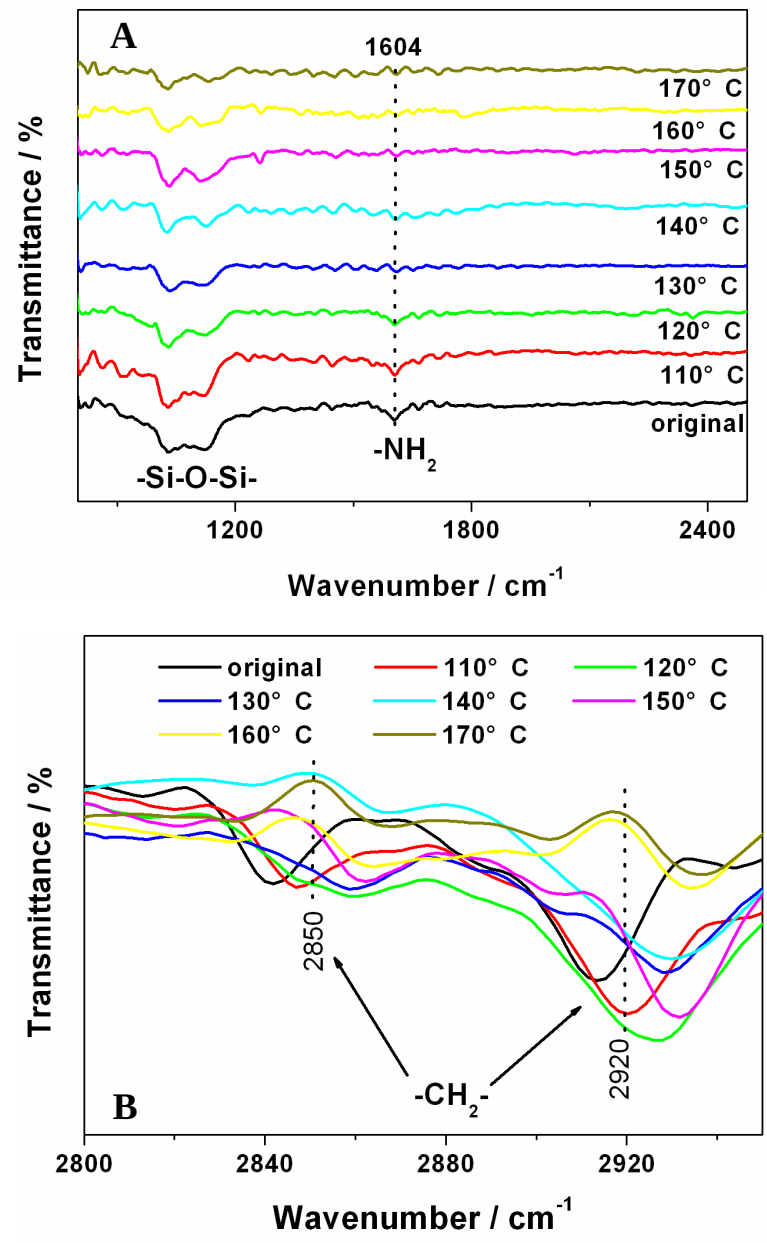

Figure 4. 28 IR spectra of the APS film heated in a vacuum oven at different temperatures: (A) the Si-O-Si and the NH regions (800 – 2500 cm^{-1}); (B) the CH region (2800 – 2950 cm^{-1}).

The bonding energy of different bonds in the APS film is shown in **Table 4. 5**. Among these bonds, the weakest one is C-N bond (308 kJ/mol). Since the C-N bond is broken since the treatment at 130°C, the -CH_2- groups result in the very big hydrophobic angles with water. After the temperature increases up to 160°C, the intensity of -CH_2- bond vibrations is reduced (**Table 4. 5**), which results from the break of the C-C bond (348

kJ/mol). After the treatment at 170°C, Si-O-Ti, Si-O-Si and Si-C bonds only exist on the titanium surface due to the stronger bonding energy.

Table 4. 5 The bonding energy for different bonds in the APS film.

	N-H	**C-N**	**C-H**	**C-C**	**Si-C**	**Si-O**
Bonding energy (kJ/mol)	391	308	413	348	418	452

4.1.2.7 Summary

In this section, a systematic investigation of silanization of APTES molecules on the titanium surface was reported in order to identify the effects of parameters on the preparation of the thin and well-ordered APS film with the $–NH_2$ functional groups and the relevant information about its stability. Overall, the results that adequate control of reaction conditions was important to obtain a desirable titanium surface by APTES.

IR spectra and water contact angles reveal the structure of the APS film deposited from toluene is largely influenced by the APTES concentration, temperature and residual water content in the solvent. The APTES concentration had a great influence on the structure of the APS film. The films formed at a concentration > 0.5 v%, show protonated $–NH_3^+$ groups on the titanium surface, while the internal loop of APTES is possibly formed on the surface when the concentration is lower than 0.1 v%. The film quality did not show strong temperature dependence. As compared to the APS film prepared at 70°C, the film prepared at 30°C was thinner because of the intensity of the Si-O-Si bonds on the IR spectra. The system with anhydrous toluene as the solvent produced well-ordered and thin film with primary amine functional groups. Therefore, under current laboratory conditions, the well-ordered and thin APS film on the surface was produced using an anhydrous toluene of 0.1~0.5 v% APTES at 30°C for 16 hours.

For the stability of the APS film, titanium samples in aqueous solutions lead to hydrolysis of the film. The Si-O-Si bond is easily hydrolyzed to form HO-Si- in hydrous solutions (the acid or alkali solutions), even quicker in the acid solution. Thus,

compared with that in the alkali aqueous solution, the APS film is less stable in the acidic solution as the Si-O-Si bonds keep the stability of the film. Moreover, under the acidic conditions, the -NH_2 functional groups trends to form protonated –NH_3^+ groups, instead of the free amine groups in alkali solution. Moreover, the formation of the –NH_3^+ groups in acidic solution leads to the disordered structure of the APS film, because of the internal loop on the surface. Under dry condition (desiccator), although there is no hydrolysis in the ambient, the APS film is still unstable due to the weak interactions between chains, and easily form cyclic and inner complexes, leading to the formation of the disordered structure of the APS film.

Further investigation of the thermal stability of the APS film in the vacuum oven from 110 to 170°C, clearly shows that the N-H and C-C bonds are broken at 130 and 160°C, respectively. The Si-O-Si and Si-O-Ti bonds are stable after the treatment at 170°C. Therefore, the film with –NH_2 functional groups on the titanium surface has a poor thermal stability.

4.2 Bioactivity of titanium with the APS film

HA coating on titanium is traditionally applied to improve the bioactivity of titanium-based implants. The existing coating methods used mainly suffer from high processing temperatures. The biomimetic approach of HA deposition is one of the methods that can promote the disadvantage of titanium as implant. Therefore, surface functionalization with self-assembling film has gained interest. So far, the inducibility of calcium phosphate (CaP) by self-assembly films with different functional groups has been studied to improve the biocompatibility of the implant surface. For example, Majewski and Allidi found that the –SOOH functionalized film showed the better inducibility of CaP compared with the –NH_2 and –SH functionalized films [Majewski 2006]. Zhu *et al.* reported that the film with the -OH group shows the best inducibility of CaP [Zhu 2002]. However, it is still a debate whether the film with -NH_2 functional group can induce calcium phosphate. Toworfe *et al.* reported that the -NH_2 functional group has inducibility of CaP in the SBF, pH 7.4 [Toworfe 2006]. Zhu *et al.* observed that the -NH_2 functional group cannot induce CaP in the SBF, pH 7.2 ~ 7.4, whereas it

can do in the SBF, pH 7.6 [Zhu 2004]. Therefore, extensive research is still being carried out in this field to improve the inducibility of CaP by the amine functional group on titanium surfaces.

In this study, the deposition of calcium phosphate was investigated on the surfaces of TiO_x and Ti with the amine group in the Simulated Body Fluid (SBF) solution to clarify whether the $–NH_2$ functional group can induce calcium phosphate. The reason to choose SBF rather than other calcium phosphate solution is that the composition of SBF is similar to that of human blood plasma. Therefore, the structure of the precipitation on the surface would be close to biological apatite in human bone. Scanning electron microscopy (SEM) analysis was performed for imaging and morphology of the surface. X-ray diffraction (XRD) and FTIR were performed for structural characterisations of titanium samples.

Titanium substrates that were chemically oxidized in the *Piranha* solution (H_2SO_4: H_2O_2= 3:1) were chosen as the control samples. The samples with the $–NH_2$ functional groups were prepared in anhydrous toluene with 0.2 v% APTES for 16 hours at 30°C, and then placed upside up in the SBF, pH 7.45 for 10 days in an incubator at 37°C, as shown in **Figure 4. 29**. Once the substrates were removed from the solution, they were washed gently with distilled water for 3 times and dried at 100°C for 30 minutes for further analysis.

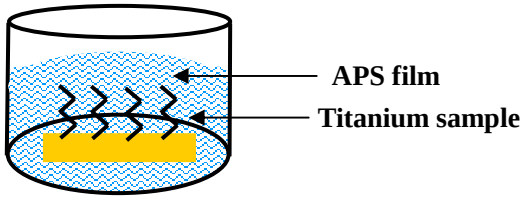

Figure 4. 29 Schematic diagram of the titanium sample with the APS film placed in the SBF.

Figure 4. 30 shows the surface morphology of the samples after 10 days immersion in SBF. Micro-sized global particles of ~ 3 μm covered on the surface of TiO_x (**Figure 4. 30A**), but the spheres are not densely covering the surface and the underlying titanium substrate can also be observed in some areas between the spheres. In comparison, a

dense film has homogenously covered the surface with the -NH_2 group, shown in **Figure 4. 30B**. The precipitate consists of a complete sublayer and a partial top layer. The spherical structure on the top layer is similar to those observed in case of TiO_x. The cracks in the sublayer as shown in **Figure 4. 30B**, might be caused by the rapid drying of the layer during evacuation of the sample chamber of the SEM.

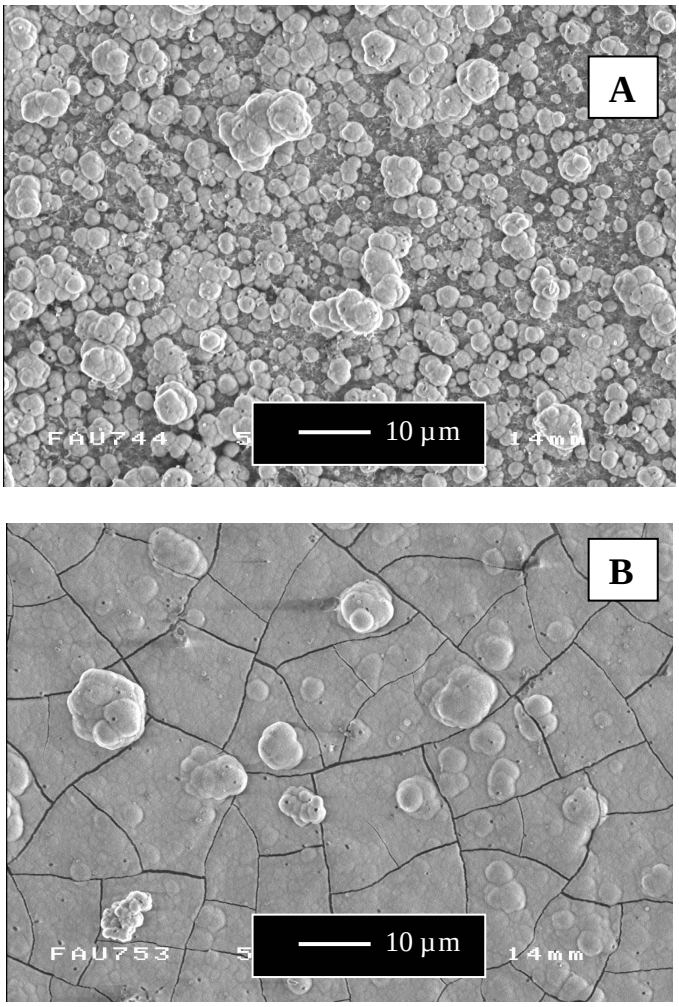

Figure 4. 30 SEM micrographs showing Ca-P precipitates on oxidized titanium (A) and titanium with the APS film (B) after immersion for 10 days immersion in SBF, pH 7.45 at 37°C.

The crystallinity of the precipitate was investigated by XRD after 10 days immersion in SBF. **Figure 4. 31** shows the evolution of XRD analysis of titanium samples placed in the SBF from 25° to 37° at 2θ. Diffraction peaks are noted and the corresponding phases have been identified. It is important to note that the main CaP phase on the surfaces is hydroxyapatite ($Ca_{10}(PO_4)_6(OH)_2$, HA) at 26° and 32°, respectively. The higher XRD peaks of HA on the XRD spectra reveal that a relatively larger quantity of HA particles

formed on the surface with the APS film compared to that on the TiO_x surface. The broad HA peaks indicate very small crystal size and/or the amorphous structure. Therefore, the XRD profiles show the poor crystalline phases of HA formed on the titanium surface.

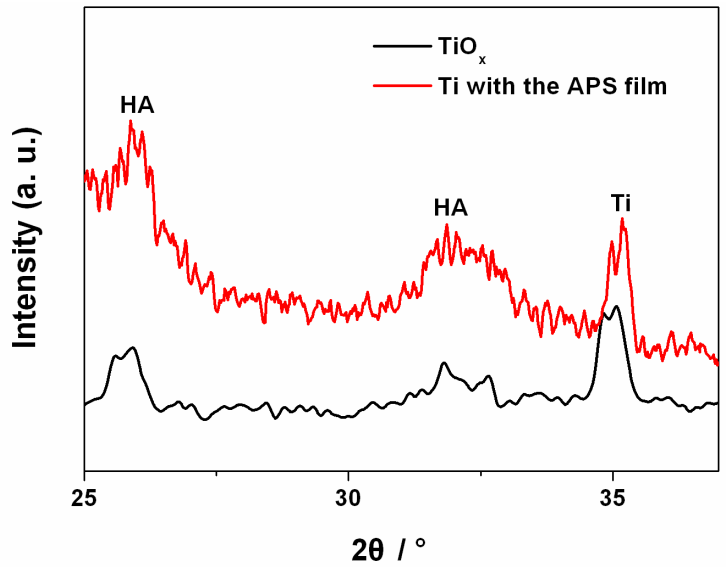

Figure 4. 31 XRD patterns on TiO_x and Ti with the APS film surfaces immersed in SBF, pH 7.45 for 10 days at 37°C. The HA and Ti mark represent the intensity of the HA and titanium, respectively.

The existence of the apatite phase in the precipitate is normally indicated by the presence of different IR vibrational modes of phosphate ions. **Figure 4. 32** presents the IR spectrum of calcium phosphate precipitate in the 400-4000 cm^{-1} regions after immersion in the SBF for 10 days at 37°C. According to the reference [Socrates 1980], two sharp bonds of phosphate (P-O) groups are observed at 560 and 598 cm^{-1} due to the vibration of P-O from -(HO)P=O and a weaker band at 871 cm^{-1} is due to P-O-C stretching. A sharp intense band at 1020 cm^{-1} and a shoulder band of P=O at 1112 cm^{-1} might result from the P-O stretching from –(OH)P=O. Two bands at 1416 and 1450 cm^{-1} are assigned for the C-O stretching, which might be due to precipitation of carbonate ions from the simulated body fluid. The P-O and C-O bonds reveal that the surface comprises of carbonated HA. One broad O-H bonds in the high-energy region at 3350 cm^{-1} is indicative of adsorbed water on the Ca-P complex.

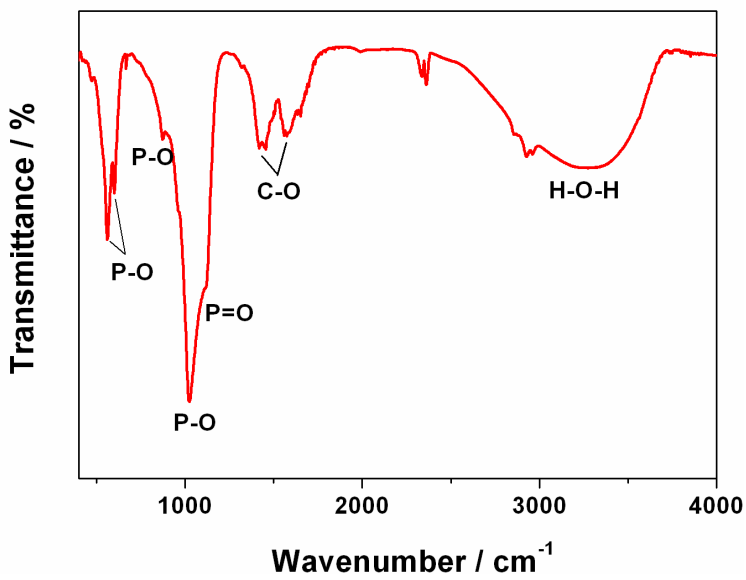

Figure 4. 32 IR spectrum of the Ca-P coating on titanium with the APS film after immersion in SBF, pH 7.45 for 10 days in the 400 – 4000 cm^{-1}.

The results from SEM, XRD and FTIR seem to confirm that the titanium samples with the $–NH_2$ functional groups greatly enhance the nucleation and growth of calcium phosphate phases in a one-step nucleation process, compared with TiO_x. The positively charged ($-NH_3^+$) functional groups firstly extract PO_4^{3-} ions by the APS film and then adsorb Ca^{2+} ions in the SBF *in vitro* processes of calcium phosphate deposition. However, the SBF solutions both showed the precipitate after the immersion, although the control SBF solution without sample was still clearly. As well-known, homogeneous nucleation can occur in unstable calcium phosphate solution, which means that there are no special objects inside. In other words, it occurs only in solution. Therefore, it is suspected that the CaP precipitate probably occurs in the SBF saturated solution and then deposit on the surface due to the gravitation. In order to avoid above nucleation process, titanium samples were hung in the SBF instead of upside up in the following experiments.

4.2.1 Formation of CaP on TiO_x and Ti with $–NH_2$

Although the SBF solution is commonly used *in vitro* to evaluate the biocompatibility of biomaterials, 1.5 SBF solution which contains 1.5 times ions concentrations than that in SBF, is also applied in many researches in order to shorten the time of nucleation time.

In order to clarify whether the $–NH_2$ functional groups can induce calcium phosphate precipitate, TiO_x and Ti with the $–NH_2$ group were hanged in the SBF and 1.5 SBF solutions, respectively, pH 7.45 for 5 days at 37°C, as shown in **Figure 4. 33**. Samples were then washed with distilled water and dried at oven for 30 minutes. The CaP precipitates on the surfaces were characterized by SEM with EDX.

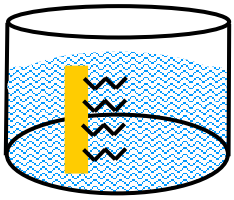

Figure 4. 33 Schematic diagram of the titanium sample with the APS film placed in the solution.

Figure 4. 34A and C show the surface morphologies and EDX profiles of TiO_x after immersing in the SBF and 1.5 SBF in the incubator at 37°C for 5 days, respectively. On the surface of TiO_x, homogeneous fine particles (**Figure 4. 34A**) and a dense film (**Figure 4. 34C**) were uniformly formed in the SBF and 1.5 SBF, respectively. **Table 4. 6** summarised the EDX elemental quantitative information (atomic %) of each specimen after the SBF and 1.5 SBF immersions for the surface of TiO_x. To determine which phase of CaP has formed, the Ca/P ratio was measured at several locations by EDX and the values were averaged. The atomic percents of P and Ca from the TiO_x surface immersed in the 1.5 SBF are over twice than those in the SBF, and the ratio of Ca to P in the 1.5 SBF (1.22) is slightly higher than that in the SBF (1.16). This is due to that the higher ionic concentrations in the 1.5 SBF can accelerate the formation of calcium phosphate. The oxidized titanium surface normally can supply the negatively charged -OH groups, which initially combined with Ca^{2+} ions to form calcium titanate, and then attract PO_4^{3-} ions to form an apatite nucleus. Once the apatite nuclei were formed, they spread out spontaneously and form the CaP layer on the surface.

Table 4. 6 Surface compositions of TiO_x and titanium with the APS film immersed in the SBF and 1.5 SBF, respectively, for 5 days by EDX elemental quantitative measurement (n=3).

	SBF (atomic %)		**1.5 SBF (atomic %)**	
	TiO_x	**APS film/Ti**	**TiO_x**	**APS film/Ti**
C	0.32	3.11	-	3.61
O	66.36	66.67	64.60	66.38
Na	-	-	-	0.22
Mg	0.58	-	1.02	-
Si	-	0.54	-	0.51
P	3.46	-	7.24	-
Ca	4.16	-	8.80	0.04
Cl	-	-	-	0.43
Ti	21.74	29.58	18.34	28.92
Ca/P	1.16	-	1.22	-

However, the surface with the amine groups seems to inhibit the nucleation and growth of HA, according to the results from SEM images and EDX profile, as shown in **Figure 4. 34B and D**. It is noticed that the surface morphology in 1.5 SBF does not shown any change on inducibility of calcium phosphate. Only small peaks of Ca, Na, Cl were found in **Figure 4. 34D**, which are assumed that small amount of CaCl and NaCl were deposited on the surface by the aqueous solution because the 1.5 SBF is super saturated solution. After the immersion, the C and Si elements are detected on the titanium surface with the APS film according to the EDX results, which indicates that the APS film still remains on the surface. However, atomic percents of C and Si in the SBF on the surface are very low, 3.11% and 0.54%, respectively, which might be due to the hydrolysis of the APS film in the aqueous solution. From above experiments, it is concluded that TiO_x surface has good inducibility of calcium phosphate, whereas the surface modified by the $–NH_2$ group has not that ability at all in SBF, pH 7.45. The same experiments were repeated three times and got the same results.

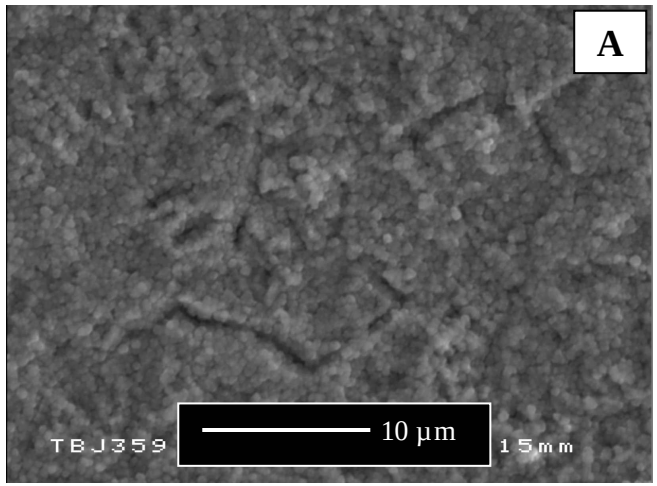
A
TBJ359
10 µm
15mm

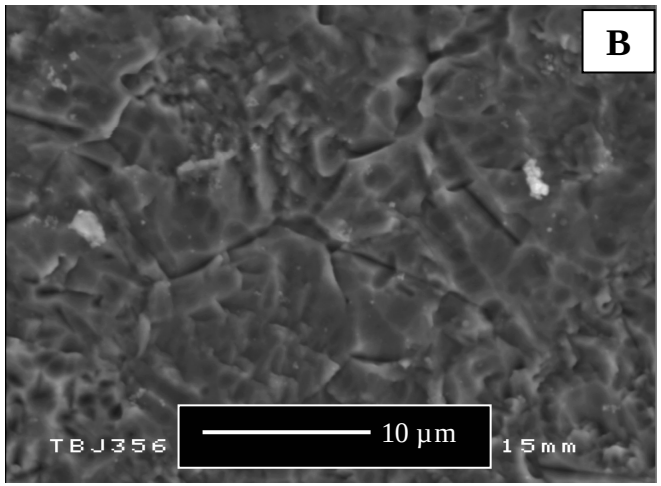
B
TBJ356
10 µm
15mm

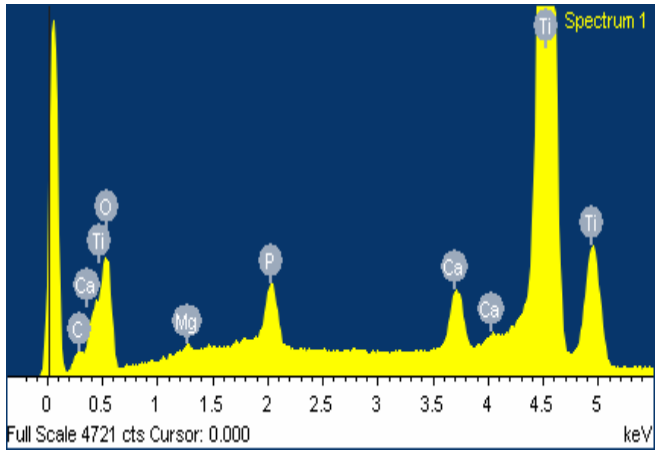
Spectrum 1
O
Ti
Ca
C
Mg
P
Ca
Ca
Ti
Ti
0 0.5 1 1.5 2 2.5 3 3.5 4 4.5 5
Full Scale 4721 cts Cursor: 0.000
keV

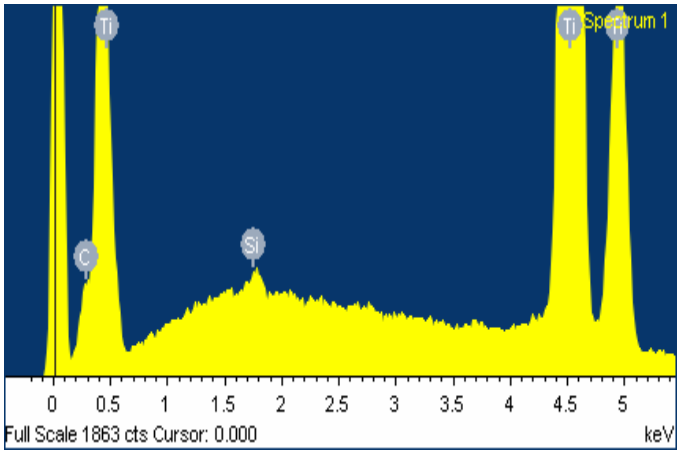
Spectrum 1
Ti
Ti
Ti
C
Si
0 0.5 1 1.5 2 2.5 3 3.5 4 4.5 5
Full Scale 1863 cts Cursor: 0.000
keV

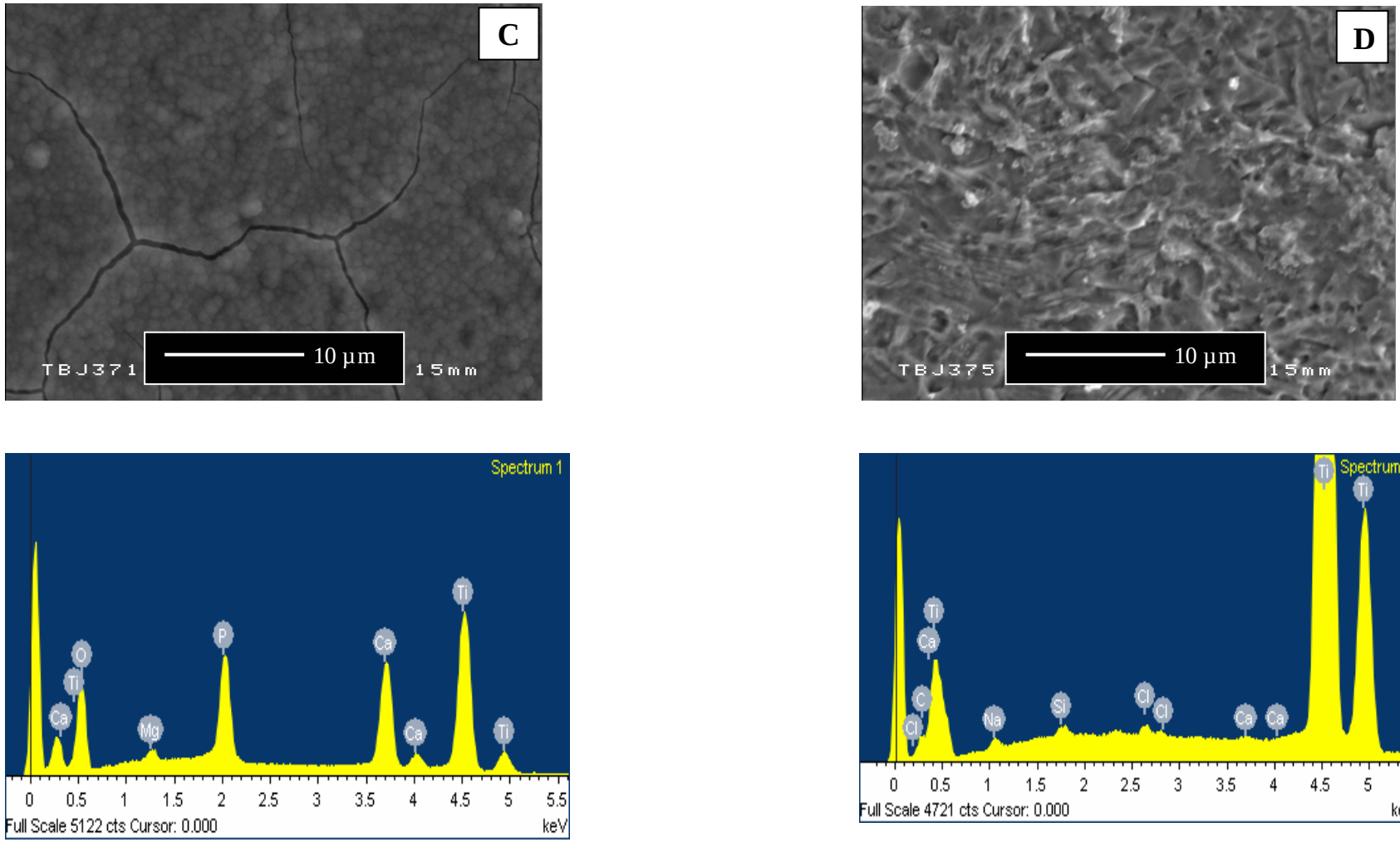

Figure 4. 34 SEM images and EDX of CaP deposited on TiO_x and titanium with the APS film surfaces after immersed in different solutions, pH 7.45 at 37°C for 5 days: (A) and (B) in the SBF; (C) and (D) in the 1.5 SBF.

The above results are totally reversed when samples were placed upside up and hanged in the solution. **Figure 4. 35** shows obvious difference of titanium surfaces treated by different functional groups: Sample A was only oxidized by the *Piranha* solution (H_2SO_4:H_2O_2=3:1) for 15 minutes at room temperature (with -OH groups); Sample B (with the –OH and –NH_2 groups) and C (with the –NH_2 groups) were silanized for 5 and 16 hours, respectively, in anhydrous toluene with 0.2 v% APTES at 30°C. They were immersed in SBF, pH 7.45 at 37°C for 5 days. The surface of sample A is fully covered by the calcium phosphate after the immersion, and the sample B is partly covered, which might result from that the APS film is not completely grown up on the whole surface. However, the surface of the sample C is not covered at all. This experiment confirms the above conclusion.

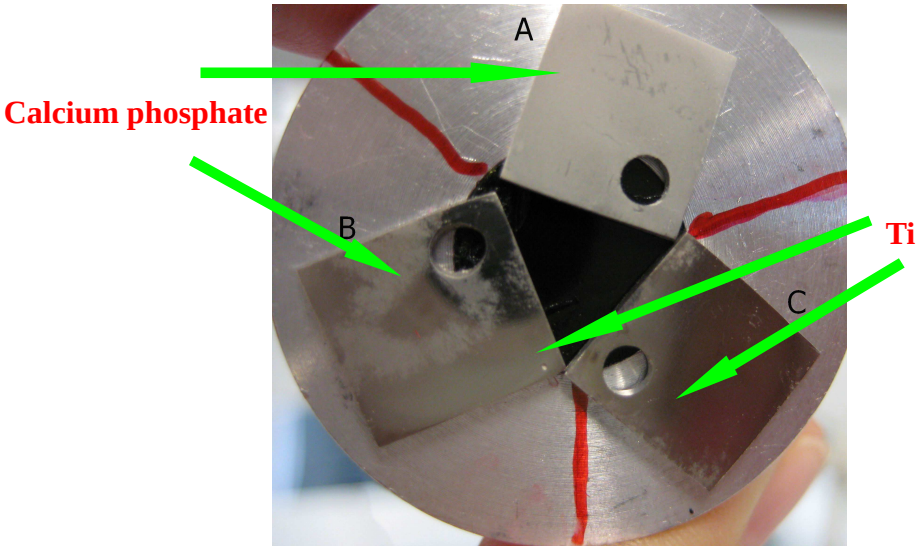

Figure 4. 35 The image of titanium samples after immersed in the SBF, pH 7.45 at 37°C for 5 days, which were prepared under different conditions: A) oxidation in the piranha solution, B) silanization for 5 hours and C) silanization for 16 hours.

4.2.2 Effect of pH in SBF on the deposition of CaP

From literature, people reported that the positively charged amine group can induce calcium phosphate in unstable solution, whereas the negatively charged hydroxyl group cannot [Zhu 2004]. It is well-known that the stability of solutions deeply depends on pH

values if other factors (temperature, ionic concentration, etc.) are fixed. Therefore, the effect of pH value in the SBF on the inducibility of calcium phosphate by the amine functional group was investigated in the following experiments. The oxidized titanium and Ti with the $–NH_2$ group samples were hanged in the SBF with a pH value of 7.0, 7.45 and 7.98 at 37°C for 5 days, respectively and SEM images are shown in **Figure 4. 36A-F**. Clearly, TiO_x samples show uniform precipitate particles on the surface (**Figure 4. 36A-C**). The particle size of calcium phosphate induced by TiO_x is increasing with the increase of pH value in the solution. This is probably due to homogeneous nucleation in the saturated solution. Apart from the calcium phosphate, magnesium phosphate was formed on the surface as well, according to the EDX elemental quantitative (**Table 4. 7**). The ratio of Ca/P deposited increases from 1.10 to 1.41, which is close to that of HA (Ca/P: 1.67). This is due to that higher pH value in the SBF can accelerate the formation of CaP on the surface.

Figure 4. 36D-E do not show any calcium phosphate precipitates on the surfaces for the titanium sample with the amine group, and **Figure 4. 36F** shows very tiny depositions including CaP, MgCl, NaCl, etc. according to EDX file. SEM images and EDX results both confirm that pH value can influence CaP deposition behaviours on the surface and in the solution, but it cannot change the behaviour on the surface with the amine group. There are probably two reasons to cause these phenomena: one is that the $–NH_2$ group cannot extract the negatively charged PO_4^{3-} ions in the SBF, like neutral groups (e.g. $–CH_3$ and $–CH=CH_2$) inhibit nucleation and growth of CaP. Another reason is that the interaction between $–NH_3^+$ and PO_4^{3-} is too weaker to produce calcium phosphate nuclei on the surface. On other words, the nuclei are easily dropped off from the surface. On the other hand, due to the presence of residual Si element in EDX profile, it is necessary to investigate the hydrolysis stability of the APS film in SBF.

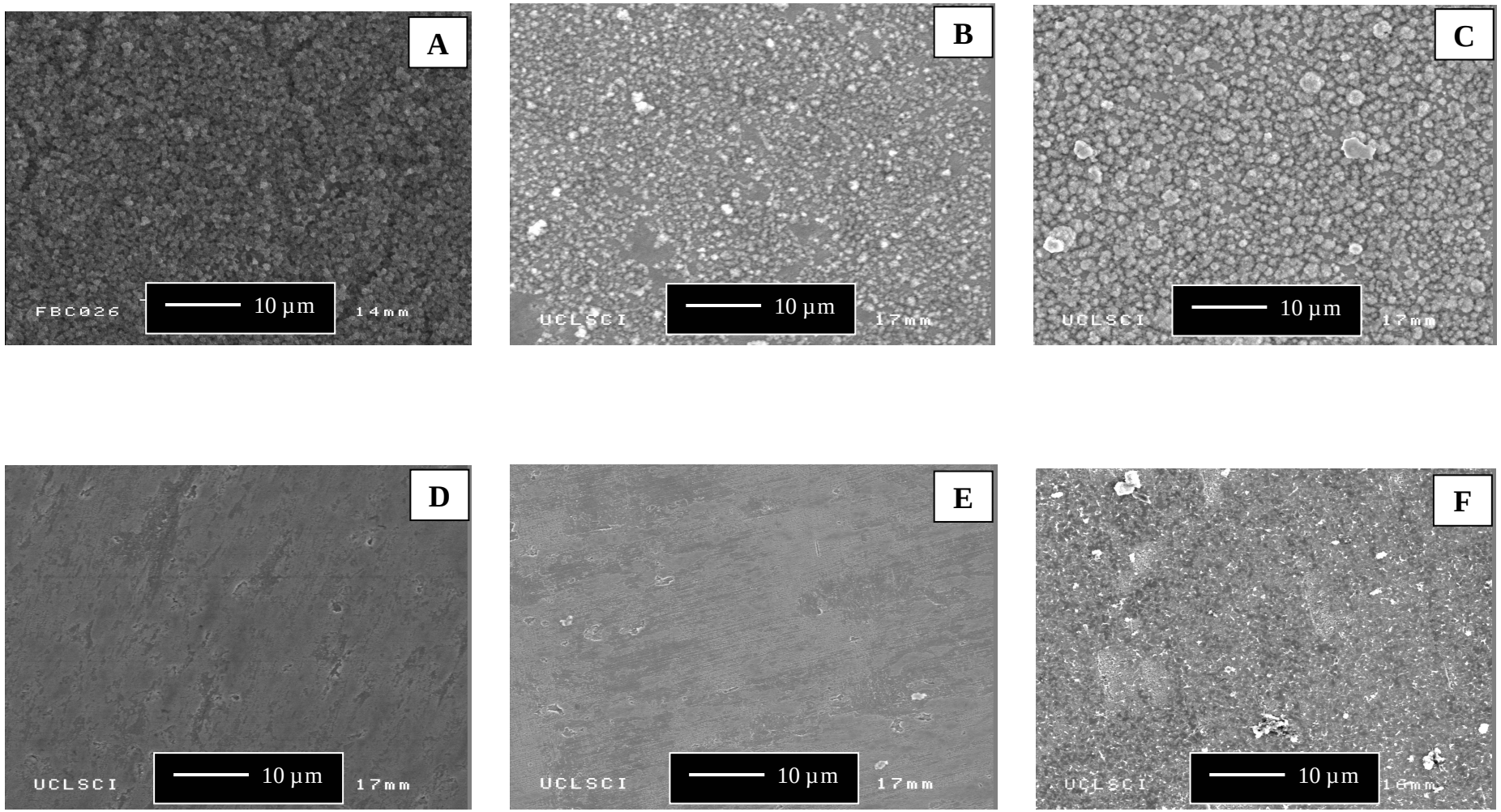

Figure 4. 36 SEM images of CaP deposited on TiO_x (above) and titanium with the APS film surfaces (bottom) after immersed for 5 days at 37°C in the SBF at different pH values: (A) and (D) at pH 7.0; (B) and (E) at pH 7.45; (C) and (F) at pH 7.98.

Table 4. 7 Surface compositions (atomic %) of TiO_x and titanium with the APS film after the SBF immersions at different pH for 5 days by EDX elemental quantitative measurement (n=3).

	SBF, pH 7.00 (atomic %)		**SBF, pH 7.45 (%) (atomic %)**		**SBF, pH 7.98 (%) (atomic %)**	
	TiO_x	**APS film/Ti**	**TiO_x**	**APS film/Ti**	**TiO_x**	**APS film/Ti**
C	0.84	3.06	0.16	2.92	-	2.15
O	66.13	65.73	65.77	66.35	63.50	65.94
Na	-	-	-	-	0.29	0.10
Mg	0.29	-	0.83	-	0.85	0.17
Si	-	0.50	-	0.51	-	0.50
P	2.34	-	5.39	-	9.04	0.85
Ca	2.58	-	6.33	-	12.74	0.92
Cl	-	-	-	-	-	0.11
Ti	27.82	30.71	20.88	30.22	13.58	29.02
Ca/P	1.10	-	1.17	-	1.41	1.08

4.2.3 Hydrolysis stability of the APS film in SBF

In order to study the hydrolysis behaviour of the APS film and the protonation of the $–NH_2$ functional group in the aqueous solution, titanium samples with the APS film were placed in the SBF, pH 7.45 at room temperature up to 72 hours. Contact angle goniometry and FTIR were preformed for the characterization of the surface at immersion time of 2, 18, 30, 48 and 72 hours, respectively. The decrease of water contact angles to 53° from 67° and the IR intensity of the Si-O-Si bond (**Figure 4. 38A)**, both imply that the hydrolysis of the APS film occurs on the surface, because the hydroxyl group is more hydrophilic than the amine group. Due to the hydrolysis of the Si-O-Si bond, the molecule with the $–NH_2$ group is continuously dropping off from the surface, which is probably a reason that the $–NH_2$ group fails to form CaP precipitate in SBF solution.

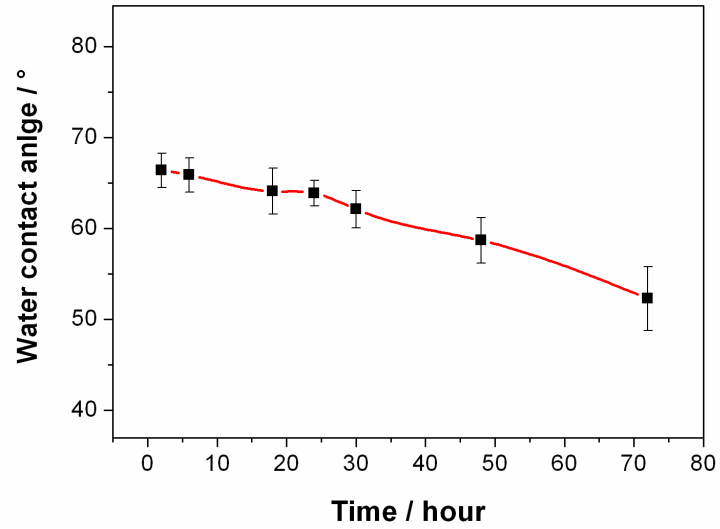

Figure 4. 37 Water contact angles of the APS film on titanium in the SBF, pH 7.45 vs. time (n=6).

In the N-H region of the IR spectra, two peaks at 1557 and 1646 cm^{-1} assigned for the vibration of the $-NH_3^+$ and one peak at 1603 cm^{-1} assigned for the deformation of the free $–NH_2$, are observed in **Figure 4. 38A** when samples were immersed up to 48 hours. Due to 4-(2-hydroxyethyl)-1-piperazineethanesulfonic acid (HEPES) as buffer agent in the SBF, the –SOOH functional group in HEPES molecule will attract with the $–NH_2$ group by the hydrogen bond: $-NH_2HOOS-$, as shown in Equation 4.2, which results in the vibration of the $–NH_3^+$ on the spectra.

$$-NH_2 + HOOS- \rightleftharpoons -NH_2\cdots HOOS- \rightleftharpoons -NH_3^+\cdots OOS- \quad \textbf{(Equation 4. 2)}$$

However, the position of the N-H deformation is primarily at 1603 cm^{-1} on the IR spectrum of the sample immersed in the SBF up to 72 hours. This is probably due to that the $–NH_2$ converting into $–NH_3^+$ alters pH value of the solution with time and HEPES as buffer agent needs release H^+ to keep the pH value in the solution, which leads to the convert of the $–NH_2$ from positively charged $–NH_3^+$. Therefore, the neutral $–NH_2$ functional groups still exist on the surface in the SBF after the immersion up to 72 hours, which will be another reason that the free amine group cannot attract the negative PO_4^{3-} ions in the solution. On the other hand, the structure of the APS film on the surface is disordered after 72 hours, as shown in **Figure 4. 38B,** as the positions of the C-H stretching modes of the alkyl chain are out the range of ~ 2850 and ~ 2918 cm^{-1}. The disordered structure of the APS film might form the inter-loop structure, which

results in that the hydrophobic group (e.g. $–CH_2$-) is exposed in the solution and further causes the failure of the inducibility of CaP.

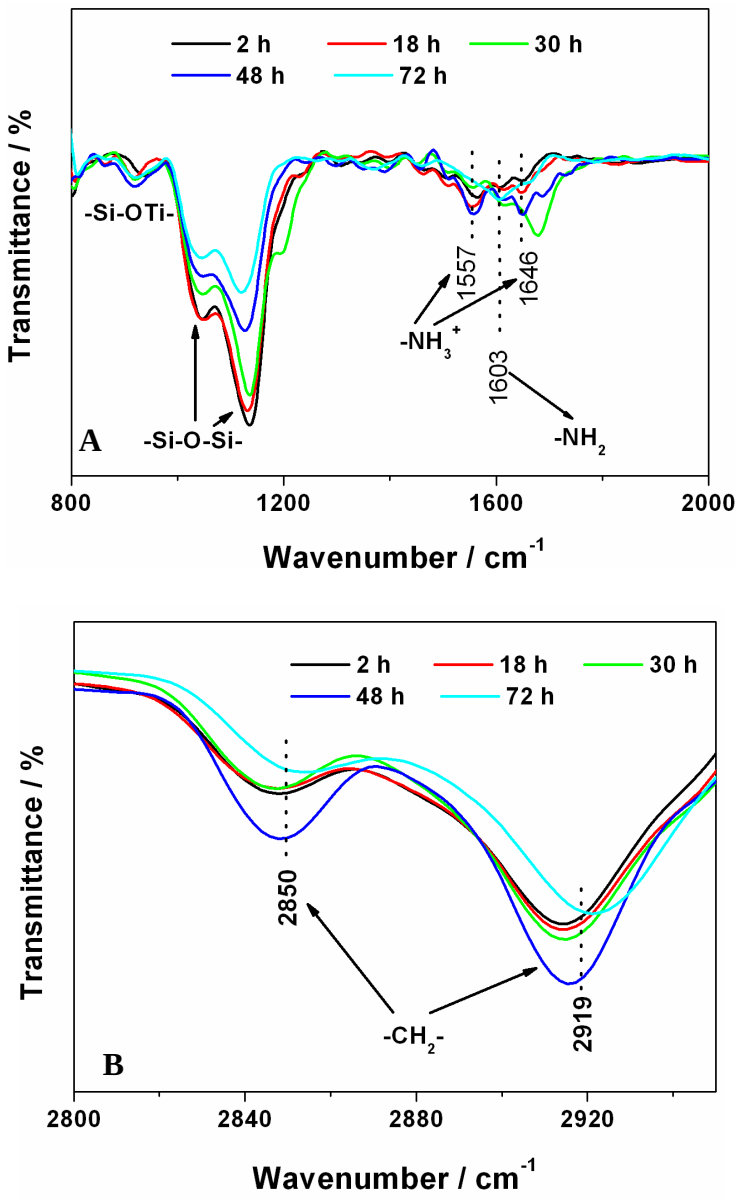

Figure 4. 38 IR spectra of the titanium surface with the APS film in the SBF, pH 7.45: (A) the Si-O-Si and the NH regions (800 – 2000 cm^{-1}); (B) the CH region (2800 – 2950 cm^{-1}).

4.2.4 Summary

Although many research have been carried out on the HA coating on titanium surface by biomimetic method, the reported data are opposite and many disputes exist in the nucleation and growth of HA. The reason is that the HA coating through biomimetic

method is highly condition-dependant and a slight change in the experimental condition could result in substantial difference. Therefore, a systematic investigation of titanium sample with the APS film was studied in order to identify the inducibility of CaP by the $–NH_2$ functional group in the simulated body fluid.

SEM images and XRD results reveal that the HA film on the TiO_x surface consists of spherical structures with flake-type crystals covering the surface of spheres because of the natively charged Ti-OH groups, but it shows poor crystalline. Higher ions concentration in the solution can accelerate nucleation and growth of HA on the surface. The deposition of HA was formed on the amine functionalized surface due to the homogenous nucleation. However, HA precipitate cannot be induced on the surface by the $–NH_2$ functional group, even in SBF with higher pH value. This might be because the APS film is continuously hydrolyzed in the SBF. According the IR spectra, the $–NH_2$ functional group is partly neutral after the immersion up to 72 hours, which can refuse attract any ions in the solution. Other reason is the exposure of the hydrophobic $–CH_2$-group in the SBF due to the disordered structure of the APS film.

4.3 Activity assay of laccase by UV-VIS spectrophotometer

Self-assembled materials are applied for the preparation of surfaces for protein and devices for nanoelectronics to strategies for biomimetic material synthesis. The self-assembled film with the $–NH_2$ functional group is able to capture CO_2 by covalent bond (-NH-C(O)-) to reduce the influence of global warming of the planet, and also to immobilize proteins (e.g. growth factors and antibody) to promote cell adhesion on the material surface or/and to heal the sick tissue. Due to the excellent functional properties, enzyme as a special protein is able to catalyse a substrate efficiently and then convert chemical to electrical energy. Oliveira *et al.* reported the immobilization of glucose oxidase and horseradish peroxidase by APTES and ascorbic acid on the titanium dioxide surface [Oliveira 2007], which is assumed to be the anodic electrode. Laccase as a multi-copper oxidase is applied in the wastewater treatment, biosensor monitoring as well as biofuel cell since it can receive 4 electrons to reduce O_2 to water. However, the

laccase (Lac) after immobilization can easily lose the activity due to change of the structure of the active site. There is no report about the Lac immobilized by APTES on the titanium-based electrode as cathode.

Our present investigation was designed to optimize the conditions of the immobilization of laccase on the surface with the APS film by carbodiimide method (EDC/NHS) to obtain the maximum activity compared with the native Lac. Particularly, the study was focused on the effects of the immobilization time, the molar ratio of EDC/NHS and pH value in the solution during immobilization on the Lac activity. Furthermore, effects of pH value and temperature in solution with substrate, and determination of the kinetic parameter (K_m) were investigated on the immobilized Lac on the surface. Finally, the stability in dry condition and aqueous solutions with pH value from 3 to 8 were studies to evaluate the possible effects of ambient on the activity of immobilized Lac.

4.3.1 Conformation of immobilized Lac on Ti with the APS film

The titanium samples with the APS film were prepared in 5 ml anhydrous toluene with 0.2 v% APTES at 30°C for 16 hours, and then immersed in 1 ml mixture solution including 200µl of 5 mM EDC, 5 mM NHS and 10 mg/L Lac, and 400µl of HEPES buffer, pH 7 in a clean vial in a refrigerator at 4°C for 8 hours, which was described in Chapter 3.1.3. Finally they were washed with the citrate buffer, pH 4.5 for three times to remove physisorbed Lac and dried very gently under argon, then analysed immediately.

Contact angles measurements were carried out to clarify the change of the chemical components on the surface using the sessile drop method. The water angle is reduced from 58° to 37° after the immobilization, as shown in **Figure 4. 39**, which is due to plenty of hydrophilic groups on the Lac surface. This change indicates that the Lac is immobilized on the surface with the APS film by EDC/NHS.

Figure 4. 39 Images of water contact angles on the surfaces with the APS film: (a) without Lac; (b) with Lac.

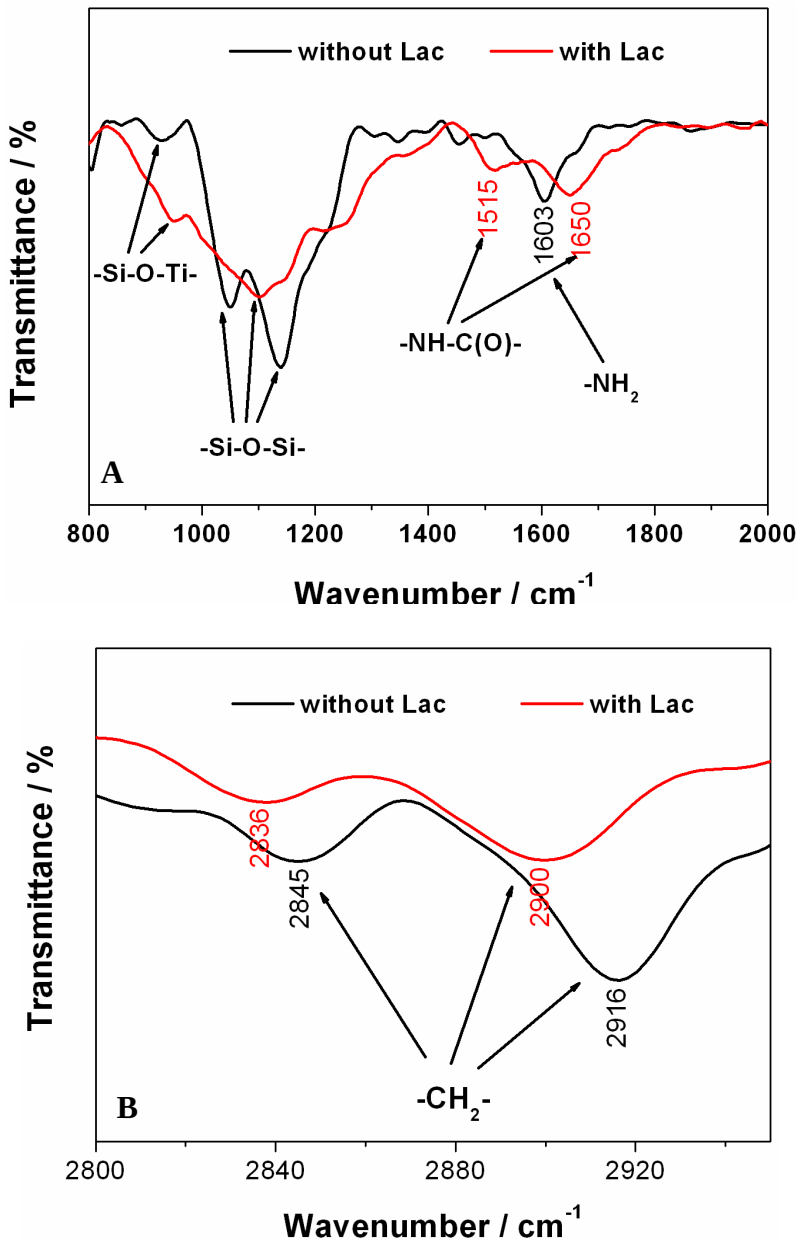

Figure 4. 40 IR spectra of titanium with the APS film with/without Lac: (A) the Si-O-Si and the NH regions (800 – 2000 cm^{-1}); (B) the CH region (2800 – 2950 cm^{-1}).

Figure 4. 40 shows the IR spectra of titanium surfaces with the APS films before and after immobilization. The Si-O-Ti band at 936 cm^{-1} blueshifting (higher wavenumber) to 944 cm^{-1}, and Si-O-Si band at 1046 and 1136 cm^{-1} merging to 1101 cm^{-1} on the IR spectra, both result from large molecules immobilized on the top of the film affecting the vibration of bonds. The peak at 1603 cm^{-1} assigned for the N-H deformation from free amine functional group, is disappeared and two new peaks are observed on the IR spectra after the immobilization: 1515 and 1650 cm^{-1}, as shown in **Figure 4. 40A**. According to IR reference book [Socrates 1980], the former is for C=O stretching and the latter is for Amide II band (N-H deformation and C-N stretching vibration), which confirm the formation of the amide bond (-NH-C(O)-). The C-H stretching vibrations redshifting (lower wavenumber) about 9-16 cm^{-1} after the Lac immobilization (**Figure 4. 40B**), indicates that a new ordered structure is formed on the surface. The contact angles and IR spectra both confirm that the Lac has been successfully immobilized on the titanium surface with the APS film by EDC/NHS.

4.3.2 Effect of molar ratio of EDC/NHS on Lac activity

The above section clearly shows that the Lac is immobilized on the surface with the APS film. Next, the activity of Lac was evaluated in 0.1 M citrate buffer, pH 4.50 with 0.2 mM 2,2'-azino-bis(3-ethylbenzthiazoline-6-sulphonic acid) (ABTS) as substrate by UV-VIS spectrophotometer, as described in Chapter 3.2.7.3. Here, it is assumed that the quantity of the $–NH_2$ functional groups in the APS film on each titanium sample is same. Therefore, the reaction rate of the Lac with ABTS only depends on the quantity of immobilized Lac on the surface: the higher reaction rate, the more actively immobilized Lac. In the carbodiimide method, EDC as the most useful activator converts the carboxyl group into a reactive unstable intermediate first and forms an amine-reactive intermediate that quickly reacts with an amino group to form an amide bond. In order to avoid reversal reaction of the unstable intermediate, NHS as an activator is normally added to convert the unstable to the stable intermediate, which will encourage the formation of the amide bond. On the other hand, since EDC and NHS are toxic, the higher concentration will lead to the inactivity of the Lac. Therefore, covalent bonding reaction depends on the amount of EDC and on the molar ratio of EDC/NHS.

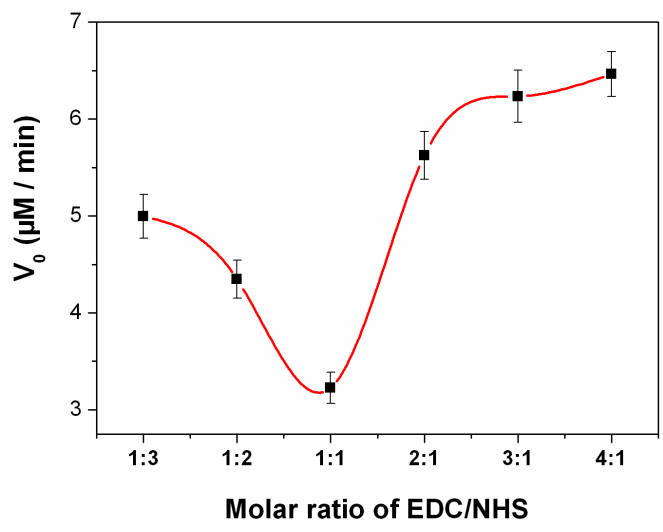

Figure 4. 41 Reaction rate (V_0) of Lac immobilized on the titanium surface with the APS film in 0.1 M citrate buffer with 0.2 mM ABTS, pH 4.5 vs. the molar ratio of EDC/NHS (n=3).

In this study, the Lac was immobilized in the mixture solution, pH 7 with different molar ratios of EDC/NHS from 1:3, 1:2, 1:1, 2:1, 3:1 and 4:1, respectively, in the refrigerator at 4°C for 8 hours, as shown in **Table 3.8**. Here, the volumes of EDC and NHS used for immobilization are 200 µl, respectively. **Figure 4. 41** shows the reaction rate of immobilized Lac vs. the molar ratio of EDC/NHS. When the concentration of NHS in the solution decreases to 1:1 from 1:3, the reaction rate of the immobilized Lac is dramatically decreasing from 5.1 to 3.3 µM/minute. This is mainly due to the failure of the formation of the amide bond from the unstable intermediate formed by EDC with the carboxyl group. On the other hand, lower concentration of EDC&NHS could also result in less active intermediate. When the concentration of EDC increases to 3:1 from 1:1, the reaction rate rapidly increases to 6.2 µM/minute, which indicates that more Lac are immobilized on the surface by EDC/NHS. When the ratio further increases to 4:1, the reaction rate slightly increases to 6.5 µM/minute, which believes that the activity of immobilized Lac on the surface has achieved maximum. The concentrations of EDC and NHS over 30 mM were used for immobilization of Lac, but the activity of Lac could not been detected by UV-VIS spectrophotometer, which suggests that higher concentration activator can kill laccase during immobilization due to the deformation of active site. Therefore, in this experiment, 3:1 (EDC of 15 mM and NHS of 5 mM) is the optimum molar ratio of EDC/NHS for the immobilization of Lac on the titanium surface with the APS film.

4.3.3 Effect of the immobilization time on the activity of Lac

In order to obtain the maximum activity of Lac on the surface, the effect of the immobilization time was investigated in the following experiment. The Lac was immobilized in a mixture of EDC/NHS (3:1), pH 7 for 2, 6, 12, 18, 20 and 24 hours, respectively at 4°C. The reaction rate of the immobilized Lac vs. immobilization time is shown in **Figure 4. 42**. In the present study, the immobilized Lac exhibits the activity with the reaction rate of 1.8 μM/min after the immobilization of 2 hours, and increases dramatically until 10 hours, which implies that the enzyme are totally covered on the surface. The reaction rate slowly increases to 7.7 μM/min for further immobilization up to 20 hours. Further prolonged immobilization time to 24 hours causes the slight reduce of the reaction rate. During the process of the immobilization, EDC and NHS are able to activate the carboxyl groups from the surface of the enzyme to form the intermediate and then form the amide bond with the $–NH_2$ functional groups. If the $–NH_2$ groups are from the surface of the Lac, the enzyme could form the multilayer on the titanium surface, which might result in that excessive Lac immobilized on the surface leads to the lower accessibility of the substrate to the active sites. Therefore, the immobilization time of 20 hours is the optimum condition to obtain the maximum activity of Lac immobilized on the surface.

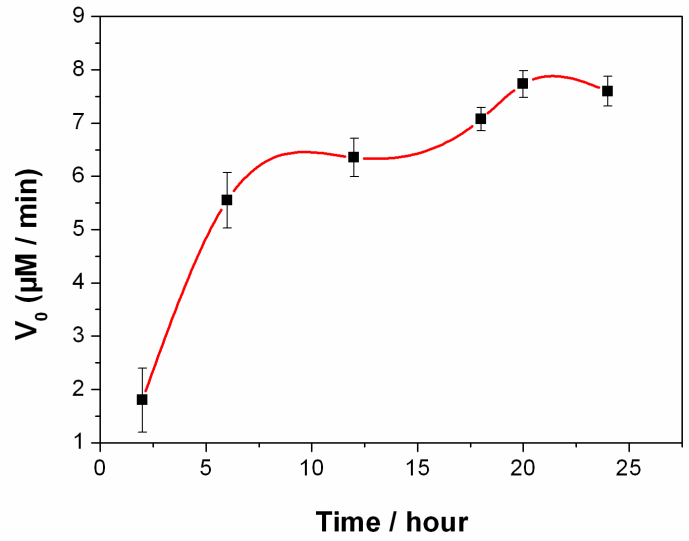

Figure 4. 42 Reaction rate (V_0) of the immobilized Lac on the titanium surface with the APS film n 0.1 M citrate buffer with 0.2 mM ABTS, pH 4.5 vs. immobilization time (n=3).

4.3.4 Effect of pH on the activity of the immobilized Lac

As known, the enzyme immobilization will be influenced easily by the ambient, which will further affect the enzyme activity. For example, pH value in the solution during the immobilization, will affect the structure of the active sites of the enzyme. Moreover, pH value will influence the activity of activators (i.e. EDC and NHS). In order to evaluate the effect of pH during the immobilization on the activity of Lac, Lac was immobilized at 4°C for 20 hours in a mixture of EDC/NHS (3:1) with pH value of 3, 4, 5, 6, 7 and 8, respectively and the reaction rate is shown in **Figure 4. 43**. The reaction rate of Lac continuously increases to 7.65 μM/min with the increase of the pH value from 3 to 7, which is probably due to that the reaction of NHS-activated molecules with primary amines is most efficient at pH 7-8. Another possible reason is that the structure of the active site of Lac is changed with higher H^+ concentration, which leads to the failure of the bonding of the substrate to the active site. However, increasing pH up to 8 results in the slight reduction of the reaction rate to 7.16 μM/min, which is possibly due to that the activation reaction with EDC is most efficient at pH 3-6. In this study, Lac should be immobilized in EDC/NHS (3:1), pH 7 for 20 hours at 4°C to obtain the maximum activity of Lac on the titanium surface with the APS film.

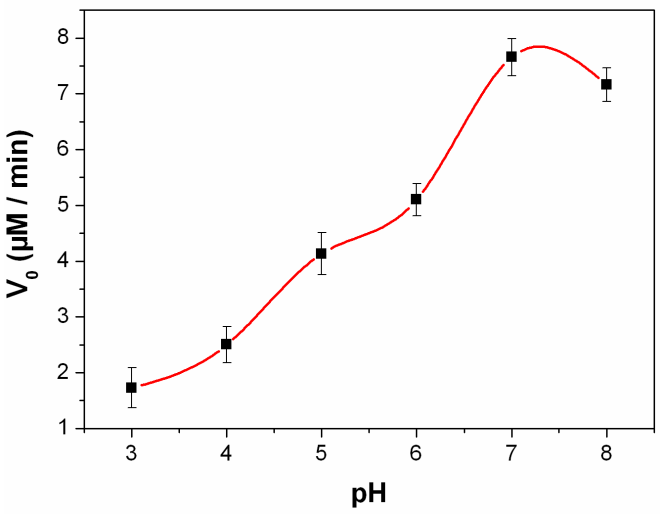

Figure 4. 43 Reaction rate (V_0) of the immobilized Lac on the titanium surface with the APS film 0.1 M citrate buffer with 0.2 mM ABTS, pH 4.5 vs. pH during the immobilization (n=3).

4.3.5 Optimum pH of the immobilized Lac

Enzymes as amphoteric molecules include a large number of acid and basic groups on their surfaces. The charges on these groups will vary with the pH of environment, which will affect the total net charge of the enzymes and their structures, in addition to the activity of the catalytic active sites. Therefore, optimization of the working pH for the immobilized enzyme is considered to be important because the ability of amino acids present at the active sites to interact with the substrate depends on their electrostatic state, which in turn depends on the pH of the solution. The Lac was immobilized on the titanium surface in the mixture of EDC/NHS (3:1), pH 7 for 20 hours at 4°C and then its activity was measured by UV-VIS spectroscopy in 0.1 M citrate buffer with 0.2 mM ABTS with the pH range of 2.5 to 6.0 at room temperature.

Figure 4. 44 shows the variety of the reaction rate of the immobilized Lac with pH value in the ABTS solution. It is clearly noticed that the reaction rate of Lac increases to 9.04 μM/min with the decrease of pH value to 3 in the solution. The pH change in the environment will influence the charge and charge distribution on the substrates, products and enzyme, which will be further reflected in changes in the binding of the

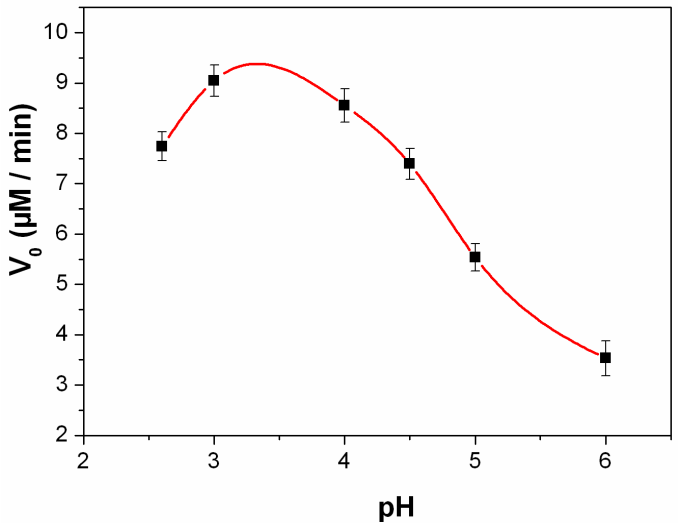

Figure 4. 44 Reaction rate (V_0) of Lac immobilized on the titanium surface with the APS film in 0.1 M citrate buffer with 0.2 mM ABTS with the pH of 2.5-6 (n=3).

substrate, the catalytic efficiency and the amount of active Lac. The effect of pH on the maximum velocity (V_{max}) of the Lac catalysed reaction may be explained below:

$$E + H^+ \underset{\kappa_{-1}}{\overset{\kappa_1}{\rightleftharpoons}} EH^+ + S \underset{\kappa_{-2}}{\overset{\kappa_2}{\rightleftharpoons}} EH^+S \xrightarrow{\kappa_3} E + P$$

(Equation 4. 3)

In this simple term, it assumes that EH^+ is the only active form of the enzyme, which believes that all of EH^+ bind the substrate to form EH^+S for the catalytic reaction.

$$\boldsymbol{[E]_0 = [E] + [EH^+] + [EH^+S]}$$ **(Equation 4. 4)**

According to **Equation 4.3,** the rate constants of κ_1 and κ_2 are written as:

$$\boldsymbol{\kappa_1 = [E][H^+] / [EH^+]}$$ **(Equation 4. 5)**

$$\boldsymbol{\kappa_2 = [EH^+][S] / [EH^+S]}$$ **(Equation 4. 6)**

Substituting **Equation 4.5** and **4.6** into **Equation 4.3**, an expression for $[E]_0$ is shown below:

$$\boldsymbol{[E]_0 = \{\kappa_1[EH^+] / [H^+]\} + [EH^+] + \{[EH^+][S] / \kappa_2\} = [EH^+]\{1 + \kappa_1 / [H^+] + [S] / \kappa_2\}}$$

(Equation 4. 7)

Substituting **Equation 4.7** to the Michaelis-Menten equation to obtain the relationship between the maximum rate of the reaction and hydrogen ion concentration, an expression is shown below:

$$\boldsymbol{V_{max} = \kappa_3 [EH^+] = (\kappa_3 [E]_0) / \{1 + \kappa_1 / [H^+] + [S] / \kappa_2\}}$$ **(Equation 4. 8)**

According to the **Equation 4.8**, the maximum velocity of Lac increase with the hydrogen

ion concentration increasing, which explains that the decrease of pH value in the ABTS solution from 6.0 to 3.0 results in the greater of the reaction rate of Lac. However, further decrease of the pH to 2.6 in the solution results in the reduction of the reaction rate to 7.74 μM/min. This is probably due to that further decreasing pH value might alter the three-dimensional shape of the enzyme, change the ionic form of the active site and the activity of the enzyme, and hence change the reaction rate. Therefore, the optimum pH for the immobilized Lac on the titanium surface with the APS film at room temperature is 3.

4.3.6 Thermal stability of the immobilized Lac

The above section clearly shows that pH 3 in the ABTS solution is the optimum pH for the immobilized Lac on the titanium surface. In some industrial applications, the enzyme will be used at higher temperature. Therefore, it is necessary to investigate the thermal stability of the immobilized Lac on the surface. The Lac was immobilized in the mixture of EDC/NHS (3:1), pH 7 for 20 hours at 4°C and then the activity of the Lac was measured in 0.1 M citrate buffer, pH 3 with 0.2 mM ABTS at the temperature in the range of 15, 22, 28, 35, 41, 50 and 55°C, respectively and the results are shown in **Figure 4. 45**.

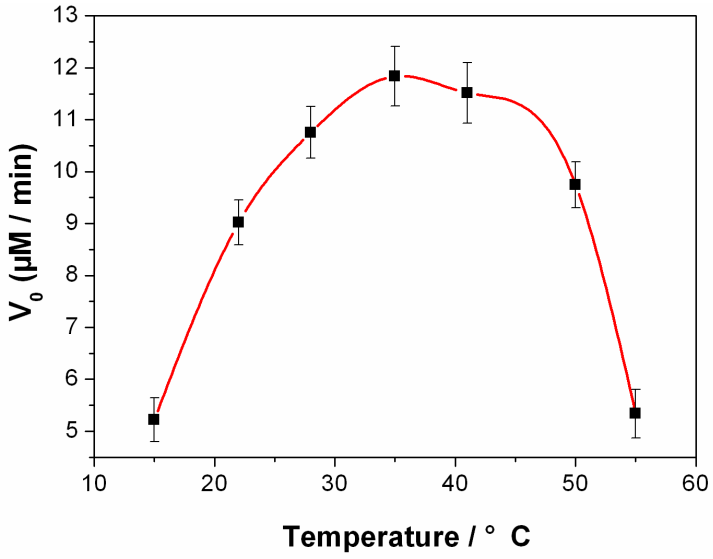

Figure 4. 45 Reaction rate of the Lac immobilized on the titanium surface with the APS film in 0.1 M citrate buffer with 0.2 mM ABTS, pH 3 at temperatures from 15 to 55°C (n=3).

Like most chemical reactions, the reaction rate of an enzyme-catalyzed reaction increases as the temperature is raised. When temperature is increasing up to 35°C, the enzyme activity dramatically gets to the maximum velocity of 11.84 μM/min, which is explained by Arrhenius equation [Trevan 1980]:

$$\ln(k) = \ln(A) - (E_a / RT) \qquad \textbf{(Equation 4. 9)}$$

where k is the rate constant of chemical reactions, R is the gas constant, T is the temperature, A is the frequency factor and E_a is the activation energy.

According to **Equation 4.9**, when the temperature (T) is increasing, the rate constant (k) is getting greater, which indicates that the reaction rate of the chemical reaction is increasing. In the case of enzymatic reactions, every five degree centigrade rise in temperature from 15 to 35 °C will increase the activity of most enzymes by 50 to 100%, as shown in **Figure 4. 45**. Normally, at low temperatures the rate of enzyme reaction is very slow. An increase in temperature increases the enzyme activity since the molecules now possess greater kinetic energy. Moreover, the collisions between enzyme and substrate on the surface are more frequent at higher temperature, which leads to the increase of the reaction rate of Lac.

However, further increase of temperature up to 55°C leads to abruptly decline of the reaction rate of the Lac to 5.33 μM/min, which indicates that higher temperatures results in the loss of Lac activity due to denaturation or unfolding. Since the Lac molecules will obtain too much kinetic energy when the temperature is increased too high, the increase in collisions between molecules could result in break or disrupt the chemical bond between the Lac and substrate. This might cause the change of shape of active site of the Lac, which indicates that the Lac is unable to combine with the substrate molecules. Therefore, the Lac become denatured and is inactive. Once the Lac has become denatured, the reaction rate would decrease as the activation energy has not been lowered. Therefore, the optimum temperature for the maximum velocity of the immobilized Lac on the titanium surface is 37~40°C.

4.3.7 Determination of the kinetic parameters (V_{max} and K_m)

Characterization of an enzyme usually includes determination of the maximum activity velocity (V_{max}) and of the Michaelis-Menten constant (K_m) for a substrate. They are the most important parameters to describe the kinetics of enzymes, which indicates how enzymes work together with substrate. In this study, the V_{max} and K_m of the immobilized Lac with ABTS as substrate were measured at room temperature by UV-VIS spectroscopy in 0.1 M citrate buffer of 1 ml, pH 3 with an ABTS concentration of 0.005, 0.01, 0.04, 0.1, 0.15, 0.2, 0.25, 0.3, 0.35, 0.4 and 0.45 mM, respectively.

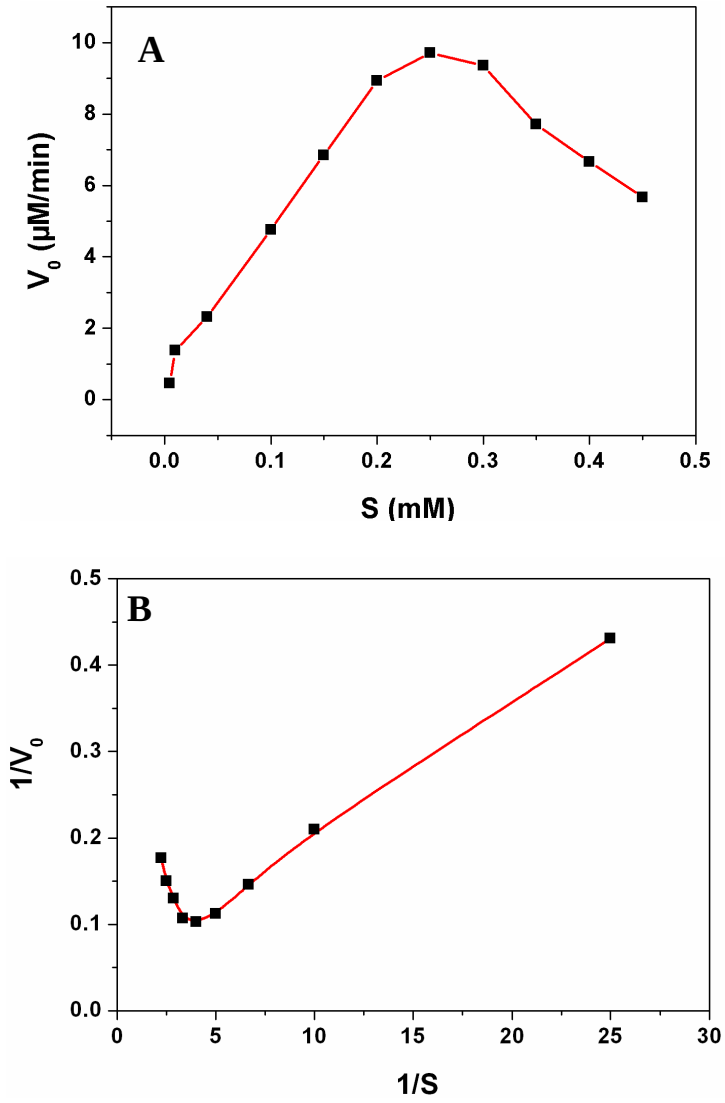

Figure 4. 46 (A) Plot of the reaction rate (V_0) against the ABTS concentration (S); (B) the Lineweaver – Burk plot of A.

The reaction rate (V_0) as a function of the substrate concentration is shown in **Figure 4. 46A**. The curve partly obeys the Michaelis-Menten equation compared with the standard hyperbolic curve shown in **Figure 3.14A**. When the ABTS concentration is higher than 0.3 mM, the reaction rate suddenly decreases, which indicates that a substrate-inhibition phenomenon occurs in this system. According to **Equation 3.15**, the results can be converted to the Lineweaver-Burk plot, as shown in **Figure 4. 46B**. The K_m and V_{max} values of the immobilized Lac on the surface are 0.271 mM and 9.77 μM/min, respectively. The immobilized Lac shows 7 times greater on the K_m value than the native Lac (0.038 mM), which implies that the immobilized Lac shows lower affinity to the substrate. It is in agreement with other researchers reporting significant decreases in affinity of enzymes after the immobilization. The diffusion resistance might mainly cause the increase in K_m, because the product accumulates near the Lac surface to an undesirable high level, leading to product inhibition for the Lac. On the other hand, the enzyme fixed on the surface by the chemical bond, cannot combine randomly with the substrate like the native one due to the space conformation.

4.3.8 Comparison the activity of the Lac immobilized on TiO_x & Ti with the APS film

In order to investigate the immobilization behaviour of laccases on TiO_x and titanium with the APS film, two samples were immersed in the mixture of EDC/NHS (3:1), pH 7 with Lac at 4°C for 20 hours, respectively and then measured by UV-VIS spectrophotometer at room temperature in 0.1 M citrate buffer, pH 3 with 0.2 mM ABTS. **Figure 4. 47** shows the progress curves of laccase-catalysed reaction within 1 minute. The slope of the curve of the titanium sample with the APS film is significantly greater than that of TiO_x. According to **Equation 3.6**, the reaction rates of Lac are calculated: 9.19 and 1.85 μM/min for the activity of Lac immobilized on titanium with the APS film and TiO_x, respectively, which confirms that the APS film can improve the activity of Lac on the titanium surface by the covalent bond.

Reaction rate (■) = (0.17053-0.005)/(0.5 × (3.6×10^4) ×1) = 9.19 μmol/min

Reaction rate (●) = (0.03446-0.001)/(0.5 × (3.6×10^4) ×1) = 1.85 μmol/min

Since TiO_x sample can only supply the hydroxyl groups on the surface instead of the carboxyl group, the Lac can be immobilized by the hydrogen bond with the amine group on the Lac surface ($^{-}H_2N^{+}\cdots HO^{-}$) rather than the amide bond. Therefore, it leads to that the majority of Lac was washed off in the citrate buffer and further results in the slow catalysed reaction.

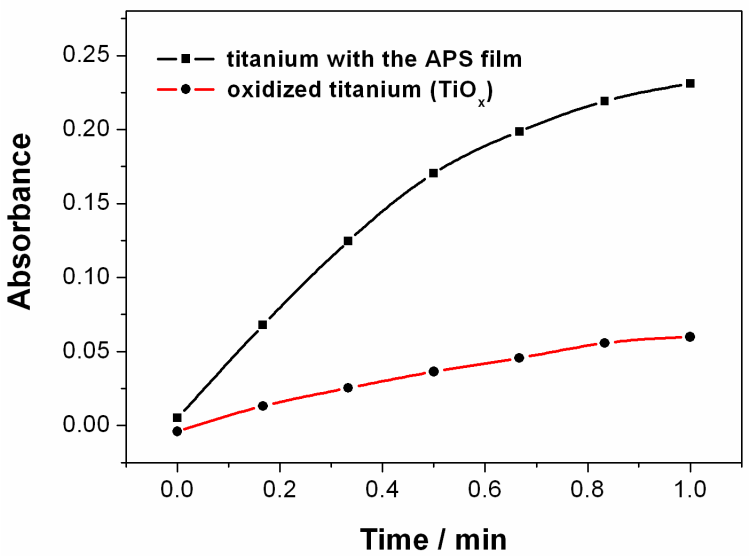

Figure 4. 47 Progress curves of laccase-catalysed reaction in 0.1 M citrate buffer, pH 3 with 0.2 mM ABTS on different surfaces.

4.3.9 Stability of the immobilized Lac

The main purpose of the immobilization is to improve the re-usability of enzyme as catalyst in the application. However, people reported that the immobilized enzymes were easily inactive after couples of hours. This is probably due to that the immobilization of enzyme on the carrier often limits its freedom to suffer drastic conformational changes, thus resulting in the increase of the denaturation. In order to investigate the stability of the immobilized Lac, titanium samples with laccase were stored in dry and aqueous HEPES buffer with a pH value of 3, 4.5, 6, 7 and 8, respectively for 7 days at 4°C to study the stability of the immobilized Lac.

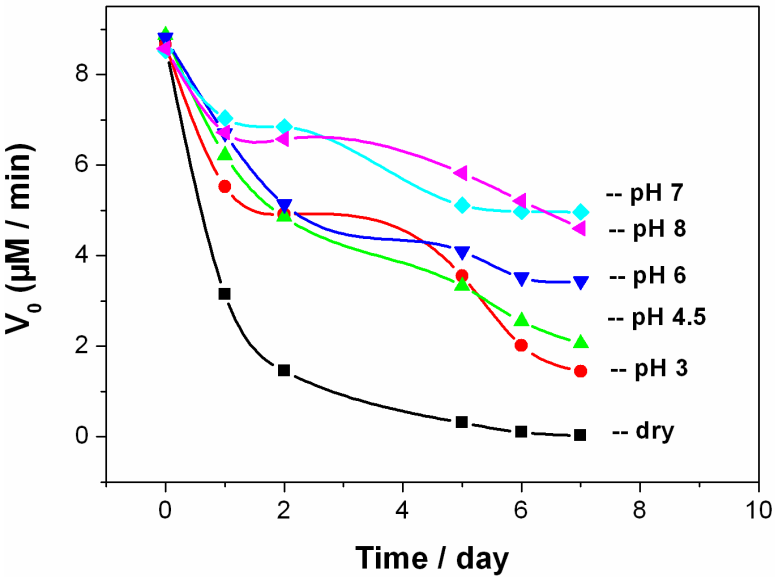

Figure 4. 48 The activity of the Lac immobilized on the titanium surface with the APS film in different storage conditions at 4°C within 7 days.

Figure 4. 48 shows the activity of the Lac on titanium in different storage conditions and corresponding activity loss within 7 days is shown in **Table 4. 8**. No matter in dry or aqueous conditions, the activity of the Lac at the first day loses faster than that in the rest of 6 days. Compared with the Lac in the aqueous solution, the immobilized Lac much easier loses the activity in the dry condition. The activity of the Lac decreases dramatically to 17% of the initial activity after 2 days and there is almost no activity obtained after one week. In the aqueous solution, the activity loss of the Lac slows down to 41.82% with the increase of the pH value to 7 within 1 week, which indicates that the Lac will remain the lower activity in the aqueous solution for the longer usability. However, the activity loss of the Lac increases to 46.39% in an aqueous solution, which indicates that the OH^- ions in the buffer might change the shape of the active site, leading to the Lac denature. On the other hand, the amide bond (-C(=O)NH-) for the immobilization, might be hydrolyzed in the presence of water. This hydrolysis process is faster in the acidic condition, which probably causes that the activity loss of the Lac reaches to 83.32% and 77.17% for pH 3 and 4.5, respectively. In this study, the optimum condition to store the immobilized laccase is an aqueous solution, pH 7, even though Lac only remains 60% of the initial activity.

Table 4. 8 Relative activity loss (%) of Lac immobilized on titanium with the APS film in different storage conditions for 1 week.

Storage conditions	Relative activity loss (%)				
	1 day	**2 days**	**5 days**	**6 days**	**7 days**
Dry	63.70	83.27	96.44	98.86	99.73
pH 3	36.23	43.28	59.03	76.76	83.02
pH 4.5	29.90	45.29	57.74	62.51	77.17
pH 6	23.95	42.79	53.52	59.11	60.48
pH 7	17.47	19.77	32.09	40.05	41.82
pH 8	21.65	23.37	32.13	39.24	46.39

4.3.10 Summary

In this section, the activity of the Lac from *Trametes versicolor* immobilized on the titanium surface with the APS film by the covalent bond, was systematically investigated by the UV-VIS spectrophotometer. The water contact angles and FTIF analyses reveal that the Lac was successfully immobilized on the surface by the carbodiimide method. To optimize the condition of the immobilization, the molar ratio of EDC/NHS, the immobilization time and pH value in the solution were studied. The Lac is immobilized in the mixture of EDC/NHS (3:1), pH 7 at 4°C for 20 hours to get the maximum activity. Compared with that on the TiO_x, the Lac on titanium with the APS film shows the higher activity due to the formation of the amide bond (–C(O)NH-).

The effects of pH value in the citrate buffer and temperature were studied on the activity of the Lac on the surface. The immobilized Lac exhibited the maximal activity at pH 3.0 compared with the native Lac at pH 4.50, which is due to the formation of $[EH^+S]$, leading to the increase of the K_{cat}. The activity of the Lac is lost when the temperature is higher than 40°C, which is the same as the native Lac. The K_m value of the immobilized Lac was 0.271 mM according to the Michaelis - Menten equation, which is much higher than that of the native Lac. It confirms that the immobilized Lac has the lower affinity towards substrate. Moreover, ABTS as a substrate is an inhibitor to the Lac due to the reduction of the activity of the Lac when the concentration of ABTS is greater than 0.3

mM. Further investigation of the stability of the immobilized Lac in different storage conditions, clearly shows that the Lac is more stable in the HEPES buffer, pH 7.0, although the activity of the Lac maintains 60% of the initial activity after one week.

4.4 Electrochemical behaviours of electrodes with Lac immobilized by the APS film

In Chapter 4.3, the catalysis activity of the immobilized Lac on the titanium surface was investigated in the ABTS solution by UV-VIS spectrophotometer. Since the Lac is capable of catalytically reducing O_2 to H_2O by receiving 4 electrons, the catalysis activity of the Lac can also be measured by the electrochemistry method. In order to investigate the electrochemical behaviours of the immobilized Lac, two different electrodes with the APS film were studied in the electrolyte with ABTS: Titanium (Ti) and Graphite (G). Titanium dioxide (also named titania, TiO_2) is one of the most widely used in electrocatalytic application due to its redox selectivity [Ronconi 2001]. For example, titania as a semiconductor to sense the amount of oxygen present in an atmosphere. Titania can also enhance the efficiency of electrolytic splitting of water into hydrogen and oxygen by photocatalysis. Moreover, Ti(IV)/Ti(III) as metal ionic redox couple was used as mediator or electron carrier [Chu 2009]. It is well known that graphite has good electrical conductivity due to the vast electron delocalization within the carbon layers from the Chapter 2.5.2.4. Therefore, it is interesting to compare the electrocatalysis activity of the Lac immobilized on Ti and G, respectively.

According to Chapter 4.3, the Lac was immobilized on electrode in the HEPES buffer by EDC/NHS of 3:1, pH 7 for 20 hours at 4°C. Then the electrode with the Lac was washed in the citrate buffer, pH 3 for three times to remove the physisorbed Lac. In the electrochemical measurement, Ag/AgCl and platinum were used as reference electrode (RE) and counter electrode (CE), respectively. According to the result from **Figure 4. 46**, the citrate buffer contains 0.2 mM ABTS is as the electrolyte during electrochemical measurements. For titanium electrode, the electrochemical behaviour was studied in the citrate buffer with mediator. For the graphite electrode, the direct electron transfer (DET) and mediated electron transfer (MET) were investigated for the catalysis activity of the

Lac. Particularly, the effects of pH value and temperature, and determination of the kinetic parameter (K_m) were studied on the activity of the Lac immobilized on G with the APS film. Normally, the graphite electrode with the Lac was stored in the HEPES buffer, pH 7 at 4°C after the measurement.

4.4.1 Titanium as electrode

In order to study the electrochemical behaviour of titanium as electrode, the $Fe(CN)_6^{4-/3-}$ redox couple is used as mediator, as shown in **Equation 3.18**, which is one of the most extensively studied redox couples in electrochemistry. Compared with titanium oxide electrode (TiO_x), the titanium sample after the oxidation was calcined in a furnace around 800°C under air to form TiO_2 layer on the titanium surface, since TiO_2 is a well-known semiconductor, which is named TiO_2 electrode. The cyclic voltammetry experiments of $Fe^{2+/3+}$ redox couple were performed by placing the TiO_x and TiO_2 electrodes in 0.1 M citrate buffer without and with 4 mM $Fe(CN)_6^{3-}$, respectively under the ambient condition by Autolab.

When TiO_x electrode was immersed in the citrate buffer, the cyclic voltammogram (solid curve) in **Figure 4. 49A** only shows the oxidation curve without the reduction one (no cathodic current), which indicates that the electron cannot freely transfer through the electrode. This is likely due to the inert inhibiting property of the titanium oxide on electron transfer through it. Normally, three types of oxides, TiO, Ti_2O_3 and TiO_2 are formed on the surface after the oxidation in the *Piranha* solution and TiO_2 is on the outermost surface [Liu 2004]. TiO can lose electrons and be oxidized to Ti_2O_3 and further to TiO_2, which results in that the electrons move from the WE to the CE when the voltage is added to the WE. However, when the voltage is added to the RE, TiO_2 on the surface can receive electrons and be reduced to Ti_2O_3 and further to TiO, which implies that the electrons cannot transfer through the titanium electrode. Therefore, this is no reversible current observed (dash curve in **Figure 4. 49A**) when the TiO_x electrode was placed in the citrate buffer with 4 mM $Fe(CN)_6^{3-}$.

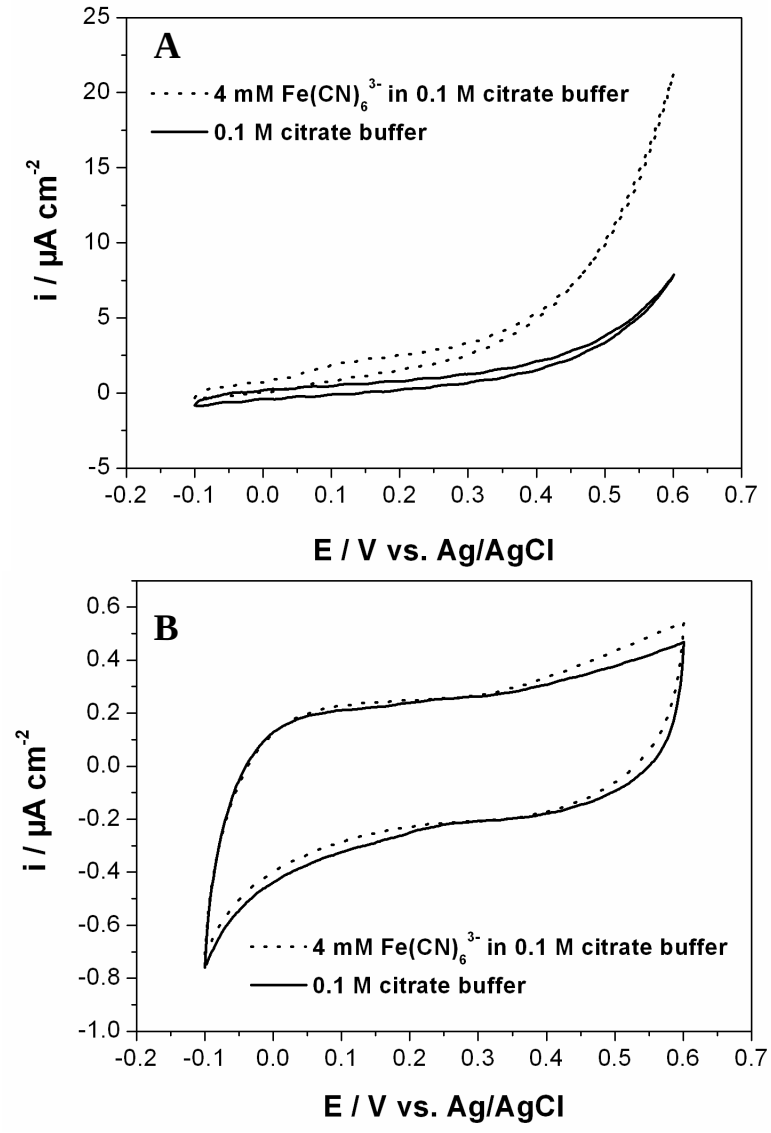

Figure 4. 49 Cyclic voltammograms at v = 20 mV/s of titanium-based electrodes in different solutions: (A) TiO_x and (B) TiO_2.

There is a standard CV curve shown in **Figure 4. 49B** (solid curve) with anodic and cathodic currents, which implies that the electrons can transfer the electrode. However, the CV curve (dash curve) of the TiO_2 electrode does not exhibit any observable redox peaks in the citrate buffer with the redox couple. This might be due to that the electrons transfer too slow to occur redox reactions. On the other hand, according to our experimental results, the TiO_2 electrode that is produced in a furnace around 800°C under air, cannot be as a substrate for the formation of the APS film. Therefore, the titanium sample treated in the *Piranha* solution is not suitable for the electrochemistry study.

4.4.2 Graphite as electrode

As known, graphite (G) is a good electrical conductor and can conduct electricity due to the vast electron delocalization within the carbon layers. Apart from the good electron transferring property, graphite has high chemical stability and mechanical strength. Moreover, compared with other electrode (e.g. gold & Pt), the graphite surface is able to supply the OH groups and further silanize APTES molecule to form the APS film. **Figure 3.19** shows the cyclic voltammogram with the oxidation and reduction peaks for the graphite electrode in the citrate buffer with 0.4 mM $Fe(CN)_6^{3-}$ and the reduction (midpoint) potential of the mediator is 185 mV vs. Ag/AgCl (sat. KCl). Today, many researchers have studied graphite as an electrode for the electrochemical applications. For example, highly ordered pyrolytic graphite and glassy carbon with carbon nanotubes-ionic liquid gel have been studied in the biofuel cells for the physisorbed Lac on the catalysis activity, whereas they could not been reusable [Liu 2007; Shleev 2005]. So far, there is no report that the Lac is immobilized on graphite with the APS film by covalent bond. The following sections are devoted to study electrochemical behaviour of the Lac immobilized on graphite.

According to the preparation methods of the APS film and enzyme immobilization on titanium, the APTES molecules were silanized on the graphite surface after the oxidation in H_2O_2 and the Lac was immobilized by the APS film through the peptide bond (-C(O)-NH-), which are confirmed by the water contact angle and FTIR. In order to investigate the DET of the Lac on graphite, Lac/APS film/G samples were analyzed by the Autolab in the citrate buffer under anaerobic and aerobic conditions, respectively. For the MET reactions, APS film/G samples were analyzed in the citrate buffer with 0.2 mM ABTS under the ambient condition to study the electrochemical behaviour. The APS film/G and Lac/APS film/G samples were both studied in the 0.2 mM ABTS solution under the oxygen-saturated condition by the cyclic voltammetry to clarify the catalysis activity of the immobilized Lac. To further clarify the effect of the scan rate, pH value and temperature on the catalysis activity of the Lac, Lac/APS film/G samples were measured at the scan rate from 10 to 200 mV/s, or at pH of 3 – 7, or at temperature of 7 – 62°C, respectively. In the study of the stability of the Lac/APS film/G electrode, the samples were stored in the HEPES buffer, pH 7.0 at 4°C for 30 days.

4.4.2.1 Confirmation of the Lac on graphite with the APS film

Like the preparation of the titanium sample, graphite was cut into approximately 10 × 10 × 1 mm^3 square shape from a graphite rod (99%, VWR). After ground and polished, the small piece of graphite was immersed in 5 ml H_2O_2 solution overnight at room temperature to form OH groups, and then washed with the distilled water in the sonicator for 5 times in order to remove the residue of the hydrogen peroxide. **Figure 4. 50** shows the SEM images of graphite surfaces before and after oxidation. After the H_2O_2 treatment, there are etching pores observed on the surface with the width of ~ 30 μm, as shown in **Figure 4. 50B**.

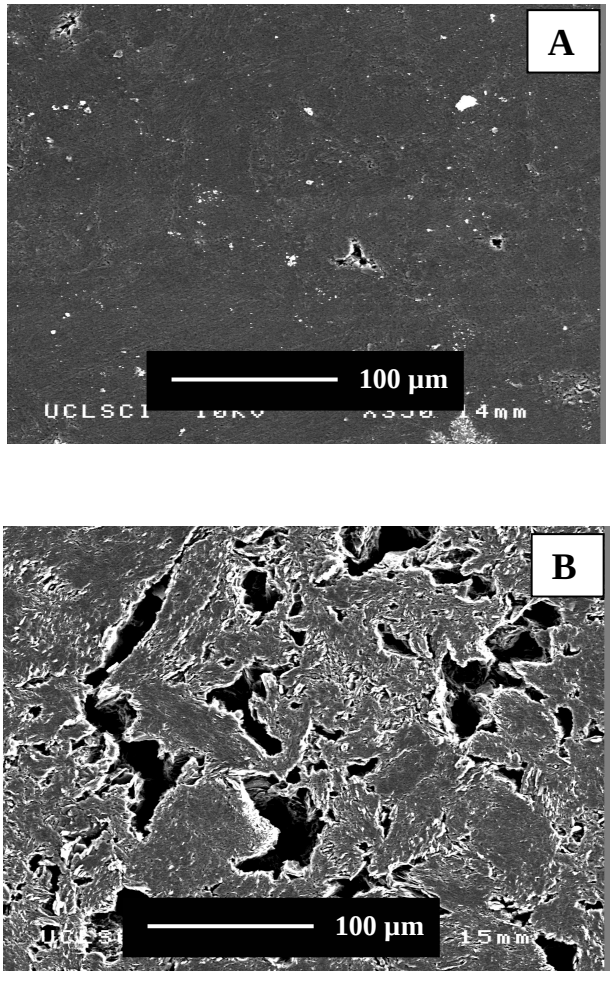

Figure 4. 50 SEM images of graphite surfaces: (A) as-received and (B) after the oxidation in H_2O_2.

The silanization of APTES molecules on graphite is the same as that on titanium. Graphite samples after oxidation were immersed in anhydrous toluene of 5 ml with 0.2

v% APETS for 16 hours at 30°C, and then washed with toluene and ethanol for 3 times in order to remove the physisorbed APS molecules. For the immobilization of the Lac, the APS film/G sample was placed in the mixture of EDC/NHS (3:1) with the Lac at 4°C for 20 hours and washed with the citrate buffer for three times to remove the physisorbed laccase. All of samples were analyzed in a few hours after being washed and dried under argon. **Figure 4. 51** shows the variation of water contact angles of graphite samples. The decrease in the value of the contact angle from 87° ±2.8° for the bare graphite to 63°±1.6° for the APS film/G electrode, implies the formation of the APS film. In the same way, the contact angle was effectively reduced to 44°±1.5°, which indicates the immobilization of the Lac on graphite with the APS film.

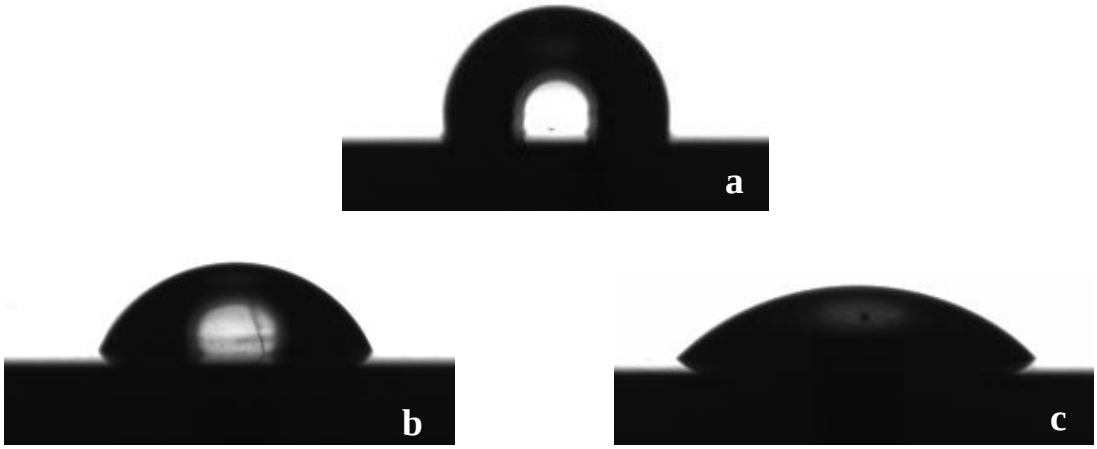

Figure 4. 51 Images of water contact angles for different graphite surfaces: (a) G after oxidation; (b) APS film/G; (c) Lac/ APS film/G.

Figure 4. 52 shows IR spectra of the APS film/G sample before and after the Lac immobilization. Intensities of two peaks at 1049 and 1085 cm^{-1} assigned for the Si-O-Si vibration, reduce after the enzyme immobilization. Moreover, the N-H deformation at 1606 cm^{-1} for the free amine functional group disappears on the spectrum of the Lac/APS film/G sample and forms two new peaks: 1518 and 1658 cm^{-1}. According to IR reference book [Socrates 1980], the former is assigned for the C=O stretching and the latter for the Amide II band (N-H deformation and C-N stretching vibration), which confirm the formation of the amide bond (-NH-C(O)-). Combined with the C-H stretching vibrations red-shift about 30 – 53 cm^{-1} after the immobilization (**Figure 4. 52B**), all of change mentioned above on the spectra indicates that the Lac is successfully immobilized on the graphite surface by the APS film.

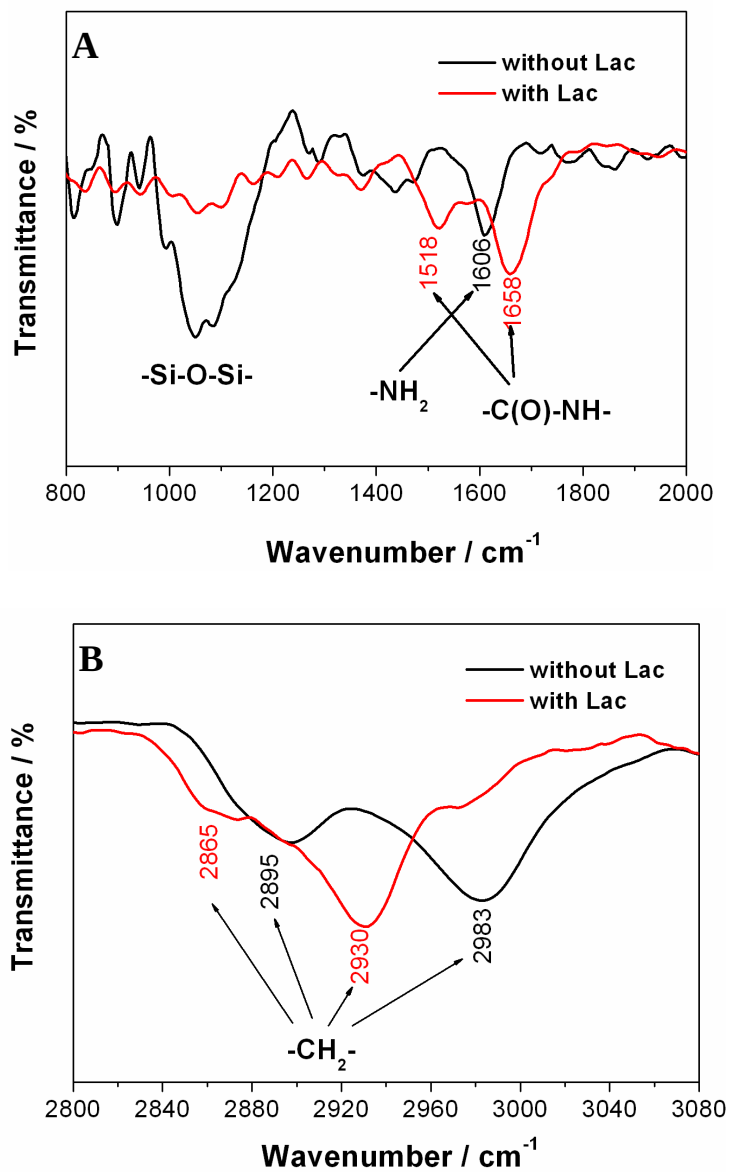

Figure 4. 52 IR spectra of the APS film/G and Lac/APS film/G samples: (A) the Si-O-Si and the NH regions (800 – 2000 cm^{-1}); (B) the C-H region (2800 – 3080 cm^{-1}).

4.4.2.2 Direct electron transfer measurements

In order to clarify the working potential range during the measurement, the APS film/G electrode was analyzed in the 0.1 M citrate buffer from -0.4 to 1 V vs Ag/AgCl under the argon-saturated and oxygen-saturated conditions, respectively and the results are shown in **Figure 4. 53**. Under the oxygen-saturated condition, cyclic voltammogram (red curve) is sharply dropping down at the potential from -0.4 to 0 V, which is probably due to the adsorption of the plenty of H^+ ions on the surface of the APS film/G electrode to

form NH_3^+ species. From 0.7 to 1 V at the working potential, the curve is obviously going up, which assumes that oxygen is adsorbed on the sample surface. Normally, the redox potential of the T1 copper of the laccase from *T. versicolor* is from 0.55 to 0.59 V vs. Ag/AgCl [Yaropolov 1994]. Moreover, the redox potential of the mediator - ABTS / $ABTS^{+\cdot}$ is 0.185 V vs. Ag/AgCl[Fernandez-Sanchez 2002]. Therefore, the range of the working potential for the electrochemistry measurement is from 0.1 to 0.7 V vs. Ag/AgCl.

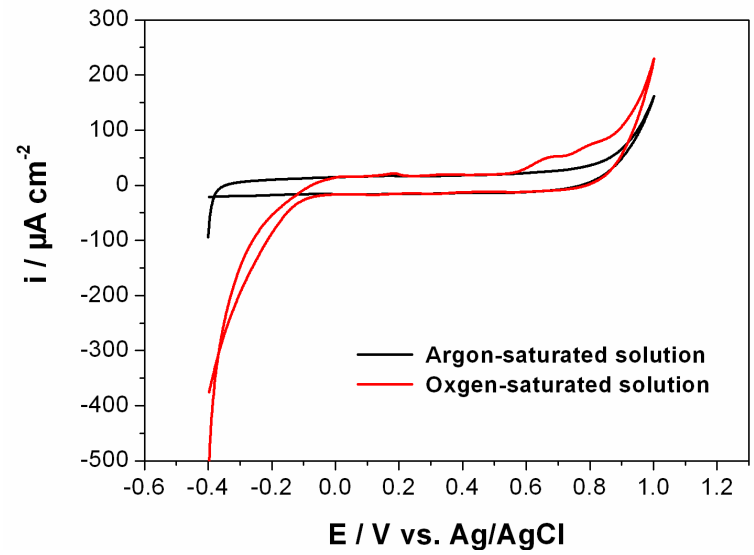

Figure 4. 53 Cyclic voltammograms of the APS film/G electrode in 0.1 M citrate buffer, pH 4.5; scan rate – 5 mV/s.

Figure 4. 54 shows cyclic voltammograms of the Lac/APS film/G electrode in 0.1 M citrate buffer at pH 4.5. There is no observed redox peaks on the cyclic voltammogram (red curve) under the oxygen-saturated condition. Since the results from Chapter 4.3 by the UV-VIS spectroscopy have confirmed that the Lac has catalysis ability, it assumes that the structure of the activity site of the Lac immobilized on graphite is changed so that the Lac cannot receive electrons to reduce O_2 to form water. According to the property of the Lac from Chapter 2.4.3.1, the copper T1 receives the electron to transfer to the T2/T3 cluster. Therefore, it is assumed that the T1 is far from the surface of the graphite electrode and cannot receive electrons. Possible structures of the Lac are shown in **Figure 4. 55**. Therefore, the Lac immobilized by the covalent bond with the APS film, cannot show the DET reactions. The following section is the investigation of the MET reactions of the Lac immobilized on graphite.

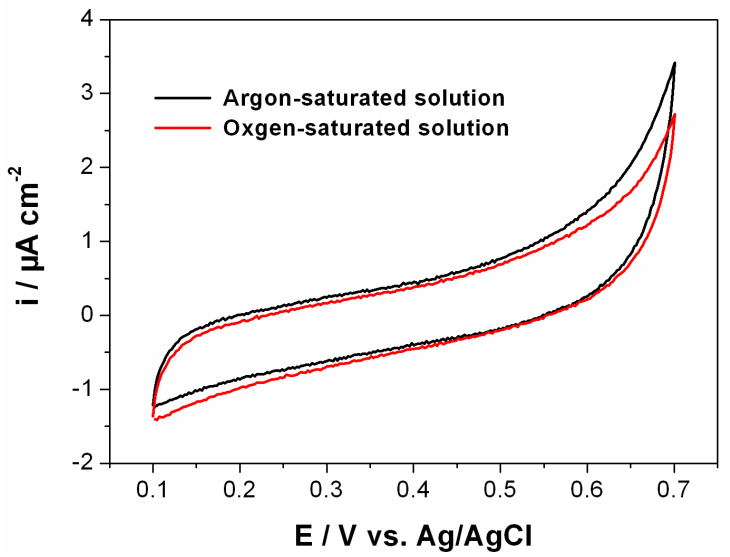

Figure 4. 54 Cyclic voltammograms of Lac/APS film/G electrode in 0.1 M citrate buffer, pH 4.5; scan rate – 5 mV/s.

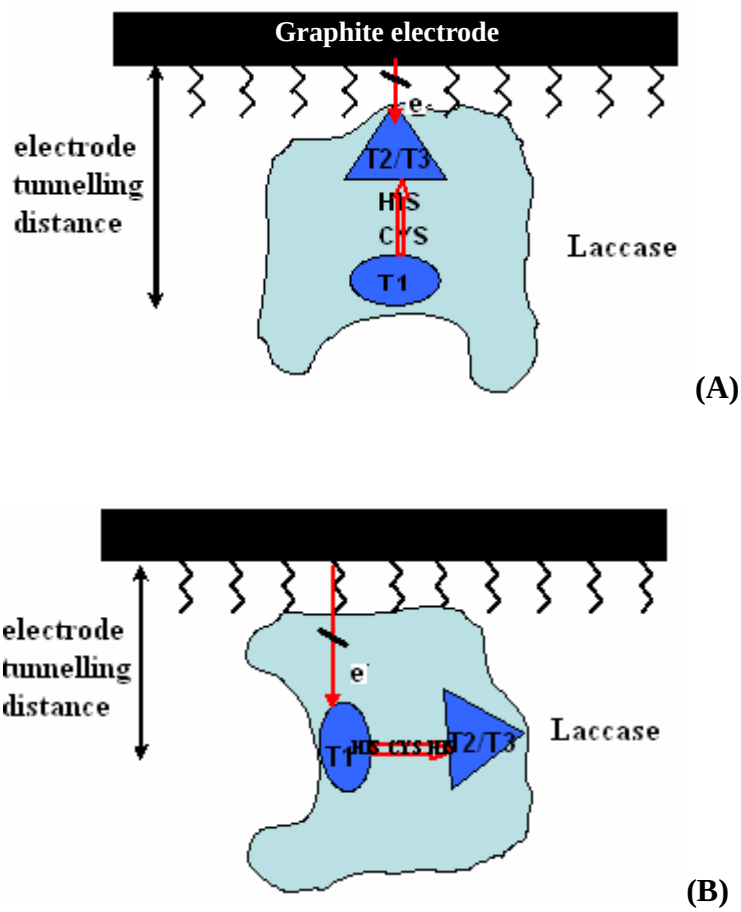

Figure 4. 55 Possible structures of the Lac immobilized on the graphite electrode for the direct electron transfer.

4.4.2.3 ABTS mediated electron transfer measurements

Since the Lac immobilized on graphite cannot show the DET reaction, a mediator will be added in the electrolyte to help transfer the electrons to the Lac. The ABTS is a good mediator to exhibit fast electron transfer kinetics between the electrode and laccase, and the sketch picture of the reduction of dioxygen to water by the Lac is shown in **Figure 2.41**. Since the graphite electrode was linked with the connector from the Autolab by a copper wire (shown in **Figure 3.22**), it is necessary to study the electrochemistry behaviour of the APS film/G electrode in the citrate buffer with 0.2 mM ABTS. **Figure 4. 56** shows the CV curve of the graphite electrode with the APS film under the argon-saturated condition in the ABTS solution. There are three sharp redox peaks observed on the CV of the APTS film/G, whose potentials of 0.345 V (anodic), 0.270 and 0.297 V (cathodic), respectively, are more negative than that of the ABTS / $ABTS^{+\cdot}$ redox couple (0.472 V vs Ag/Ag/Cl) [Bourbonnais 1998]. It is assumed that these peaks probably originate from the copper wire and reactions are happened as below:

$$Cu \underset{+e^-}{\overset{-e^-}{\rightleftharpoons}} Cu^{(I)} \underset{+e^-}{\overset{-e^-}{\rightleftharpoons}} Cu^{(II)} \qquad \textbf{(Equation 4. 10)}$$

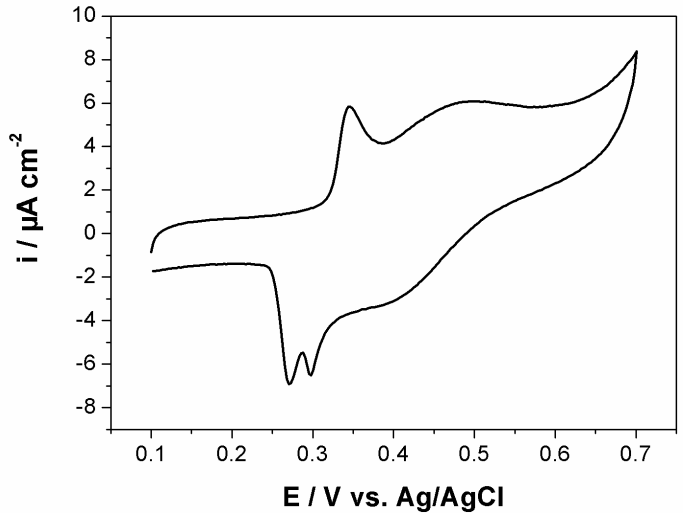

Figure 4. 56 Cyclic voltammogram of the APS film/G electrode under argon atmosphere in 0.1 M citrate buffer, pH 4.5 with 0.2 mM ABTS. Scan rate: 10 mV/s.

Figure 4. 57 shows the effect of the scan rate on the electrochemistry behaviour of the APS film/G electrode. The redox potential of the ABTS for the graphite electrode is + 0.435 V vs. Ag/AgCl, as shown in **Figure 4. 57A**. **Figure 4. 57B** shows the linear dependence of peak current on square root of the scan rate from 5 to 50 mV/s, which indicates that the redox process of the ABTS on the graphite electrode is controlled by the mass transport. It indicates that the relatively large mediator molecule can easily penetrate the APS film.

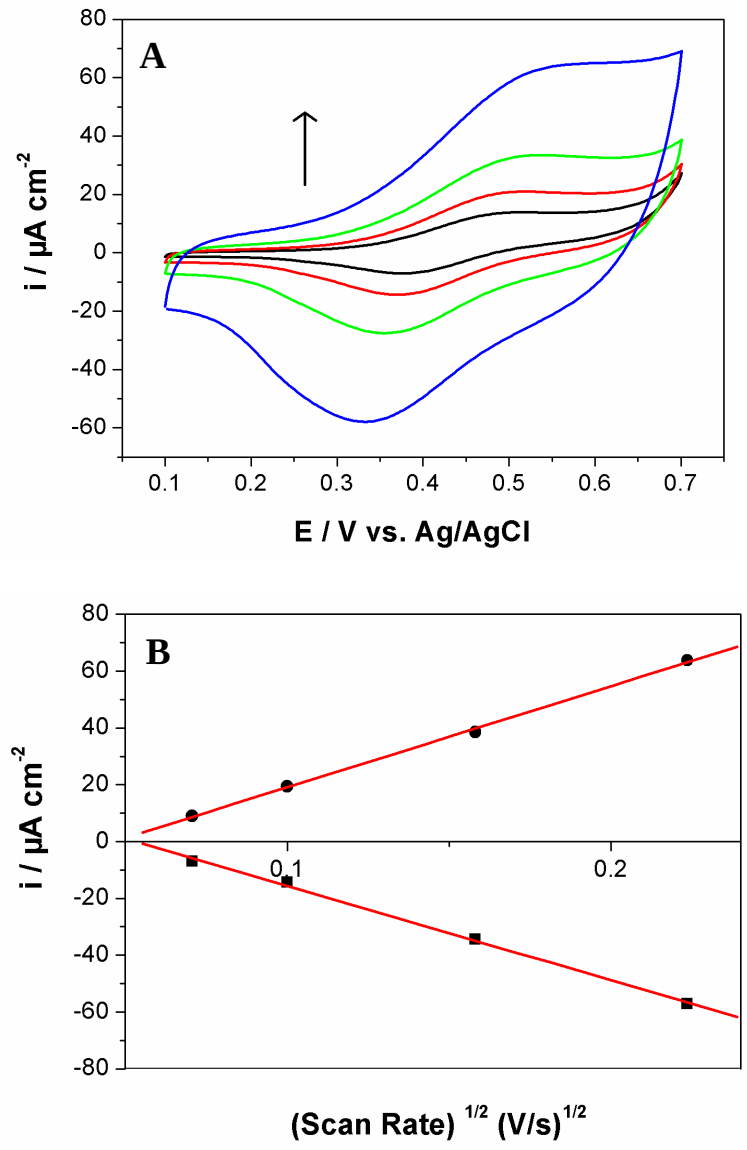

Figure 4. 57 (A)Cyclic voltammograms of the APS film/G electrode in 0.1 M citrate buffer with 0.2 mM ABTS, pH 4.5 at various potential scan rates: 50, 20, 10, 5 mV/s. (B) Plot of peak current density vs. square root of scan rate under oxygen atmosphere: (●) – anodic current and (■) – cathodic current.

Figure 4. 58 shows CVs of graphite electrodes in the oxygen-saturated solution containing 0.2 mM ABTS. In **Figure 4. 58**, a pair of redox peaks of the ABTS with the redox potential of 0.435 V (vs. Ag/AgCl) is observed on the CV of the APS film/graphite electrode. When the Lac is present on the electrode, the cyclic voltammogram (red curve) shows a sigmoidal cathodic wave for the catalytic reduction, which shows that the reduction peak current clearly increases and the oxidation peak current decreases, by comparison with that of the APS film/G electrode (blue curve). This process represents a typically electrocatalytic reduction of the oxygen by the Lac, which is agreeing with the previously reported results [Liu 2007; Zawisza 2006]. These phenomena imply that the Lac has been stably immobilized on the APS film/G electrode surface and especially, retains the good catalytic activity. There is a noticeable pair of redox peaks on the CV of the Lac/APS film/G electrode at 0.345V (anodic) and 0.273 (cathodic), which are probably due to free Cu ions from the active site of the physisorbed Lac on the electrode. MET measurements confirm that the conformation changing of the immobilized Lac on the graphite surface results in no catalysis current observed for the DET reaction of the reduction of oxygen.

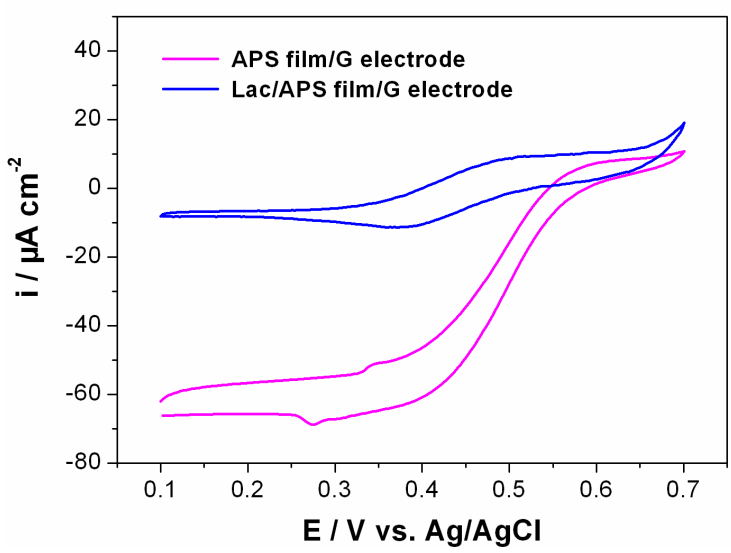

Figure 4. 58 Cyclic voltammograms of the graphite-based electrodes in 0.1 M citrate buffer with 0.2 mM ABTS, pH 4.5 under the oxygen-saturated condition. Scan rate: 5 mV/s.

Figure 4. 59A and B show the CVs of the Lac/APS film/G electrode in 0.1 M citrate buffer with 0.2 mM ABTS under argon and oxygen-saturated conditions, respectively at different scan rates. In the absence of the Lac, CV curves (**Figure 4. 59A**) are almost

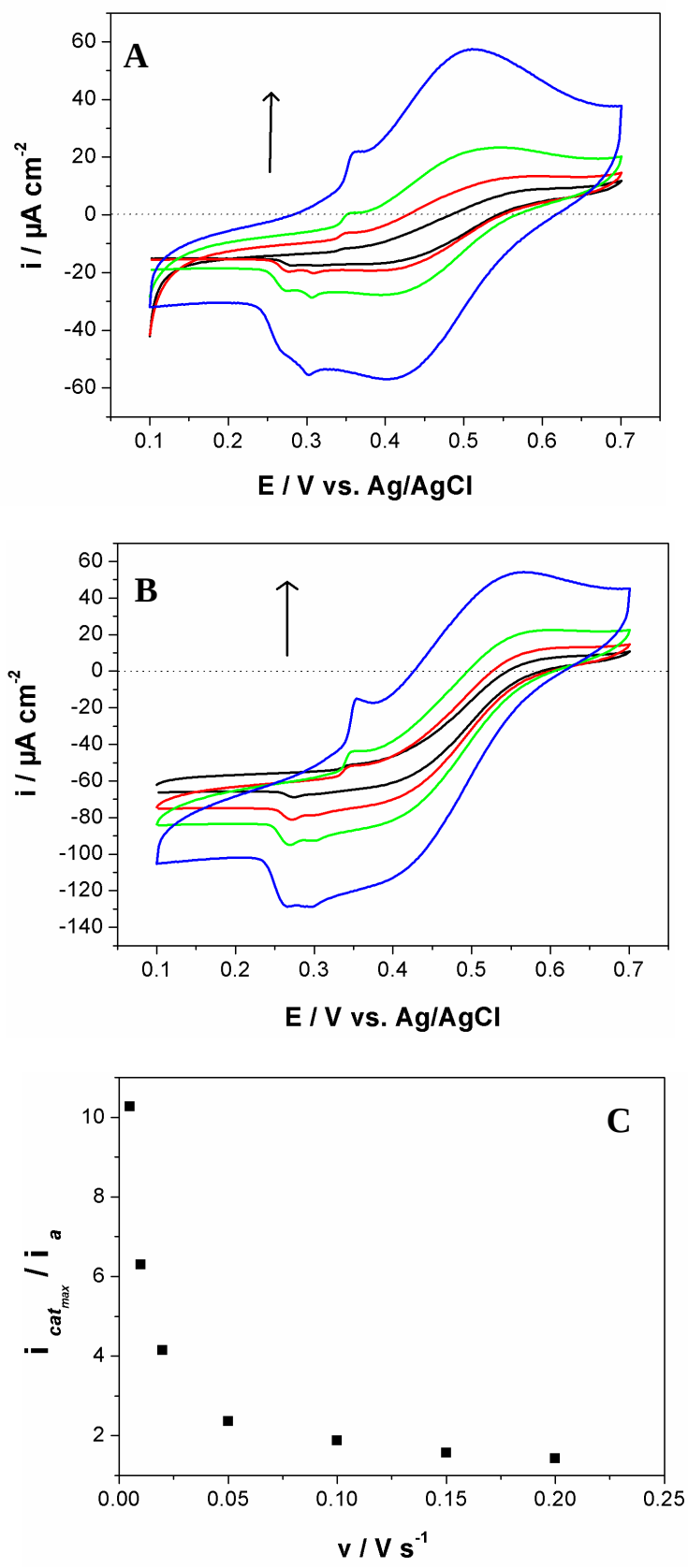

Figure 4. 59 Cyclic voltammograms of 0.2 mM ABTS in 0.1 M citrate buffer solution, pH 4.5 at various can rates: 5, 10, 20 and 50 mV/s for Lac/APS film/G electrode: (A) argon-saturated solution; (B) oxygen- saturated solution; (C) Plot of the ratio of the cathodic to anodic currents on scan rate under oxygen-saturated condition.

symmetric with the anodic and cathodic current well developed indicating the mass transport controlled process. However, the electrocatalytic reaction is still observed immediately after the immersion of the electrode at low scan rate (= 5 mV/s) because the solution is not 100% argon-saturated. For the Lac/APS film/G electrode under the oxygen-saturated condition, the anodic current is negligible at low scan rate (= 5 mV/s) (**Figure 4. 59B**). At larger scan rates the anodic peak appears due to the diffusion controlled oxidation of ABTS. **Figure 4. 59C** shows the ratio of the cathodic to anodic currents with the scan rates from 5 to 200 mV/s. The ratio decreases with the increase of the scan rate approaching unity for $\nu \leq 50$ mV/s. These experiments indicate that the electron transfer from the mediator to the Lac is too slow and time longer than 12 seconds is required to observe the electrocatalytic process.

The observed above changes in the cyclic voltammograms can be explained by the electrocatalytic reduction of O_2 by the Lac in the presence of the mediator. There are three steps of the electron transfer during the processes. The first one is the reduction reaction of $ABTS^{+\cdot}$, involving the electrons transferred from the electrode surface to ABTS:

$$4ABTS^{+\cdot} + 4e^- \longrightarrow 4ABTS \qquad \textbf{(Equation 4. 11)}$$

At the second step, ABTS is oxidized by the Lac to form $ABTS^{+\cdot}$. Meanwhile, four electrons transfer from ABTS to the T1 centre of the Lac, including the reduction of Cu^{2+} to Cu^{+}.

$$Lac4Cu^{(II)} + 4ABTS \longrightarrow 4ABTS^{+\cdot} + Lac4Cu^{(I)} + 4e^- \qquad \textbf{(Equation 4. 12)}$$

Finally, four electrons transfer from the T1 to T2/T3 copper cluster by three-peptide linker and Cu^{+} ion is re-oxidized to Cu^{2+}, and then O_2 is reduced to the H_2O by the Lac.

$$Lac4Cu^{(I)} + O_2 + 4H^+ + 4e^- \longrightarrow 2H_2O + Lac4Cu^{(II)} \qquad \textbf{(Equation 4. 13)}$$

During the redox reactions, the first and third steps are relative fast compared the

second one. According to the MET experimental results, the reduction of fully oxidized four Cu atoms in the Lac is the slowest reaction in the catalytic cycle. $ABTS^{+\cdot}$ radical is produced by the electron transfer to Cu(II) at T1 centre. Next electrons are shuttled to T3/T2 trinuclei centres to oxidize remaining part of the enzyme [Lee 2002]. This nuclear centre is the binding site of molecular oxygen and the site of its catalytic reduction to H_2O. The catalytic reaction requires re-oxidation of fully reduced Cu(I) atoms in enzyme to regenerate the enzyme. Slow catalytic reaction explains the disappearance of cathodic catalytic current at higher scan rates. Therefore, at slow scan rates time constant is sufficient to observe the catalytic process and the steady-state current is reached.

4.4.2.4 Effect of temperature on the catalytic activity of the Lac

In order to study the effect of temperature on the catalytic activity of the Lac, the Lac/APS film/G electrode was prepared following the method from Chapter 4.4.2.1 and performed in 0.2 mM ABTS solution, pH 4.5 in the water bath of 7 – 62°C under oxygen-saturated condition and the results are shown in **Figure 4. 60**. The catalytic ability of the Lac immobilized on graphite dramatically increases with the temperature until 19°C. When the temperature increases to 50°C, the reaction rate of the Lac increases with the temperature and the Lac immobilized on graphite obviously exhibits the maximum ratio of cathode to anodic currents (**Figure 4. 60B**), which indicates that reaction rate of the immobilized laccase obtains maximum. The catalytic ability of the Lac decreases suddenly at the temperature above 50°C, which might be due to the change of the configuration of the active site at the higher temperature leading to the denaturation of the enzyme. In general, the activity of enzymes is strongly dependent on the temperature. According to the property of the protein, at the temperature > 60°C, the secondary helical structure of the active site in the enzyme will disappear, which leads to the failure of the combination of the oxygen with the T2/T3 cluster centre, finally resulting in the decay in the catalysis activity. Therefore, the optimum temperature of the Lac from *T. versicolor* immobilized on graphite with the APS film is around 50°C.

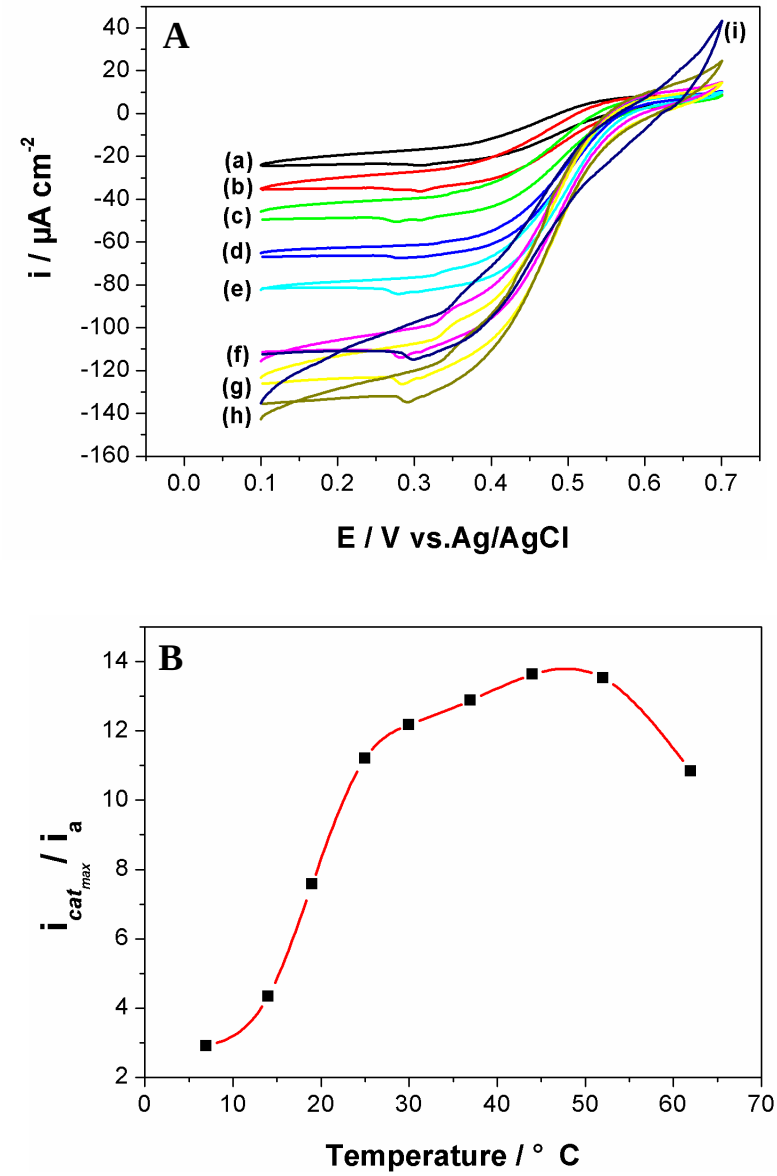

Figure 4. 60 (A) Cyclic voltammograms of the Lac/APS film/G electrode in 0.1 M citrate buffer with 0.2 mM ABTS, pH 4.5 under oxygen atmosphere vs. 5 mV/s at different temperature: (a) 7°C, (b)14°C, (c) 19°C, (d) 25°C, (e) 30°C, (f) 37°C, (g) 44°C, (h) 52°C, (i) 62°C. (B) Plot of the ratio of catalytic current over anodic current for $ABTS^{\cdot+}$ reduction for the same electrode vs. temperature.

4.4.2.5 Effect of pH on catalytic activity of the Lac

One of the most important characteristics of the Lac for the catalytic activity is the pH dependence, which can influence the ionization property of active site in enzyme. In order to investigate the effect of pH value on the catalytic activity of the Lac, the Lac/APS film/G electrode is measured in 0.2 mM ABTS solution over the pH range of 2.5-5.0 at room temperature under the oxygen-saturated condition and the results are

shown in **Figure 4. 61**. The catalytic current of the Lac is increasing with the decrease of the pH value until 3, and then decrease at the pH of 2.5 (**Figure 4. 61A**). The ratio of cathodic to anodic currents with the pH in **Figure 4. 61B** shows the same trend.

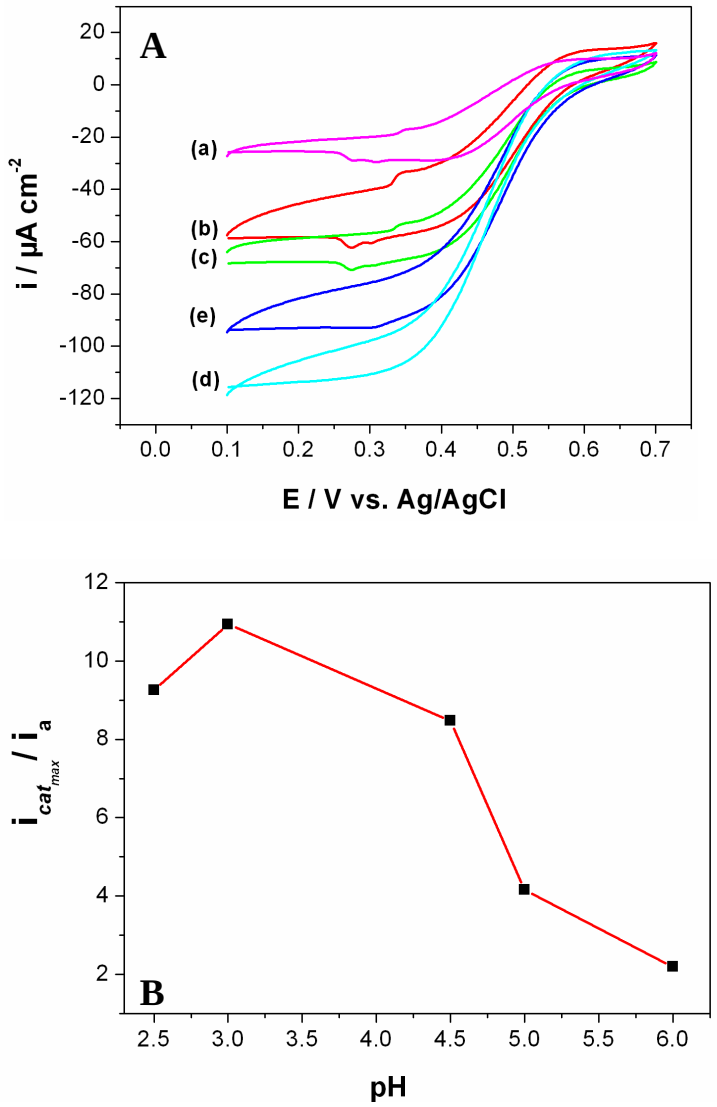

Figure 4. 61 (A) Cyclic voltammograms at v = 5 mV/s of the Lac/APS film/G electrode in 0.1 M citrate buffer with 0.2 mM ABTS under oxygen atmosphere at various pH values during the measurement: (a) 6, (b) 5, (c) 4.5, (d) 3, (e) 2.5. (B) Plot of the ratio of catalytic over anodic currents for the same electrode vs. pH.

In general, the activity of the Lac is contributed by various structural and mechanistic factors of enzymes and substrates. According to the result reported by Xu *et al.*, the dependence of the enzyme activity on pH is governed by the potential difference between redox potential of the Lac and the mediator and OH^- inhibition effect [Xu 1997]. The redox potential of the Lac is normally pH independent [Duran 2004], so the

effect of the potential difference is mainly determined by that of the mediator. However, the redox potential of ABTS remains constant at the pH range studies [Fernandez-Sanchez 2002], which means the formation of ABTS cation radical does not involve proton transfer and the redox potential of ABTS is pH independent. Thus the effect of the potential difference between redox potential of Lac & mediator is pH independent. Therefore, the contribution of the OH^- inhibition is dominant over the whole pH range. At higher pH range, the OH^- will inhibit T2/T3 site of the Lac to bind with the substrate, which will cause the descending of the catalytic activity. At lower pH range, excessive H^+ ions might affect the shape of the active site and the charge property of the substrate so that either the substrate cannot bind to the Lac or it cannot undergo catalysis. According to the above results, the Lac immobilized on graphite shows the maximum catalytic current at pH 3 in the citrate buffer with 0.2 M ABTS.

4.4.2.6 Calculation of Michaelis-Menten constant (K_m)

Michaelis-Menten constant (K_m) is an important parameter in enzyme kinetics, and can evaluate the affinity of enzyme bonding with substrate which is related to the catalysis ability. The enzyme kinetics of the Lac immobilized on the APS film/G electrode was studied at room temperature by UV-VIS spectroscopy in the citrate buffer of 1 ml with different ABTS concentrations. The initial reaction velocity as a function of the substrate concentration is shown in **Figure 4. 62A** and the corresponding Lineweaver-Burk plot is shown in **Figure 4. 62B**. There is a dramatic drop of the initial velocity when the ABTS concentration is greater than 0.4 mM, which is due to the substrate-inhibition phenomenon. According to the Lineweaver-Burk plot in **Figure 4. 62B**, Michaelis-Menten parameters V_m and K_m are 60.98305 µM/min and 0.146 mM, respectively. Actually, the inhibition by ABTS has been observed also with the Lac from other origins. Compared with the K_m of the native Lac of 0.036 mM, K_m of 0.146 mM for the immobilized Lac implies that the affinity of the Lac is around 4 times reduced, which might be due to the limitation of the diffusion of the immobilized Lac.

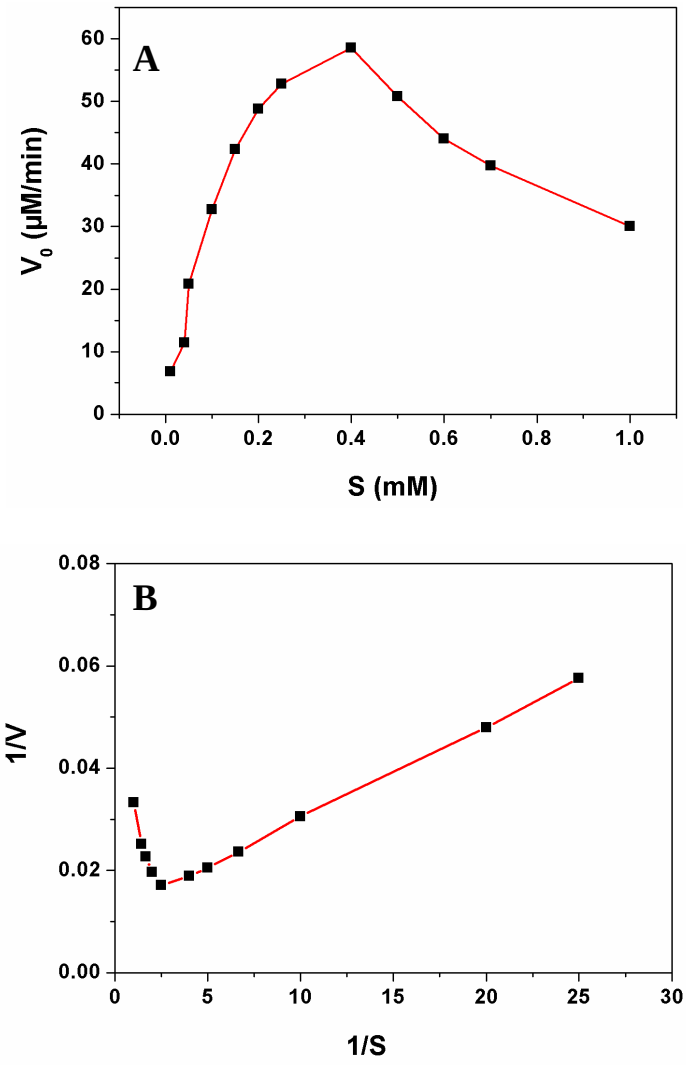

Figure 4. 62 Initial velocity of the Lac immobilized on the Lac/APS film/G electrode with ABTS concentration from 0.005 to 1.0 mM in 0.1 mM citrate buffer, pH 3: (A) points (experimental), line (Michaelis-Menten equation). (B) Lineweaver-Burk plot.

4.4.2.7 Stability of the laccase immobilized on graphite

To investigate the stability of the Lac on the APS film/G electrode, graphite samples were stored in 20 mM HEPES buffer, pH 7 at 4°C before used, and then tested in 0.1 citrate buffer, pH 3.0 by the cyclic voltammetry method at regular intervals for 30 days. **Figure 4. 63** shows the plot of the ratio of cathodic and anodic currents with the storage time. Within 30 days, the Lac on the electrode still has a good catalytic activity, in agreement with the result from **Table 4. 9** that shows the graphite electrode still remains about 84% of the initial catalytic activity. These imply that the immobilized Lac on the APS film/G electrode has good stability.

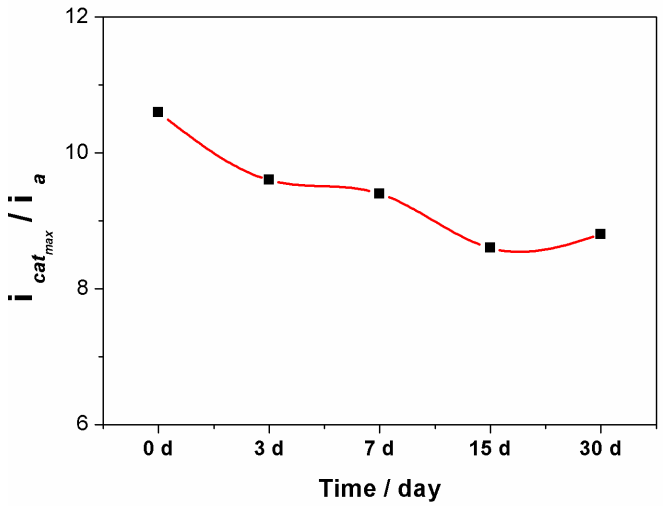

Figure 4. 63 Plot of the ratio of catalytic current over anodic current for the $ABTS^{\bullet+}$ reduction on Lac/APS film/G immersed in 20 mM HEPES buffer, pH 7 for different durations.

Table 4. 9 Activity loss of the Lac immobilized on graphite with the APS film stored in 0.2 mM HEPES buffer, pH 7 for 30 days.

	0 d	3 d	7 d	15 d	30 d
Activity loss	100%	9.43%	11.32%	18.87%	16.98%

4.4.3 Summary

In this section, electrochemical behaviours of the Lac immobilized on titanium and graphite by the cyclic voltammetry method were investigated, respectively. For titanium as electrode, amorphous TiO_x film on the surface cannot show the proper electron conductivity in the citrate buffer, which might be due to the inert electron transferring property. TiO_2 film on the titanium surface prepared in the furnace cannot show the redox reaction in the citrate buffer with $Fe(CN)_6^{3-}$ as a mediator, which is due to far slowness of electron transferring.

For graphite as electrode, the formation of the amide bond at 1518 and 1650 cm^{-1} on the IR spectrum and changing of the water contact angles, reveal that the Lac was successfully immobilized on the graphite surface with the APS film. The direct electron transfer reaction was not detected under oxygen-saturated condition, which might result from the barrier of the electron transfer between the T1 centre and the electrode surface. For the MET reaction with ABTS as a mediator, the catalytic current of the Lac to the

oxygen reduction was observed at lower scan rate (≤ 50 mV/s). The optimal temperature and pH of the Lac immobilized on graphite were 50°C and 3, respectively. The K_m value of the immobilized Lac was 0.146 mM, 4 times higher than that free Lac (0.036 mM), which shows lower affinity with ABTS. However, the Lac on graphite has a relative good stability in HEPES buffer, pH 7 within 30 days.

CHAPTER 5

GENERAL DISCUSSION

5.1 General issues of self-assembling APTES

Considering the fact that silane-based SAMs (e.g., Octadecyltrichlorosilane, OTS) have been successfully formed on the oxidized Si surfaces and served as model systems for many years, but limited work was reported the growth of SAMs on the titanium surface, especially for the hydrophilic end group, such as 3-aminopropyltriethoxysilane (APTES). The APTES as a silane agent can bond inorganic materials such as glass and silicon by self-assembly technology with the hydroxyl groups, hence it has been used widely for many applications. However, the APTES with short chain has less stability in aqueous media and at high temperatures, which will influence its applications. Moreover, APTES is an amphiphilic molecule after hydrolysis: the -OH group as head group and the $–NH_2$ group as end group, so it will form multilayers and/or irregular structure on the surfaces without control, although it may be useful for some applications, e.g., the thick APS layers can be detrimental if depositing on spatially constrained regions. Therefore, it is very important to ensure that APTES deposits a thin and ordered film on the surface. Many experimental efforts have been devoted to the growth of silane molecules including the APTES molecule, but the results are very patchy, often inconsistent and lack of due interpretation, particularly alkylsilane molecules self-assembled on titanium has not been well studied before. Therefore, a clear understanding of the important factors which influence the growth of APTES on titanium is highly desirable.

In this project, titanium with the APS film is applied in bio-implant and immobilization of enzymes in biofuel cells. Although some experimental efforts have been devoted to the inducibility of calcium phosphate (CaP) by the $–NH_2$ functional groups, there is still a debate whether the amine group can induce CaP. On the other hand, the $–NH_2$ functional group can immobilize the enzyme by the covalent bond (-C(O)-NH-).

However, the immobilized enzyme can be easily inactive due to the change of the configuration, resulting in the short life time. Therefore, it is necessary to investigate the ability of catalysis and electrochemistry, and stability of the immobilized enzyme.

Hence, the main objectives of this study were set: 1) to determine the effects of pre-treatment, temperature, molecular concentration and water content in solvent on the preparation of the relative thin and ordered APS film on titanium; 2) to evaluate the stability of the APS film on titanium in aqueous solutions with different pH values; 3) to evaluate the inducibility of calcium phosphate by the $-NH_2$ functional groups in the simulated body fluid (SBF); 4) to improve the stability of the immobilized laccase on electrode surface; and 5) to improve the ability of electrochemistry of the immobilized laccase on graphite. The overall aims are to form well-ordered self-assembling film on surface and that the APS film can be successfully applied in bio-implant and bio-fuel cells. The general discussion is organised in line with the objectives.

5.2 Effect of pre-treatment by *Piranha* solution

Various titanium surface modification methods have been suggested in literature as a beneficial measure to improve its biological applications. In order to obtain clean and/or TiO_x layer on the surface, the *Piranha* solution was used. In general, the *Piranha* treatment improves the surface hydrophilicity with a contact angle reduction from 78° to 16° (**Figure 4.1 and Table 4.1**). Advincula *et al.* have reported similar water contact angle of 20° on the *Piranha* treated Ti layer (with its native oxide) thermally evaporated on Si wafers [Advincula 2005]. Moreover, Liu *et al.* have shown a reduction in the water contact angle of titanium substrate from 68° to 40° after the *Piranha* treatment [Liu 2004]. Such reduction can result from the removal of organic contaminants and/or an increase in the density of surface hydroxyl groups. Majewski *et al.* have also applied the *Piranha* treatment on a Ti foil substrate and claim the facilitated hydroxylation of the Ti surface without showing supportive data [Majewski 2006].

However, the *Piranha* treatment resulted in high surface roughness (**Table 4.1**), which might not be desirable for the formation of a well-ordered self-assembled film for laboratory characterisation, though rough surfaces can be desirable for bony tissue ingrowth in practical applications. Therefore, reducing temperature or the immersion time or changing the concentration of the acid in the *Piranha* solution can tailor the surface roughness, e.g. generating a relatively smooth surface. The AFM images (**Figure 4.2**) show that changing temperature did affect the surface roughness significantly and the surface remains quite rough with a local RMS roughness of ~ 37.71 nm. Moreover, the surface wettability changed slightly from 24° to 16°, which might be mainly affected by the surface roughness rather than the chemical component on the surface, according to the Wenzel equation.

Prolonged treatment duration revealed no considerable difference in the local RMS roughness of the surfaces of 6.57 ~ 7.26 nm (**Table 4.2**). This was explained by the fact that the *Piranha* solution is a very strong etching reagent and even with a short exposure most of the porous native oxide layer is dissolved. However, a slight increase in surface hydrophilicity (**Figure 4.4**) was observed with prolonged processing durations from 5 to 30 minutes, which indicates that prolonged processing exposure to the *Piranha* solution further cleaned the surface without affecting its roughness (**Figure 4.5**).

In order to clarify the roles of H_2SO_4 and H_2O_2 in the *Piranha* solution, respectively, different concentrations of solutions were applied for the surface treatment. Water contact angles (**Figure 4.6**) show the *Piranha* solution has better ability to clean titanium surface compared with only H_2O_2 or H_2SO_4, respectively. With the increase of the concentration of H_2SO_4, the surface hydrophilicity increases with contact angles of 45° to 15° (**Figure 4.6**) and XPS analysis also shows that the level of the carbon contamination decreased as well (**Figure 4.7 C**). Therefore, it is suggested that the role of the acid in the solution was to remove the contaminant. XPS spectra (**Figure 4.7 Ti2P**) also show that the *Piranha* treatment can form an oxide layer, mainly TiO_2, and H_2O_2 can oxide thoroughly Ti element with higher concentration of H_2SO_4 in the *Piranha* solution. Therefore, according to the above findings, the acid in the *Piranha* solution can enlarge the oxidation ability of H_2O_2.

However, XPS results show that the amount of surface hydroxyl groups remained relatively the same with varying *Piranha* solutions (**Figure 4.7**). Therefore, it was concluded that the increased hydrophilicity was due to the decontamination – not further hydroxylation of the titanium surface. This was further confirmed by water contact measurements that showed increased hydrophilicity with the same trend observed for the evolution of carbon contamination (**Figure 4.6 and 4.7 C**).

5.3 Effect of molecular concentration on growth of the APS film

The adsorption of APTES molecules on the *Piranha* treated titanium surfaces was carried out in the solvent with 1 v% APTES following the preparation conditions of the silane-based SAMs on silicon [Zhu 2004]. The strongest cross-linking of Si-O-Si stretching and free amine (N-H) deformation peaks were formed in the FTIR spectrum (**Figure 4.8A**), which is in the agreement with the report by other people [Chiang 1980; Hooper 2001]. A peak at 940 cm^{-1} in the spectrum was assigned for the Si-O-Ti vibration, which is agreed with the previous report [Matininna 2004]. White and Tripp suggested that the peak should be assigned for the Si-OH vibration, which is assumed that the hydrolyzed molecules are not crosslinked completely [White 2000]. When the APS film on titanium was heated up to 160°C, the intensity of this peak was not changed with the increase of the Si-OH groups (**Figure 4.28A**), which confirms the Si-O-Ti bond at 940 cm^{-1}. However, assessment of the APS film order by FTIR (**Figure 4.8B**) shows that the film is not well-organized and packed due to the position of the C-H vibrations. In order to clarify the above issue, the molecular concentration is further discussed below.

It is well known that the most important driving force of the formation of SAM is the chemisorption of the head group to the substrate surface, which are highly affected by the molecular concentration and water content in the solvent [Schreiber 2000; Ulman 1991]. A lot of research has been carried out the effect of molecular concentration on the formation of SAMs. For instant, Rozlosnik *et al.* have shown that the optimum OTS concentration is 25 μmM to 2.5 mM (equal to ~ 0.013 v%), as a high solution

concentration causes a polymerized but weakly bound film, while a low solution concentration would result in a covalently bound monolayer [Rozlosnik 2003]. Other people reported that the molecular concentration was around 10 mM (equal to 0.05 v%) [Foisner 2003; Wang 2003; Yasseri 2006] for the OTS-based SAMs. However, Hooper considered that 0.2 v% was best concentration for the SAMs with APTES on silicon [Hooper 2001]. The concentration of 0.5 v% was used for the APTES to form the APS film on the titanium surface [Matinlinna 2004; Zhu 2004]. To confirm this, different concentration of APTES in the solvent from 0.02 to 3 v% were used for the investigation of the formation of a self-assembled film on titanium. The water contact angle of APTES-treated surfaces are range from 67 – 90° (**Figure 4.9**), compared with 16° for the oxidized titanium. It was discussed that the increased hydrophobicity gives information about the surface coverage with the alkyl chain of the APS molecules, since head and end groups in the APS molecule are both hydrophilic. Therefore, an increase in the surface hydrophobicity can support the assumptions of the disordered structure of the APS film on the surface.

Before the discussion of the effect of molecular concentration, it is necessary to identify the chemical reactions during the silanization. According to Chapter 2.3.2.2, there are generally three steps: (1) the alkanesilane molecule is hydrolyzed by the water which is from in the solvent and/or on the surface; (2) the hydroxyl groups from the molecules react with the hydroxyl group from the surface to form the covalent bond; (3) the hydrolyzed molecules on the surface condense to crosslink. The hydrolysis and condensation process of silane molecules are highly influenced by the pH value in the solvent [Plueddemann 1982], which means that acidic or alkali solvent will accelerate the hydrolysis or condensation.

For the alkylalkoxysilanes, although the Isoelectric point of APTES is 9 [Matinlinna 2004], the aggregation of ethanol after the hydrolysis will result in the pH of the solvent to be neutral at lower concentration, further leading to slow down of the reaction. Since the reaction is too slow, the free amine group is possible protonated by water from the condensation. According to the assessment of the ordering of the APS film by FTIR (**Figure 4.11**), the APS molecules were probably not vertically aligned on the surfaces, which were prepared at the concentrations lower than 0.1 v%, due to the

presence of $–NH_3^+$ rather than $–NH_2$ vibration peaks. It is assumed that the protonated amine groups will form the loop structure with the OH groups from the surface (**Figure 4.10**). Moreover, the water contact angles are over 90° and there exists a relatively large scatter for titanium samples (**Figure 4.9**). It was explained that the looping of the $–NH_2$ end group with –OH groups on the Ti surface leads to some of the hydrophobic $–CH_2$- groups from the APTES chain were exposed over the titanium surface. A similar phenomenon has been reported by Akkerman *et al*. for relatively low-concentration dithiol solutions, which results in looping of the –SH end group with surface atoms [Akkerman 2008]. Although the current APTES chain is not very long, compared with the dithiol chain, the bulky steric structure of the tri-ethoxyl head groups in APTES may over-shadow unbonded –OH groups on the Ti surface, and subsequent to its hydrolysis, for the amine end-group to bend and loop with such –OH groups to expose the $–CH_2$- chain over the surface, particularly with APTES molecules are far apart at low concentrations. **Figure 4.11A-B** provides the evidence of the disordered film formed on the surface at lower concentrations. On the other hand, OTS molecule has hydrophobic end group ($-CH_3$) with longer chain, which is prone to assemble together, rather than bend towards the surface. Moreover, HCl is one of products after the hydrolysis in OTS-based SAMs, which could accelerate the reaction rate. Therefore, well-ordered films are obtained from OTS at very lower molecular concentration.

When the APTES concentration increases from 0.2 to 3 v%, the contact angle increases again, from 67° to 78°. A similar contact angle of 63° was reported for the $–NH_2$ functionalized thiol-based SAMs [Faucheux 2004; Matinlinna 2004]. Majewski *et al.* showed that the water contact angle of the SAMs with $–NH_2$ group on Ti was 45° [Majewski 2006]. Due to the plenty of APTES molecules in the solvent at higher concentrations, the hydrolysis and condensation reactions are still fast, although C_2H_5OH presents in the ambient. However, due to the fast adsorption kinetics, the growth of the APTES on the Ti surface is out of control, so a network structure of $HO\cdots NH_2$- in the APS film was formed. Disordered structures of the APS film prepared at higher concentrations were detected by FTIR according to the C-H vibration (**Figure 4.11B**).

Such behaviour has been explained by the fact that very lower concentrations is too slow to form the covalent bonding of Si-O-Ti and crosslinker of the Si-O-Si; at very high concentrations the adsorption of the APTES molecules on titanium is too fast to allow the formation of well-ordered and densely packed films. In this case, the surface is probably blocked by irregular chemisorption of the adsorbate molecules during the initial phase of the growth process. To avoid too fast or slow adsorption of the molecules in an irregular manner, the concentration of 0.2 v% was chosen for the APTES to form the well-ordered film on the titanium surface.

5.4 Stability of the APS film in the aqueous solutions

Although several synthetic approaches for the self-assembled technology have been reported, there has been little effort to study the hydrolytic stability of the SAMs. Hydrolytic stability is the key parameter that determines the applications of final materials and it is critical in choosing a synthetic strategy for surface functionalization. Therefore, the APS films on the Ti surfaces were immersed in different aqueous solutions with pH values of 4, 6.5 and 10 up to 72 hours to further investigate the hydrolytic stability.

In terms of the structure of the APS film, the hydrolytic stability of the film is mainly depend on the covalent bonds of Si-O-Ti and Si-O-Si. In the acidic aqueous solution, the APS film was hydrolyzed rapidly in the acidic aqueous solution, due to that the vibration of the Si-O-Ti was not detected by the FTIR up to 72 hours (**Figure 4.13A**) and the water contact angles reduced from 68° to 26° (**Figure 4.12**). The results obtained agree well with literature [Marcinko 2003] that acidic solutions hydrolyzed the monolayers faster. Due to the hydrolysis of the Si-O-Ti bond, the part of the APS film was dropped off from the surface, so the value of contact angle of the surface is close to that of the oxidized Ti surface. In the neutral and alkali aqueous solutions, the APS film is hydrolyzed continuously, but slower than that in the acidic solution, which is confirmed by the presence of the Si-O-Ti bond on the surface (**Figure 4.15A and 4.17A**). However, Marcinko *et al*. found the monolayers of $C_{18}H_{37}Si(CH_3)_2Cl$ were hydrolyzed almost completely within 3 – 24 hours in the solution at neutral pH [Marcinko 2003]. It is probably because that the APS film as tri-functional silane

primarily supply stronger bonding, including siloxane (Si-O-Si), hydrogen bonds (Si-OH…HO-Si) and van der Walls interactions between chains. Therefore, the film from trifunctional silanes is more stable than that from monofunctional silanes.

As the position of CH_2 peak is an indicator of the conformation of hydrocarbon chains [Kessel 1991], the evolution of the film ordering in different aqueous solutions was investigated by the FTIR spectra. The shift of the peak towards a higher frequency after 2-hour immersion in the acidic solution (**Figure 4.13B**) confirmed that the film started disordering. However, in the alkali solution, the disorder structure of the film was formed after 48-hour immersion (**Figure 4.17B**). It was explained that the -NH_2 functional group with IEP of ~ 9 was easily protonated in the acidic solution, further resulting in the formation of hydrogen bond with the hydroxyl group from phosphate group or silanols. In the neutral solution, the Si-O-Si bond is hydrolyzed to form the –Si-OH, so protonated amine group forms the hydrogen bond with the silanols, leading to the disordered structure (**Figure 4.15B**). **Figure 4.14** also provides clear evidence by the change of the water contact angles.

To avoid the hydrolysis of the APS film, titanium samples were stored in a desiccator under vacuum up to 72 hours. It is noticed that the film after 2 hours was disordered due to the shift of the C-H vibration to higher wavenumber (**Figure 4.19B**). It was explained that the van de Waals force between the chains is very weak due to the short chain with 3-carbon length, which further results in the bend of the chains. The hydrophobicity of the surface (**Figure 4.18**) also confirms that the CH_2 groups are exposed over the titanium surface due to the bending of the –NH_2 end group with –OH groups. Therefore, the results showed that the APS film was not stable under dry condition, too. On the other hand, although the position of the C-H vibration confirms the ordering of the film, the real structure of the ordering film is not as the same as the ‘idea’ structure – molecules aligns one by one, and it might be like dendritic structure.

5.5 Effects of temperature and water content on growth of the APS film

The adsorption of APTES molecules on the titanium surface is a complex process. To date, there is little effort on the mechanisms of formation of self-assembled film. There are two assumptions for the growth of the SAMs: one is that individual molecules are adsorbed on the surface on vertical direction and then crosslink together on horizontal direction; another one is that once one molecule is adsorbed on the surface, other molecules will spread out in the central of the adsorbed molecule on the surface by the crosslink [Schreiber 2000]. To confirm this, the adsorption of APTES molecules was carried out on Ti surface with different times.

Figure 4.21 shows once adsorbed on the Ti surface, the APTES molecules further react with water and other APTES molecules in the vicinity to form small aggregates. These aggregates can then be imaged readily by AFM to monitor a potential site-specific adsorption. It is in the agreement with the report from Balgar *et al.* [Balgar 2003]. They found that two types of islands have been identified on the oxidized Si with OTS molecules: small circular islands with a diameter around 0.1 μm and larger islands with branched shape indicative for a diffusion limited aggregation-type growth mechanism. Britt and Hlady also reported that condensed 'island-like' and expanded 'liquid-like'domains of OTS were formed on mica [Britt 1996]. The AFM analysis showed that the surface with the lower density was completely covered with island-type clusters after 2 hours, which is consistent with that the water contact angle of the APS film is stable around 63° (**Figure 4.20**). Although the surface was covered with high dense film up to 16 hours, the film with multilayers was observed on the surface. Poirier and Pylant also found that the monolayer formation follows a two-step process that begins with condensation of low-density crystalline islands, which will transit to a denser phase by realignment of the molecular axes with the surface normal [Poirier 1996].

The line-measurement by AFM in **Figure 4.22** suggests that the cross-polymerization of the APS molecules occurs in a vertical direction, rather than horizontal direction. It

was explained that there was a probability for a surface hydroxyl group to be close to the first adsorption site of an APS molecule. In this case, vertical polymerization could occur, resulting in the formation of polysilane aggregates. Such behaviour was possible caused by the adsorption of APTES on the surface at higher temperature. Yamada *et al.* reported that the higher the temperature of the solution, the larger the size of the well-ordered domain. Moreover, the number of the vacancy islands of the gold surface decreased [Yamada 2000]. Once a monolayer was formed, further polymerization continued on the APS molecules at the edges of the monolayer leading to the formation of large aggregates as observed by AFM (**Figure 4.21**).

As for the temperature, the existence of a critical temperature (*Tc*) has been confirmed to be an intrinsic property of alkylsilane on surface and it is independent of the solvent used for the reaction [Brzoska 1992]. According to Parikh *et al.* [Parikh 1994], films prepared above *Tc* exhibit a low surface coverage and a high conformational disorder, while below *Tc*, well-ordered films are formed. They have reported a critical temperature of 28±5°C for the growth of the OTS-based SAMs on the silicon surface. According to the FTIR spectra of the APS film at varying temperatures (**Figure 4.24**), the C-H vibration related to an organized film from 30 to 70°C was observed at frequencies representative of a well-ordered film, although the peaks shifts to higher wavenumber at higher temperature. This result confirms that temperature does not affect the ordering o the APS film on the surface.

For low temperatures, a majority of the water presents in the system was adsorbed on the surface, which limited the silanes to react primarily at the substrate surface. As temperature was increased, it seems to lead to the formation of multilayers on the surface. This has been proved in **Figure 4.24A** for the IR spectra of the peak intensity of –Si-O-Si bond with temperature. During the silanization, water molecules from the surface are released into the solvent phase at the higher temperature, which results in that the hydrolysis and condensation happen in the solvent instead of the surface and then growth of the film is likely affected. On the other hand, the higher temperature leads to speed up the collision between molecules, and further accelerate the reaction rate. Moreover, as layers of APTES are built up, underlying APTES molecules which have not fully been hydrolyzed become isolated and the hydrolyzation reaction

becomes diffusion limited. For APTES films to hydrolyze, ethoxy groups must have access to water molecules. Thick films with an initial cross-linking between APTES molecules may prevent complete hydrolyzation by creating an impenetrable fully hydrolyzed surface film which protects the underlying APTES molecules from interaction with water. Thus, slowly developing film will occur at low temperature. In this set of experiments, since the FTIR is not enough sensitive to detect the chemical bond in the APS film prepared under 30°C, the optimum temperature is 30°C under our experimental conditions, which is in agreement of the results from Wang [Wang 2003].

The variation of water contact angles about the film with the -NH_2 functional groups are reported in literature. The water contact angle obtained here is 60°. Majewski *et al.* reported that the water contact angle of film with the -NH_2 group is 45° [Majewski 2006] and 42° was reported by Toworfe *et al.* [Toworfe 2006]. However, Faucheux *et al.* reported that 60° and 40° were for advancing and receding water contact angles, respectively [Faucheux 2004]. The different results imply that the film with the -NH_2 groups is very unstable in the aqueous solution as the –NH_2 can react with water molecules by the hydrogen bonding.

It is well known that the process of the chemisorption for the growth of the APTES is highly affected by the water content on the substrate and/or in the solution. This is because silane adsorption does not occur in the absence of water. However, the presence of water also results in deposition of polymerized products and the lack of reproducibility arises from a competition between formation of chemisorbed and polymerized products [White 2000]. Therefore, the further investigate about the effect of water content during silanization was done for the APS film on the surface.

The growth of the APS film in hydrous solution results in the formation of the disordered structure with the indicator of the C-H and N-H vibrations on the IR spectra (**Figure 4.26**). Moreover, hydrophobic surface formed in hydrous solution also confirms that some of –CH_2 groups are exposed over the surface (**Figure 4.25**). It is explained that the presence of water in the solution causes the polymerisation of APTES in the solution before molecules attach on the surface, leading to the deposition of aggregates.

Although water on the surface or in the solution was more favourable than a totally anhydrous system, water may favour the cross-polymerization of APS molecules in the solution and formation of aggregates that may deposit on the surface and block the surface adsorption sites.

It has been shown that a thin water layer on the surface could act as a water reservoir for the hydrolysis of molecules and serve as a lubricating layer for the adsorbed molecules to move laterally on the surface and gather into a densely packed monolayer. Moreover, by using a hydrophobic solvent, the water molecules on the substrate tend to stay on the surface and hydrolyze the arriving molecules only on the substrate surface. In current experiment conditions, a dry hydrophobic toluene was used to avoid cross-polymerization of the APTES molecules in the solution and to keep any water at the solution/substrate interface within a thin layer, so that inevitable traces of water can also induce the adsorption of the APTES molecules to the Ti surface. It is still not clear if the reaction directly occurs through the hydrolysis of the silane molecules by the surface hydroxyl groups, or the molecules needs to be pre-hydrolysed before reacting with the surface hydroxyl groups.

5.6 Nucleation of HA by the $–NH_2$ functional group

One of objectives of this project is to improve the biocompatibility of titanium as implant by the self-assembled film. The titanium samples with the APS film used here were prepared with 0.2 v% APTES in 5 ml anhydrous toluene at 30°C for 16 hours, and immersed in the simulated body fluid to investigate its inducibility of calcium phosphate. However, samples placed upside up and hanged in the solution leads to the difference inducibility of the $–NH_2$ group. The results involve two different mechanism nucleations of HA: homogeneous & heterogeneous nucleations. Homogeneous nucleation occurs spontaneously in solution and depends on the degree of supersaturation, and heterogeneous nucleation occurs on the surface with foreign bodies [Tanahashi 1997; Zhu 2004], which results from the difference nucleation barrier.

The investigations on the nucleation and growth of HA on the surface with varying surface chemistry showed that the inducibility of HA highly depend on the surface properties of the underlying substrate. According to the classical nucleation theory, nucleation is defined as a process during which the nuclei with a size larger than the critical size is created by overcoming the nucleation barrier [Jiang 2004]. Once this barrier is overcome, the growth from the nuclei into large crystals starts [Liu 2000a]. In fact, the nucleation and growth of HA depends on two main factors:

1. A positive thermodynamic driving force ($\Delta\mu$) is required, which drives the nucleation and growth and is given by **Equation 5.1** [Jiang 2004]:

$$\Delta\mu = kT\ln(1+\sigma) = kT\ln\frac{[a(Ca^{2+})]^5[a(PO_4^{3-})]^3[a(OH^-)]}{K_{sp}(HA)} \qquad \textbf{(Equation 5. 1)}$$

Where k is the Boltzmann constant, T is the absolute temperature, α is the actual activity of a given ion, K_{sp} is the solubility product and σ is the supersaturation of the solution - the source of the driving force for the mineralization in the solution.

2. The nucleation barrier (ΔG^*) at a given thermodynamic driving force ($\Delta\mu$) that needs to be overcome in order to start the nucleation. In the presence of foreign particles (e.g. a substrate), the heterogeneous nucleation barrier (ΔG^*_{heter}) is given by **Equation 5.2** [Jiang 2004; Liu 2000a, 2000b]:

$$\Delta G^*_{heter} = \Delta G^*_{hom\,o}\, f \qquad \textbf{with } 0 \le f \le 1 \textbf{ and } \Delta G^*_{hom\,o} = \frac{16\pi\gamma_{cf}^3\Omega^2}{3\Delta\mu} \qquad \textbf{(Equation 5. 2)}$$

Where $\Delta G^*_{hom\,o}$ is the homogeneous nucleation barrier, f is the interfacial correlation function related to the reduction of $\Delta G^*_{hom\,o}$ to ΔG^*_{heter} due to the occurrence of foreign bodies (e.g. a substrate), γ_{cf} is the specific interfacial free energy between the crystal and the solution, and Ω is the volume of the growth unit. $f \rightarrow 0$ means that the interaction between the nucleating phase and the substrate is optimal and the

heterogeneous nucleation is favored. However, $f \rightarrow 1$ means that the substrate does not have any influence on the nucleation barrier and homogeneous nucleation occurs.

Therefore, according to **Equation 5.1-5.2**, at low supersaturation, nucleation will be controlled by the process with a small interfacial correlation function f, which results from a strong interaction and good structural match between the foreign bodies and the crystallizing phase [Liu 2000a]. Strong evidence for heterogeneous nucleation has been found on TiO_x surfaces (**Figure 4.34A&C and Figure 4.36A-B**). The behaviour of oxidized titanium surface in SBF has been explained in detail by Rohanizadeh *et al.* [Rohanizadeh 2004]. According to their results, the Ti-OH groups on the surface as active site shows negatively charged at pH 7.45 due to the isoelectric point (IEP) of titanium oxide is 5-6 [Brunette 2001]. Ca^{2+} cations could be attracted to the negative charge of the OH^- groups and the phosphate groups ($H_2PO_4^-$, HPO_4^{2-} or PO_4^{3-}) could be attracted to the Ti^+ cations, then forming HA coating. At higher supersaturation, nucleation on foreign particles having a weak interaction and poor structural match with the crystallizing phase, which results in a big interfacial correlation function and the formation of homogeneous nucleation [Liu 2000a] (**Figure 4.30A**). On the other hand, since the SBF with higher pH value has greater driving force ($\Delta\mu$), lower $\Delta G^*_{\mathrm{hom}\,o}$ will be obtained, which results in that the homogeneous nucleation easily occurs in SBF with higher pH value (**Figure 4.36C**).

When Ti sample with the APS film was upside up placed in a high supersaturation, it is possible that calcium phosphate critical nuclei in solution is formed, started to grow and then adsorbed onto the substrates, which result in the HA formation on the surface with the $-NH_2$ group (**Figure 4.30**), which is in agreement with the finding from Majewski *et al.* [Majewski 2006]. Zhu *et al.* also suggested that the hydrogen bond was formed between particles of calcium phosphate and the amine groups in unstable solution [Zhu 2003], and then precipitation grew progressively into a thin film. When titanium samples were hanged in the solution with higher ionic concentration or with higher pH value, the conclusion is that the $-NH_2$ functional group cannot induce calcium phosphate in SBF. In general, some of the possible reactions for the nucleation in SBF considering the compositions in SBF are as follows:

$$Ca^{2+} + HPO_4^{2-} + 2H_2O = CaHPO_4 \bullet 2H_2O \quad \textbf{(Equation 5. 3)}$$

$$3Ca^{2+} + 2PO_4^{3-} = Ca_3(PO_4)_2 \quad \textbf{(Equation 5. 4)}$$

$$5Ca^{2+} + 3PO_4^{3-} + OH^- = Ca_5(PO_4)_3OH \quad \textbf{(Equation 5. 5)}$$

Due to that pK_a value of the –NH_2 in APTES molecule is 8.0 – 9.7 from Table of selected pK_a values, the –NH_2 functional group should be positively charged. According to **Equation 5.3-5.5**, protonated –NH_3^+ should attract negatively charged phosphated groups, then absorb cation Ca^{2+} to form calcium phosphate. However, EDX files in **Figure 4.43 C&D** do not show phosphate element on the surface. Tanahashi *et al.* explained that positively charged –NH_3^+ group could form very weak interaction with negatively charged phosphate groups, which results in the failure of heterogeneous nucleation by the -NH_2 functional group [Tanahashi 1997]. The interaction modes between participating ionic species and surface functional groups are represented in **Figure 5.1**. On other words, even if Ca^{2+} is attracted by the phosphate group on the surface, the nuclei could be dropped into the solution due to the weak interaction.

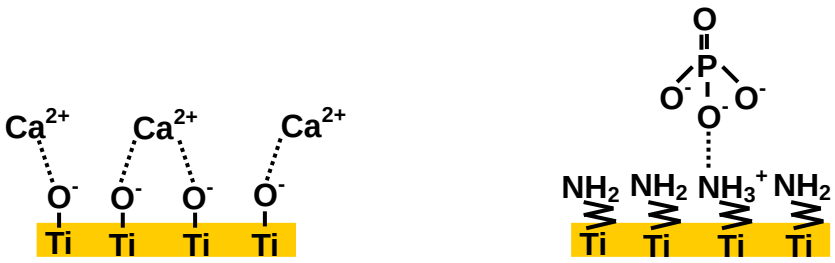

Figure 5. 1 Interaction modes between calcium and phosphate ions and surface functional groups as an initial step for calcium phosphate formation.

Although the trace of the silicon element in the EDX files indicate the presence of the APS film on the surface (**Table 4.6-4.7**), the IR spectra (**Figure 4.38A**) shows that the APS film is continuously hydrolyzing with immersion time due to the decrease of intensity of the Si-O-Si bond. Therefore, the APS molecules with the –NH_2 group are dropping off from the surface, which also results in no CaP precipitation observed on the surface.

According to the study from Tanahashi and Matsuda, since the $CONH_2$ group is non-ionic in the aqueous solution, it will form ionic-dipolar interaction with calcium ion complexation [Tanahashi 1997]. However, this interaction is much weaker than electrostatic interaction between Ca ion and the negatively charged groups, which may be responsible for a low calcium phosphate formation. Therefore, it is possible for the $–NH_2$ group in solution to be non-ionic (neutral). This point is shown in **Figure 4.38A**, where the IR vibration of the $–NH_2$ group at 1603 cm^{-1} present, instead of the vibration of the $–NH_3^+$ after 72-hour immersion. The neutral amine group cannot attack any phosphate ions in the solution, which results in that heterogeneous nucleation cannot happen. Moreover, the disordered structure of the APS film occurs in the solution after longer immersion (**Figure 4.38B**), which results in the exposure of the hydrophobic group ($-CH_2-$) on the surface. As well-known, the hydrophobic group (e.g. CH_3-, $-CH=CH_2$) cannot induce calcium phosphate in SBF. However, this is different from the result by Toworfe *et al.* [Toworfe 2006], in which calcium phosphate precipitate induced by the $–NH_2$ functional groups was reported after immersion for 7 days. This phenomena can be explained that the homogenous nucleation occurs in the solution, resulting in the formation of CaP precipitation on the $–NH_2$ functionalized surface.

5.7 Comparison of the activity of the immobilized Lac

Traditional enzyme immobilization by covalent bond is to use the –COOH groups from the surface to react with the $–NH_2$ group from enzyme surface. For example, Mendes *et al.* reported that horseradish peroxidase (HRP) was immobilized on gold by SAMs with the -COOH groups [Mendes 2008]. However, in silane-based SAMs, molecules with the –COOH groups normally have longer chain length, which will influence the electrochemical behaviour of enzyme on electrode. Therefore, the APTES molecules as a linker immobilize the laccase through the amide bond by the carboxyl group from the laccase surface. Therefore, peaks of amide bond on the IR spectrum are directly determined whether enzyme has been immobilized on the surface by APTS film. **Figure 4.40A** and **4.52A** both confirm the formation of amide bond on the surface: peaks at 1515-1518 cm^{-1} and 1655-1658 cm^{-1} assigned for the –C=O- and –NH- bonds, respectively. These are different from the result by Arya *et al.* [Arya

2007], in which the –C=O- and –NH- bonds are reported at 1537 and 1637 cm^{-1}, respectively. The difference is possible due to that the difference of surface leads to the peak shift. On the other hand, IR spectra in **Figure 4.13A**, **4.15A** and **4.17A** show the peaks at ~1557 and ~1646 cm^{-1}, which confirms the electrostatic adhesion between $–NH_3^+$ and –COOH, or $–NH_3^+$ and $–H_2PO_4^-$, as the carboxyl or phosphate groups cannot form the amide bond in the solution without activators. The decrease of the water contact angles in **Figure 4.39** and **4.51** also confirm the immobilization of laccase on the surface.

The pH value is a factor in the stability of enzymes. Extremely high or low pH values generally result in the loss of activity for most enzymes. It is necessary to study the most favourable pH value – the point where the enzyme is most active, also called optimum pH. The optimal pH for the laccase immobilized by EDC/NHS shifts slightly toward a more acidic region compared to the native laccase (pH 4.5). Such shifts have previously been detected for various immobilized enzymes [Shleev 2005b; Yu 2002] [Quan 2004; Zawisza 2006]. The shift is caused by the certain enzymatic reactions or charge of carrier. One explanation of this behaviour is based on the electrostatic field produced by a highly charged carrier, in which the pH shift is caused by an unequal distribution of hydrogen and hydroxyl ions between the polyelectrolyte phase on which the enzyme is immobilized and the external solution [Zaborsky 1974]. On the other word, enzymes are immobilized in a charged film as a result of a change in the microenvironment of the enzyme [Trevan 1980]. In essence, the hydrogen ion concentration in the immediate vicinity of a positively charged APS film is lower than its concentration in the external solution. Thus, the optimum pH for the laccases bound to a positively charged APS film is displaced toward lower pH values. In addition, Xu reported that mechanism involving the OH^- inhibition of laccase was dominant for the nonphenolic substrates (e.g., ABTS and $K_4Fe(CN_6)$), resulting in the decrease of the reaction rate with the increase of pH in the solution [Xiu 1997].

The thermal stability was also investigated for the activity of the immobilized laccase, since most existing enzymatic industrial processes are carried out at elevated temperatures. Temperature effect on enzyme activity is very complex and able to affect a lot of different factors, such as the speeds of molecules, the activation energy of the

catalytic reaction and the combination binding of the enzyme and substrate. When the temperature increases to 40°C, the activity of the laccase on Ti (**Figure 4.45**) or graphite (**Figure 4.60**) is both increasing greatly. Like most chemical reactions, this is due to increasing the energy of molecules, resulting in more collisions per unit time. However, after 40°C, the activity of the laccase on Ti reduces dramatically, while the activity on graphite still slightly increases until 50°C, then decrease afterwards. This different is due to the result of the surfaces after treatment in the H_2SO_4/H_2O_2 solution. Normally, an increase in temperature to certain point (normally 37~40°C) leads to the protein unfolding and less ordered - inactivation. On the titanium surface, due to the dense surface, such unfolding behaviour directly results in disassembling of the three-dimensional structure. On the graphite surface, due to the porous surface (**Figure 4.50B**), the unfolding structure can be re-assembled to new structures, which is different from the native laccase conformation. Finally, these incorrect structures at higher temperature remain in the laccase, resulting in inactivation. It has been previously reported that this influence is significantly different for the laccase of different origins. Jiang *et al*. reported that the thermal stability of immobilized laccase from *Rhus vernicifera* on chitosan is the same as that of native one [Jiang 2005]. Arya and his coworkers developed cholesterol oxidase immobilized by APTES and demonstrated that the optimum temperature is 50°C by UV-VIS spectroscopy [Arya 2007]. Quan *et al.* used APTES to immobilize laccase from *Coriolus hirsitus* on platinum and found that the temperature profile of the immobilized laccase was very similar to that of free enzyme, in which the activity of the laccase starts to decrease above 60~65°C [Quan 2004]. Liu *et al.* reported that the laccase immobilized on hydrophobic graphite by carbon nanotubes, shows maximum activity at 70°C [Liu 2007]. They explained that the microenvironment of carbon nanotube gel can protect the secondary structure of protein not to be destroyed by thermal treatment process.

In order to investigate the kinetics of immobilized laccase on the solid surface, the Michaelis-Menten constants of laccase were further determined on titanium and graphite, respectively. The Michaelis-Menten constant, K_m, is one of the most important and useful parameters in enzyme kinetics, which determines the affinity between enzyme and substrate. The K_m values of the laccase immobilized either on titanium (**Figure 4.46**) or on graphite (**Figure 4.62**), are both far greater than that of

native laccase. This is in agreement with the reports in literature [Arya 2007; Fernandez-Sanchez 2002; Jiang 2005]. So far, the discussion of the Michaelis-Menten constant for immobilized enzyme has corresponded to diffusion limitations. Higher concentrations of substrates and products near the laccase could change the microenvironment and lead to activity inhibition of enzymes. On the other hand, covalent bond as one of chemical immobilization methods can change the conformation and properties of the laccase, which causes that the immobilized enzymes could not bond substrate like the native ones.

The K_m of the laccase on titanium (0.271 mM) is almost 2 times greater than that on graphite (0.146 mM). Moreover, the V_{max} value of the laccase on titanium (9.8 μm/min) is approximately 5.8 times smaller than that on graphite (57 μm/min). This is due to the formation of etching pores on graphite after oxidation of H_2O_2. The pores of ~30 μm on the surface increase the surface area of graphite, which results in more laccase immobilized on the surface. On the other hand, the laccase can be entrapped in the pores, which greatly improve the combination between the active site and substrate. Consequently, the laccase immobilized on the graphite surface shows greater affinity with the substrate (lower K_m value) and maximum reaction rate.

The storage stability of the immobilized laccase is largely determined by its conformational stability. No matter in dry condition or aqueous solution, the relative activity of the immobilized laccase lost 18 ~ 64% at the first day (**Table 4.8**). This might be due to that dilute enzyme concentration easily results in the inactivation [Elsenthal 1993; Trevan 1980] and the details has not been cleared yet. Compared with dry condition, the laccases from *Trametes versicolor* on the surface prefer aqueous solution (**Figure 4.48**), which possibly results from the stability of the APS film in aqueous solution. The disordered structure of the APS film under dry condition will cause structure unfolding of the active site in the laccase, leading to the denaturation. Although the APS film in the solution, pH 7 is more stable than in other solutions, the Si-O-Si bond is still slowly hydrolyzed, causing that the APS molecules are dropping off from the surface. In the same way, the laccase can be falling off with the APS film, resulting in the activity loss. It is interesting that in the aqueous solution of pH 7, the activity of immobilized laccase on graphite (**Figure 4.63** and **Table 4.9**) last longer than

that on titanium (**Figure 4.48** and **Table 4.8**). This is probably due to the chemistry property of the surface pre-treated in oxidized solution, resulting in breaking or making of new bond with enzyme. In the buffer solution of pH 7, titanium surface after oxidation shows almost neutral as the IEP of titanium oxide is 6-7 [Brunette 2001], while the graphite surface after oxidation of H_2O_2 shows negatively charged as its IEP is 5-6. The negatively charged graphite surface will attract positively charged laccase by electrostatic force, which could enhance the stability of laccase immobilized on solid support. On the other hand, the covalent bond Si-O-C is more stable than Si-O-Ti in the aqueous solution as the Si-O-Ti bond involves ionic bond.

The laccase cannot only oxidize ABTS to $ABTS^{+\cdot}$, but also reduce O_2 to form H_2O by receiving 4 electrons. Thus, laccase immobilized on electrode has been studied by cyclic voltammetry (CV) to investigate the catalytic activity of redox active enzyme with electrode material [Liu 2007; Nogala 2006; Zawisza 2006]. Firstly, it is important to study the electrical conductivity of electrodes without immobilization of enzymes. Compared with the titanium electrode oxidized in the piranha solution, TiO_2 electrode shows electroconductivity, which is due to the formation of crystal structure like semiconductor. However, there is no redox current peaks observed on the CV curve of TiO_2 in the solution with potassium ferricyanide ($K_3Fe(CN)_6$) (**Figure 4.49**). It is assumed that the amorphous structure is still present in the TiO_2 electrode. Some research works have been done to modify titanium electrochemical surface. For example, Sirivisoot and Webster demonstrated multiwalled carbon nanotubes (MWCNTs) grown on anodized titanium and a well-defined redox peak appears in the solution with $K_3Fe(CN)_6$ [Sirivisoot 2008]. They believed that the electrolyte-electrode interface barriers are reduced by MWCNTs because they facilitate double-layer effects. Since the charge in the electrolyte solution causes the layer to be more compact, this compact layer can rapidly exchange electrons with the surface of the MWCNTs modified titanium electrode. Liu *et al.* immobilized horseradish peroxidase on TiO_2 nanotube arrays and the reduction potential range is between -0.7 and 0.0 V [Liu 2005]. However, only reduction peaks of the immobilized enzymes are observed and no oxidative peaks can be seen in the reverse potential scan because of the low electrical conductivity of the TiO_2 nanotubes.

In order to investigate the electrochemical behaviour of the immobilized laccase on the APS film, graphite was chosen as electrode because of the good electrical conductivity (**Figure 3.19**), which shows well-defined redox peaks with anodic and cathodic potentials at 250 and 125 mV, respectively, when graphite was immersed in the solution with potassium ferricyanide. The study of direct electron transfer (DET) between enzyme and electrode can supply important information on the kinetics of the redox process. However, **Figure 4.54** does not show any catalysis curve on the CV in the oxygen-saturated condition. Since the results in **Figure 4.62-63** confirm that the immobilized laccase still can oxidize substrate to product, a main reason for the failure of DET according to **Figure 2.33**, is that the T1 Cu(II) cannot receive electron from the electrode to be reduced to Cu(I). Due to the formation of the chemical bond between the surface of the enzyme and the electrode, the structure of the active site of the laccase might be changed, resulting in block of the tunnel for electron transferring (**Figure 4.55A**). The APS film might be too thick to enlarge the tunnel distance between the electrode and T1 copper (**Figure 4.55B**), causing the failure of T1 copper receiving electron. So far, the DET is only happened with the laccase physisorbed on the electrode, as the conformation of enzyme immobilized is almost unchanged [Christenson 2004; Shleev 2005a].

When ABTS as mediator was added in the electrolyte, the catalysis current was observed on the CV (**Figure 4.58**). The maximum catalytic current can obtain 68 $\mu A/cm^2$, which are greater than previous reports [Liu 2007; Zawisza 2006]. This is due to that the entrap method by gel can limit the attachment between enzyme and mediator. Mendes *et al.* compared the electrochemical activity of horseradish peroxidase by SAMs with different groups (e.g. $–NH_2$ and –COOH) in the electrolyte with a mediator [Mendes 2008]. They found monolayers possess the $–NH_2$ terminal groups provided the best results. This might be due to that the $–NH_2$ terminal group from the film can protect the active site of the enzyme. Blanford and coworkers developed redox film on the graphite surface to immobilize laccase and gain a maximum catalysis current with 60 $\mu m/cm^2$ [Blanford 2007]. The redox film can help T1 centre receive electrons from the electrode.

CHAPTER 6

CONCLUSIONS

A systematic investigation of the formation of an 3-aminopropylsilane (APS) film on titanium has been successfully performed with 3-aminopropyltriethoxysilane (APTES) molecules in organic toluene solutions. The effects of pre-treatment of titanium, APTES concentration, silanized temperature and water content in the organic solution on the formation of the APS film are characterised using water contact goniometry, Atomic Force Microscopy (AFM), Fourier Transform Infrared spectroscopy (FTIR), X-ray Photoelectron Spectroscopy (XPS). The thermal and hydrolyzed stabilities of the APS film have been clearly identified using FT-IR.

Formation of an APS film on Ti surface was first considered for the surface modification of biomaterials, to assess its ability of inducing calcium phosphates by the $–NH_2$ functional group. The effects of ions concentrations and pH values in the simulated body fluid (SBF) are characterised using SEM with EDX, X-Ray Diffraction (XRD) and FTIR. Then, the APS film was applied to laccase immobilization by covalent bonding in biofuel cells. The optimum conditions for enzyme immobilization, including molar ratio of EDC/NHS, time and pH value, have been studied in order to maximise the activity of the laccase on electrode surfaces. Apart from calculation of Michaelis-Menten constant (K_m), the influences of pH and temperature in the substrate solution on the activity of the immobilized laccase on titanium and on graphite have been investigated by UV-VIS spectrophotometry and electrochemistry (Autolab), respectively. Since the laccase can reduce O_2 to H_2O, the electrochemical behaviour of direct electron transfer (DET) and mediated electron transfer (MET) by the laccase were also investigated. The findings are very helpful in the development of the $–NH_2$ functionalized self assembled film on the titanium surface with a well ordered and relative thin structure. With consideration of the findings, the following specific conclusions may be drawn from the investigation.

1) Oxidation of titanium in the *Piranha* solution (H_2O_2 + H_2SO_4) has been shown to be an important factor of influencing the surface properties of titanium. Exposure at a higher temperature and/or for a longer period of immersion in a *Piranha* solution result in the formation of rough surfaces. Increasing the concentration of acid in the solution does not cause the change of the relative density of surface hydroxyl groups. A relative flat, clean and fresh oxidized film with maximum –OH groups on titanium, is obtained in the 3:1 (H_2SO_4 : H_2O_2) piranha solution for 15 minutes at room temperature.

2) During silanization, higher or lower concentrations of APTES molecules in toluene can lead to formation of multilayers and/or protonated amine groups (-NH_2•••HO-) on the titanium surface. Too high an APTES concentration leads to a disordered film with –NH_3^+ groups, whereas too low a concentration causes end groups of the adsorbed APTES to loop with the –OH groups on the surface. Therefore, a relative thin and well-ordered film with free amine functional groups on titanium is prepared in ~ 0.2 v% APTES in 5 ml anhydrous toluene for 16 hours at 30°C.

3) For stability of the APS film under different conditions, dry condition leads to a disordered structure, as confirmed by contact angle and FTIR. In the aqueous solution, the APS film is hydrolyzed rapidly in an acidic buffer solution and relatively slowly in a basic buffer solution, according to the intensity of the Si-O-Si bond in the IR spectra. Under acidic conditions, amine groups on the surface are easily protonated to form –NH_3^+ by hydrogen bonding or electrostatic forces. Under basic conditions, although the major functional groups are free –NH_2 groups after 72-hour immersion, the APS film forms a disordered structure on the surface.

4) AFM images reveal that the APS film is formed within 2 hours at 70°C. However, line measurement by AFM can confirm the formation of the APTES aggregate at the early stages. This phenomenon is believed to result from an increase of the collision between molecules at high temperatures. Increasing the temperature of silanization from 30 to 70°C does not seem to affect the ordering of the film, but

is likely to generate a multilayer film. It is therefore desirable to control the temperature at a relatively low level, e.g. 30°C.

5) Comparison of the effects of water from the surface and from the solution for the formation of the APS film shows clearly that water from the solution results in formation of the disordered multilayer film with the $-NH_3^+$ and $-NH_2$ groups, whereas water from the surface leads to formation of a well-ordered structure with the $-NH_2$ group only. This is because the presence of excess water in the solvent causes polymerization of APTES molecules before them being attached on the surface. Therefore, using anhydrous toluene as a solvent can produce well-ordered and thin film with primary amine functional groups.

6) For thermal stability, the IR spectra reveal that the APS film can be stable below 130°C, since the free amine groups will break off from the titanium surface at 130°C through the weakest bond, the C-N bond (308 kJ/mol), in the APS film.

7) SEM micrographs reveal that titanium samples with positively charged group ($-NH_2$) have better homogenous calcium phosphate nucleation, compared with negatively charged (-OH) samples. XRD reveals that the precipitate of calcium phosphate on titanium is of relatively poor crystallinity. However, the $-NH_2$ groups cannot induce heterogeneous calcium phosphate nucleation in the SBF with different ionic concentration or pH value from 7.0 to 7.98, as confirmed by SEM with EDX. This is because of the weak interaction between the $-NH_2$ and phosphate groups, and/or the neutral amine groups in the aqueous solution, and/or the exposure of the hydrophobic $-CH_2-$ groups in APS film on the surface.

8) For the immobilization of the laccase by the covalent bonding method, the IR spectrum which reveals the vibration of the –C(=O)NH- bond at 1515 and 1650 cm^{-1}, and water contact angles both confirm that the laccase has been successfully immobilized on the surface by the APS film. Effects of molar ratio of EDC/NHS, pH value and immersion time during immobilization on the activity of the laccase have been demonstrated. In order to reach the maximum reaction rate, the laccase should be immobilized by the $-NH_2$ groups on the

titanium surface in HEPE buffer, pH 7 with 3:1 of EDC/NHS for 20 hours at 4°C.

9) A comparative study of the laccase immobilized on titanium and graphite both with the APS film, indicates that the optimum pH for activity of the laccase immobilized is 3. Compared with native laccase (pH 4.5), the optimum pH slightly decrease, which is mainly due to K_{cat} getting greater by hydrogen ions binding on active site of the laccases in the acidic condition. However, the optimum temperature is 40°C and 50°C for the laccase on titanium and graphite, respectively, which is due to the graphite surface structure after the pre-treatment.

10) The Michaelis-Menten constant (K_m) is an important parameter to describe the mechanism of the kinetics on the activity of the laccase. UV-VIS spectrophotometry reveals that the K_m values of immobilized laccases are 0.271 mM and 0.146 mM for the laccase on titanium and graphite, respectively; both cases show lower affinity towards substrate ABTS than that of free laccase (0.038 mM). Due to the limitation of the diffusion of the laccases, ABTS can inhibit the activity of the laccase when the substrate concentration is greater than 0.4 mM. Further comparison of K_m of immobilized laccase on different surfaces clearly shows that the K_m value for laccase on Ti is almost twice as high as that on graphite, which mainly results from the surface topography of graphite after pre-treatment.

11) For the stability of immobilized laccase, the laccase on titanium will prefer aqueous solution with pH 7, whereas it will lose most of its activity under dry conditions, which might be related to the stability of the APS film under different conditions. Compared with the laccase on titanium that shows a relative activity of 58% within 7 days, the laccase on graphite in the HEPES buffer, pH 7, has much improved storage stability with a relative activity of 83% within 30 days, because the surface pores on the graphite after treatment can supply more space for configurational change in the active site of the laccase.

12) Titanium samples treated in the *Piranha* solution or calcined at 750°C cannot be applied for electrochemistry as electrode, because it readily forms a surface oxide

layer, which is a poor conductor. The laccase immobilized on graphite does not show any direct electron transfer reaction in 0.1 M citrate buffer under oxygen-saturated conditions by Autolab, which is due to the failure of the electrons transferring to the centre T1 from the electrode surface.

13) For the electrochemical behaviour in mediated electron transfer, the redox process of the ABTS on the graphite electrode with the APS film is controlled by the mass transport, because of the linear dependence of peak current on square root of the scan rate. The laccase on graphite in ABTS solution shows the catalysis current of 60 $\mu A/cm^2$ at 5 mV/s, which indicates that the electron transferring is very slow between the laccase and mediator.

CHAPTER 7

FUTURE WORK

From the present findings, a number of issues warrant further investigation, which range from preparation of the APS film to its applications in biomaterials and biofuel cells. These are outline as follows:

1) To identify the statuses of amine functional group ($-NH_3^+$ or $–NH_2$) on the surface by X-ray Photoelectron Spectroscopy (XPS) during experiments, although Fourier Transform Infrared spectroscopy (FTIR) can show the evidence. For example, for investigation of stability of the APS film on titanium in the aqueous solutions with different pH values, the decreases of total quantities of N1S and Si1S on the surface strongly confirm the hydrolysis of the APS film and quantify the level of the hydrolysis. Moreover, when the APS film on titanium was placed in the simulated body fluid (SBF), the status of amine functional groups can further confirm the reason that the $–NH_2$ groups could not induce calcium phosphate.

2) To clarify the thickness of the APS film on the surface by Ellipsometer. According to the applications, the well-ordered APS film has to be as thin as monolayer, because multilayer film has less stability in aqueous solution. Atomic Force Microscopy (AFM) is only able to measure the surface morphology at atomic level. However, one requirement for ellipsometry measurement is that the first layer should be very flat, which is a challenge for the titanium surface prepared in the piranha solution. Electropholish method can be a choice to gain a flat surface for titanium, but it is still a doubt whether this method can supply water layers on the surface for silanization.

3) To immobilize small peptides (e.g., RGD) or growth factors by the $–NH_2$ functional groups to improve biocompatibility of implant surface, although the $–NH_2$ groups cannot induce calcium phosphate in SBF. It is well-known that the small peptides or growth factors can be recognized by the ligands in bone cells, whose differentiation is able to improve the integration between implant and bone tissue by osteoinductivity.

4) According to the Michaelis-Menten Equation, the different of the K_m value results from the K_{cat} (rate constant at catalytic step), as it is assumed that the concentration of laccase immobilized is same for all of experiments. However, the challenge is to know the concentration of immobilized enzyme on the surface. This might be calculated from the quantity of the $–NH_2$ groups in the APS film.

5) Since ABTS as a mediator at higher concentration can inhibit the activity of the laccase, direct electron transfer of the laccase need to be improved by redox particles or good mediator. The T1 centre cannot receive electrons from the electrode surface because of longer electron tunnel, so redox particles or mediator can be fixed in the APS film to help transfer electrons to the active site.

REFERENCES

A:

Advincula M, Fan XW, Lemons JFC, *et al.* (2005). *Colloids and Surfaces B - Biointerface* **42**: 29-43.

Akkerman HB, Kronemeijer AJ, Van Hal PA, *et al.* (2008). *Small* **4**: 100-104.

Alexandre G and Zhulin IB (2000). *Trends in Biotechnology* **18**: 41-42.

Allara DL, Parikh AN and Rondelez F (1995). *Langmuir* **11**: 2357-2360.

Andrade JD and Hlady V (1986). *Advances in Polymer Science* **79**: 1-63.

Angst DL and Simmons GW (1991). *Langmuir* **7**: 2236-2242.

Anselme K (2000). *Biomaterials* **21**: 667-681.

Antonietti M and Forster S (2003). *Advanced Materials* **15**: 1323-1333.

Aoki H (1991). 'Science and medical applications of hydroxyapatite'. Takayama Press. Tokyo.

Arica MY (2000). *Polymer International* **49**: 775-781.

Ariga K, Hill JP, Lee MV, *et al.* (2008). *Science and Technology of Advanced Materials* **9**: 14109-14205.

Arya SK, Prusty AK, Singh SP, *et al.* (2007). *Analytical Biochemistry* **363**: 210-218.

B:

Babensee JE, Mclntire LV and Mikos AG (2000). *Pharmaceutical Research* **17**: 497-504.

Bailey JE and Ollis DF (1986). "Biochemical Engineering Fundamentals." 2nd edition, McGraw-Hill, New York, p.157.

Bain CD, Troughton EB, Tao YT, *et al.* (1989). *Journal of the American Chemical Society* **111**: 321-335.

Baldrian P (2006). *FEMS Microbiology Reviews* **30**: 215-242.

Balgar T, Bautista R, Hartmann N, *et al.* (2003). *Surface Science* **532**: 963-969.

Banerjee R, Nag S and Fraser HL (2005). *Materials Science and Engineering C* **25**: 282-289.

Bangham AD and Horne RW (1964). *Journal of Molecular Biology* **8**: 660-&.

Barrena E, Ocal C and Salmeron M (1999). *Journal of Chemical Physics* **111**: 9797-9802.

Barton SC, Gallaway J and Atanassov P (2004). *Chemical Reviews* **104**: 4867-4886.

Black J (1992). 'Biological performance of materials: Fundamentals of biocompatibility.' 4th Edition, Taylor & Francis and CRC press, New York.

Blanford CF, Heath RS and Armstrong FA (2007). *Chemical Communications* **17**: 1710-1712.

Bonfield W (1987). *Journal of the Institute of Metals* **3**: 712-716.

Boudet AM (2000). *Plant Physiology and Biochemistry* **38**: 81-96.

Bourbonnais R, Leech D and Paice MG (1998). *Biochimica et Biophysica Acta* **1379**: 381-390.

Boukherroub R, Morin S, Bensebaa F, *et al*. (1999). *Langmuir* **15**: 3831-3835.

Brandriss S and Margel S (1993). *Langmuir* **9**: 1232-1240.

Brian LF and Robert MC (1996). *Analytical Chemistry* **68**: 3187-3193.

Britt DW and Hlady V (1996). *Journal of Colloid and Interface Science* **178**: 775-784.

Brown TD and Ferguson AB (1980). *Acta Orthopaedica Scandinavica* **51**: 429-437.

Brunette DM, Tengvall P, Textor P, *et al*. (2001). 'Titanium in Medicine', 1st Edition, Springer-Verlag, Berlin Heidelberg.

Brzoska JB, Shahidzadeh N and Rondelez F (1992). *Nature* **360**: 719-721.

Bullen RA, Arnot TC, Lakeman JB, *et al*. (2006). *Biosensors and Bioelectronics* **21**: 2015-2045.

Buriak JM (2002). *Chemical Reviews* **102**: 1271-1308.

Buser D, Schenk RK, Steinemann S, *et al.* (1991). *Journal of Biomedical Materials Research* **25**: 889-902.

Byloos M, Al-Maznai H and Morin M (2001). *Journal of Physical Chemistry B* **105**: 5900-5905.

C:

Cahn RW, Haasen P and Kramer EJ (1991). 'Medical and Dental Materials', 67th Edition, John Wiley & Sons, New York.

Call HP and Mucke I (1997). *Journal of Biotechnology* **53**: 163-202.

Callister WD (1994). 'Materials Science and Engineering: an introduction'. 6th Ediiton, John Wiley and Sons, New York.

Camarero S, Garcia O, Vidal T, *et al*. (2004). *Enzyme and Microbial Technology* **35**: 113-120.

Cao WP and Hench LL (1996). *Ceramics International* **22**: 493-507.

Chai CS, Gross KA and Ben-Nissan B (1998). *Biomaterials* **19**: 2291-2296.

Chehroudi B, McDonnell D, and Brunette DM (1997). *Journal of Biomedical Materials Research* **34**: 279-290.

Chen MS, Santra AK and Goodman DW (2004). *Physical Review B* **69**: 155404(1-7).

Chiang CH, Ishida H and Koenig JL (1980). *Journal of Colloid and Interface Science* **74**: 396-404.

Chowdhury PB and Luckham PF (1998). *Colloids and Surfaces A* **143**: 53-57.

Christenson A, Dimcheva N, Ferapontova EE, *et al*. (2004).*Electroanalysis* **16**: 1074-1092.

Christenson HK and Claesson PM (2001). *Advances in Colloid and Interface Science* **91**: 391-436.

Christoffersen J and Landis WJ (1991). *Anatomical Record* **230**: 435-450.

Chu DB, Hou YY, He JG, etal. (2009). *Journal of Nanoparticle Research* 11: 1805-1809.

Clarke A. and Partridge A (2006). 'A Strategic Review of the Surface Engineering Industry in the UK'. National metals technology centre.

Collis JJ and Embery G (1992). *Biomaterials* **13**: 548-552.

Cowin SC (1989). 'Mechanics of materials: Bone mechanics.' CRC Press, p15-42.

Creager SE and Olsen KG (1995). *Analytica Chimica Acta* **307**: 277-289.

Currey JD (2006). 'Bones: structure and mechanics.' New Edition, Princeton University Press, New Jersey.

D:

Damien CJ and Parsons JR (1991). *Journal of Applied Biomaterials* **2**: 187-208.

Dannenberger O, Wolff JJ and Buck M (1998). *Langmuir* **14**: 4679-4682.

Datsyuk V, Kalyva M, Papagelis K, *et al*. (2008). *Carbon* **46**: 833-840.

Davis S and Burns RG (1992). *Applied Microbiology and Biotechnology* **37**: 474-479.

De Sena LA, De Andrade MC, Rossi AM, *et al*. (2002). *Journal of Biomedical Materials Research* **60**: 1-7.

DeBono RF, Loucks GD, DellaManna D, *et al*. (1996). *Canadian Journal of Chemistry-Revue Canadienne de Chimie* **74**: 677-688.

Depalma V and Tillman N (1989). *Langmuir* **5**: 868-872.

Diebold U (2003). *Surface Science Reports* **48**: 53-229.

Ding SJ, Ju CP, Lin JHC (1999). *Journal of Biomedical Materials Research* **44**: 266-279.

Ding SJ (2003). *Biomaterials* **24**: 4233-4238.

Delecrin J, Daculsi G, Passutin N, *et al*. (1994). *Cells and Materials* **4**: 51-62.

Doudevski I and Schwartz DK (2001). *Journal of the American Chemical Society* **123**: 6867-6872.

Duran N, Rosa MA, D'Annibale A, *et al.* (2002). *Enzyme and Microbial Technology* **31**: 907-931.

E:

Eberhardt A, Fenter P and Eisenberger P (1998). *Surface Science* **397**: L285-L290.

Eddowes MJ and Hill H (1977). *Journal of the Chemical Society-Chemical Communications* **21**: 771-772.

Edwards JT, Brunski JB and Higuchi HW (1997). *Journal of Biomedical Materials Research* **36**: 454-468.

Elsenthal R. and Danson J.M. (1993). 'Enzyme assays: a practical approach.' Oxford University Press, Oxford, UK

Elwing H, Ivarsson B and Lundstrom I (1987). *Journal of Biomedical Materials Research* **21**: 263-267.

Evans FG (1976). *Anatomical Record* **185**: 1-12.

F:

Faucheux N, Schweiss R, Lutzow K, *et al.* (2004). *Biomaterials* **25**: 2721-2730.

Feng B, Weng J, Yang BC, *et al.* (2001). *Biomaterials* **25**: 3421-3428.

Fernandez-Sanchez C, Tzanov T, Gubitz GM, *et al.* (2002). *Bioelectrochemistry* **58**: 149-156.

Finklea HO, Robinson LR, Blackburn A, *et al.* (1986). *Langmuir* **2**: 239-244.

Foisner J, Glaser A, Kattner J, *et al.* (2003). *Langmuir* **19**: 3741-3746.

Freire RS, Duran N and Kubora LT (2001). *Talanta* **54**: 681-686.

Fujibayashi S, Neo M, Kim HM, *et al.* (2003). *Biomaterials* **24**: 1349-1356.

G:

Gainers GL (1996). 'Insoluble monolayers at liquid-gas interfaces.' John Wiley & Sons, New York.

Gil GC, Chang IS, Kim BH, *et al.* (2003). *Biosensors and Bioelectronics* **18**: 327-334.

Glimcher MJ (1968). *Clinical Orthopaedics and Related Research* **61**: 16-&.

Glorieux FH, Travers R, Taylor A, *et al.* (2000). *Bone* **26**: 103-109.

Golub AA, Zubenko AI and Zhmud BV (1996). *Journal of Colloid and Interface Science* **179**: 482-487.

Golz-Berner K, Walzel B, Zastrow L, *et al.* (2004). 'Cosmetic and dermatological preparation containing copper-binding proteins for skin lightening'. International patent application number WO2004017931.

Gooding JJ, Erokhin P, Losic D, *et al.* (2001). *Analytical Sciences* **17**: 3-9.

Gooding JJ and Hibbert DB (1999). *TRAC - Trends in Analytical Chemistry* **18**: 525-533.

Gronowicz G and McCarthy MB (1996). *Journal of Orthopaedic Research* **14**: 878-887.

Groot KD, Wen HB, Li Y, *et al.* (2000). *Materials Research Society Symposium Proceedings* **599**: 109-116.

Gun J, Iscovici R and Sagiv J (1984). *Journal of Colloid and Interface Science* **101**: 201-213.

H:

Habibovic P, Barrere F, Van Blitterswijk CA, *et al.* (2002). *Journal of the American Ceramic Society* **85**: 517-522.

Han Y, Fu T, Lu J, *et al.* (2001). *Journal of Biomedical Materials Research* **54**: 96-101.

Hanefeld U, Gardossi L and Magner E (2009). *Chemical Society Reviews* **38**: 453-468.

Hanker JS and Giammara BL (1988). *Science* **242**: 885-892.

Hartland Stanley (2004). 'Surface and interfacial tension: Measurement, Theory and Applications.' Marcel Dekker, New York.

Hench LL (1997). *Current Opinion in Solid State & Materials Science* **2**: 604-610.

Hench LL and Ethridge EC (1982). 'Biomaterials: An interfacial approach'. Academic Press, New York

Hench LL and Wilson J (1993). 'An introduction to bioceramics'. 1st Edition, World Scientific Publishing Co Ltd., New York.

Himmelhaus M, Eisert F, Buck M, *et al.* (2000). *Journal of Physical Chemistry B* **104**: 576-584.

Ho WF, Ju CP and Lin JHC (1999). *Biomaterials* **20**: 2115-2122.

Hoffmann PW, Stelzle M and Rabolt JF (1997). *Langmuir* **13**: 1877-1880.

Hooper AE, Werho D, Hopson T, *et al.* (2001). *Surface and Interface Analysis* **31**: 809-814.

Hou HM, Zhou JT, Wang J, *et al.* (2004). *Process Biochemistry* **39**: 1415-1419.

Howarter JA and Youngblood JP (2006). *Langmuir* **22**: 11142-11147.

Hsieh S, Ku HY, Ke YT, *et al.* (2007). *Journal of Mass Spectrometry* **42**: 1628-1636.

Huang J, Disilvio L, Wang M, *et al.* (1997). *Journal of Materials Science -Materials in Medicine* **8**: 775-779.

Huiskes R, Weinans H and Vanrietbergen B (1992). *Clinical Orthopaedics and Related Research* **274**: 124-134.

Humphries MJ, Akiyama SK, Komoriya A, *et al.* (1986). *Journal of Cell Biology* **103**: 2637-2647.

I:

Imamura M, Haruyama T, Kobatake E, *et al.* (1995). *Sensors and Actuators B* **24**: 113-116.

Ishida H (1984). *Polymer Composites* **5**: 101-123.

J:

James SL (2003). *Chemical Society Reviews* **32**: 276-288.

Jiang DS, Long SY, Huang J, *et al.* (2005). *Biochemical Engineering Journal* **25**: 15-23.

Jiang HD and Liu XY (2004). *Journal of Biological Chemistry* **279**: 41286-41293.

Jolivalt C, Brenon S, Caminade E, *et al.* (2000). *Journal of Membrane Science* **180**: 103-113.

Jones VW, Kenseth JR, Porter MD, *et al.* (1998). *Analytical Chemistry* **70**: 1233-1241.

Jonsson U, Olofsson G, Malmqvist M, *et al.* (1985). *Thin Solid Films* **124**: 117-123.

Jung C, Dannenberger O, Xu Y, *et al.* (1998). *Langmuir* **14**: 1103-1107.

K:

Kam L, Shain W, Turner JN, *et al.* (2002). *Biomaterials* **23**: 511-515.

Kane KR, Deheer H, Owens SR, *et al.* (1994). *Journal of Applied Biomaterials* **5**: 353-360.

Kang JF, Liao S, Jordan R, *et al.* (1998). *Journal of the American Ceramic Society* **120**: 9662-9667.

Karpovich DS and Blanchard GJ (1994). *Langmuir* **10**: 3315-3322.

Kasemo B and Lausmaa J (1986). *CRC Critical Reviews in Biocompatibility* **2**: 335-380.

Katz E, Willner I and Kotlyar AB (1999). *Journal of Electroanalytical Chemistry* **479**: 64-68.

Kessel CR and Granick S (1991). *Langmuir* **7**: 532-538.

Kilpadi DV, Raikar GN, Liu J, *et al.* (1998). *Journal of Biomedical Materials Research* **40**: 646-659.

Kim HM, Miyaji F, Kokubo T, *et al.* (1997). *Journal of Materials Science -Materials in Medicine* **8**: 341-347.

Kim HJ, Park HS, Hyun MS, *et al.* (2002). *Enzyme and Microbial Technology* **30**: 145-152.

Kim RH, Shapiro HS, Li JJ, *et al.* (1994). *Matrix Biology* **14**: 31-40.

Kilpadi KL, Chang PL and Bellis SL (2001). *Journal of Biomedical Materials Research* **57**: 258-267.

Kitsugi T, Yamamuro T, Nakamura T, *et al.* (1993). *Biomaterials* **14**: 216-224.

Kleinfeld D, Kahler KH and Hockberger PE (1988). *Journal of Neuroscience* **8**: 4098-4120.

Klinger A, Steinberg D, Kohavi D, *et al.* (1997). *Journal of Biomedical Materials Research* **36**: 387-392.

Kokubo T (1991). *Biomaterials* **12**: 155-163.

Kokubo T, Kim HM and Kawashita M (2003). *Biomaterials* **24**: 2161-2175.

Kuroda D, Niinomi M, Morinaga M, *et al.* (1998). *Materials Science and Engineering A* **243**: 244-249.

Kuroda D, Kawasaki H, Yamamoto A, *et al.* (2005). *Materials Science and Engineering C* **25**: 312-320.

L:

Landis WJ, Song MJ, Leith A, *et al.* (1993). *Journal of Structural Biology* **110**: 39-54.

Lang G. and Cotteret J (1999). "Hair dye composition containing a laccase." (L'Oreal, France) International patent application number WO9936036.

Larminie J and Dicks A (2000). 'Fuel Cell Systems Explained'. 2nd Edition, John Wiley & Sons Ltd., Chichester.

Larsson C, Thomsen P, Lausmaa J, *et al.* (1994). *Biomaterials* **15**: 1062-1074.

Lee CW, Gray HB and Anson FC (1984). *Journal of Electroanalytical Chemistry* **172**: 289-300.

Lee SK, George SD, Antholine WE, *et al.* (2002). *Journal of the American Ceramic Society* **124**: 6180-6193.

Leech D and Daigle F (1998). *Analyst* **123**: 1971-1974.

Legeros RZ (2002). *Clinical Orthopaedics and Related Research* **395**: 81-98.

Legrange JD, Markham JL and Kurkjian CR (1993). *Langmuir* **9**: 1749-1753.

Leonowicz A, Sarkar JM and Bollag JM (1988). *Applied Microbiology and Biotechnology* **29**: 129-135.

Lewington TA, Alexander MR, Thompson GE, *et al.* (2002). *Surface Engineering* **18**: 228-232.

Li F, Feng QL, Cui FZ, *et al.* (2002). *Surface & Coatings Technology* **154**: 88-93.

Li TT, Lee JH, Kobayashi T, *et al.* (1996). *Journal of Materials Science-Materials in Medicine*

7: 355-357.

Lin H, Xu HC and Degroot K (1992). *Journal of Biomedical Materials Research* **26**: 7-18.

Linford MR and Chidsey CED (1993). *Journal of the American Ceramic Society* **115**: 12631-12632.

Lisdat F, Dronov R, Mohwald H, *et al.* (2009). *Chemical Communications* **3**: 274-283.

Liu DM, Troczynski T and Tseng WJ (2001). *Biomaterials* **22**: 1721-1730.

Liu Q, Ding J, Mante FK, *et al.* (2002). *Biomaterials* **23**: 3103-3111.

Liu SQ and Chen AC (2005). *Langmuir* **21**: 8409-8413.

Liu XY (2000). *Langmuir* **16**: 7337-7345.

Liu XY (2000). *Journal of Chemical Physics* **112**: 9949-9955.

Liu XY, Chu PK and Ding CX (2004). *Materials Science & Engineering R* **47**: 49-121.

Liu Y, Huang LJ and Dong SJ (2007). *Biosensors and Bioelectronics* **23**: 35-41.

Logan BE, Hamelers B, Rozendal RA, *et al.* (2006). *Environmental Science & Technology* **40**: 5181-5192.

Love JC, Estroff LA, Kriebel JK, *et al.* (2005). *Chemical Reviews* **105**: 1103-1169.

M:

Ma J, Wang C and Peng KW (2003). *Biomaterials* **24**: 3505-3510.

Maasen S (2006). 'The assembled self of nanotechnology: the career of self-assembled as a metaphor'. EASST Conference, Lausanne.

Macanovic A, Marquette C, Polychronakos C and Lawrence MF (1993). *Nucleic Acids Research* **32**: e20.

Majewski PJ and Allidi G (2006). *Materials Science and Engineering A* **420**: 13-20.

Mandler D and Turyan I (1996). " *Electroanalysis* **8**: 207-213.

Manso M, Jimenez C, Morant C, *et al.* (2000). *Biomaterials* **21**: 1755-1761.

Manso M, Langlet M, Jimenez C, *et al.* (2002). *Biomolecular Engineering* **19**: 63-66.

Marcinko S and Fadeev AY (2003). *Langmuir* **19**: 2752-2755.

Marler JJ, Upton J, Langer R, *et al.* (1998). *Advanced Drug Delivery Reviews* **33**: 165-182.

Mathauer K and Frank CW (1993). *Langmuir* **9**: 3446-3451.

Matinlinna JP, Areva S, Jassila LVJ, *et al.* (2004). *Surface and Interface Analysis* **36**: 1314-1322.

Matsuura T, Hosokawa R, Okamoto K, *et al.* (2000). *Biomaterials* **21**: 1121-1127.

Mavis B and Tas AC (2000). *Journal of the American Ceramic Society* **83**: 989-991.

Maxian SH, Zawadsky JP and Dunn MG (1993). *Journal of Biomedical Materials Research* **27**: 717-728.

Mayer AM and Harel E (1979). *Phytochemistry* **18**: 193-215.

McConnell D (1962). *Clinical Orthopaedics and Related Research* **23**: 253-268.

McGovern ME, Kallury KMR and Thompson M (1994). *Langmuir* **10**: 3607-3614.

Mendes RK, Carvalhal RF and Kubota LT (2008). *Journal of Electroanalytical Chemistry* **612**: 164-172.

Messing RA (1975). 'Immobilized enzymes for industrial reactors.' Academic Press, New York, p. 225.

Milstein O, Nicklas B and Huettermann A (1989). *Applied Microbiology and Biotechnology* **31**: 70-74.

Minier M, Salmain M, Yacoubi N, *et al.* (2005). *Langmuir* **21**: 5957-5965.

Mrksich M (1998). *Cellular and Molecular Life Sciences* **54**: 653-662.

Mueller U, Schubert M, Teich F, *et al.* (2006). *Journal of Materials Chemistry* **16**: 626-636.

Murai K, Takeshita F, Ayukawa Y, *et al.* (1996). *Journal of Biomedical Materials Research* **30**: 523-533.

Murugan R and Ramakrishna S (2005). *Composites Science and Technology* **65**: 2385-2406.

N:

Nogala W, Roznіecka E, Zawisza I, *et al.* (2006). *Electrochemistry Communications* **8**: 1850-1854.

Nuzzo RG and Allara DL (1983). *Journal of the American Chemical Society* **105**: 4481-4483.

Nyquist RM, Eberhardt AS, Silks LA, *et al.* (2000). *Langmuir* **16**: 1793-1800.

O:

Oberg K, Persson P, Shchukarev A, *et al.* (2001). *Thin Solid Films* **397**: 102-108.

Oji MO, Wood JV and Downes S (1999). *Journal of Materials Science -Materials in Medicine* **10**: 869-872.

Okahata Y, Kawase M, Niikura K, *et al.* (1998). *Analytical Chemistry* **70**: 1288-1296.

Oliveira AL, Elvira C, Reis RL, *et al.* (1999). *Journal of Materials Science - Materials in Medicine* **10**: 827-835.

Oliveira EM, Beyer S and Heinze J (2007). *Bioelectrochemistry* **71**: 186-191.

Olszta MJ, Cheng XG, Jee SS, *et al.* (2007). *Materials Science & Engineering R* **58**: 77-116.

Ong JL and Lucas LC (1994). *Biomaterials* **15**: 337-341.

Osiadacz J, Al-Adhami AJH, Bajraszewska D, *et al.* (1999). *Journal of Biotechnology* **72**: 141-149.

P:

Palmore GTR and Kim HH (1999). *Journal of Electroanalytical Chemistry* **464**: 110-117.

Palmore GTR and Whitesides GM (1994). *Americal Chemical Society Symposium Series*, **566**: 271-290.

Pan J, Liao H, Leygraf C, *et al.* (1998). *Journal of Biomedical Materials Research* **40**: 244-256.

Parikh AN, Allara DL Azouzib, *et al.* (1994). *Journal of Physical Chemistry* **98**: 7577-7590.

Park JB (1984). 'Biomaterials science and engineering' Plenum Press, New York.

Patel N, Davies MC, Hartshorne M, *et al.* (1997). *Langmuir* **13**: 6485-6490.

Peterlinz KA and Georgiadis R (1996). *Langmuir* **12**: 4731-4740.

Peters RD, Nealey PF, Crain JN, *et al.* (2002). *Langmuir* **18**: 1250-1256.

Petitjean M, Proust N and Chapeaublanc JF (1990). *Applied Surface Science* **46**: 189-194.

Petty MC (1996). 'Langmuir-Blodgett films: an introduction'. 1st Edition, Cambridge University Press, Cambridge.

Philp D and Stoddart JF (1996). *Angewandte Chemie-International Edition* **35**: 1154-1196.

Piacquadio P, Destefano G, Sammartino M, *et al.* (1997). *Biotechnology Techniques* **11**: 515-517.

Piontek K, Antorini M and Choinowski T (2002). *Journal of Biological Chemistry* **277**: 37663-37669.

Plant AL, Chen CS, Groves JT, *et al.* (2003). *Langmuir* **19**: 1449-1450.

Plueddemann EP (1982). 'Silane Coupling Agents'. 2nd Edition, Plenum Press, New York.

Poirier GE (1999). *Langmuir* **15**: 1167-1175.

Poirier GE and Pylant ED (1996). *Science* **272**: 1145-1148.

Puleo DA and Nanci A (1999). *Biomaterials* **20**: 2311-2321.

Q:

Quan D, Kim Y and Shin W (2004). *Journal of Electroanalytical Chemistry* **561**: 181-189.

R:

Rao AB and Rubin ES (2002). *Environmental Science & Technology* **36**: 4467-4475.

Ratner BD (1993). *Journal of Biomedical Materials Research* **27**: 837-850.

Ratner BD, Hoffman AS, *et al.* (1996). 'Biomaterial science: An introduction to materials in medicine'. Academic Press, New York.

Reilly DT and Burstein AH (1975). *Journal of Biomechanics* **8**: 393-&.

Reinhamm B (1970). *Biocheimica et Biophysica Acta* **205**: 35-&.

Rey C, Miquel JL, Facchini L, *et al.* (1995). *Bone* **16**: 583-586.

Rezania A and Healy KE (1999). *Biotechnology Progress* **15**: 19-32.

Robey PG, Bianco P, and Termine JD (1992). 'The cell biology and molecular biology of bone formation'. New York, Raven Press.

Rogalski J, Wojtaswasilewska M, Apalovic R, *et al.* (1991). *Biotechnology and Bioengineering* **37**: 770-777.

Rohanizadeh R, Al-Sadeq M and LeGeros RZ (2004). *Journal of Biomedical Materials Research Part A* **71A**: 343-352.

Rozlosnik N, Gerstenberg MC and Larsen NB (2003). *Langmuir* **19**: 1182-1188.

S:

Sakiyama-Elbert SE and Hubbell JA (2001). *Annual Review of Materials Research* **31**: 183-201.

Sampath S and Lev O (1997). *Advanced Materials* **9**: 410-&.

Sato K, Kumagai Y and Tanaka T (2000). *Journal of Biomedical Materials Research* **50**:16-20.

Sauer GR and Wuthier RE (1988). *Journal of Biological Chemistry* **263**: 13718-13724.

Scherer J, Vogt MR, Magnussen OM, *et al.* (1997). *Langmuir* **13**: 7045-7051.

Schreiber F (2000). *Progress in Surface Science* **65**: 151-256.

Schreiber F (2004). *Journal of Physics-Condensed Matter* **16**: R881-R900.

Schwartz DK, Steinberg S, Israelachvili J, *et al.* (1992). *Physical Review Letters* **69**: 3354-3357.

Schweizer M, Hagenstrom H and Kolb DM (2001). *Surface Science* **490**: L627-L636.

Serro AP, Fernandes AC, Saramago B, *et al.* (1997). *Biomaterials* **18**: 963-968.

Shin H, Jo S and Mikos AG (2003). *Biomaterials* **24**: 4353-4364.

Shleev S, Jarosz-Wikolazka A, Khalunina A, *et al*. (2005). *Bioelectrochemistry* **67**: 115-124.

Shleev S, Christenson A, Serezhenkov V, *et al.* (2005). *Biochemical Journal* **385**: 745-754.

Sigal GB, Bamdad C, Barberis A, *et al.* (1996). *Analytical Chemistry* **68**: 490-497.

Silberzan P, Leger L, Ausserre D, *et al.* (1991). *Langmuir* **7**: 1647 -1651.

Silin V, Weetall H and Vanderah DJ (1997). *Journal of Colloid and Interface Science* **185**: 94-103.

Sirivisoot S and Webster TJ (2008). *Nanotechnology* **19**: 295101.

Smith BC (1996). 'Fundamentals of Fourier Transform Infrared spectroscopy'. CRC Press, Boca Raton.

Snyder RG, Strauss HL and Elliger CA (1982). *Journal of Physical Chemistry* **86**: 5145-5150.

Socrates G. (1980). 'Infrared Characteristic Group Frequencies'. 1st Ediiton, John Wiley & Sons Ltd, New York.

Solomon EI, Sundaram UM and Machonkin TE (1996). *Chemical Reviews* **96**: 2563-2605.

Steinemann SG (1994). 'Compatibility of Biomedical Implants'. California, USA.

Sterjiades R, Dean JFD and Eriksson KEL (1992). *Plant Physiology* **99**: 1162-1168.

Sun LM, Berndt CC, Gross KA, *et al.* (2001). *Journal of Biomedical Materials Research* **58**: 570-592.

Susana RC and Jose LTH (2006). *Biotechnology Advances* **24**: 500-513.

Suzuki R and Frangos JA (2000). *Clinical Orthopaedics and Related Research* 280-289.

T:

Takeichi M (1995). *Current Opinion in Cell Biology* **7**: 619-627.

Tanahashi M and Matsuda T (1997). *Journal of Biomedical Materials Research* **34**: 305-315.

Tao YT and Lee MT (1994). *Thin Solid Films* **244**: 810-814.

Tengvall P, Lundstrom I, Sjoqvist L, *et al.* (1989). *Biomaterials* **10**: 166-175.

Thomas RC, Sun L, Crooks RM, *et al.* (1991). *Langmuir* **7**: 620-622.

Thurston CF (1994). *Microbiology-SGM* **140**: 19-26.

Tolles WM (2000). *MRS Bulletin*, **25**: 36-48.

Toworfe GK, Composto RJ, Shapiro IM, *et al.* (2006). *Biomaterials* **27**: 631-642.

Trevan Michael D (1980). 'Immobilized enzymes: an introduction and applications in biotechnology'. 2nd Edition, John Wiley & Sons Ltd, Chichester, UK.

Tripp CP and Hair ML (1992). *Langmuir* **8**: 1120-1126.

Tripp CP and Hair ML (1995). *Langmuir* **11**: 149-155.

U:

Ulman A (1990). *Advanced Materials* **2**: 573-582.

Ulman A (1991). 'An introduction to ultrathin organic films: From Langmuir-Blodgett to Self-assembly'. 1st Edition, Academic Press, Boston.

Ungersbock A, Perren SM and Pohler O (1994). *Journal of Materials Science -Materials in Medicine* **5**: 788-792.

V:

Valiokas R (2000). PhD thesis, 'Intrefacial design and characterization of oligo (ethylene glycol) self-assembled monolayers'. Linkopings University, Sweden.

Vallant T, Brunner H, Mayer U, *et al.* (1998). *Journal of Physical Chemistry B* **102**: 7190-7197.

Van Alsten JG (1999). *Langmuir* **15**: 7605-7614.

Van Blitterswijk CA, GroteJJ, Kuijpers W, *et al.* (1986). *Biomaterials* **7**: 137-143.

Veis A, Bhatnaga RS, Shuttlew CA, *et al.* (1970). *Biochimica et Biophysica Acta* **200**: 97-&.

Vericat C, Andreasen G, Vela ME, *et al.* (2001). *Journal of Chemical Physics* **115**: 6672-6678.

W:

Walivaara B, Aronsson BO, Rodahl M, *et al.* (1994). *Biomaterials* **15**: 827-834.

Wang MJ, Liechti KM, Wang Q, *et al.* (2005). *Langmuir* **21**: 1848-1857.

Wang X.X, Hayakawa S, Tsuru K, *et al.* (2002). *Biomaterials* **23**: 1353-1357.

Wang YL and Lieberman M (2003). *Langmuir* **19**: 1159-1167.

Wasserman SR, Tao YT and Whitesides GM (1989). *Langmuir* **5**: 1074-1087.

Weiner S and Wagner HD (1998). *Annual Review of Materials Science* **28**: 271-298.

Wen HB, Liu Q, De Wijn JR, *et al.* (1998). *Journal of Materials Science - Materials in Medicine* **9**: 121-128.

West JL and Hubbell JA (1999). *Macromolecules* **32**: 241-244.

Whitaker MJ, Quirk RA, Howdle SM, *et al.* (2001). *Journal of Pharmacy and Pharmacology* **53**: 1427-1437.

White LD and Tripp CP (2000). *Journal of Colloid and Interface Science* **11**: 417-424.

White LD and Tripp CP (2000). *Journal of Colloid and Interface Science* **232**: 400-407.

Whitesides GM, Mathias JP and Seto CT (1991). *Science* **254**: 1312-1319.

Wikstrom P, Mandenius CF and Larsson PO (1988). *Journal of Chromatography* **455**: 105-117.

Williams B, Waddington D, Murray DH, *et al.* (2004). *Calcified Tissue International* **74**: 236-245.

Wilt PM (1986). *Journal of Colloid and Interface Science* **112**: 530-538.

Wirth MJ, Fairbank RWP and Fatunmbi HO (1997). *Science* **275**: 44-47.

Wolke JGC, Vandijk K, Schaeken HG, *et al.* (1994). *Journal of Biomedical Materials Research* **28**: 1477-1484.

Wong M, Eulenberger J, Schenk R, *et al.* (1995). *Journal of Biomedical Materials Research* **29**: 1567-1575.

Woodward JT, Ulman A and Schwartz DK (1996). *Langmuir* **12**: 3626-3629.

X:

Xiao XD, Hu J, Charych DH, *et al.* (1996). *Langmuir* **12**: 235-237.

Xu F (1997). *Journal of Biological Chemistry* **272**: 924-928.

Xu F, Palmer AE, Yaver DS, *et al.* (1999). *Journal of Biological Chemistry* **274**: 12372-12375.

Y:

Yamada R, Wano H and Uosaki K (2000). *Langmuir* **16**: 5523-5525.

Yang YZ, Kim KH and Ong JL (2005). *Biomaterials* **26**: 327-337.

Yaropolov AI, Skorobogatko OV, Vartanov SS, *et al.* (1994). *Applied Biochemistry and Biotechnology* **49**: 257-280.

Yasseri AA, Sharma S and Kamins TI (2006). *Applied Physics Letters* **89**: 153121.

Yu JH and Ju HX (2002). *Analytical Chemistry* **74**: 3579-3583.

Z:

Zaborsky O.R. (1974). 'Immobilized enzymes'. CRC Press, USA, p.175.

Zawisza I, Rogalski J and Opallo M (2006). *Journal of Electroanalytical Chemistry* **58**: 244-252.

Zhao XL and Kopelman R (1996). *Journal of Physical Chemistry* **100**: 11014-11018.

Zhitomirsky I (2000). *Materials Letters* **42**: 262-271.

Zhu PX, Ishikawa M, Seo WS, *et al.* (2002). *Journal of Biomedical Materials Research* **59**: 294-304.

Zhu PX, Masuda Y, Yonezawa T, *et al.* (2003). *Journal of the American Ceramic Society* **86**: 782-790.

Zhu PX, Masuda Y and Koumoto K (2004). *Biomaterials* **25**: 3915-3921.

Zisman WA, Pickett DL and Bigelow, WC (1946). *Journal of Colloid Science* **1**: 513-538.

Web pages:

W1. "http://en.wikipedia.org/wiki/File:System2.gif."

W2. "http://en.wikipedia.org/wiki/Carbodiimide."

W3. "http://en.wikipedia.org/wiki/Enzyme."

W4. "http://publish.uwo.ca/%7Ehnie/image-1/set-up.gif."

W5. "http://www.ntmdt.com/spm-principles/view/non-contact-techniques."

W6. "http://en.wikipedia.org/wiki/Michaelis_constant."

W7. "http://www.azom.com/details.asp?articleid=1630#_Electrical_Applications."

W8. "http://www.stryker.co.uk/index/st_pat_about-us/uk_pag_about-us-industry.htm."

APPENDIX: Publications

Q. Gu, Dongmei Sun and Z.X. Guo, ‘‘*Covalent immobilization of laccase from Trametes versicolor on graphite with the APS film for bioelectrocatalytic reduction of of oxygen*’’, (Drafted, intend to submit to **Journal of Electroanalytical Chemistry**)

Q. Gu, X.S. Lu and Z.X. Guo, ‘‘*Self-assembly of 3-Aminopropyltriethoxysilane on a TiOx/Ti surface*’’, (Accepted to **Journal of Chemical Technology & Biotechnology**)

Q. Gu and Z.X. Guo (2006) *Surface modification of biomedical Ti alloys by a Self-Assembly technique*, 21st European Conference on Biomaterials 2007, Brighton, UK **(Awarded Andrew Carnegie Research Fund, IMMM, UK)**

Q. Gu, T.F. Hong and Z.X. Guo (2004) *Surface Modification of Bio- Titanium Associated by Self-Assembly*, Materials congress 2006, London, UK (**Awarded Best Poster Prize**)